Durham E-Theses

New Luminescent Organic and Organomatallic Materials for OLED Applications

ZHENG, YONGHAO

How to cite:

Use policy

New Luminescent Organic and Organomatallic Materials for OLED Applications

Yonghao Zheng

Trevelyan College

Department of Chemistry

University of Durham

A Thesis submitted for the degree of Doctor of Philosophy
at the University of Durham

January 2011

Statement of Copyright

Declaration

The work described in this thesis was carried out in the Department of Chemistry at the University of Durham between October 2008 and January 2011. All the work was carried out by the author unless otherwise stated and has not previously been submitted for a degree at this or any other university.

Publications

Yonghao Zheng, Andrei S. Batsanov, and Martin R. Bryce
"Unusual Dinuclear and Mononuclear Cyclometalated Iridium Complexes of 2,5-Diaryl-1,3,4-oxadiazole derivatives" *Inorg. Chem.* 2011, **50**, 3354-3362

Yonghao Zheng, Andrei S. Batsanov, Vygintas Jankus, John Dickinson, Fernando B. Dias, Martin R. Bryce and Andrew P. Monkman
"Ambipolar Molecules with High Triplet Energies: Synthesis, Structural and Optoelectronic Properties" Manuscript in preparation, submission expected June 2011.

Yonghao Zheng, Robert M. Edkins, Andrei S. Batsanov, Andrew Beeby and Martin R. Bryce
"Phosphorescent *mer* and *fac* Cyclometalated Iridium(III) Complexes of 2-Phenylpyrido[4,3-*b*]indole Derivatives: An Unusual Thermally-Induced Defluorination Reaction of a Homoleptic Complex"
Manuscript in preparation, submission expected May 2011.

Mustafa Tavasli, Tom N. Moore, Yonghao. Zheng, Martin R. Bryce, Mark A. Fox, Gareth C. Griffiths, Vygintas Jankus, Hameed A. Al-Attar and Andrew P. Monkman
"High Efficiency Colour Tuneable Electrophosphorescent Devices Using Tris-Cyclometalated Iridium(III) Complexes of 2-(Carbazol-3'/2'-yl)-pyridine Ligands with Trifluoromethyl and Methoxy Substituents"
Manuscript in preparation, submission expected June 2011

Shashi U. Pandya, Hameed A. Al Attar, Vygintas Jankus, Yonghao Zheng, Martin R. Bryce and Andrew P. Monkman
"Solution-Processable Ambipolar Host Polymers with High Triplet Energies for Phosphorescent Green Emitters"
Manuscript submitted to *Marcomolecules*.

Table of Contents

Abstract

The design, synthesis and photophysics is presented for a new series of fluorescent carbazole-2,5-diphenyl-1,3,4-oxadiazole dyad molecules and in which the topology and electronic properties are systematically varied by chemical modification. Cyclic voltammetric data, HOMO-LUMO calculations, and X-ray crystallographic analyses are also presented. Our study sheds new light on designing ambipolar molecules and we demonstrate a strategy for precisely tuning the singlet and triplet levels in charge transfer molecules.
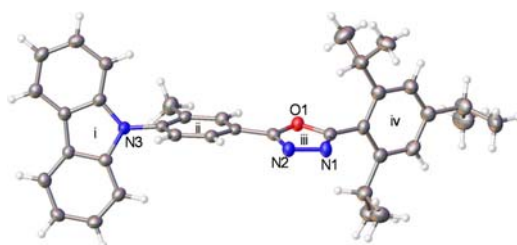
X-ray crystal structure of compound **77**

A family of new 2,5-diphenyl-1,3,4-oxadiazole (OXDs) derivatives bearing *ortho*-alkyl substituents on one of the phenyl rings is reported. The reactions of these OXDs with IrCl$_3$ under standard cyclometalating conditions did not give the usual μ-dichloro bridged diiridium OXDs complexes. Instead, novel diiridium complexes and monoiridium complexes were isolated and characterised by X-ray crystallography. It is proposed that the unusual structures arise due to the *ortho*-alkyl substituents leading to a substantial twisting of part of the OXDs system which, for steric reasons, changes the normal course of the metal-ligand coordination reactions.
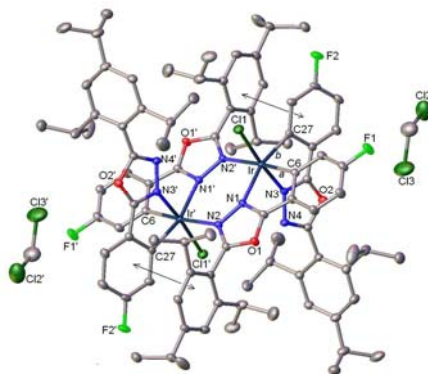
X-ray crystal structure of complex **87**

A new high triplet host polymer was synthesised and characterised. Photophysical studies and device data are presented. The triplet energy of this polymer is 2.73 eV. Also, the unoptimised device efficiency (device architecture: ITO/PEDOT:PSS/8% **145** and 40 wt% OXD-7 doped in polymer **133**/Ba:Al) is 4.5 cd/A. Our study sheds new light on designing high triplet polymers and we demonstrate a strategy for possessing a high triplet level in a polymer by interrupting the conjugation on the polymer backbone.
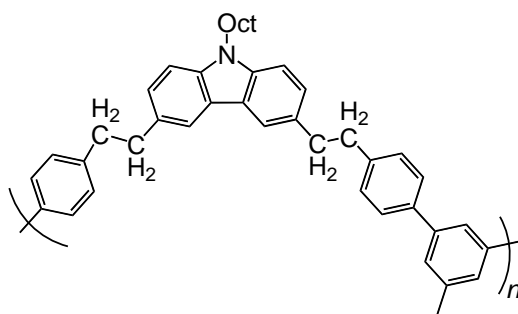
Polymer **133**

Acknowledgement

Abbreviations

acac	Acetylacetonate
AcOH	Acetic acid
B3LYP	Becke's three-parameter hybrid exchange functional with Lee-Yang-Parr gradient-corrected correlation functional
BCP	2,9-Dimethyl-4,7-diphenyl-1,10-phenanthroline
BPhen	4,7-Diphenyl-1,10-phenanthroline
bpy	2,2′-Bipyridine
^{n}BuLi	n-Butyllithium
CBP	[4,4′-Di(N-carbazolyl)biphenyl]
$CDCl_3$	Deuterated chloroform
CRT	Cathode ray tubes
CuI	Copper iodide
CV	Cyclic voltammetry
DCB	[N-[4-(N-Carbazolylphenyl)]-4,7-bis(N,N-dicarbazolyl)carbazole]
DCM	Dichloromethane
DFT	Density functional theory
DMF	N,N-Dimethylformamide
DMSO	Dimethylsulphoxide
p-DPA-TDAB	[1,3,5-Tris[N-(4-diphenylaminophenyl)-phenylamino]benzene]
EL	Electroluminescence
EQE	External quantum efficiency
E_T	Triplet energy
ET	Electron-transporting
EtOAc	Ethyl acetate
fac	Facial
FcMe	Decamethyl ferrocene
FIr6	Iridium(III) bis(4,6-difluorophenylpyridinato)tetrakis(1-pyrazolyl)
FIrpic	Iridium(III) bis[(4,6-difluorophenyl)-pyridinato-

	N,C^2]picolinate
HOMO	Highest occupied molecular orbital
HPLC	High-performance liquid chromatography
HT	Hole-transporting
ICT	Intramolecular charge transfer
Ir(ppy)$_3$	Tris(2-phenylpyridine)iridium
ITO	Indium tin oxide
K$_2$CO$_3$	Potassium carbonate
LCDs	Liquid crystal displays
LUMO	Lowest unoccupied molecular orbital
mCP	3,5′-*N,N*′-Dicarbazolylbenzene
MeOH	Methanol
mer	Meridional
MLCT	Metal-to-ligand charge-transfer
mp	Melting point
o-, *m*-, *p*-MTDAPB	[1,3,5-Tris[4-(methylphenylphenyl -amino)phenyl]benzenes]
M$_w$	Weight-average molecular weight
NaN$_3$	Sodium azide
NBS	*N*-Bromosuccinimide
NEt$_3$	Triethylamine
NH$_4$Cl	Ammonium chloride
NMR	Nuclear magnetic resonance
OLED	Organic light emitting diode
OXD-7	[1,3-Bis[5-(*p-tert*-butylphenyl)-1,3,4-oxadiazol-2-yl]benzene]
OXDs	2,5-Diaryl-1,3,4-oxadiazoles
PBD	5-(4-Biphenyl)-2-(4-*tert*-butylphenyl)-1,3,4-oxadiazole
PDI	Polydispersity index
Pd(PPh$_3$)$_2$Cl$_2$	Dichlorobis(triphenylphosphine)palladium(II)
Pd(PPh$_3$)$_4$	Tetrakis(triphenylphoshine)palladium(0)
Pd(P(*o*-Tol)$_3$)$_2$Cl$_2$	Dichlorobis(tri-*o*-toluenephosphine)palladium(II)
PPLEDs	Phosphorescent polymer light-emitting diodes
PVK	Poly(9-vinylcarbazole)
PVKH	High molecular weight PVK

PVKL	Low molecular weight PVK
PEDOT:PSS	Poly(3,4-ethylenedioxythiophene) doped with poly(styrene sulfonic acid)
PFs	Polyfluorenes
pic	Picolinate
PL	Photoluminescent
PLED	Polymeric light emitting diode
PLQY	Photoluminescence quantum yield
$POCl_3$	Phosphorus oxychloride
PPPs	Polyphenylenes
PPVs	Poly(*p*-phenylenevinylene)
PTs	Polythiophenes
S_1	Singlet state
$SOCl_2$	Thionyl chloride
Spiro-TAD	[2,2′,7,7′-Tetrakis-(*N,N*-diphenylamino)-9,9′-spirobifluorene]
T_1	Triplet state
TAPC	1,1-Bis[(di-4-tolylamino)phenyl]cyclohexane
TAZ	[3-(Biphenyl-4-yl)-4-phenyl-5-(4-*tert*-butylphenyl)-1,2,4-triazole]
TBFAPB	[4,4′,4″-Tris[bis(9,9-dimethylfluoren-2-yl)amino]triphenylbenzene]
TCTA	[4,4′,4″-Tri(*N*-carbazolyl)triphenylamine]
T_g	Glass transition temperature
THF	Tetrahydrofuran
TLC	Thin Layer Chromatography
TMSA	Trimethylsilylacetylene
TPD	*N,N*′-Diphenyl-*N,N*′-bis(3-methylphenyl)(1,1′-biphenyl)-4,4′-diamine
TPBI	[2,2′,2″-(1,3,5-Benzenetriyl)tris-[1-phenyl-1*H*-benzimidazole]]
TPOB	[1,3,5-Tris(4-*tert*-butylphenyl-1,3,4-oxadiazolyl)benzene]
3TPYMB	Tris[3-(3-pyridyl)mesityl]borane
UV-vis	Ultraviolet-visible

Chapter 1 – Introduction

1.1 Organics for Photonics Applications

For thousands of years, humans have used wood and candle as light sources. Then, a century ago, cathode ray tubes (CRT) and the tungsten light bulb were invented, which have since dominated. However, these lighting sources have their own disadvantages. For the tungsten bulb, the drawbacks are that they are energy inefficient, whereby over 90% of electricity is transformed into heat, and they have a short lifetime (*ca*. 1000 hours). Fluorescent lighting is less energy consuming, but toxic mercury contained in the tubes makes disposal more difficult. By contrast, solid-state lighting (both inorganic and organic) has the potential to be a future light source which offers lifetimes of over 100,000 hours and better energy efficiency. Inorganic LEDs have already been applied in day to day life as light sources.

Currently, the displays market is dominated by liquid crystal displays (LCDs) and plasma displays. However, they both have their own disadvantages. Organic light-emitting diode (OLED) displays show great potential to overcome the drawbacks of current displays, with properties such as quick response time (microseconds), high viewing angle, higher contrast and no need for a backlight. Also, OLED displays can be flexible and very thin, which are bonus properties for the next generation display technology. Products with small OLED screens (<3 inch diameter) are already commercial available, such as mobile phones and MP3 players. Energy efficiency is one of main advantages of OLEDs. Therefore, OLED lighting has attracted great industrial interest.[1] Finally, General Electric have demonstrated an OLED lighting panel (Figure 1.1).[2] This Chapter will highlight areas in OLED technology which are of current interest, with emphasis on those topics which are relevant to the work described later in the thesis.

Organic electroluminescent materials can emit light over a range of colours due to their tunable band gaps. Small molecules as emissive materials have been used in commercial OLED products, due to their high colour purity, high energy efficiency and long lifetimes. However, a huge drawback which has made them unfavourable is that ca. 95% of the materials are wasted during the vacuum deposition fabrication

process. In contrast, polymeric emissive materials are fabricated by a spin-coating method onto the device, which does not waste any materials and is easy to operate.

Figure 1.1. General Electric OLED lighting panel (from ref. 2).

Polymeric emissive materials have attracted considerable attention in the last decade. Several types of conjugated polymer have been well studied (see Figure 1.2), including poly(*p*-phenylenevinylene) (**PPVs**),[3,4] polyphenylenes (**PPPs**),[5] polyfluorenes (**PFs**)[6] and polythiophenes (**PTs**).[7]
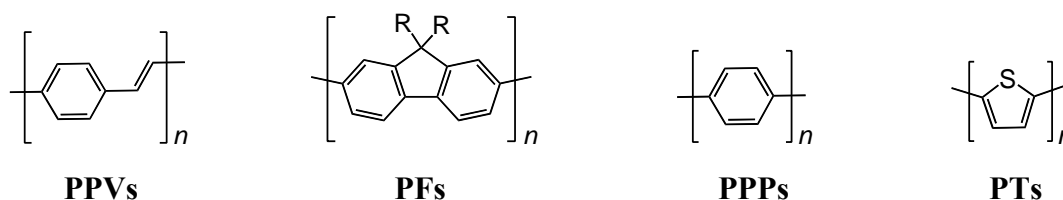
PPVs   **PFs**   **PPPs**   **PTs**

Figure 1.2. Structures of polymers **PPVs**, **PFs**, **PPPs** and **PTs**.

PPVs and PFs are the favoured materials for OLED applications. These two families of compounds have already shown some promising results which include high efficiency, high brightness and long lifetime devices. Also, a wide range of colour emissions has been achieved. In particular, polyfluorene derivatives have come under the spotlight due to their large photoluminescent (PL) quantum efficiency and their good chemical and thermal stability properties.[6]

Organic small molecules and polymers emit light *via* the recombination of singlet excitons (fluorescence). Therefore, the maximum output is 25% of the input due to the recombination ratio of 3 (triplet):1 (singlet). By contrast, phosphorescent

materials approach a 100% internal quantum efficiency by utilising both singlet and triplet excitons. Incorporation of heavy metal atoms, such as iridium or platinum, can overcome selection rules and enable the harvesting of both singlet and triplet excited states.

1.2 OLED Devices

The basic concept of OLEDs is to generate light by injecting electrons and positive holes into electroluminescent materials. The first OLED device was designed as a sandwich-like single-layer system. Electroluminescent materials are assembled between a cathode [electrons are injected into the lowest unoccupied molecular orbital (LUMO) to form anion radicals] and an anode [positive holes are injected into the highest occupied molecular orbital (HOMO) to form cation radicals]. When these two polarons meet at the electroluminescent layer, an excited state with either singlet or triplet multiplicity is formed. The emitted light is one of the end results of the relaxation of the excited state. For the cathode, an atmospherically degradable metal coated with a non-reactive metal is required.[8]

However, single-layer devices (Figure 1.3)[9] are generally not reliable, efficient or long-lived, mainly due to polaron quenching by escaped opposite charges. Therefore, a better charge injection balanced system is necessary for improving device performance. The multiple-layer device design has been widely explored to achieve this goal.
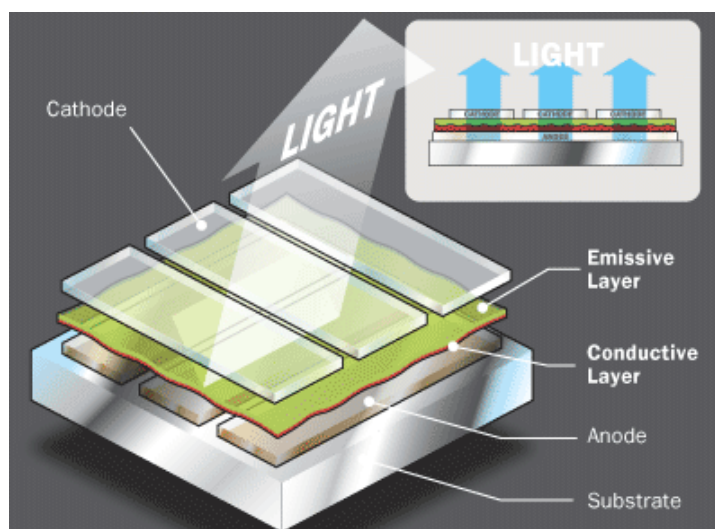
Figure 1.3. An illustration of the structure of an OLED device (from ref. 9).

In this design, extra functionalised layers are introduced in the device. Hole-transporting (HT) and electron-transporting (ET) materials are used to facilitate charge migration into the emitting layer (recombination zone). Ideally, the HOMO of the HT material should lie close to the work function of the anode and the HOMO of the emissive layer. In contrast, the LUMO of the ET material should lie close to the work function of the cathode and the LUMO of the emissive layer. On the other hand, hole-blocking and electron-blocking materials are also introduced in the device, to avoid hole and electron movement beyond the materials, respectively.[8]

1.3 Hole-Transporting Materials

The positioning of the HOMO and LUMO are the main considerations for designing HT materials. For receiving positive holes from the anode, it is important for the HOMO level to lie close to the work function of the anode. Furthermore, the HOMO level of the HT materials should lie slightly higher than that of the emissive molecule which would allow for easier hole injection. In addition, indium tin oxide (ITO) is a commonly used anode with a work function of between -4.7 to -4.9 eV; also it forms transparent films which allow light to pass through. On the other hand, a high lying LUMO level is important for preventing escaped electrons from reaching the anode. Specifically, the LUMO level of the HT materials must be higher than that of the emissive molecule. The greater the LUMO energy differences the better the electron blocking ability. In other words, HT materials should posses low ionisation potentials and electron affinities. Finally, hole mobility and the ability to form reversible stable cation radicals and stable homogenous thin films of HT materials play very important roles in device performance.[10]

In devices, a material with a low solid-state ionisation potential, called a hole-injection buffer layer, is applied on the top of ITO and acts as the HT material. Poly(3,4-ethylenedioxythiophene) doped with poly(styrene sulfonic acid) (PEDOT:PSS) is the most commonly used hole-injection buffer layer, with a HOMO level of ca. -5.1 eV. However, its ability to transport holes from the buffer layer into the emissive layer is limited due to the large energy barrier. One way to reduce the energy barrier, and increase hole-transporting efficiency, is to apply a second hole-

transporting layer on top of the buffer layer. In addition, the second hole-transporting layer should possess a higher ionisation potential than the buffer layer.

Amines have been widely used as excellent second layer hole-transporting layers. Moreover, the high glass transition temperature (T_g) materials can be used to fabricate thermally stable OLED devices.[10] Representative structures, which have been well studied, are shown in Figure 1.4.
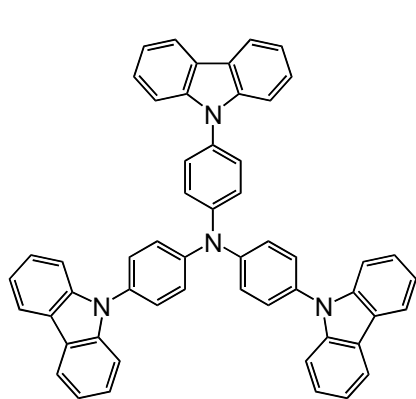
1 TCTA (T_g= 151 °C)[11]
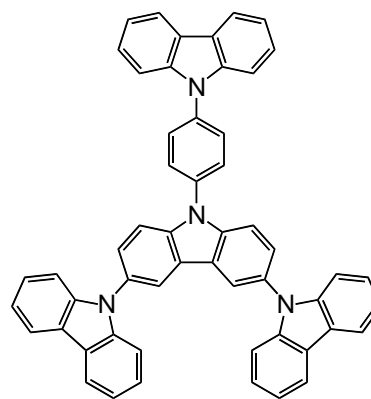
2 DCB[12]
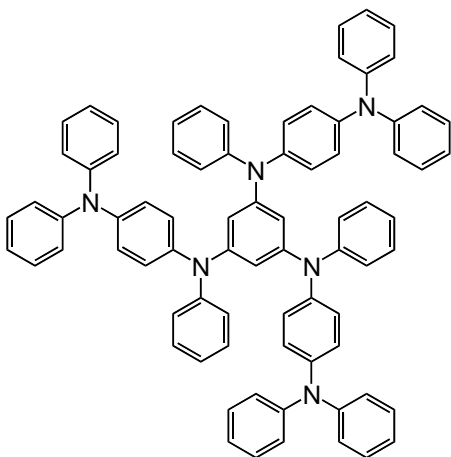
3 *p*-DPA-TDAB (T_g= 108 °C)[13]
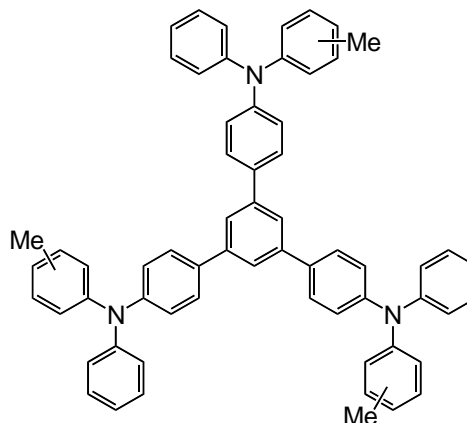
4-6 *o*-, *m*-, *p*-MTDAPB (T_g= 105-110 °C)[14]

7 TBFAPB[15]

8 PPD (T$_g$= 152 °C)[16]

9 CBP[17]

10 Spiro-TAD (T$_g$= 152 °C)[18]
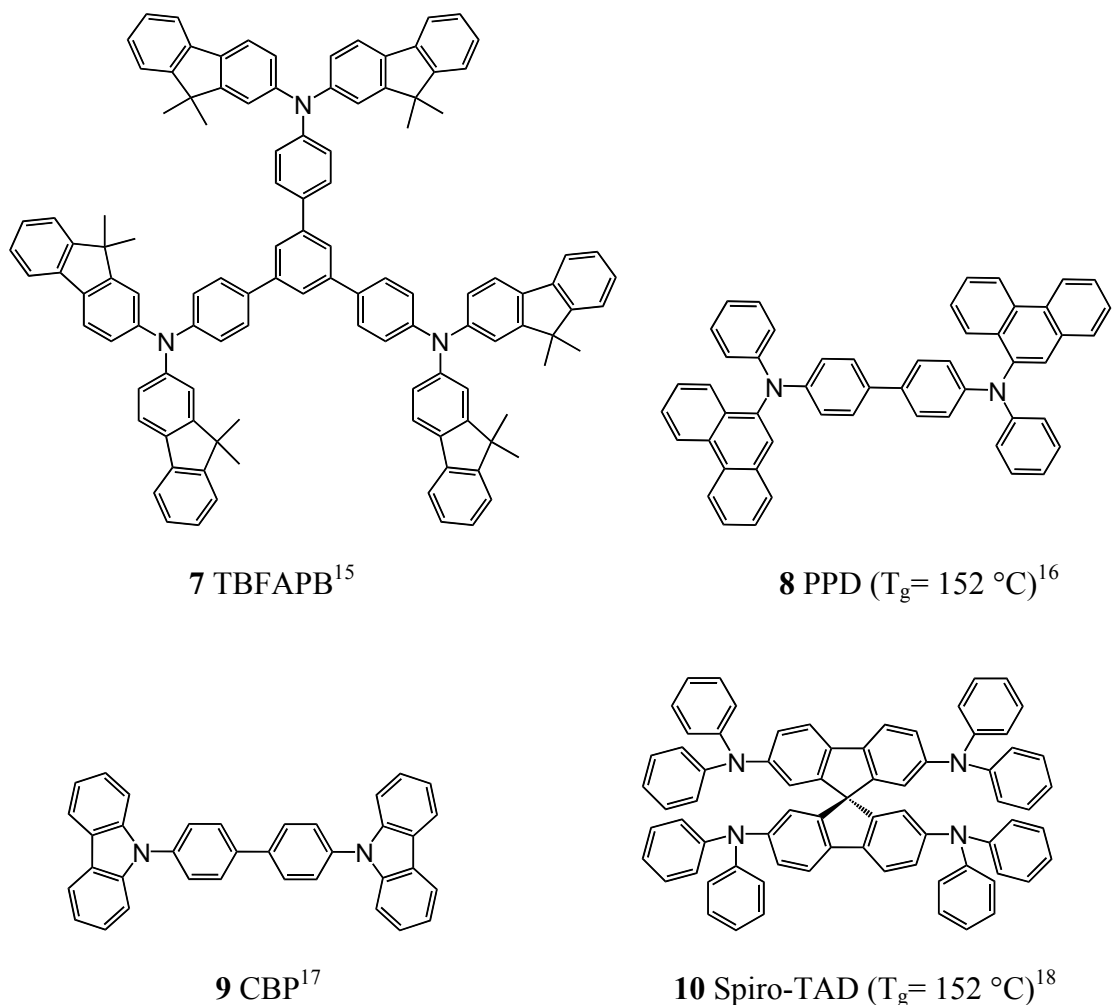
1 TCTA [4,4′,4″-Tri(*N*-carbazolyl)triphenylamine]

2 DCB [*N*-[4-(*N*-Carbazolylphenyl)]-4,7-bis(*N,N*- dicarbazolyl)carbazole]

3 *p*-DPA-TDAB [1,3,5-Tris[*N*-(4-diphenylaminophenyl)-phenylamino]benzene]

4-6 *o*-, *m*-, *p*-MTDAPB [1,3,5-Tris[4-(methylphenylphenyl-amino)phenyl]benzene]

7 TBFAPB [4,4′,4″-Tris[bis(9,9-dimethylfluoren-2-yl)amino]triphenylbenzene]

8 PPD [*N,N*′-Diphenyl-*N,N*′-bis(9-phenanthryl)4,4'-biphenyl]

9 CBP [4,4′-Di(*N*-carbazolyl)biphenyl]

10 Spiro-TAD [2,2′,7,7′-Tetrakis-(*N,N*-diphenylamino)-9,9′-spirobifluorene]

Figure 1.4. Structures of compounds **1-10**.

The hole-transporting and electron-blocking properties of **9** are commonly used in devices. Also, CBP has been used as host material to host phosphorescent emitters.[19]

1.4 Electron-Transporting Materials

For receiving electrons from the cathode, it is important for the LUMO level of the ET material to lie close to the work function of the cathode. A low lying HOMO level is also important for preventing escaped holes from reaching the cathode. The HOMO level of the ET materials must be lower than the emissive molecule. The greater the HOMO energy differences the better the hole-blocking ability. In addition, electron mobility, the ability to form reversibly stable anion radicals and stable homogenous thin films of HT materials are very important properties for improving device performance. A few families of ET materials have been developed, including oxadiazole, triazole and benzimidazole derivatives (see Figure 1.5).
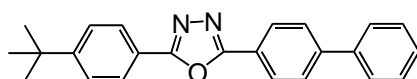
11 PBD[20]
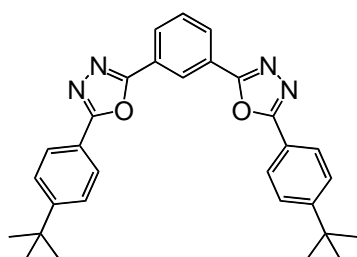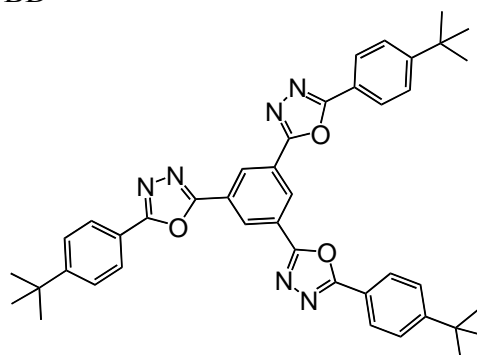
12 OXD-7[21]   **13** TPOB[22,23]
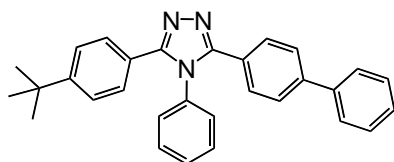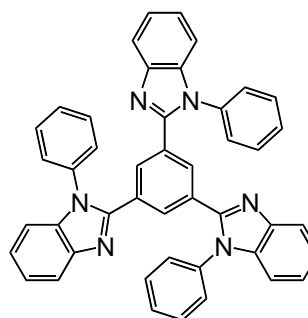
14 TAZ[24]   **15** TPBI[25]

11 PBD [2-(Biphenyl-4-yl)-5-(*tert*-butylphenyl)-1,3,4-oxadiazole]

12 OXD-7 [1,3-Bis[5-(*p-tert*-butylphenyl)-1,3,4-oxadiazol-2-yl]benzene]

13 TPOB [1,3,5-Tris(4-*tert*-butylphenyl-1,3,4-oxadiazolyl)benzene]

14 TAZ [3-(Biphenyl-4-yl)-4-phenyl-5-(4-*tert*-butylphenyl)-1,2,4-triazole]

15 TPBI [2,2′,2″-(1,3,5-Benzenetriyl)tris-[1-phenyl-1*H*-benzimidazole]]

Figure 1.5. Structures of compounds **11-15**.

Finding the right HOMO and LUMO levels for HT and ET materials for emitters is essential for well-performing devices. Moreover, HT and ET materials can also act as electron-blocking and hole-blocking materials, respectively.[10] OXD-7 and PBD have been widely studied in devices for their electron-transporting and hole blocking properties.[26]

1.5 Host Materials

A basic requirement of host materials is for them to have a higher triplet energy than the phosphorescent emitter in order to stop energy transfer from emitter to the host. Phosphorescent materials are doped in the host materials to allow for energy transfer from host to emitter with high efficiency.

Host materials are analogous to a combination of both hole-transporting and electron-transporting materials and act as media to facilitate the transfer of energy. At the same time, host materials should not quench the phosphorescent emission. The exciton binding energy and exchange energy (the singlet-triplet difference) are important for determining how easily energy can be transferred onto the phosphorescent emitter.[27]

Many high triplet energy materials have been developed to host phosphorescent materials. Carbazole derivatives are some of the most promising and popular candidates for hosting higher energy triplet emitters. Carbazole is commercially available, chemically and thermally stable and most importantly has a high triplet energy (3.0 eV).[28] In addition, carbazole is easy to functionalise.[29]

1.5.1 Small Molecules as Host

Brunner *et al.* have developed a series of carbazole-based host materials (see Figure 1.6).[30] The HOMO level and the triplet energy of these carbazole compounds are tuned by varying the position of substitution.

16 **17**

18 **19**

20 **21**
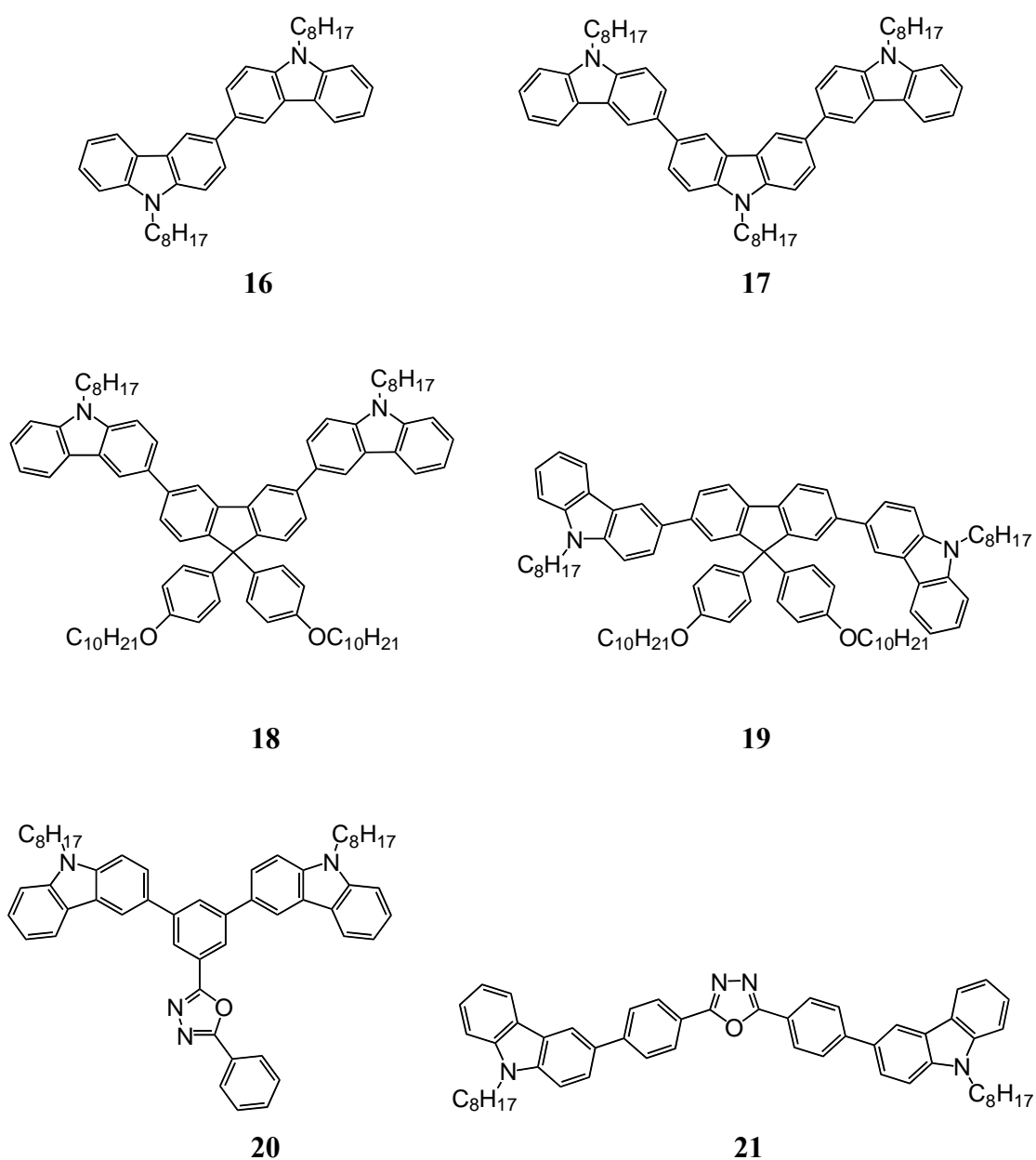
Figure 1.6. Structures of compounds **16-21**.

Fluorene and oxadiazole units are incorporated with carbazole units to balance the hole and the charge distribution due to their possession of electron-transporting properties. The HOMO levels and the triplet energies of these compounds are shown below (Table 1.1).

Table 1.1. The HOMO levels and the triplet energies of carbazole-based compounds.[30]

Compound	HOMO level (eV)	Triplet energy T_1 (eV)
16	-5.60	2.75
17	-5.57	2.73
18	-5.94	2.73
19	-5.80	2.38
20	-5.94	2.70
21	-5.94	2.44

The HOMO level and the triplet energy of the parent unsubstituted carbazole are -5.88 and 3.0 eV, respectively. Carbazole units are coupled *via meta* linkages to form dimer **16** and trimer **17**. The triplet energy of the dimer is considerably lower than the monomer but slightly higher than the trimer. It is suggested that the delocalisation of the triplet wavefunction between carbazole units does not extend significantly beyond two carbazole units.

Compound **18** has the same triplet energy as the trimer **17**. Also, the HOMO level is -0.37 eV lower which is due to the high ionisation potential of the fluorene unit. In contrast, the HOMO level of compound **19** is slightly higher than compound **18**, but the triplet energy is significantly lower than compound **18**. This is because of the greater π-conjugation resulting from 2/7 linkages. In addition, oxadiazole compounds **20** and **21** show similar trends to **18** and **19** respectively, which can be explained in the same way as the fluorene-based compounds.[30]

Recently, Wu *et al.* reported triphenylsilyl- and trityl-substituted carbazole-based host materials for blue electrophosphorescence (compounds **22-24**).[31] To achieve high triplet energies, they built these molecules *via* carbazole 3/6 linkages, which are the least conjugated positions. In addition, triphenylsilyl and trityl groups are non-conjugated (see Figure 1.7).

22 A= C, B= C
23 A= C, B= Si
24 A= Si, B= Si
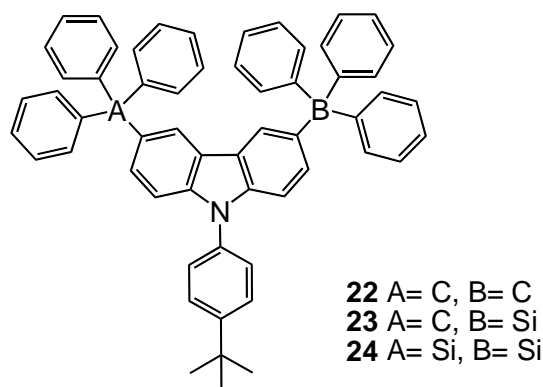
Figure 1.7. Structures of compounds **22-24**.

The triplet energies of compounds **22**, **23** and **24** are 2.97, 2.98 and 3.02 eV, respectively, which are very close to carbazole itself. Furthermore, the profiles of the phosphorescence spectra of **22-24** are very similar to carbazole. The HOMO levels of **22-24** are ca. -5.9 eV. In multi-layer devices, compounds **22**, **23** and **24** have external quantum efficiencies of 12.9%, 14.2% and 15.7%, respectively. In addition, high power efficiencies of 25.9, 25.0 and 26.7 lm/W have been obtained for these compounds.

In summary, decreasing the π-conjugation between aromatic units has been a successful method for obtaining high triplet energy hosts. However, the drawback is the resulting low HOMO level (ca. -5.9 eV) which leads to more energy being needed to inject holes into the HOMO orbital.

1.5.2 Bipolar Host Materials

Bipolar small host molecules have attracted considerable interest in recent years, due to their combined hole- and electron-transporting abilities. The drawback of bipolar materials is the compression of the band gap due to intramolecular charge transfer between the electron donating and the electron withdrawing moieties, which results in the lowering of the triplet energy. This problem can be solved by adjusting the π-conjugation between the electron donating and the electron withdrawing moieties.

Kido *et al.* have reported a highly efficient blue host material, **25**, with 24% external quantum efficiency and 46 lm/W power efficiency.[32] Subsequently, a highly

efficient green host material, **26**, was developed by Ma *et al.*, which has an external quantum efficiency for EL of 20.2%.[33]
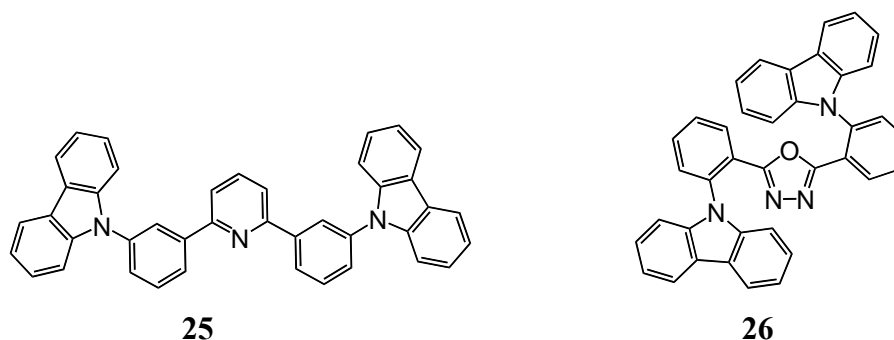
Figure 1.8. Structures of compounds **25** and **26**.

Compound **25** has a triplet energy of 2.71 eV which is higher than the iridium(III) bis(4,6-(difluorophenyl)pyridinato-N,C^2)picolinate complex (FIrpic)[34] which is a blue phosphorescent emitter (T_1= 2.62 eV). In theory, energy transfer from guest to host can be avoided. Another reason these materials have such good device performance is the well matched energy levels between the host materials and the hole- and the electron-transporting layers.

The way that the π-conjugation in compound **25** is interrupted to build the molecule *via meta* linkages. On the other hand, in compound **26**, twisting between the carbazole unit and the N-phenyl ring is capable of interrupting the π-conjugation. In the crystal structure of **26** (see Figure 1.9) this dihedral angle is 51.4°. Also, the authors claimed that the twist in the structure leads to the reduction of the π-conjugation between the carbazole and the oxadiazole moieties.
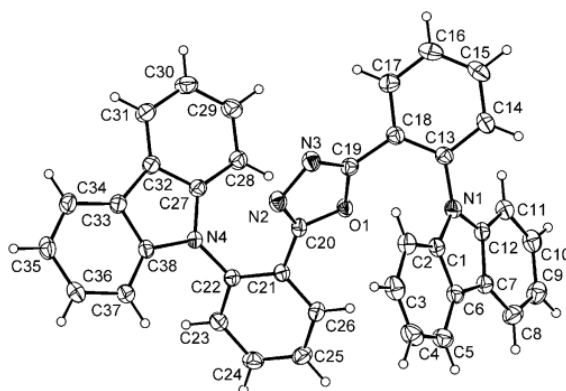
Figure 1.9. X-ray crystal structure of compound **26** (from ref. 33).

The triplet energy of compound **26** is 2.68 eV.[33] The HOMO and the LUMO energy levels are -5.55 eV and -2.56 eV, respectively. A direct comparison study with **26** and a CBP host (HOMO: -6.0 eV, LUMO: -2.9 eV) suggested that compound **26** is a better host than CBP.[17] The reason for this is that the HOMO energy level of molecule **26** is closer to that of the hole-transporting layer, 1,4-bis[(1-naphthylphenyl)amino]biphenyl NPB (HOMO: -5.4 eV).[35] In addition, compound **26** shows maximum external quantum efficiencies of 20.2% for green and 18.5% for deep red emitters.

Pyridine and oxadiazole compounds are good electron-transporting units, which have shown some promising results as components in host materials. However, what about other good ET materials? Novel host materials **27-30** with high triplet energy levels have been developed by Kim *et al.* (see Figure 1.10). These molecules, which have triplet energies from 2.8 to 3.0 eV, are based on carbazole and 1,2,4-triazole (TAZ) moieties.[36]

27   **28**

29   **30**
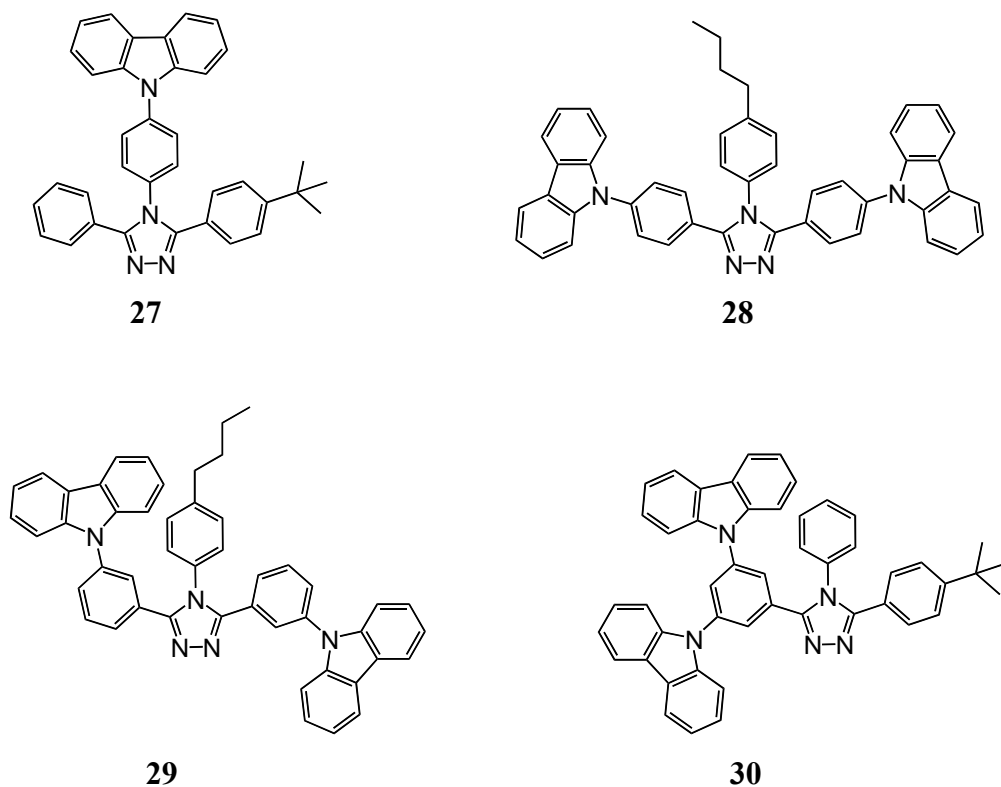
Figure 1.10. Structures of compounds **27-30**.

These molecules are linked through different positions. The HOMO-LUMO gaps of these molecules (from 3.49 to 3.59 eV) are similar to 9-phenylcarbazole which suggests there is no significant influence from changing the position of substitution. The maximum photometric efficiency of compound **30** in devices is 14.2 cd/A at a current density of 1.1 mA/cm^2.[36]

In conclusion, bipolar hosts have already shown some impressive results in terms of external quantum efficiency and power efficiency values. The HOMO level of bipolar hosts is closer than non-bipolar hosts to that of ITO. However, the negative effect of relatively low HOMO levels is the narrowing of the band gap which also means the lowering of the triplet energy of the host.

1.5.3 Polymeric Host Materials

A major problem for small molecule hosts is that ca. 95% of the materials are wasted during the vacuum deposition layering process, which is not acceptable for commercial production. Hence, polymeric hosts have come under the spotlight for development of future phosphorescent host materials, due to their ability to be processed from solution; polymeric light emitting diode (PLED) devices are prepared by either spin coating or inkjet printing. Poly(9-vinylcarbazole) (PVK) is the most commonly used polymeric host, with a triplet energy of 3.0 eV.[37] PVK is used to host blue phosphorescent materials. However, its poor electron-transporting ability and low lying HOMO level (ca. -5.9 eV) are the main issues preventing the production of high performance devices. For polymeric hosts, high triplet energies play a key role in devices. Also, it is important to have the HOMO and the LUMO levels close enough to the work functions of the electrodes, which leads to low energy barriers for injecting charges.

Van dijken *et al.* have reported a series of co-polymeric host materials (compounds **31-35**).[38] Biscarbazole is the main building block for these polymers which contain ET materials, such as oxadiazole and fluorine (see Figure 1.11).

31 (E_T= 2.29 eV)   **32** (E_T = 2.57 eV)

33 (E_T = 2.57 eV)   **34** (E_T = 2.29 eV)

35 (E_T = 2.57 eV)
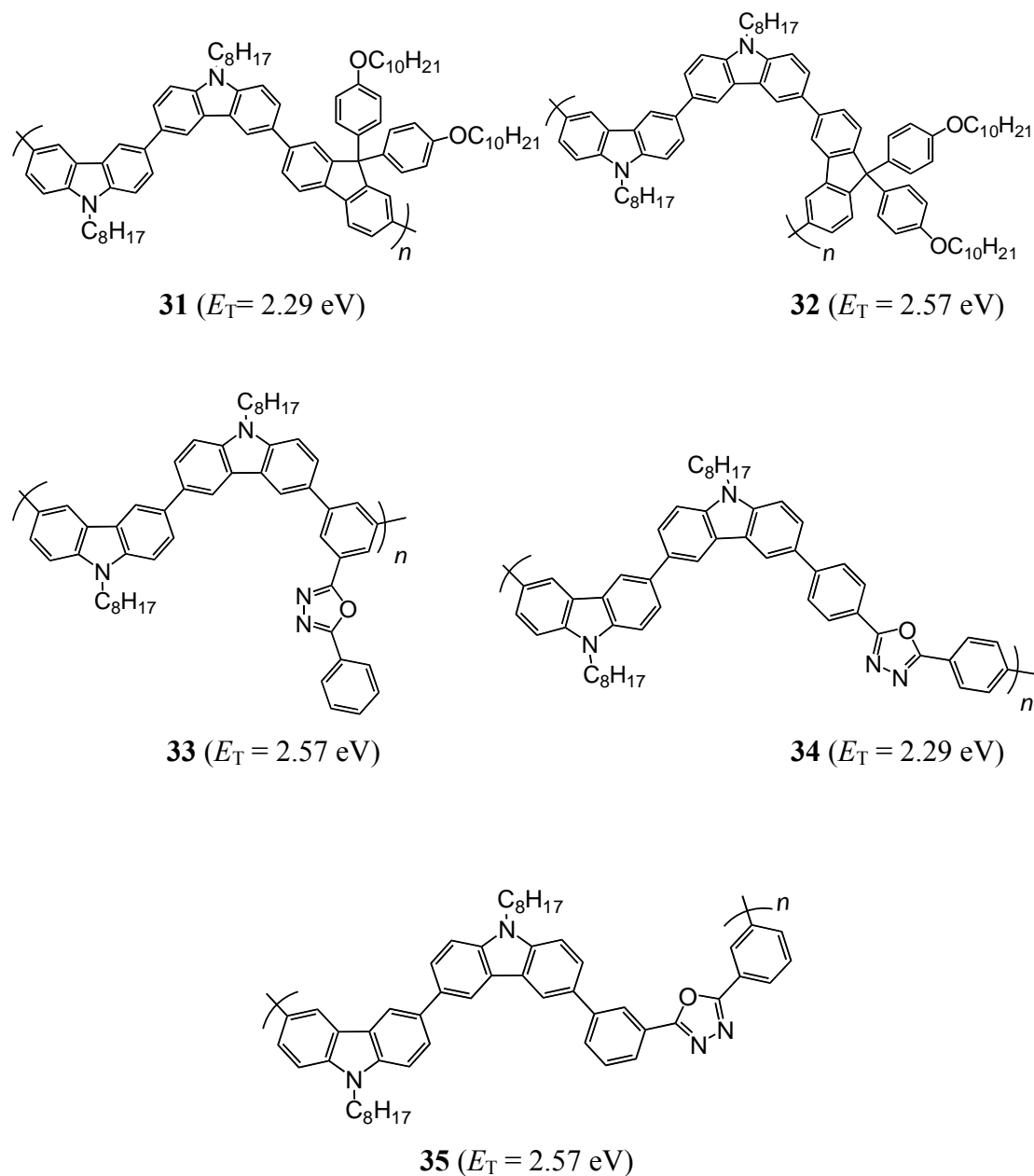
Figure 1.11. Structures of polymers **31-35**.

The half-wave oxidation potentials of these copolymers are ca. 0.74 V (versus Ag/AgCl in THF solvent). Biscarbazole units in copolymer **31** were substituted by mono-carbazole, leading to an increased half-wave oxidation potential of up to 0.94 V.

Poly(3,3'-carbazole) has a triplet energy of 2.60 eV. Copolymers **32**, **33** and **35** have triplet energies of around 2.57 eV, which are similar to the homo-carbazole polymer. As discussed above, in small molecules with carbazole units coupled *via* the 3,3'-positions, the delocalisation of the triplet wavefunction does not extend significantly beyond two carbazole units. The carbazole dimer has a triplet energy of 2.75 eV. However, the homo-carbazole polymer, with hundreds of carbazole units,

still has a triplet energy of 2.60 eV. Therefore, it can be concluded that the delocalisation of the triplet wavefunction ceases to increase after a certain number of repeating units is reached in the polymer. Copolymers **31** and **32** are engineered through different coupling positions, leading to a great impact on their triplet energies. The triplet energy of copolymer **31** is lowered from 2.57 to 2.29 eV, which is due to the greater π conjugation through the 2/7 linkages on fluorene. Furthermore, copolymers **33**, **35** and **34** obey the same rule as for **31** and **32**. Copolymers **33** and **35** are coupled *via* the *meta* positions on the diaryloxadiazole units. The triplet energies of copolymers **33** and **35** are the same, 2.57 eV. However, copolymer **34** which is coupled *via* the *para* position on the diaryloxadiazole units, has a lower triplet energy of 2.29 eV. Hence, the combination of biscarbazole and diaryloxadiazole follows the same rule as for **31** and **32**. Finally, carbazole-oxadiazole copolymers hosting green phosphorescent emitters show a high efficiency of 23 cd/A which does not change at high current densities and high luminance levels.[38]

Recently, Ma *et al.* have reported the tuning of the triplet energies of carbazole-oxadiazole copolymers by using different coupling positions. They built oxadiazole into the 9-position of carbazole rather than in the backbone. The triplet energy of copolymers made *via* 3/6, 3,6/2,7 and 2/7 linkage are 2.52, 2.42 and 2.32 eV, respectively. These can be explained by the greater π conjugation, which lowers the triplet energy. However, the maximum current efficiencies for these copolymer-based devices are 0.59, 1.33 and 1.67 cd/A, respectively.[39]

One of the main problems of carbazole-based polymers is the low triplet energy states. To achieve higher triplet energy hosts for blue electrophosphorescent materials, Brunner *et al.* introduced twisting effects between molecules. They located a methoxy group at the 2-position of carbazole and then coupled these units *via* the 3,3'-position to form the twisted biscarbazole derivative **36** (see Figure 1.12). Phosphorescence measurements have suggested that the triplet energy of **36** is 2.97 eV, which is 0.22 eV higher than biscarbazole **16** and just slightly lower than carbazole itself (3.0 eV). As a consequence, interrupting the conjugation between carbazole has a positive effect on increasing the triplet energy level of the molecule.

36 ($E_T = 2.97$ eV)　　　　　　　**37** ($E_T = 2.73$ eV)
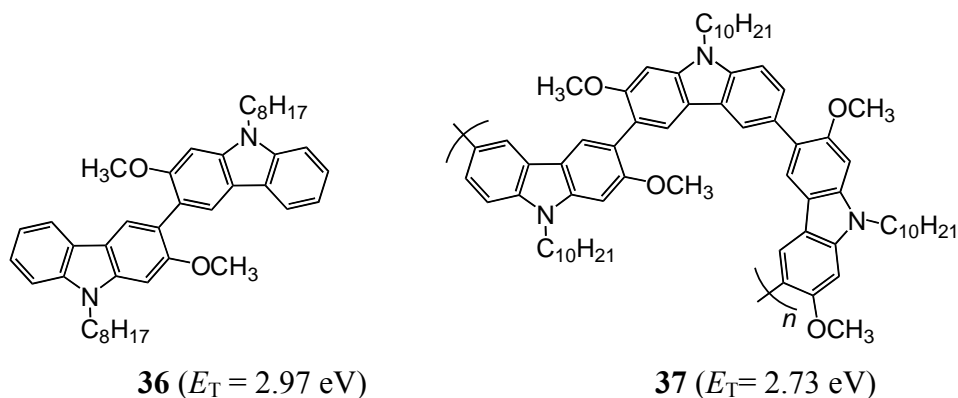
Figure 1.12. Structures of compound **36** and polymer **37**.

Similar twist-inducing carbazole units have also been incorporated into the backbone of polymer **37**. The triplet energy of **37** is 2.73 eV which is 0.13 eV higher than the homo-carbazole polymer. Furthermore, the half-wave oxidation potential of **37** (0.65 V) is 0.1 V higher than that of the homo-carbazole polymer (0.55 V versus Ag/AgCl in THF solvent).[40]

Recently, a wide band gap polymer **38** (Figure 1.13) has been developed by Fei *et al.*[41] and used as the host for iridium complexes; the maximum luminous efficiencies for green and blue devices were 27.6 and 3.4 cd/A, respectively.

38
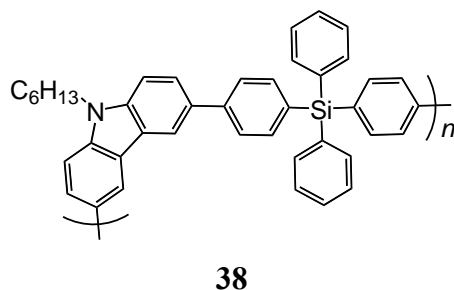
Figure 1.13. Structure of polymer **38**.

In summary, polymers have displayed great potential for hosting high energy phosphorescent emitters. Incorporating twist-inducing molecules into the polymer backbone leads to higher triplet energy levels which are suitable for hosting blue phosphorescent materials.

1.6 Phosphorescent Emitters

Heavy transition metal (ruthenium, osmium, platinum and iridium)[42-45] organometallic complexes have received intensive interest in photonic applications, due to their 100% theoretical efficiency by harvesting both singlet and triplet excitons.[46,47] In contrast, fluorescent molecules can utilise only the singlet excitons, leading to 25% theoretical maximum efficiency.[48] Cyclometalated Ir(III) complexes have gained special attention for optoelectronic applications, notably as dopants for harvesting the otherwise non-emissive triplet states formed in OLEDs. Furthermore, they have been widely used in optoelectronic applications because of their thermal stability, colour tuning ability and high external quantum efficiency in OLEDs.[49]

Organic transition-metal complexes with octahedral d^6-electronic configuration can overcome the selection rule due to the spin-orbit coupling mediated by the heavy metal core and mixed ^{3}MLCT/^{3}LC states. The Jablonski diagram shown in Figure 1.14 summarises the possible transition routes.
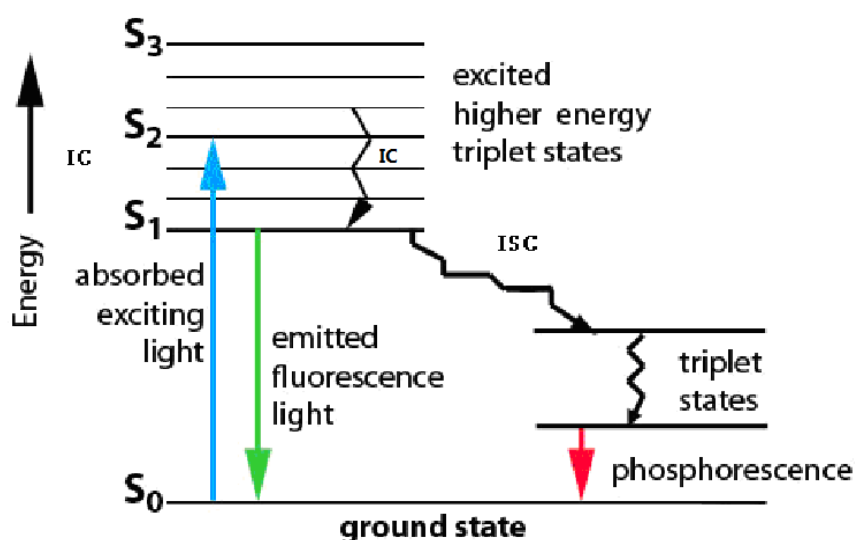
Figure 1.14. Jablonski diagram.[50]

1.6.1 Synthesis and Structure of Ir(*C^N*) Complexes

Two types of neutral Ir complexes have been widely studied. One is the homoleptic Ir(III) complex, in which the three chelating ligands are the same. The other is the heteroleptic Ir(III) complex, which has two chelating ligands the same and a different auxiliary ligand. Charged Ir(III) complexes will not be discussed here.

1.6.2 Homoleptic Ir(III) Complexes

Ir(III) tris-complexes with asymmetric chelated ligands can be of either a facial (*fac*) or a meridional (*mer*) configuration. The two isomers show differences in thermal stability and photophysical properties. For example, *fac*-isomers are more thermally stable than the corresponding *mer*-isomers at high temperature.[44] The structural difference between *fac*- and *mer*-isomers is the mode of ligand coordination. As shown in Figure 1.15, for *fac*-isomers, all three nitrogen atoms are parallel to the carbon atoms, leading to symmetric complexes. By contrast, two of the nitrogen atoms are parallel to each other in *mer*-isomers, which gives an asymmetric complex. In the ^{1}H NMR spectrum, the number of proton signals for a *fac*-Ir(III) complex is the same as the number of protons in the uncomplexed ligand. However, *mer*-isomers give more complicated spectra.[44] Usually the *fac*- and *mer*-isomers can be separated by thin layer chromatography, due to their different polarities.
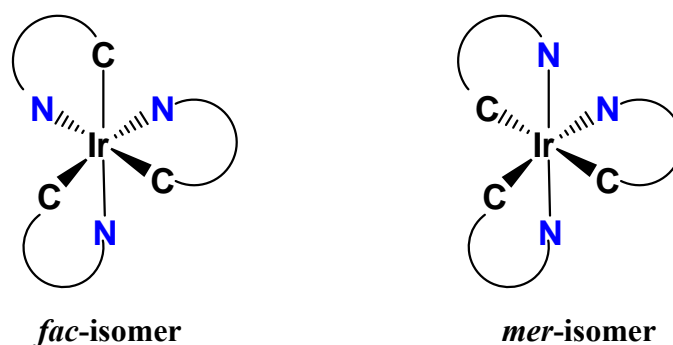
Figure 1.15. Structure of *fac*- and *mer*-isomers.

There are three synthetic pathways to obtain Ir(III) tris-complexes (see Scheme 1.1):

Method A:

$$Ir(acac)_3 \ + \ 3C\wedge NH \ \xrightarrow[\triangle]{glycerol} \ Ir(C\wedge N)_3 \ + \ 3acacH$$

Method B:

$$+ \ C\wedge NH \ \xrightarrow[\triangle]{glycerol} \ Ir(C\wedge N)_3 \ + \ acacH$$

Method C:

$$+ \ 2C\wedge NH \ \xrightarrow[\triangle]{glycerol,\ K_2CO_3} \ Ir(C\wedge N)_3 \ + \ 2KCl \ + \ H_2O \ + \ CO_2$$
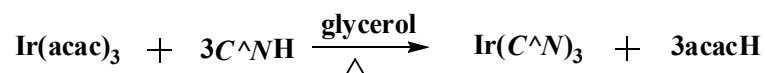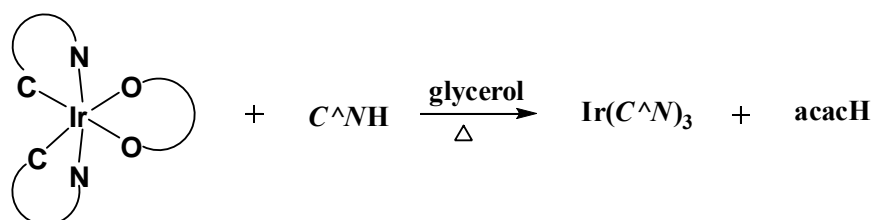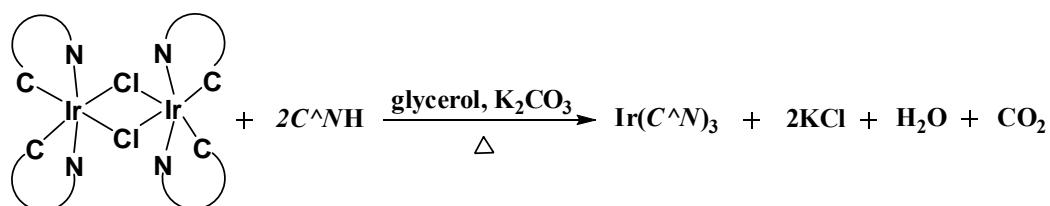
Scheme 1.1. Formation of homoleptic Ir(III) complex *via* different approaches.

Methods B and C have advantages over method A. Pre-cyclometalated Ir(III) complexes are easily synthesised under mild conditions in high yield.[34] Cyclometalated Ir(III) μ-chloro-bridged dimers (Method C) were first developed by Nonoyama, by refluxing $IrCl_3.xH_2O$ with 2-2.5 equiv of ligand in a 3:1 mixture of 2-ethoxyethanol and water. Meanwhile, simple purifications were applied and this is generally a high yielding process.[51]

Temperature is a key parameter to selectively form either the *fac-* or *mer-* isomer. *fac-*isomers are the thermodynamically favoured species. Therefore, when the reaction temperature is above 200 °C, the *fac-*isomer is the major product. On the other hand, *mer-*isomers are more kinetically favourable and their formation requires a lower temperature (below 150 °C). There are two approaches to convert *mer-* to *fac-*isomers, as shown in Scheme 1.2.

$$mer\text{-Ir}(C^\wedge N)_3 \xrightarrow[\text{heat or UV irradiation}]{\text{glycerol}} fac\text{-Ir}(C^\wedge N)_3$$
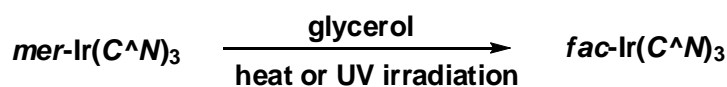
Scheme 1.2. Conversion of *mer*-isomer to *fac*-isomer

The *mer*-isomers normally have large nonradiative rate constants, which suggest that in the excited state, a bond rupture process may occur. The reason is that the Ir-C and Ir-N bonds in *mer*-isomers are normally longer than that in the *fac*-isomers. Karatsu *et al.* observed complete conversion from *mer*- to *fac*-isomer under UV irradiation for 200 min.[52]

1.6.3 Heteroleptic Ir(III) Complexes

Heteroleptic Ir(III) complexes can be synthesised by reacting the corresponding chloro-bridged dimer complexes with monodendate or bidentate ligands under relatively mild conditions.[53,54] An alcohol solvent (boiling point lower than 130 $^{\circ}$C), base and an auxiliary ligand are required for the reaction. The general procedure is shown in Scheme 1.3.
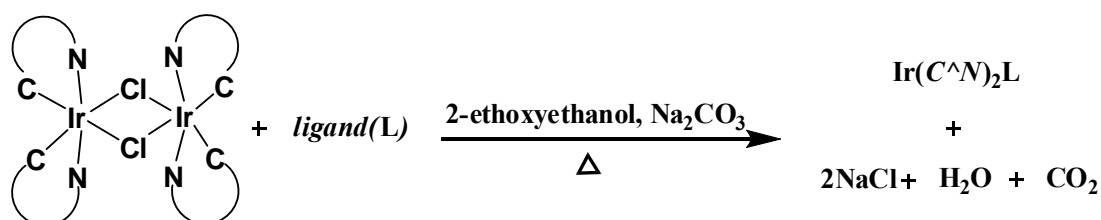
Scheme 1.3. Formation of heteroleptic Ir(III) complexes.

Unlike homoleptic Ir(III) complexes, the electro-optical properties of heteroleptic complexes can be easily modulated by changing the auxiliary ligand. Acetoacetonate (acac), picolinate (pic), 2,2′-Bipyridine (bpy), and their structural analogues, have been heavily investigated as an auxiliary ligand. Also, the purification of heteroleptic complexes is usually simpler, due to fewer side products being formed. Structural isomers for heteroleptic complexes are rare. Only a few isomerised complexes have been reported.[55]

1.6.4 Colour Tuning

Besides the high photoluminescence efficiencies and relatively short (µs range) phosphorescence lifetimes of Ir(III)-based complexes, their colour tuning ability is another great advantage. Covering the whole visible range of emission is necessary for full colour displays. Blue (450-480 nm), green (500-530 nm) and red (610-650 nm) are the primary colours. Ir(III) complexes have shown great potential in this respect for OLED applications. The complexes emission can be finely tuned by modifying ligands in the complexes.

1.6.5 2-Phenylpyridine Based Ligands

2-Phenylpyridine is the most popular parent ligand, since it is chemically stable and relatively easy to modify. *fac*-**Ir(ppy)₃** (ppy = 2-phenylpyridine) is the model complex for modification and comparison; it possesses a 97% PLQY and emits at λ_{max} 508 nm (green) at 298 K.[56] A considerable volume of work has been done on modifying the ppy ligand to tune the properties of derived complexes, especially, colour tuning. DFT calculations on Ir(ppy)₃ were employed to optimise the electronic structure. The basis set B3LYP was used. The HOMO and LUMO of Ir(ppy)₃ complex are shown in Figure 1.16.
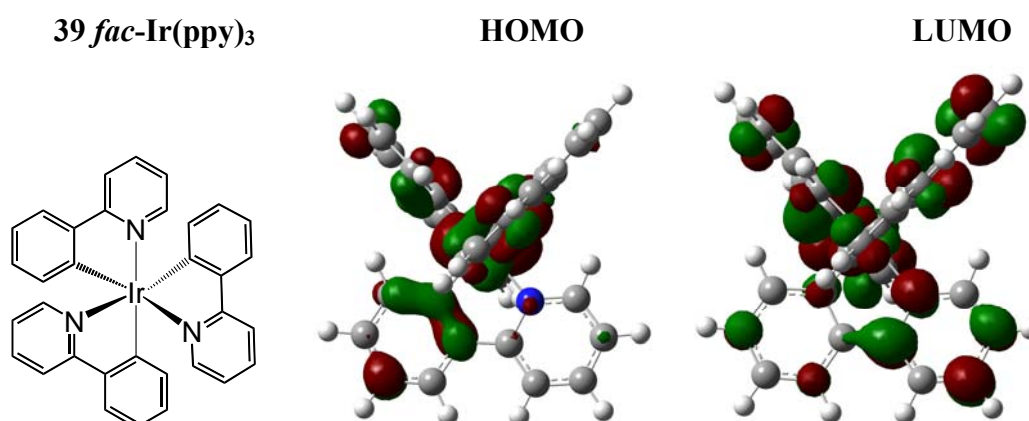
Figure 1.16. HOMO and LUMO orbitals of *fac*-Ir(ppy)₃ (N atoms shown in blue).

The emissive state is believed to be from a HOMO that is localised on the phenyl rings and iridium *d* orbitals, while the LUMO is located predominantly on the

pyridine rings. Approaches to tuning the emission colour by varying the HOMO and LUMO levels of Ir(ppy)$_3$ derivatives are shown below.

Blue shift the emission:

Approach 1: Destabilise the HOMO by attachment of electron withdrawing groups (see Figure 1.17)
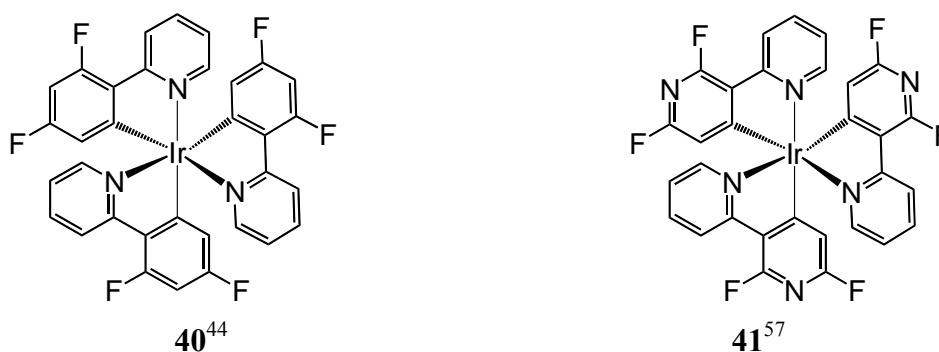
Figure 1.17. Structures of compounds **40** and **41**.

Approach 2: Destabilise the LUMO by attachment of electron donating groups (see Figure 1.18)
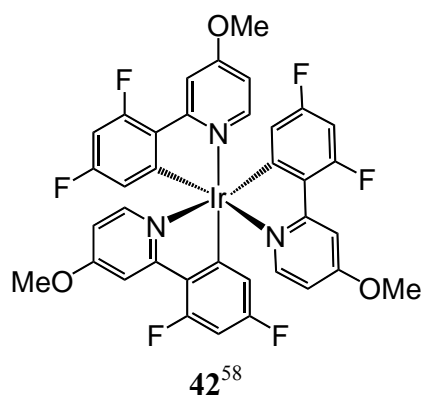
Figure 1.18. Structure of compound **42**.

Approach 3: Incorporate strong σ-donating ligands to stabilise the iridium core (see Figure 1.19)

43[59]
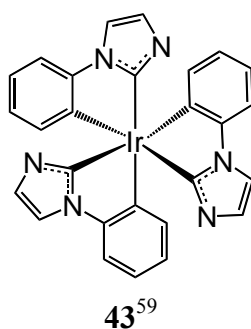
Figure 1.19. Structure of compound **43**.

Red shift the emission:

Approach 4: Stabilise the HOMO by attachment of electron donating groups (see Figure 1.20)

44[60]
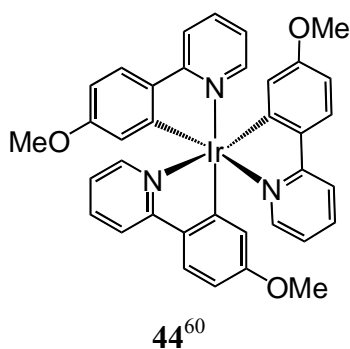
Figure 1.20. Structure of compound **44**.

Approach 5: Extend the π-conjugation on the units which have the major effect on either the HOMO or LUMO levels (see Figure 1.21)
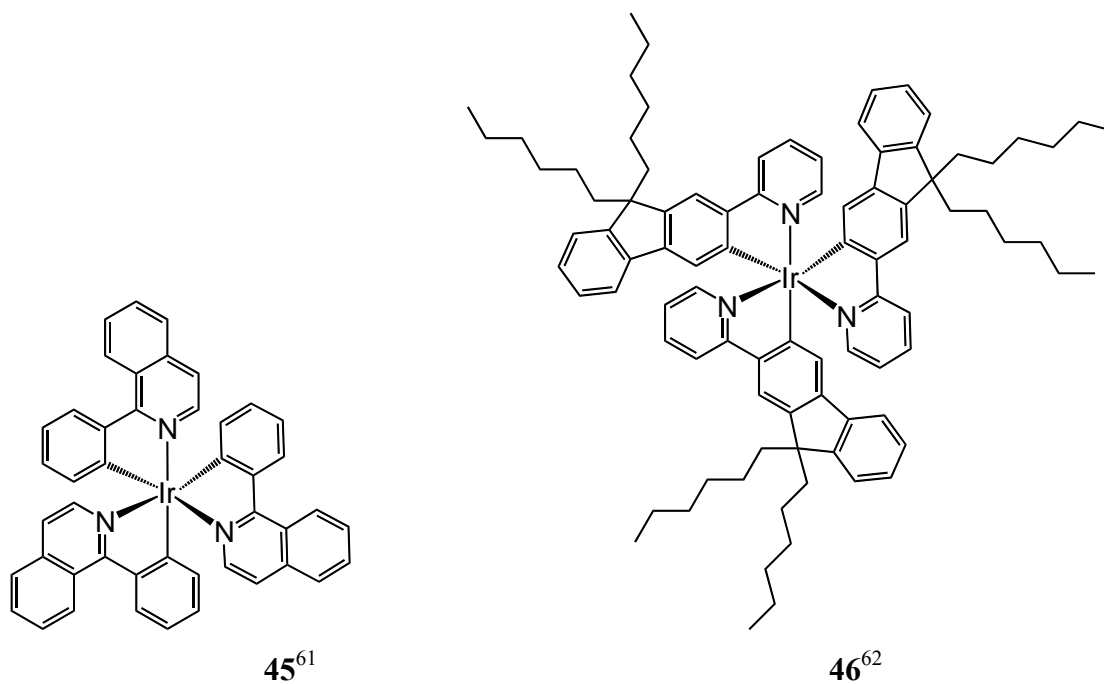
Figure 1.21. Structures of compounds **45** and **46**.

Approach 6: Stabilise the LUMO by attachment of electron withdrawing groups (see Figure 1.22)
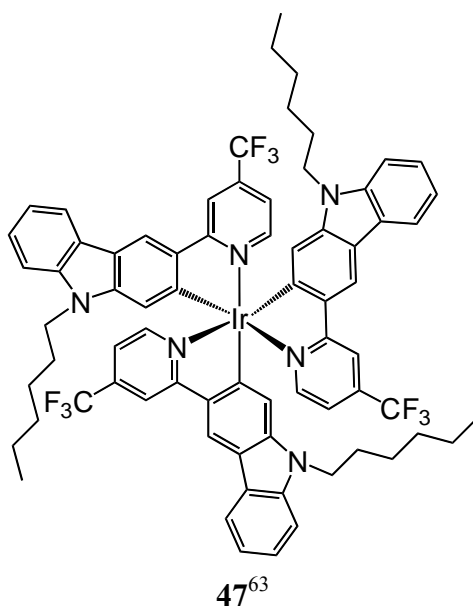
Figure 1.22. Structure of compound **47**.

Table 1.2. Photophysical studies on the *fac*-isomer of complexes.

Complex	Emission (nm) at 298 K	Quantum yields (Φ_f)	Lifetime (μs)
Ir(ppy)$_3$[b]	508	0.97	1.6
[a]40[44]	468	0.43	1.6
[b]41[57]	438	0.71	-
[b]42[58]	471	0.95	0.74
[b]43[59]	380	0.02	0.4
[d,e]44[60]	539	-	2.86
[b]45[61]	558	-	-
[c]46[62]	620	0.26	0.74
[c]47[63]	652	0.19	0.74

298 K emission and lifetime measurements were carried out in [a]2-methyltetrahydrofuran, [b]CH$_2$Cl$_2$, [c]toluene, [d]ethanol/methanol and [e]MeCN

The emission of complexes **Ir(ppy)$_3$**, **40** and **41** (Table 1.2) is remarkably shifted from 508 to 438 nm by introducing electron withdrawing groups on the HOMO level. However, the emission of complex **42** did not change as expected. In theory, introducing the electron donating groups on the pyridine ring should destabilise the LUMO level, and lead to a bigger HOMO-LUMO gap. However, it was found that adding extra electron donating groups on the LUMO level has limited effect. In addition, using strong σ-donating ligands, such as carbene in an Ir(III) complex has a huge potential to blue shift the emission, although, the quantum yield of complex **43** is very low, 2% only.

Red shifting the complex emission has been demonstrated with complexes **44** to **47**. Among the different approaches, extending the π-conjugation on either HOMO or LUMO side has proved to be the most effective approach (shift >100 nm).

The emission of heteroleptic complexes can be tuned by the same approaches as homoleptic complexes. Additionally, it can also be achieved by using different ancillary ligands. Electron deficient ancillary ligands blue shift the emission, while

electron rich ancillary ligands (like acetylacetonate) red shift the emission. Selected examples are shown below to illustrate this effect.

Blue shift the emission by electron deficient ancillary ligands (see Figure 1.23):

48 FIrpic (470, 494 nm)[53]   **49** (459, 489 nm)[54]

50 (460, 489 nm)[54]
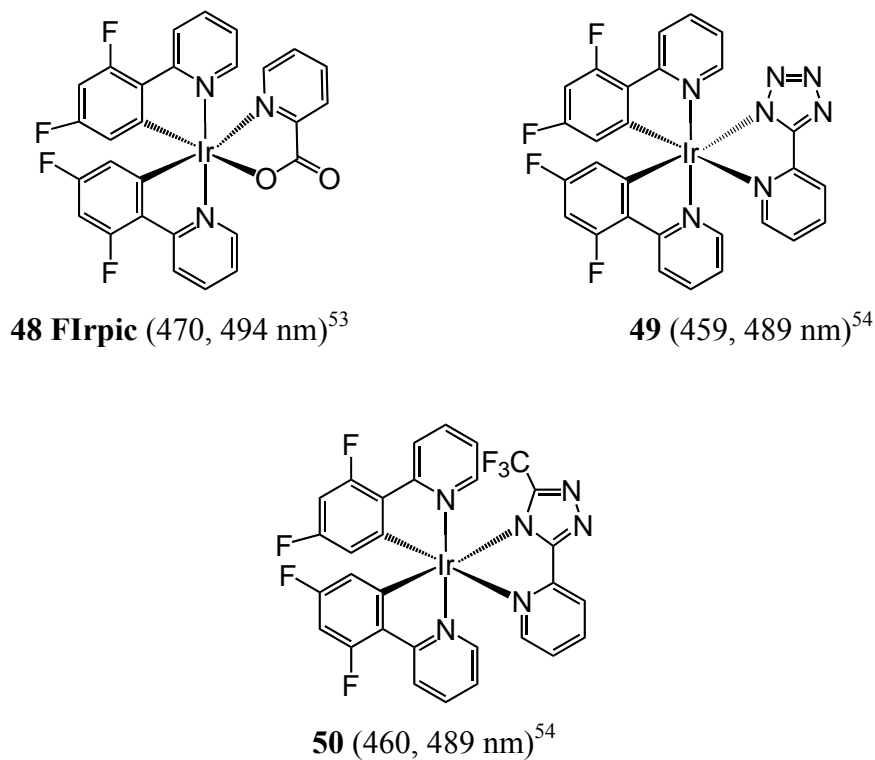
Figure 1.23. Structures of compounds **48-50**. Emission measurements at 298 K were carried out in CH$_2$Cl$_2$.

Red shift the emission by electron rich ancillary ligands (see Figure 1.24):

51 (528 nm)[53]   **52** (488 nm)[53]
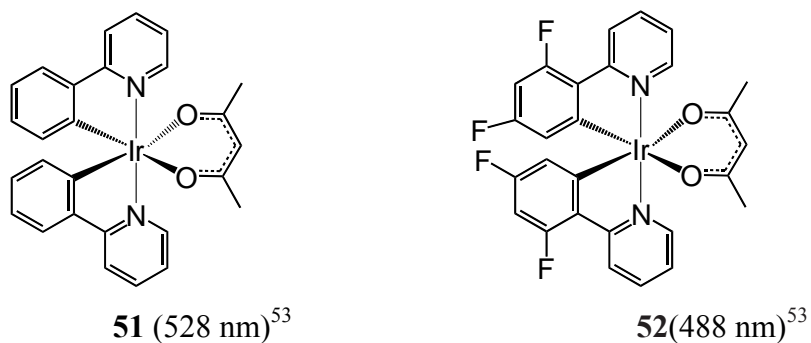
Figure 1.24. Structures of compounds **51** and **52**. Emission measurements at 298 K were carried out in CH$_2$Cl$_2$.

1.6.6 Multi-Hetetroatom Ligands

In the search for new iridium complexes with balanced charge transport and colour tuning in OLEDs, multi-heteroatom ligands have also been exploited, such as 1,3,4-oxadiazole (**53**), triazole (**54**) and pyrazole (**55**) derivatives (see Figure 1.25). These complexes have interesting properties. For example, complex **54** is a highly efficient deep blue emitter and complex **55** has the dual phosphorescent feature. However, compared to phenylpyridine based complexes, the properties of multi-heteroatom complexes are less predictable and more difficult to modify.

53[64]   **54**[65]   **55**[66]
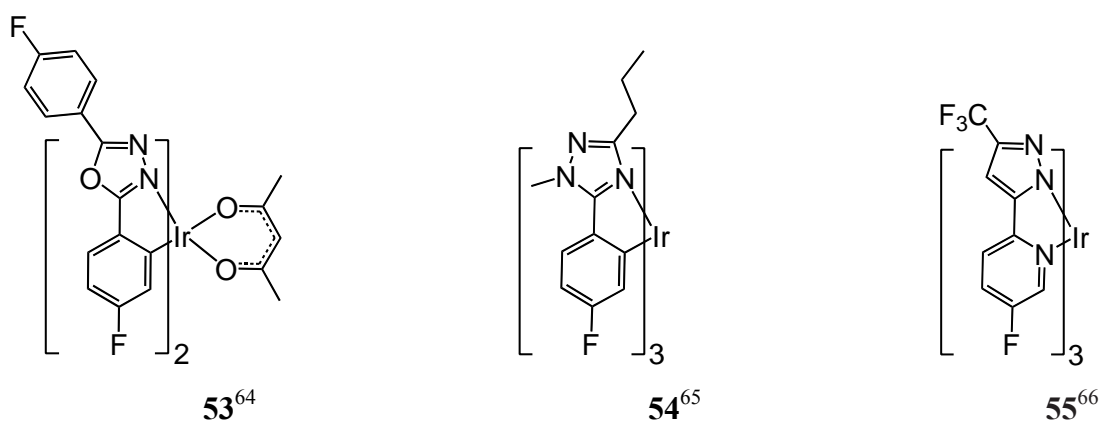
Figure 1.25. Structures of compounds **43-55**.

1.7 Conclusions

OLEDs materials have received intensive interest from both academic and industry based research in recent years due to the fundamental scientific challenges and their potential applications. Displays and lighting panels are now commercially available. However, long lifetime, stable and low cost OLED devices still remain a great challenge in materials and engineering science. In this chapter, recent progress in several contemporary topics in OLED research has been reviewed, including the use of nitrogen-contain small molecules as HT materials, ET materials, host materials and iridium complexes.

Chapter 2 – Ambipolar Molecules with High Triplet Energies: Synthesis, Structural and Optoelectronic Properties

2.1 Introduction

Energy transfer processes[67] in functional π-systems are of fundamental interest and of relevance to applied research. Controlling energy transfer is a central concept in the design of materials for the emerging technologies of molecular electronics[68] and optoelectronic devices,[69] including photovoltaic cells[70] and OLEDs.[71] Numerous families of small molecules[72] and polymers have been studied with the aims of optimising the extent of π-conjugation, the energies of singlet and triplet excited states, energy transfer processes and subsequent decay pathways that mediate electronic communication. For example, interchromophore separation,[73] *meta* versus *para* phenyl substitution[74,75] in the backbone, and molecular twisting controlled by steric effects[19] have all been exploited to chemically tailor the energy levels and the optoelectronic properties of conjugated π-systems.

Ambipolar molecules, with the propensity to accept and transport both holes and electrons, are attractive candidates for optoelectronic studies.[76-78] In the OLED field, a major drawback of ambipolar materials is the compression of the HOMO-LUMO gap due to intramolecular charge transfer (ICT) between the electron donating (D) and the electron accepting (A) moieties. This results in lowering of the singlet and triplet energies[38] which, in turn, leads to back-transfer of energy from the guest to the host thereby reducing the device efficiency. It is a significant challenge, therefore, to obtain a high triplet energy state in an ambipolar system.

Our approach, which is described in this Chapter, has been to systematically modulate the π-conjugation within an ambipolar system by means of steric effects and to probe the structure-property relationships in the resulting series of compounds. For this study we chose carbazole as the electron donor moiety. Carbazole (Cz) is a popular component of optoelectronic materials:[79-81] it is commercially widely available, chemically and thermally stable, has a high triplet energy (3.05 eV)[28] and

29

demonstrates good hole-transporting ability. For example, **9** (CBP) is a conventional host material for phosphorescent emitters.[82] The shortcomings of CBP are a low triplet energy (2.56 eV),[83] unbalanced injection of holes and electrons, and the presence in CBP films of low energy triplet traps which further reduce the emission from the dopant. By combining carbazole with electron-transporting moieties, such as 2,5-Diaryl-1,3,4-oxadiazoles (OXDs) derivatives, balanced injection and transport of holes and electrons can be achieved. For example, **12** (OXD-7) has found widespread use as electron-transporting materials. However, both **11** (PBD) and OXD-7 have low triplet energies (2.5 and 2.7 eV, respectively).[84,85] In order to achieve high triplet energy in an ambipolar host, both the hole and electron-transporting fragments should possess high triplet energy.

The original concept of utilising carbazole and diaryloxadiaozle as a bipolar host was developed by Ma *et al*.[33] The aim of their work was to interrupt the π-conjugation between carbazole and diaryloxadiazole units. They claimed that the twist in the structure is the reason for the reduction of the π-conjugation between carbazole and oxadiazole moieties which leads to the high triplet energy for the molecule (the crystal structure of **26** is shown in Figure 1.9 in Chapter 1). However, we do not totally agree with them. From their crystal structure, the aryloxadiazole unit was twisted. The phenyl and the oxadiazole rings were no longer in the same plane. They did not comment on this point. Furthermore, the conjugation between the carbazole and aryloxadiazole unit is poor due to coupling *via* C-N linkages. Hence, our proposal is that the reduction of the π-conjugation between the phenyl and oxadiazole rings is more important than between the carbazole and adjacent phenyl ring. Therefore, we attempted to vary the triplet energy of diaryloxadiazole moieties by introducing steric effects.

OXDs derivatives, which were first synthesised in 1955.[86] Syntheses of OXDs use cheap, available materials and generally proceed in high yields. The reactions to form the heterocycle are an elimination-cyclisation sequence. There are two general routes to synthesise OXDs derivatives which involve either hydrazide or tetrazole precursors (Scheme 2.1). Route 1 is to react a hydrazide with an acid chloride in basic solution (such as pyridine) to form OXDs. Meanwhile, hydrazides can be easily obtained from acid chlorides, carboxylic acids and esters, which are commercially available. The intermediate diacyl hydrazine, is then converted to the oxadiazole by

refluxing in a dehydrating solvent such as thionyl chloride ($SOCl_2$) or phosphorus oxychloride ($POCl_3$).[87] On the other hand, the second route using tetrazoles was developed by Huisgen in 1960.[88] Tetrazoles are easily synthesised from cyano precursors. This step is high yielding and isolation of the product is straightforward. Then, an acid chloride reacts with the tetrazole to form the desired oxadiazole compound.
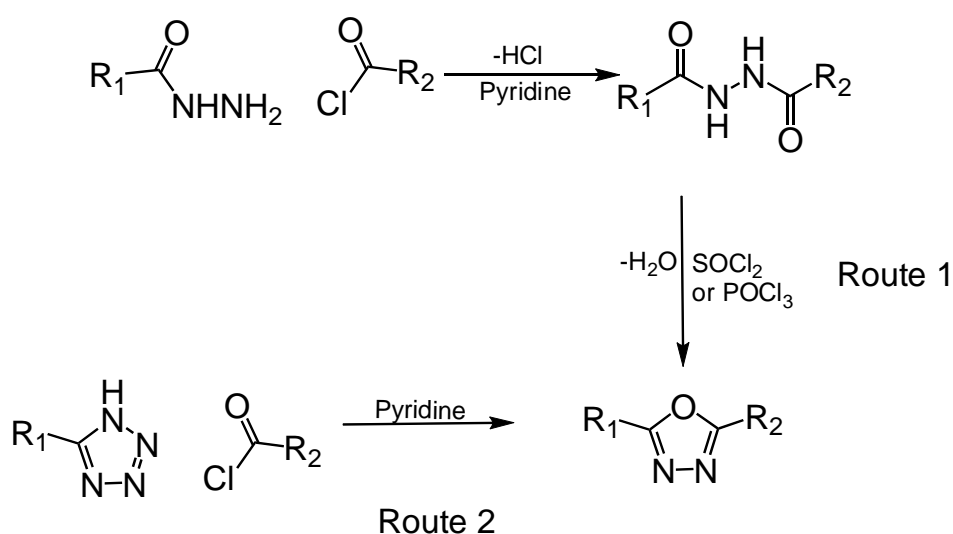
Scheme 2.1. Hydrazide and tetrazole routes to 1,3,4-oxadiazole derivatives
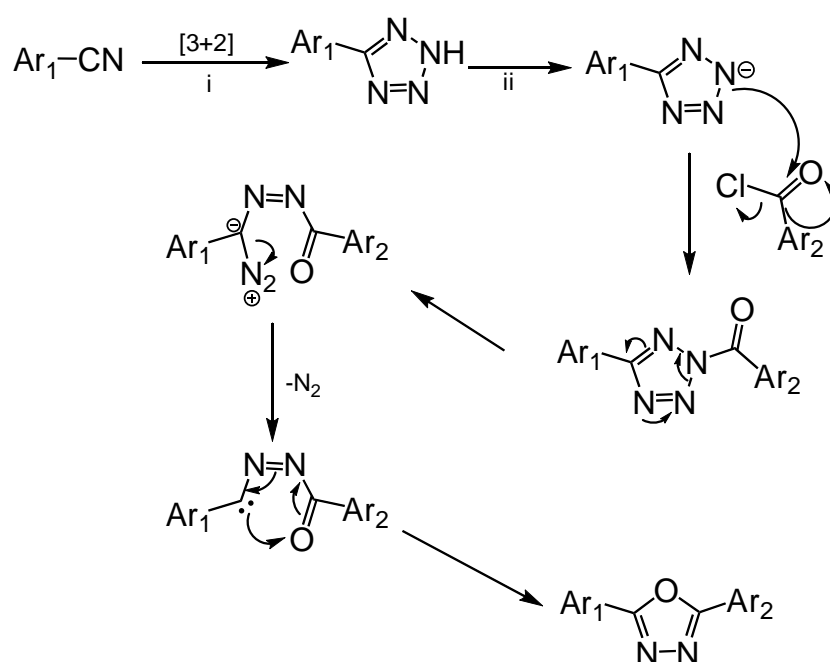
Scheme 2.2. The mechanism of synthesising OXDs *via* tetrazole precursors Reagents and conditions: i: NH_4Cl, NaN_3, DMF, 105 °C, ii: pyridine, reflux.

Tetrazole formation involves [3+2] cycloaddition of azide to a cyano group. This is followed by deprotonation of the tetrazole NH group and attack of the resulting anion on an acid chloride. Rearrangements with N_2 as a leaving group drive cyclisation to form the oxadiazole as shown in Scheme 2.2.[88]

The focus of the current work is the rational design, synthesis and photophysics of a new series of fluorescent Cz-OXD dyad molecules **71-81** in which the topology and electronic properties are systematically varied by chemical modification. Cyclic voltammetric data, HOMO-LUMO calculations, and X-ray crystallographic analyses are also presented. Our Cz-OXD dyads are structurally different from those reported by Thomas *et al.*[89], Ma *et al.*[33] and Guan *et al.*[90] Furthermore, these authors did not report systematic variations to probe structure/property relationships. Our study demonstrates a strategy for precisely tuning the singlet and triplet levels in ambipolar molecules.

2.2 Results and Discussion

2.2.1 Syntheses of Carbazole-Oxadiazole Ambipolar Compounds

The torsion angles in the Cz-OXD systems were systematically varied by alkyl substitution on one, or both, of the aryl rings of the OXDs portion of the molecules **71-81**. Schemes 2.3 outlines the routes used for their synthesis. Benzonitrile derivatives **56** and **57** were converted into **58**[91] and **59**, which were reacted with benzoyl chloride derivatives **60-63** in refluxing pyridine to afford **64-70**. In the final step, S_NAr reactions[33] of carbazole or 2,7-dimethoxycarbazole at the C-F bond of **64-70** gave **71-79**. Comparable reactions of **82** gave **80** and **81** (Scheme 2.4). All reactions proceeded in moderate or high yields. The structures of the 11 compounds studied in this work are shown in Figure 2.1.
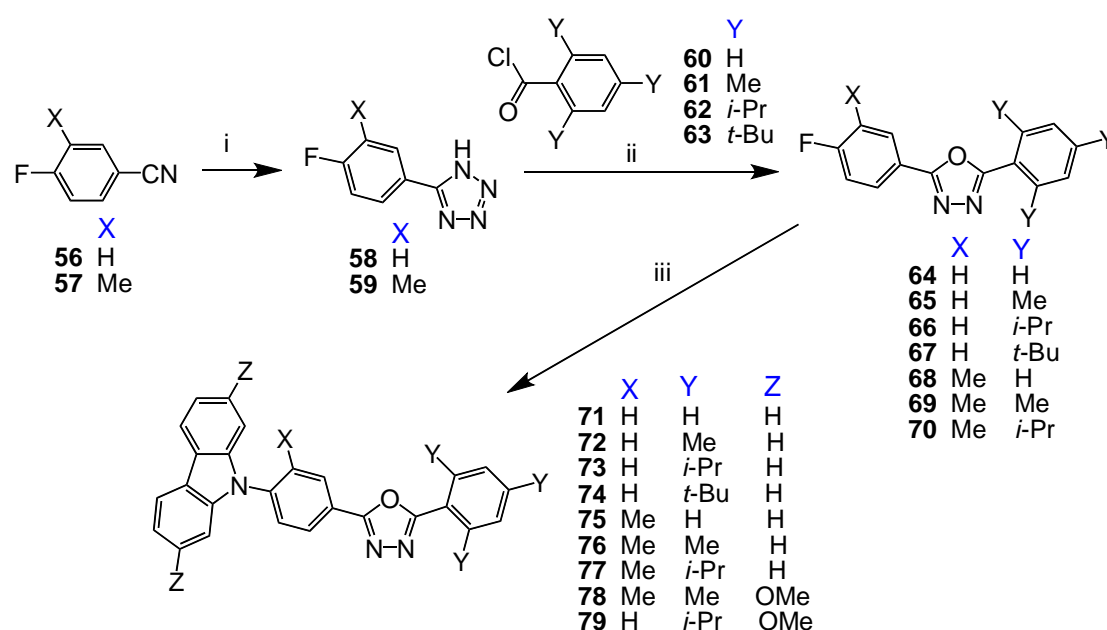
Scheme 2.3. Synthetic route to **71-79**: i: NH₄Cl, NaN₃, DMF, 105 °C (66-78% yields), ii: **60-63**, pyridine, reflux (47-85% yields), iii: carbazole or 2,7-dimethoxycarbazole, K₂CO₃, DMSO, 150 °C (45-60% yields).
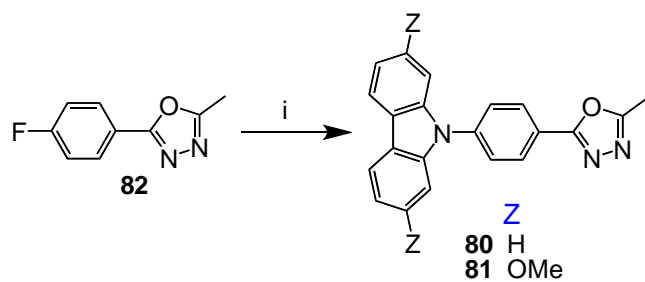
Scheme 2.4. Synthetic route to **80-81**: i: carbazole or 2,7-dimethoxycarbazole, K_2CO_3, DMSO, 150 °C (61-73% yields)

71

72

73

74

75

76

77

78

79   **80**   **81**
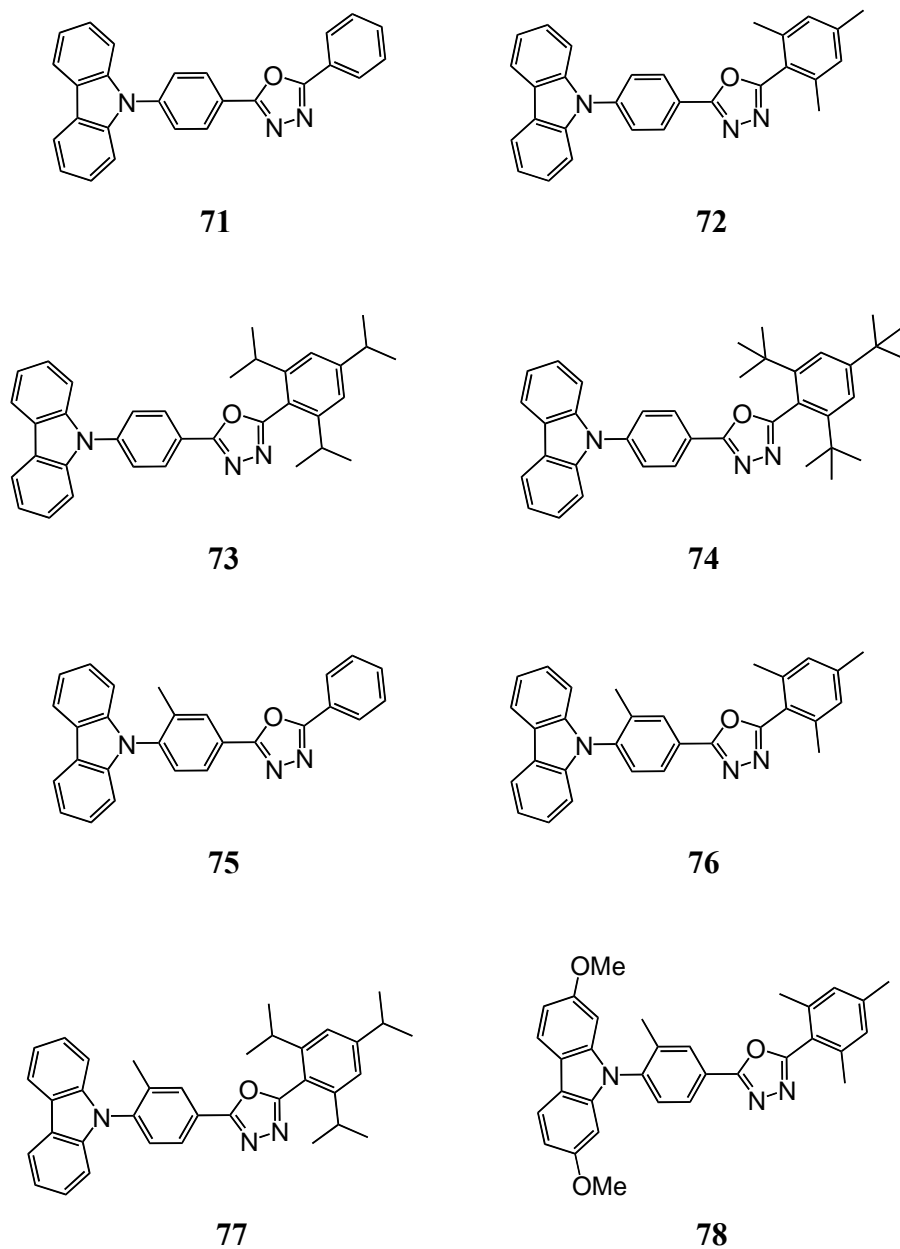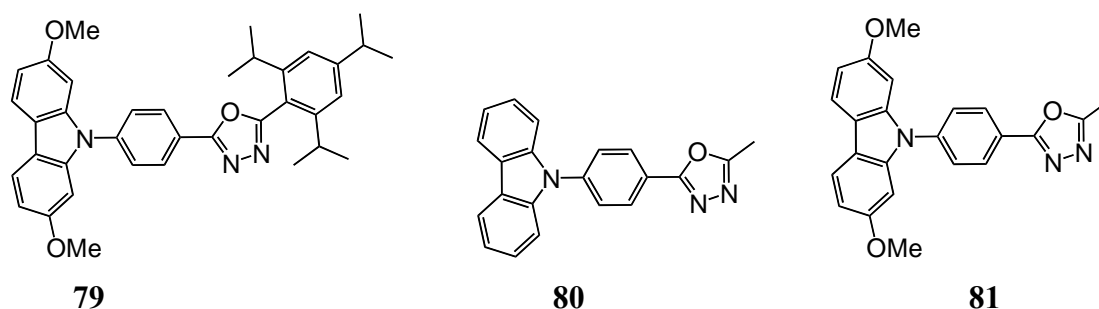
Figure 2.1. Structures of compounds **71-81**.

2.2.2 X-ray Crystal Structures

Single-crystal X-ray diffraction studies were performed by Dr Andrei Batsanov on **73**, **74, 77** and **80** to probe the effects of substitution on the inter-ring twist angles (see Figure 2.2 for **77**). The twist angle between the essentially planar carbazole group (i) and the benzene ring (ii) is similar in **73** (53.8º), **74** (58.3º) and **80** (54.1º), whereas in **77** it widens to 82.2º due to the methyl substituent at ring ii. The twist between the oxadiazole ring (iii) and benzene ring (iv) is also large due to bulky *peri*-substituents at the latter; it is somewhat larger in the *tert*-butyl substituted **74** (86.3º) than in *iso*-propyl-substituted **73** (77.4º) and **77** (78.5º). The twist between rings ii and iii varies erratically, viz. 4.3º in **73**, 22.5º in **74**, 11.8º in **77** and 1.6º in **80**, probably due to packing effects. A search of the May 2010 issue of the CSD[92] revealed 121 organic structures with 235 unique oxadiazolyl-phenyl links without *peri*-substituents at the phenyl ring or other important steric hindrances; the twist angle ranges from 0 to 31º with the average of 8º. In these cases, this twist is not big enough to prevent conjugation, unlike the new systems described herein.
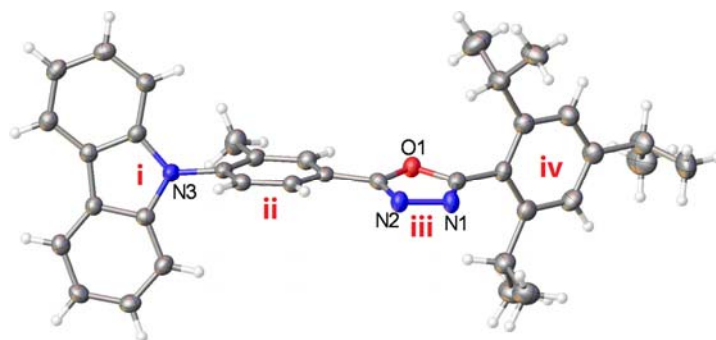
Figure 2.2. X-ray molecular structure of **77**, showing thermal ellipsoids of 50% probability. Twist angles (º): i/ii 82.2; ii/iii 10.0; iii/iv 78.5.

2.2.3 Theoretical Studies

To explore the HOMO-LUMO levels and minimum energy conformations of the molecules, the geometrical and electronic properties of compound **71-81** were performed with the Gaussian 03 program package. The calculation was optimised by means of the B3LYP (Becke three parameters hybrid functional with Lee-Yang-Perdew correlation functionals) with the 6-31G(d) atomic basis set 32. Molecular orbitals were visualised using Gaussview (see Figure 2.3, 2.4 and 2.5). The ring notation used in the section, is shown in Figure 2.2.

HOMO   **LUMO**

71

72

73

74

80
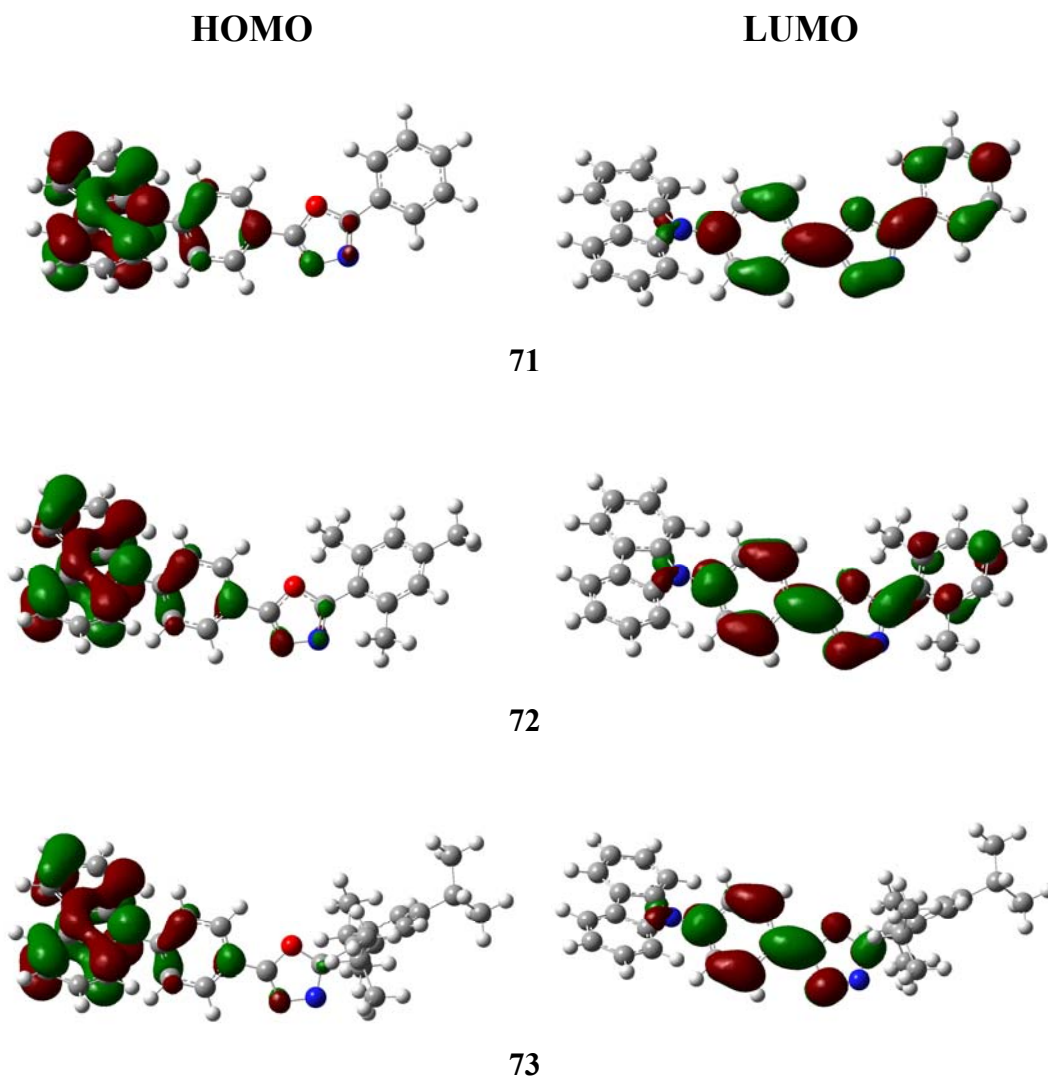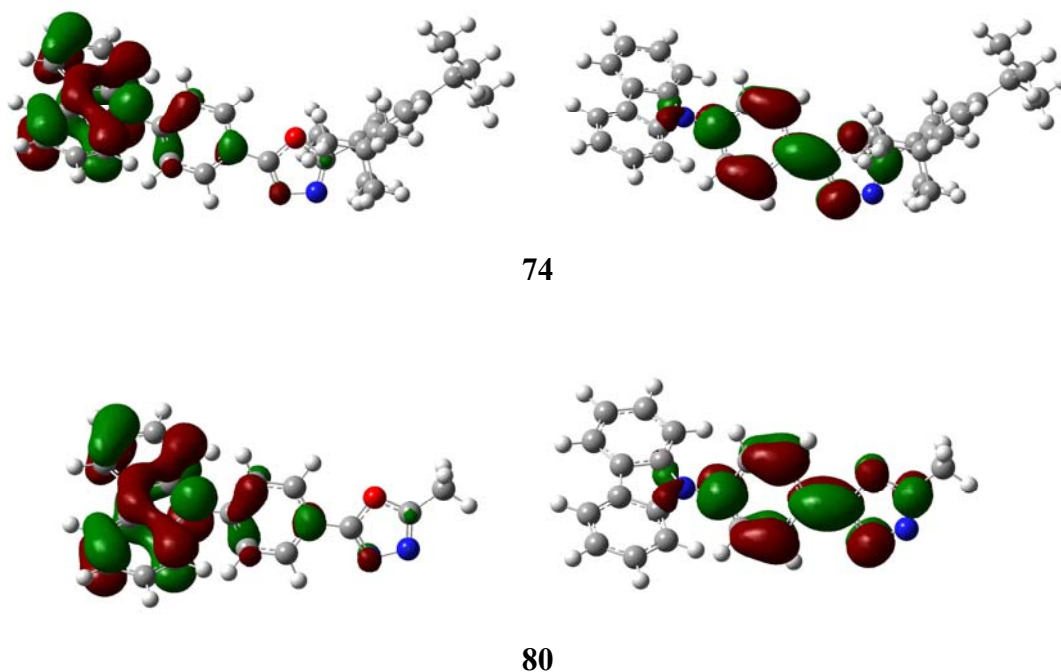
Figure 2.3. HOMO-LUMO maps of compound **71-74** and **80**. (N atoms shown in blue. Oxygen atoms shown in red).

The HOMO orbital distribution in compounds from **71-74** and **80** is rather similar, and mainly located on the carbazole moiety. Less than 5% of the HOMO electron density is located on the diaryloxadiazole moiety. Hence, these compounds have similar HOMO energy levels (ca. -5.48 eV). On the other hand, the majority of the LUMO orbital is on the diaryoxadiazole. The LUMO electronic density on the end phenyl unit decreases from **71** to **74**, due to a reduction of the π-conjugation within the oxadiazole moieties. Hence, the LUMO levels of **71** to **74** increase from -1.77 to -1.51 eV. Moreover, **74** and **80** have very similar HOMO-LUMO distributions and energy levels, which suggest that the sterically bulky groups break the conjugation between rings iii and iv.

HOMO   **LUMO**

76

77
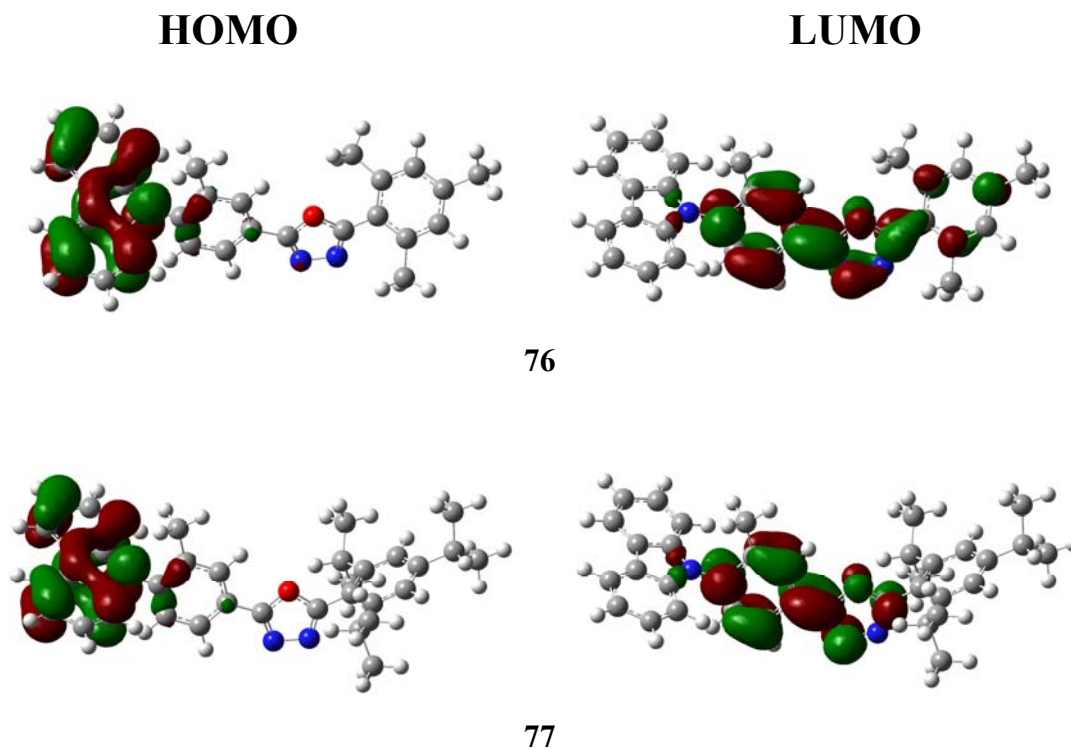
Figure 2.4. HOMO-LUMO maps of compound **76** and **77**. (N atoms shown in blue. Oxygen atoms shown in red).

The HOMO electron density located on ring ii decreases from **72** to **76** (see Figure 2.3 and 2.4). These data suggest that introducing a methyl group on phenyl ring ii will reduce conjugation between rings i and ii, i.e. the carbazole and diaryloxadiazole moieties. On the other hand, the LUMO orbitals of **72** and **76** are almost identical. Therefore, adding a methyl group to ring ii has an effect on the electron density of HOMO but not the LUMO orbital. Moreover, **73** and **77** have similar HOMO and LUMO features as **72** and **76**.

HOMO   **LUMO**

78
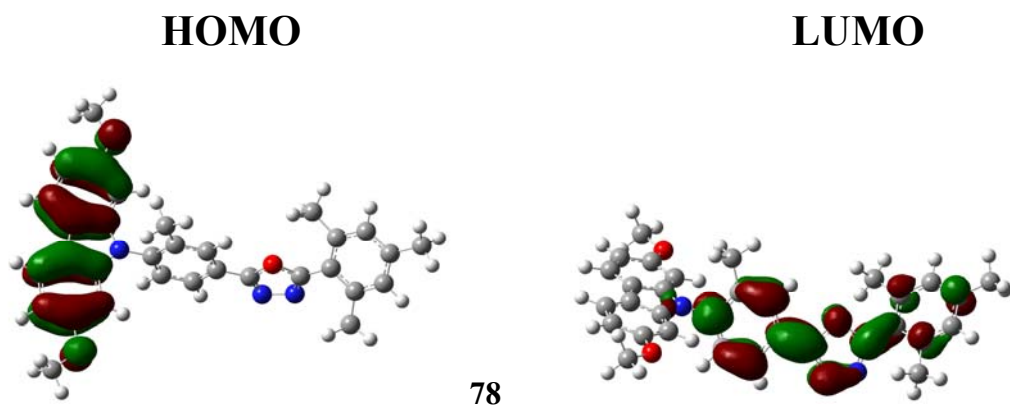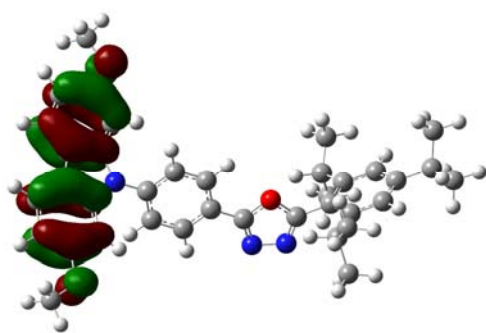
79
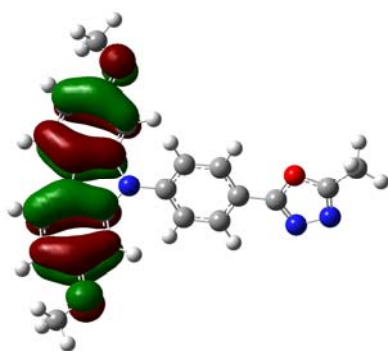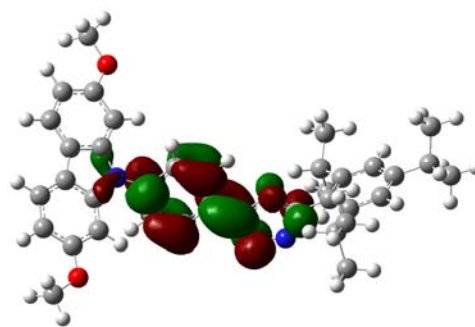
81
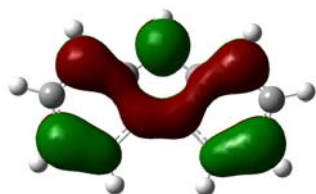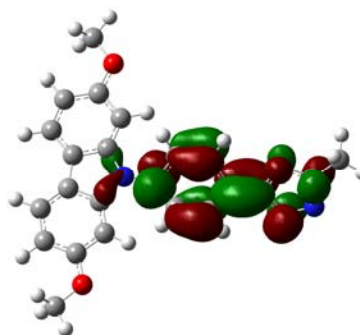
83
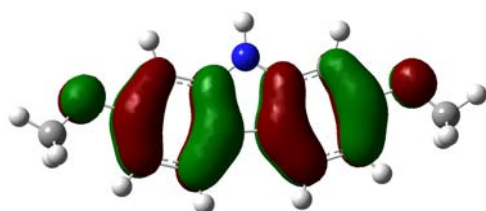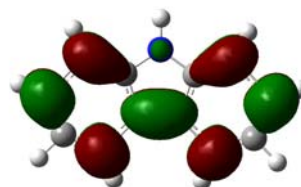
84
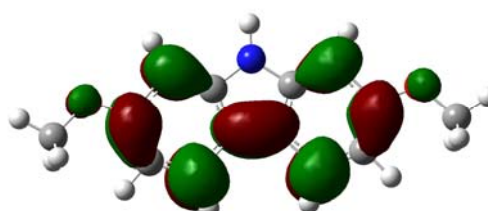
Figure 2.5. HOMO-LUMO maps of compound **78-79, 81, 83** and **84**. (N atoms shown in blue. Oxygen atoms shown in red).

The HOMO level of **84** (2,7-dimethoxycarbazole) is raised from -5.44 of **83** (carbazole) to -4.98 eV. The electron donating ability of carbazole was increased by adding two methoxy groups at the 2,7-positions. The HOMO-LUMO calculations of **78-79** and **81** show no HOMO orbital overlaps between the 2,7-dimethoxycarbazole (**84**) and diaryloxadiazole moieties, in comparison to **76**, **73** and **80**. The reason could be that no HOMO electron density is observed on the nitrogen of 2,7-dimethoxycarbazole which leads to no HOMO orbital overlapping with diaryloxadiazole. The situation is different for carbazole. The values of the LUMO and HOMO levels and torsion angles of the optimised molecules are shown in Table 2.1.

Table 2.1. Calculated torsion angles, singlet energy, LUMO and HOMO levels.

Compound	Angle between rings (iii) and (iv) (^{o})	Angle between rings (i) and (ii) (^{o})	Angle between rings (ii) and (iii) (^{o})	E_S (eV)	LUMO (eV)	HOMO (eV)
71	0	51.8	0.2	3.71	-1.77	-5.48
72	52.3	52.2	1.4	3.83	-1.62	-5.45
73	84.2	52.5	0.1	3.96	-1.51	-5.47
74	88.7	52.8	0.2	3.95	-1.52	-5.47
75	0	83.0	1.1	3.71	-1.78	-5.49
76	53.8	70.7	0.3	3.84	-1.64	-5.48
77	82.6	73.0	0.5	3.95	-1.53	-5.48
78	50.3	69.2	2.9	3.54	-1.52	-5.06
79	84.8	52.2	0.4	3.72	-1.39	-5.11
80	-	52.1	1.0	3.94	-1.54	-5.48
81	-	51.5	1.1	3.71	-1.41	-5.12

2.2.4 Electrochemical Studies

The electrochemical properties of **71-81** were studied by cyclic voltammetry (see Figure 2.6) in THF solution. Cyclic voltammograms were recorded at a scan rate 100 mVs^{-1} for five cycles at room temperature using an air-tight single-compartment three-electrode cell equipped with a Pt disk working electrode, Pt wire counter electrode, and Pt wire pseudo-reference electrode. The cell was connected to a computer-controlled Autolab PG-STAT 30 potentiostat. The solutions contained the compound together with n-Bu$_4$NPF$_6$ (0.1 M) as the supporting electrolyte in dichloromethane. All potentials are reported with reference to an internal standard of the ferrocene/ferrocenium couple (Fc/Fc$^+$ = 0.00 V).

71

72

73

74

75

76

77

80
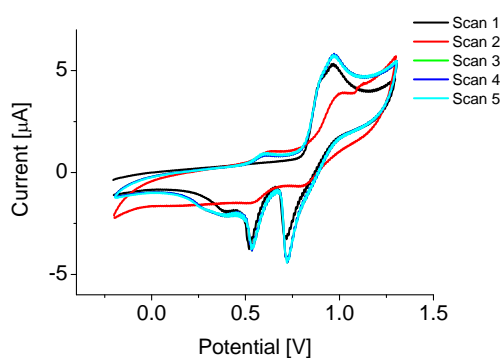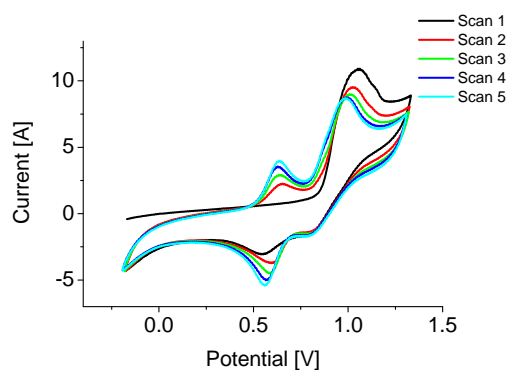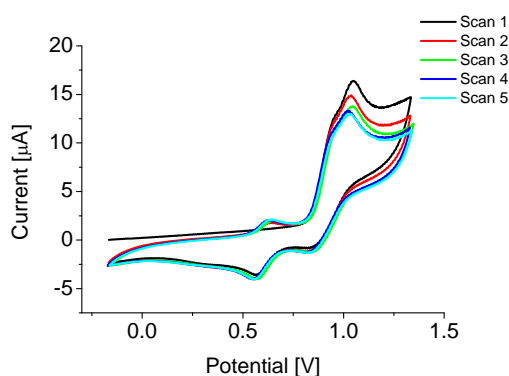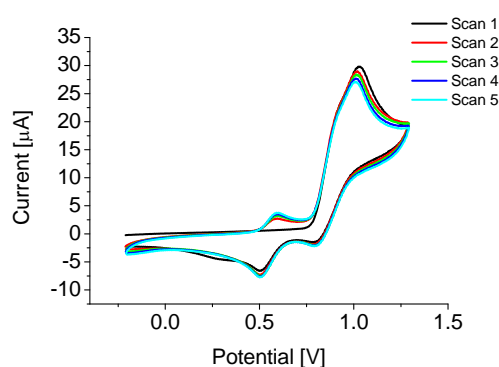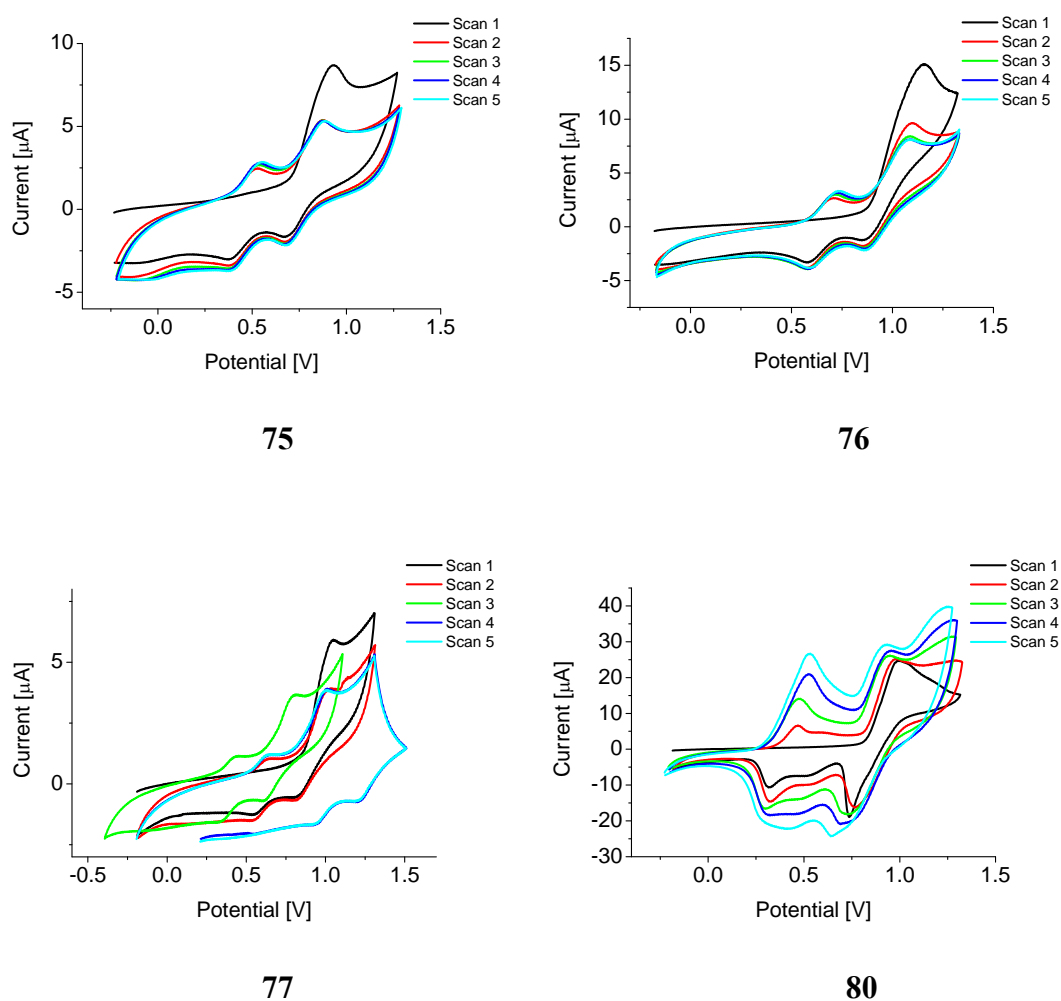
Figure 2.6. Cyclic voltammograms of compound **71-77**and **80**.

For the above CVs, scans 1-5 are shown as labelled (Scan 1 to Scan 5). All these compounds show a quasi-reversible oxidation on the first scan, to form a cation radical species. However, from scans 2 to 5, an additional peak at ca. 0.6 V was seen, most likely resulting from electrochemical dimerisation at C3 and C6 of the carbazole unit.[93] Notably, the current of the additional peak in the CV trace of compound **80** increases significantly with successive scans (Figure 2.6).

78

79

81
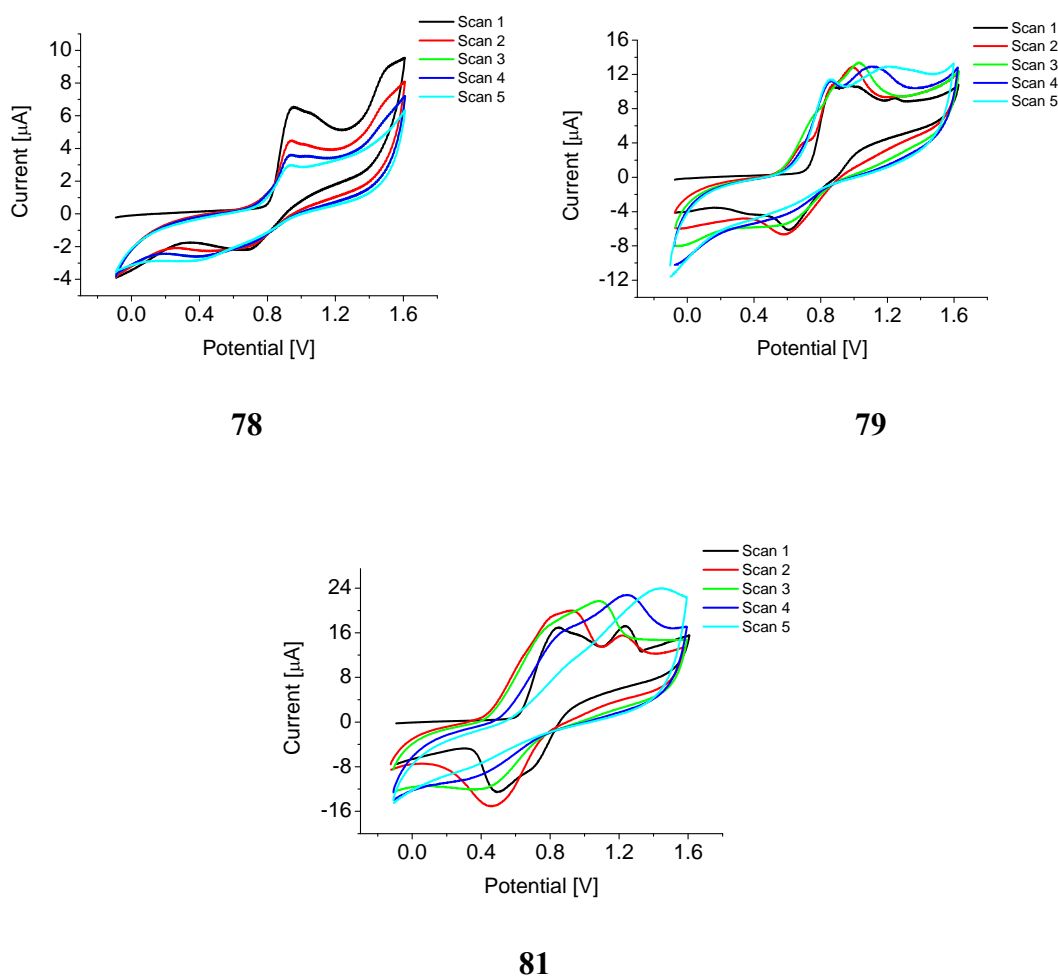
Figure 2.7. Cyclic voltammograms of compound **78-79** and **81**.

All the dimethoxycarbazole-oxadiazole compounds **78-79** and **81** display quasi-reversible oxidations on the first scan (Figure 2.7). The oxidation waves become more difficult to assign from scans 2 to 5, which is consistent with the electrochemical dimerisation at C3 and C6 of the 2.7-dimethoxycarbazole. Moreover, the oxidative waves are shifted to lower potential than the carbazole analogues, due to the electron donating effect of the methoxy substituents. Scans in the range 0 V to -2.0 V did not show any clear peaks for all the 11 compounds from a reduction of the OXDs unit, due to the high LUMO level. The values of E_{ox}^{onset} of all 11 compounds are shown in Table 2.2.

2.2.5 Photophysical Studies

Solution photophysical studies of compound **71-81** were carried out by Fernando B. Dias and John Dickinson in the Physics Department of Durham University. The ambipolar compounds investigated in this work show excited state intramolecular charge transfer, with the carbazole moiety acting as the donor and the oxadiazole as the acceptor. Figure 2.8 shows the absorption and emission spectra of **71** in non-polar methylcyclohexane (MCH) and polar ethanol (EtOH). While the effect of solvent polarity in the absorption spectrum of **71** is minimal, the fluorescence spectrum in EtOH appears broadened and red-shifted when compared with the emission obtained in MCH. The enhanced excited state dipole moment of the solute upon excitation induces local dipole-dipole interactions that force the reorientation of the polar solvent molecules around the excited solute. This is accompanied by the molecular structural relaxation and gives rise to inhomogeneous broadening of the fluorescence spectrum with emission occurring from a relaxed state at lower energy. With increasing solvent polarity the energy of the emissive relaxed state further decreases giving an emission spectrum with a larger red-shift. Similar observations have been made for all the other compounds in Figure 2.1.
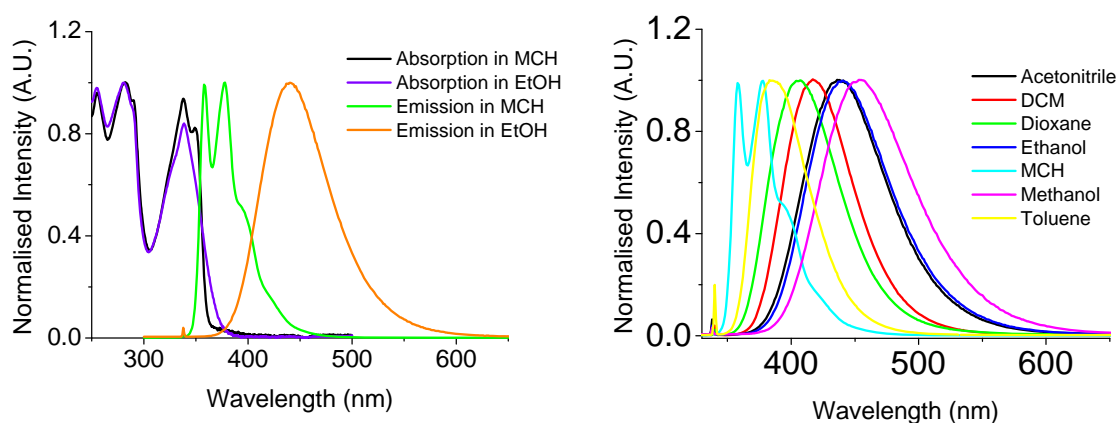
Figure 2.8. Normalised absorption and emission of **71** in MCH and EtOH solution (left). Emission of **71** in solvents with different polarity (right).

The fluorescence lifetime of **71** in non-polar MCH is well described by a single exponential decay with 1.43 ns (see Figure 2.9). However in ethanol, due to the more complex excited state dynamics, emission decays can only be fitted by a sum of two exponentials, with a fast time constant around 23 ps and a longer decay term of 4.96 ns.

The pre-exponential amplitude associated with the longer decay component appears positive independently of the emission wavelength. This component appears always as a decay term and clearly represents the lifetime of the emissive relaxed state. The fast decay component around 23 ps appears with positive pre-exponential amplitude at shorter wavelengths (400 nm), but with negative pre-exponential amplitude at longer wavelengths (500 nm). This component appears as emission decay at shorter wavelengths and as an emission rise-time at longer wavelengths, and is associated with the excited state relaxation described above. Local dipole-dipole interactions occurring during the solute excited state lifetime leads to a shift to longer wavelengths of the fluorescence spectrum as a function of time, and this makes the fluorescence intensity collected at a constant wavelength to drop on the high energy side of the emission spectrum, and to build-in at longer wavelengths.
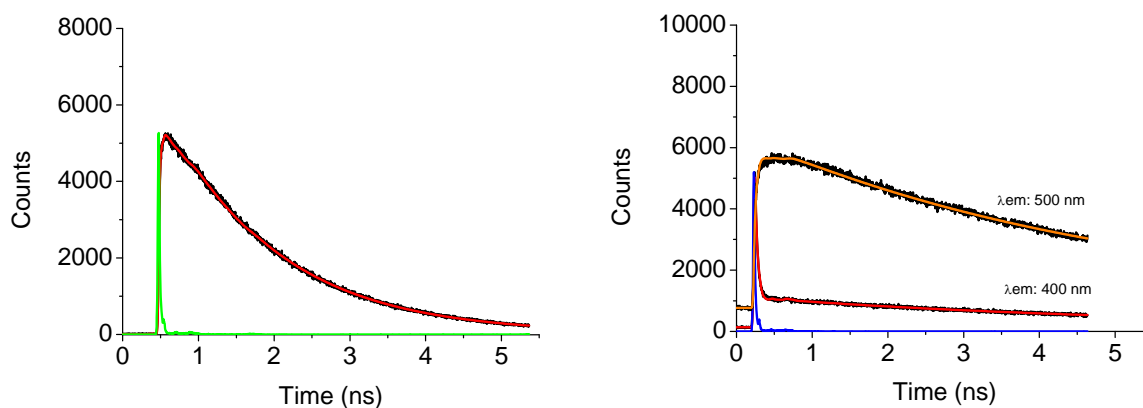
Figure 2.9. Fluorescesce decay of **71** in MCH at RT with emission collected at 373 nm (left). Fluorescence decay of **71** in ethanol at RT with emission collected at 400 and 500 nm (right). Excitation wavelength at 363 nm in both cases.

Interestingly, while compounds **71** to **77** and **80** keep good emission yields in all the solvents used in this study, the methoxy substituted compounds **78**, **79** and **81**

show almost no emission in ethanol and other polar solvents, suggesting an enhanced triplet yield in these derivatives, which has been confirmed by the emission temperature dependence studies.

The emission temperature dependence of **71** shows a shift to shorter wavelengths with decreasing temperature, as a result of a slower solvent reorganisation around the excited solute at low temperatures, but no further emissive state is observed (Figure 2.10). This is a common observation in compounds showing excited state intramolecular charge transfer, decreasing the temperature makes the solvent more viscous and the solvent reorganisation takes a longer time to occur, as a consequence the emission from non relaxed states starts to compete and progressively, as temperature drops, emission occurs from a state closer in energy to the Franck-Condon state. Emission from the triplet state is usually unlikely to be observed in steady state conditions. Phosphorescence is normally much weaker than fluorescence, which makes almost impossible for observation. Acquisition gated methods have generally to be used to collect phosphorescence spectra, these use a delay time between the excitation pulse and the emission acquisition in order to separate the weak phosphorescence and the strong fluorescence signals. However, in the case of compound **78** even phosphorescence emission is clearly observed together with fluorescence in a simple steady-state emission acquisition at low temperatures. The decreased emission yield observed at RT and the strong phosphorescence observed at low temperature strongly suggests an increase in the triplet yield of dimethoxy substituted compounds.
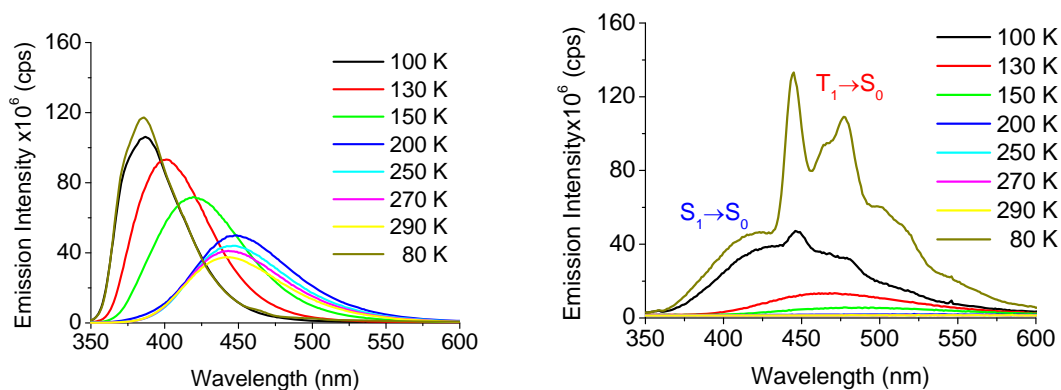
Figure 2.10. Emission spectrum of **71** (left) and **78** (right) in EtOH solution as a function of temperature.

Solid state photophysical studies of compound **71-81** were carried out by Vygintas Jankus in the Physics Department of Durham University. All fluorescence and phosphorescence spectra were obtained for thin film samples prepared by spin-coating. The concentration in zeonex was ~1E-4 mass to mass ratio. The zeonex solution of the materials was drop cast onto sapphire substrates of 12 mm diameter. The normalised fluorescence and phosphorescence spectra of compounds **71-74** are shown in Figure 2.11. The triplet levels of all four compounds are higher than those of CBP, PBD and the level increases sequentially (**71** < **72** < **73** < **74**) with increasing torsion angle between rings iii and iv (Table 2.2) due to a reduction of π-conjugation in this part of the molecules. The singlet levels are similarly raised (**71** < **72** < **73** = **74**) with increasing the torsion angle.
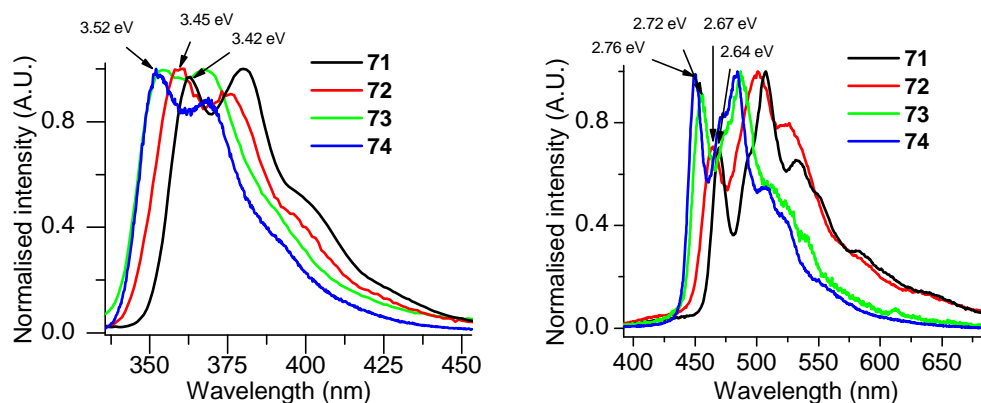
Figure 2.11. Normalised fluorescence (left) and phosphorescence spectra (right) of compounds **71-74**. Peak energies (triplet and singlet levels) are indicated on the spectra.

Figure 2.12 shows a comparison of **71**, **80** and **81**. It can be seen that replacing phenyl ring iv with a methyl substituent has the same effect in raising the triplet and singlet energy levels as introducing a large torsion angle between rings iii and iv, for example with *t*-butyl groups (for both **74** and **80**: E_T 2.76; E_S 3.52 eV). This further confirms that effective reduction of π-conjugation in the oxadiazole moieties is responsible for increasing both the triplet and singlet levels by ca. 0.1 eV, compared with the parent compound **71**.

Introduction of 2,7-dimethoxy substituents onto the Cz moiety (compound **81**) shifts E_S by 0.15 eV to the red in comparison to **80**, but E_T is unaffected, which means that the singlet-triplet gap in **81** is reduced to 0.61 eV.
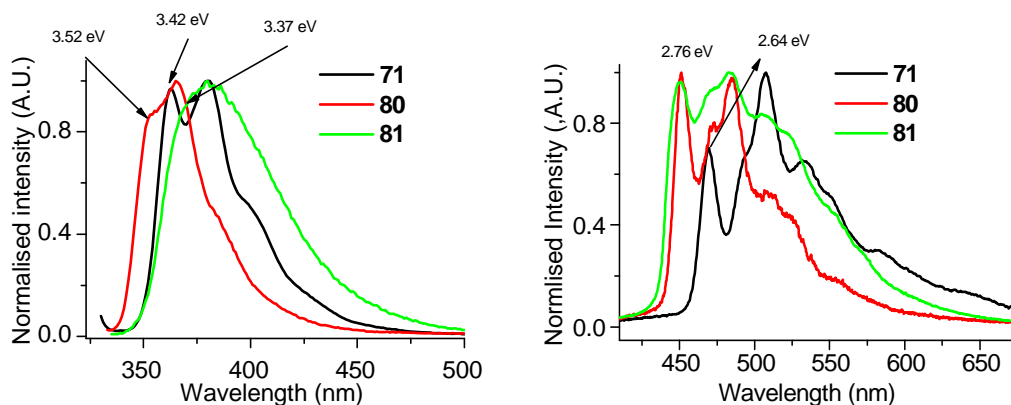
Figure 2.12. Normalised fluorescence (left) and phosphorescence spectra (right) of thin films of **71**, **80** and **81**. Peak energies (triplet and singlet levels) are indicated on the spectra.

The room temperature steady state fluorescence spectrum of **81** is very broad (see Figure 2.12), probably due to the introduction of new vibrational modes arising from the methoxy substituents. For the spectrum recorded at 11 K (see Figure 2.13) the features are more resolved and the difference between the vibrational peaks of **80** and **81** is the same (0.13 eV) with a red shift observed for **81**. This indicates that the broad spectrum of **81** at room temperature arises from comparable transitions as **80** but is red-shifted and less structured. Thus, 3.37 eV which was the highest energy peak in the fluorescence spectrum peak at 11 K, was taken as the singlet level for **81**. In the 11 K spectrum, at around 450 nm, phosphorescence was observed in a steady state *not* gated spectrum, indicating especially efficient phosphorescence emission. Similarly broadened spectra at room temperature are observed for the dimethoxycarbazole derivatives **78** and **79** compared to **73** and **76** (see Figure 2.14) with a red shift in E_S and no change in E_T.
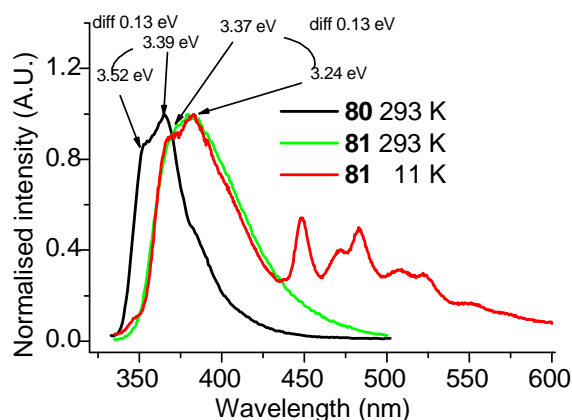
Figure 2.13. Normalised phosphorescence spectra of **80** at room temperature, and **81** at room temperature and 11 K. Energies of the main peaks, as well as the difference between them are indicated on the spectra.
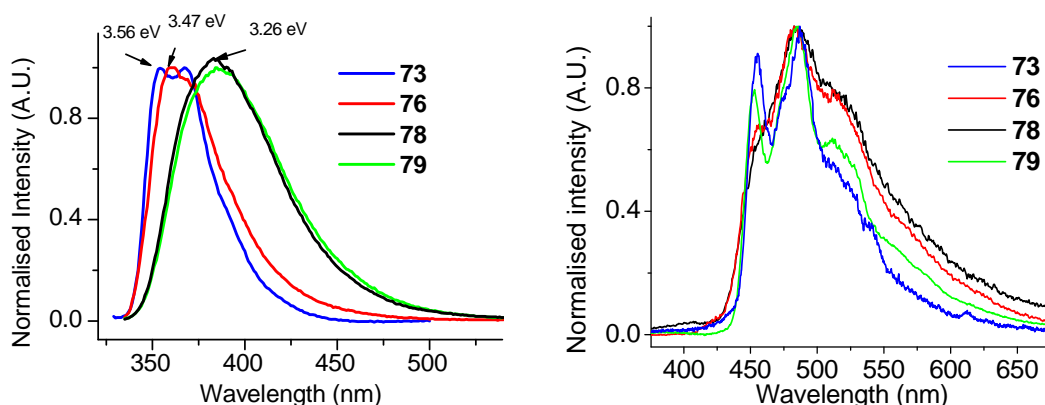
Figure 2.14. Normalised fluorescence (left) and phosphorescene spectra (right) of **73**, **76**, **78** and **79**. Peak energies (triplet and singlet levels) are indicated on the spectra.

From the above data we conclude that the triplet excited state wavefunction is located mostly on the diphenyloxadiazole unit of the molecules as the methoxy substituents on the carbazole unit do not affect the triplet level. This is reasonable as carbazole has triplet energy at 3.05 eV, whereas OXDs derivatives, e.g. PBD and OXD-7, have lower triplet levels than carbazole. The excited triplet state will be located primarily on the part of the molecule with the lower triplet energy level. This means that changes in triplet energy can be engineered by chemical modification to the diaryloxadiazole moiety (twisting it, reducing conjugation, etc.) whereas

modification to the Cz moiety (higher triplet than diaryloxadiazole) will change E_S but not E_T.

Furthermore, we observed an increase of triplet and singlet levels when a methyl group is introduced on ring ii adjacent to ring i (structures **75-78**) (see Figure 2.15). **77** has a larger blue shift of E_T in comparison with **73** (0.05 eV and ~0.06 eV shift for E_S). Figure 2.15 shows that **76** is affected by methyl substitution on ring ii in a similar manner to **77**.
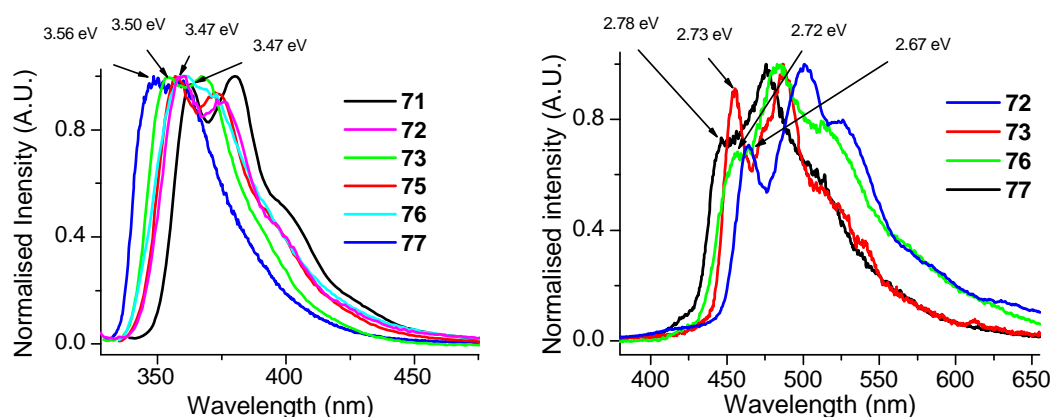
Figure 2.15. Normalised fluorescence spectra of **71**, **72**, **73**, **75**, **76**, **77** and normalised phosphorescence spectra of **72**, **73**, **76**, **77** and. Peak energies (triplet and singlet levels) are indicated on the spectra.

The triplet state lifetime (Table 2.2) for all of the compounds exceeds 400 ms and decays exponentially at 15 K which is reasonable bearing in mind that molecules in a zeonex matrix are isolated (1E-4 mass to mass ratio) thus reducing the probability of any type of energy transfer (see Figure 2.16). The triplet lifetime increases with an increase of torsion angle between the phenyl ring iv and oxadiazole ring iii. A similar progression is observed for the compounds **77** and **76**. This is consistent with Kasha's rule for radiationless transitions which states that with an increase of the bandgap there is a decrease in the decay rate of radiationless transitions (i.e. the overall lifetime increases).
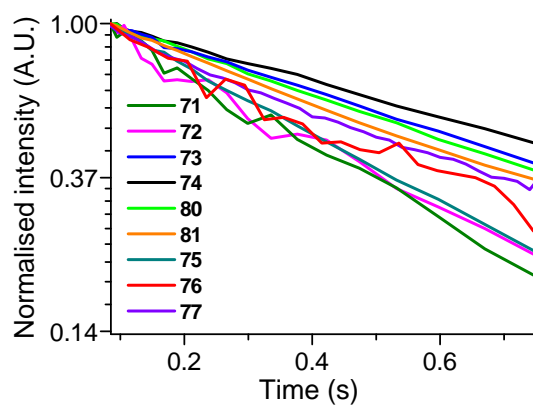
Figure 2.16. Normalised phosphorescence decays of all materials in linear-ln scale. Fitted exponential lifetimes can be found in Table 2.2.

Table 2.2. Measured and calculated torsion angles, measured and calculated triplet and singlet energy levels as well as their difference, calculated LUMO and HOMO levels, triplet lifetimes and oxidation potential onset.

Compound	E_{ox}^{onset} (V)	Twist angle between rings (iii) and (iv) (°)	Twist angle between rings (i) and (ii) (°)	Twist angle between rings (ii) and (iii) (°)	Triplet energy, E_T (eV)	Singlet energy, E_S (eV)	S_1-T_1 (eV)	LUMO (eV)	HOMO (eV)	T_1 Lifetime at 15 K, (ms)	Absorption λ_{max} (nm)
71	**(0.82)**	0	51.8	0.2	**(2.64)**	3.71(**3.42**)	0.78	-1.77	-5.48	**(416)**	**(341)**
72	**(0.85)**	52.3	52.2	1.4	**(2.67)**	3.83(**3.45**)	0.76	-1.62	-5.45	**(454)**	**(340)**
73	**(0.84)**	84.2(**77.4**)	52.5(**53.8**)	0.1(**3.3**)	**(2.73)**	3.96(**3.52**)	0.79	-1.51	-5.47	**(740)**	**(339)**
74	**(0.79)**	88.7(**86.3**)	52.8(**58.3**)	0.2(**23.1**)	**(2.76)**	3.95(**3.52**)	0.76	-1.52	-5.47	**(858)**	**(339)**
75	**(0.71)**	0	83	1.1	**(2.64)**	3.71(**3.47**)	0.81	-1.78	-5.49	**(448)**	**(339)**
76	**(0.88)**	53.8	70.7	0.3	**(2.73)**	3.84(**3.47**)	0.75	-1.64	-5.48	**(546)**	**(338)**
77	**(0.87)**	82.6(**78.5**)	73(**82.2**)	0.5(**10.0**)	**(2.79)**	3.95(**3.56**)	0.79	-1.53	-5.48	**(627)**	**(337)**
78	**(0.73)**	50.3	69.2	2.9	**(2.73)**	3.54(**3.37**)	0.64	-1.52	-5.06	**(641)**	**(319)**
79	**(0.81)**	84.8	52.2	0.4	**(2.73)**	3.72(**3.37**)	0.64	-1.39	-5.11	**(709)**	**(318)**
80	**(0.82)**	-	52.1(**54.1**)	1.0(**1.6**)	**(2.76)**	3.94(**3.52**)	0.77	-1.54	-5.48	**(686)**	**(339)**
81	**(0.63)**	-	51.5	1.1	**(2.76)**	3.71(**3.37**)	0.61	-1.41	-5.12	**(626)**	**(318)**

The values in brackets are all from experimental results.
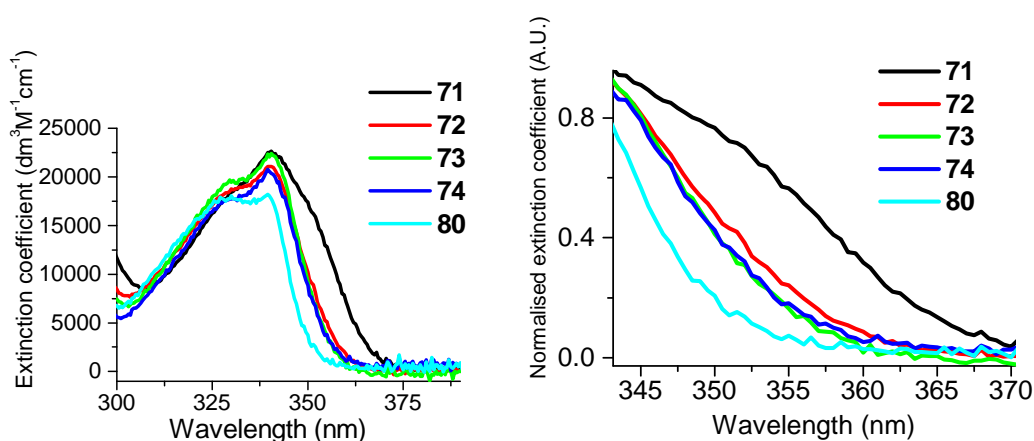
Figure 2.17. Extinction coefficients of **71-74** and **80** in toluene solution (left). Absorption spectra zoomed in between 345 nm and 370 nm. Each curve is normalised at the peak wavelength (right).
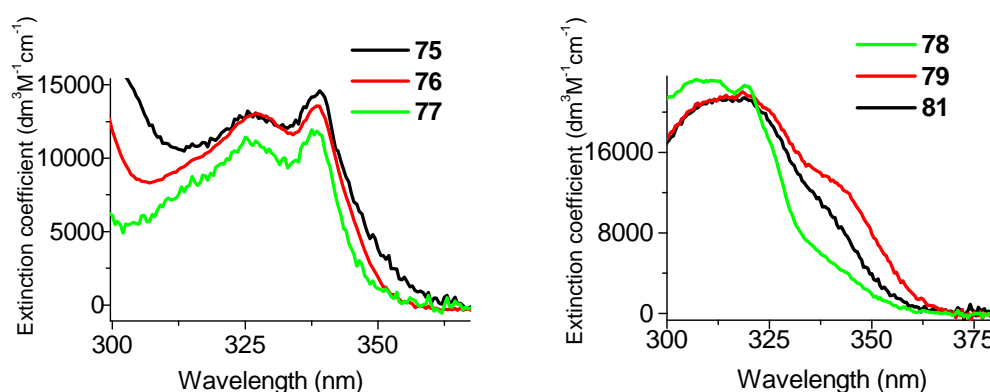
Figure 2.18. Extinction coefficients of **75-77** in toluene (left). Extinction coefficients of **78**, **79** and **81** in toluene (right).

Absorption spectra follow a very similar pattern as the triplet and singlet spectra – they blue shift for the series of compounds **71-74**, **80** and for the series **75-77**. At the peak wavelength the extinction coefficients of most of the compounds are slightly more than 20000 dm³mol⁻¹cm⁻¹ with an exception of **75-77** (Figures 2.17 and 2.18) where introduction of the methyl substituent on ring ii reduces the oscillator strength of absorption to ~15000 dm³mol⁻¹cm⁻¹.

2.3 Conclusions

New Cz-OXD hybrid molecules have been synthesised in order to evaluate electronic and conformational effects on the singlet and triplet energies. Introducing more bulky alkyl substituents onto the diaryloxadiazole fragment systematically increases the singlet and triplet levels and blue shifts the absorption and emission bands. The triplet energy of **74** with the largest twist between rings iii and iv is 0.12 eV higher than the parent compound **71**. Replacement of the terminal phenyl unit by a methyl group has a similar effect. In contrast, the Cz-OXD system reported by Ma *et al.*[33] did not comment on the importance of twisting between phenyl and oxadiazole ring. Also, an addition of methyl group on ring ii blue shifts the absorption and emission.

Interestingly, by introducing electron donating groups (methoxy) at the 2,7-positions of the carbazole moiety the singlet level is decreased without changing the triplet excited state, thereby reducing the singlet-triplet energy gap. The HOMO energy levels of all the dimethoxy subsitutied compounds are increased. However, the LUMO energies of these compounds mostly remain unchanged. Furthermore, dimethoxy substituted compounds show another intresting feature: phosphorescence is observed together with fluorescence emission at low temperatures. The decreased fluorescence emission yield observed at RT and the strong phosphorescence observed at low temperature strongly suggests an increase in the triplet yield of dimethoxy substituted compounds.

In conclusion, these modifications enable fine-tuning of the photophysical properties in Cz-OXD systems. These design features should aid the search for new charge transfer molecules for various optoelectronic applications.

Chapter 3 – Novel Cyclometalated Iridium Complexes

3.1 Introduction

As already discussed in chapter 1.6, Ir(III) phosphorescent emitters have been actively studied for OLED applications due to their colour tuning ability and 100% theoretical efficiency by harvesting both singlet and triplet excitons. Among them, Ir(ppy)₃ based complexes have been widely examined for tuning the emission wavelength,[94] improving the performance in devices and exploring other applications.[95]

48 (Flrpic) is one of the most popular sky-blue complexes for testing new high triplet hole and electron-transporting materials, and its analogues have been widely developed[96,97,98] However, thermal instability and limited solubility in organic solvents have restricted its applications. Sivasubramaniam *et al.* reported that Flrpic decomposition occurred under the thermal evaporation conditions used to obtain thin films for devices, which leads to reduced efficiency of the devices.[99] Moreover, the insolubility of Flrpic precludes its incorporation into devices by solution processing (spin-coating) techniques. Hence, looking for stable, soluble and efficient blue iridium complexes as replacements for FIrpic still remains a great challenge.

Much research is focused on deeper blue, thermally stable and device efficient Ir(III) complexes.[54,57,59] Here, ligands containing more heteroatoms came into the spotlight. Burn *et al.* developed new triazole ligands to achieve stable deep blue emission. However, these complexes did not produce efficient devices due to triplet quenching by ET materials.[65] Other multi-heteroatom ligand Ir(III) complexes have been exploited,[66,100,101] but only a very few iridium complexes with oxadiazole ligands have been reported.[64,102,103] 2,5-Diaryl-1,3,4-oxadiazoles (OXDs) are widely used as electron-transporting and hole blocking materials in OLEDs due to their moderate electron affinity, high photoluminescence quantum yield, and good thermal and chemical stabilities.[104] We reasoned that iridium complexes with twisted 2,5-diaryl-1,3,4-oxadiazole ligands should be blue emitters due to their high triplet energy. In this Chapter we discuss our work on this topic, which gave rise to novel structures different from our expectations. Furthermore, functionalised pyridine-carbazole and azacarbazole based iridium complexes are also reported.

3.2 Results and discussion

3.2.1 Synthesis of Cyclometalated Iridium Complexes of 2,5-Diaryl-1,3,4-oxadiazole Ligands.

The synthesis of the twisted diaryloxadiazole ligands **65, 66** and **67** was discussed in chapter 2. These OXDs ligands were then reacted with iridium chloride under standard conditions to form a bridged µ-dichloro-bridged diiridium C^N ligand complex (Scheme 3.1). This afforded complexes **86-89** in 10-40% yield. Subsequent reactions of **87** with acetylacetone and picolinic acid, and **89** with picolinic acid yielded the acac and picolinate complexes **90** (61%), **91** (28%) and **92** (69%), respectively (Scheme 3.1). The structures of the complexes **86-92** are shown in Figure 3.1.
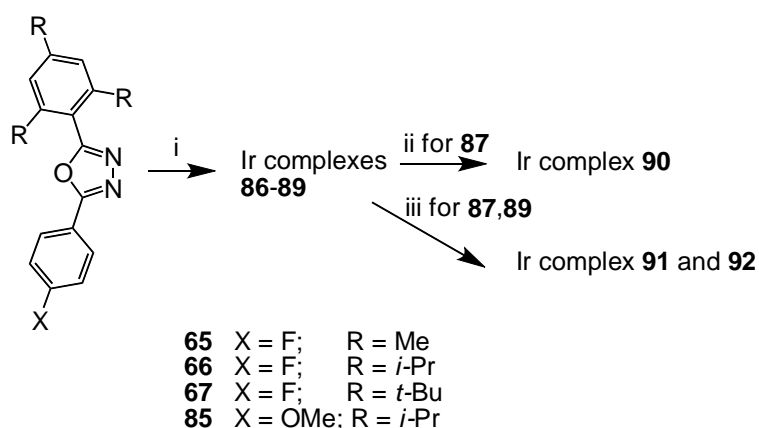
Scheme 3.1. Synthetic routes to complexes **86-92**: (i) IrCl₃, 2-ethoxyethanol, water, 120 °C; (ii) **87**, acetylacetone, Na₂CO₃, 2-ethoxyethanol, 120 °C; (iii) **89**, picolinic acid, Na₂CO₃, 2-ethoxyethanol, 120 °C.

86 R = Me; X = F
87 R = *i*-Pr; X = F
88 R = *i*-Pr; X = OMe

89 R = *t*-Bu

90 R = *i*-Pr

91 R = *i*-Pr
92 R = *t*-Bu
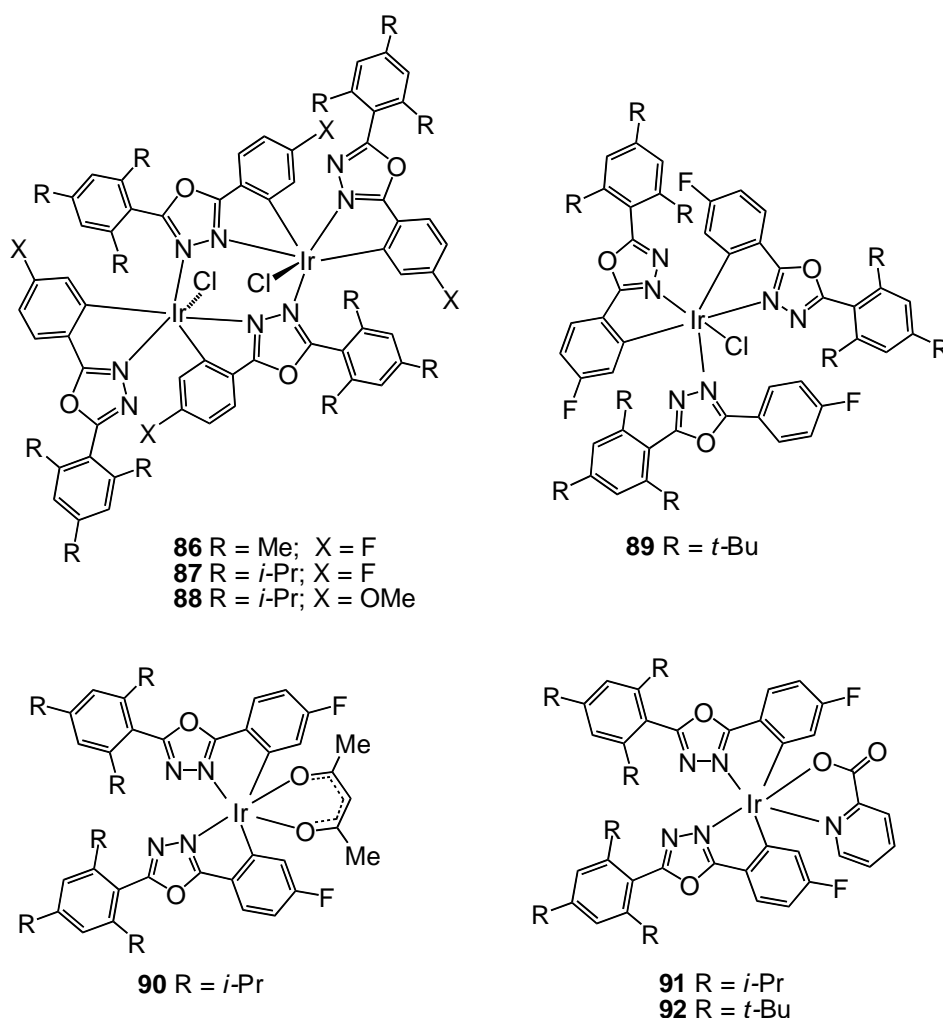
Figure 3.1. Structures of diaryloxadiazole iridium complexes **86-92**.

First, complex **90** was characterised by NMR, MS and X-ray diffraction. The X-ray crystal structure revealed that a mononuclear complex with an unusual structure was formed under standard cyclometalation conditions (see Figure 3.2). The ligand coordination differs from the majority of iridium complexes formed under the same conditions. The nitrogen atom to iridium coordination plane is approximately linear with the cyclometalated C atom of the second OXDs ligand. This is a very unusual conformation for heteroleptic complexes. In the literature, there are only a few complexes reported with a similar coordination mode to **90**.[55,105] However, the synthetic approach is completely different. For example, complex **93** was obtained by mixing the ligand with ZnCl$_2$ to form organozinc reagents, then reacting it with the ancillary ligand. The possible structure of the organozinc intermediate was not reported.

Figure 3.2. Crystal structure of **90** (molecule *A*, thermal ellipsoids at 50% probability level, disorder and all H atoms are omitted). Selected bond distances (Å) in two independent molecules: Ir-O(3) 2.040(2) & 2.040(3), Ir-O(4) 2.118(3) & 2.131(3), Ir-N(1) 1.985(3) & 2.010(3), Ir-N(3) 2.158(3) & 2.093(3), Ir-C(12) 2.006(4) & 2.000(4), Ir-C(32) 2.023(4) & 2.010(4).
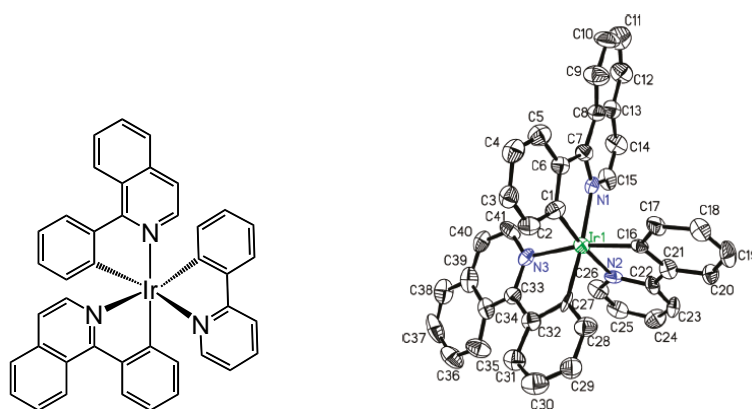
Figure 3.3. Crystal structure of complex **93** (from ref. 105).

On the other hand, Xu *et al.* have reported the crystal structure of the oxadiazole complex with acac as the ancillary ligand, **94**[103] (see Figure 3.4), formed under standard conditions, which did not show a similar coordination mode to **90**.
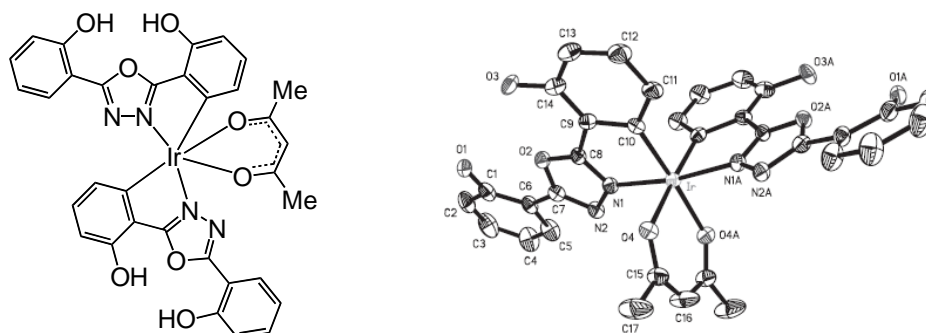
Figure 3.4. Crystal structure of complex **94** (from ref. 103).

For our series of complexes, X-ray crystal structures of **86-90** and **92** revealed that dinuclear and mononuclear complexes with unusual structures were formed under standard cyclometalation conditions as a result of the *ortho*-alkyl substituents inducing steric overcrowding, which changes the normal course of the metal-ligand coordination reactions. All these crystal structures (solved by Dr Andrei S. Batsanov) are discussed below.

3.2.2 X-ray Crystal Structure Studies

In all the complexes **86-90** and **92**, iridium atoms adopted a distorted octahedral coordination. Complexes **86**, **87** and **88** have similar dimeric structures to each other (Figure 3.1, Table 3.1). The first two crystallised with largely similar crystal lattices and packing motifs, with the asymmetric unit comprising half of the dimer (which lies at a crystallographic inversion centre) and also with one solvent molecule (DMSO in **86** or DCM in **87**), whereas the unsolvated crystal of **88** has one independent molecule in a general position (but still pseudo-centrosymmetric). There are four OXD ligands in each complex. Two of the ligands chelate the Ir atom in a bidentate C,N-fashion, whereas two of the ligands are tridentate, chelating one Ir atom in the same C,N-fashion and coordinating the other Ir *via* the remaining nitrogen atom. The chloro ligands are terminal; thus **86-88** differs from the diiridium OXDs complexes reported previously, all of which had [(OXD)$_2$Ir]$_2$(μ-Cl)$_2$ type structures with two chloro-bridges.[106] Complex **89** (crystallised as DCM monosolvate, Figure 3.6) is mononuclear, with two N,C-chelating, one N-monodentate OXDs ligand and one terminal chloro ligand. Hence, it can be regarded as analogous to the monomeric units of **86-88**, except for the monodentate OXDs being coordinated through a

different nitrogen atom. In each OXDs ligand the tri-R-aryl ring is twisted with respect to the oxadiazole ring due to steric overcrowding, the interplanar angle τ varying from 63 to 88°. The angle (φ) between the planes of the oxadiazole and the metallated aryl rings is negligible in **86**, **87**, **89** and also for the one bridging ligand of **88**. Three other ligands of the latter display a substantial folding (rather than twist) of *ca*. 12°, while the monodentate OXDs ligand in **89** is twisted with φ=60.5°. In each of the dimers, the two bridging aryloxadiazole moieties and the Ir atoms are roughly coplanar. And there are two cases of intramolecular π-π stacking (see Figure 3.5) between a tri-R- and a 4-X-substituted aryl unit, with the interplanar angles of 6° (**86**), 17° (**87**), 10° and 17° (**88**) and the mean interplanar separations of 3.32, 3.43, 3.40 and 3.55 Å, respectively.

Although the N,N′-bridging coordination of OXDs has been observed before (in Co, Mn, Re, Cu, Ag, though never in Ir[92] complexes), the only known example of such bridging combined with cyclometalation is (2,5-diphenyl-1,3,4-oxadiazole)[Mn(CO)$_4$], where *both* metal atoms are C,N-chelated.[107] Diiridium complexes with N,N′-bridging pyrazolyl ligands are well known, but most of these contain a direct metal-metal bond.[108] In [{IrH(O$_2$CCF$_3$)(CNBu^t)$_2$}$_2$(μ-pz)$_2$] and [{(PhO)$_3$PIrH(Cl)-(CO)}$_2$(μ-pz)$_2$][109] where octahedral, 18-electron iridium(III) centers are bridged by two N,N′-pyrazolyl rings, the Ir$_2$(pz)$_2$ moiety adopts a folded (butterfly) conformation with the Ir…Ir distances (3.803 and 3.770 Å, respectively), much shorter than in **86-88**.

The asymmetric unit of **90** comprises two molecules (A and B) with the same coordination mode (comprising two C,N-chelating OXDs and one acac ligand) but substantially different conformations. The cyclometalated aryloxadiazole moiety *L1* is folded in molecules A (φ=15.6°) and both folded and twisted in B (φ=10.0º). The *L2* moiety is twisted in both molecules, but the φ angles are rather different in magnitude (14.6 and 7.5°) and of opposite sense. The Ir−N(3) bond is inclined to the oxadiazole plane by 20.2° in molecule A and only 10.8° in B, the iridium atom deviating from that plane by 0.74 and 0.39 Å, respectively. This probably causes this bond to be much longer in A than in B (2.158(3) vs 2.093(3) Å), whereas other bond distances are similar. The Ir-acac metallacycle is folded along the O…O vector by 12.4° (A) or 16.0° (B) in opposite directions. Complex **92** (crystallising as a DCM monosolvate) has a similar conformation mode with the replacement of O,N- for O,O-acac chelation (Figure 3.7). It shows weaker distortions with φ=6 and 8°.
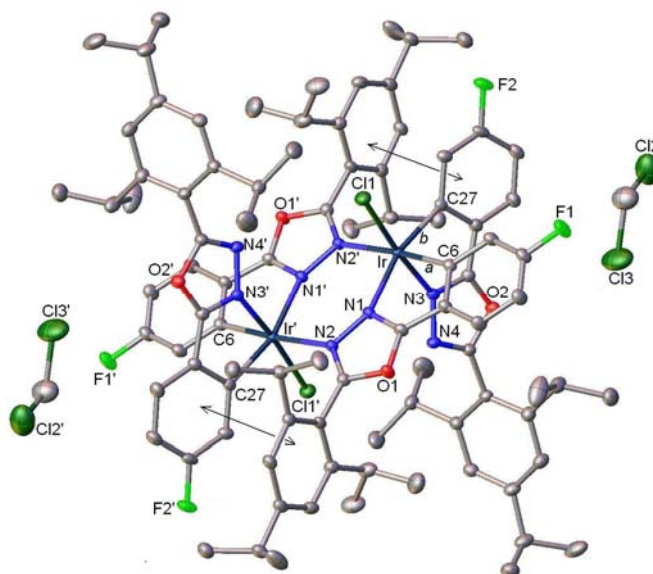
Figure 3.5. Crystal structure of **87**•2CH$_2$Cl$_2$ (thermal ellipsoids at 50% probability level, disorder and all H atoms are omitted). Primed atoms are generated by the inversion centre. Arrows show intramolecular π-π stacking interactions.
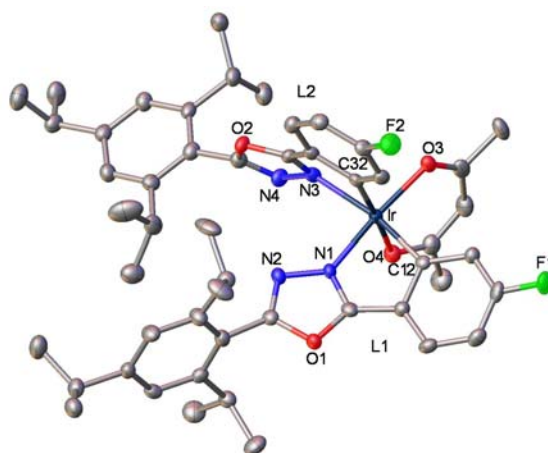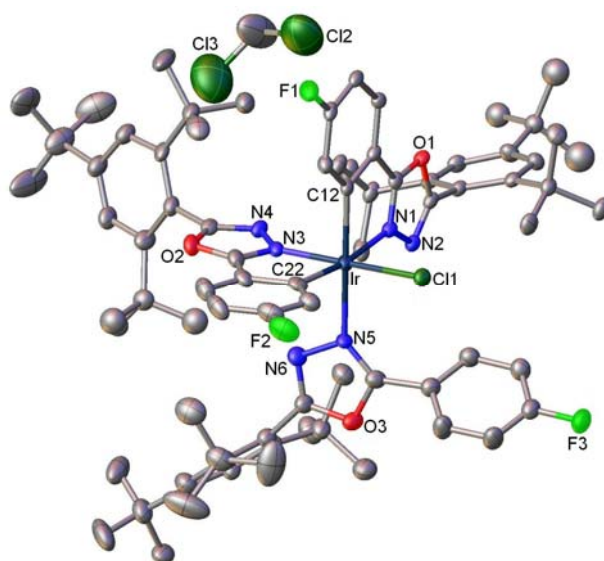

Figure 3.6. Crystal structure of **89**•CH$_2$Cl$_2$ (thermal ellipsoids at 30% probability level, disorder and all H atoms are omitted). Selected bond distances (Å): Ir-Cl(1) 2.357(1), Ir-N(1) 2.131(4), Ir-N(3) 2.019(4), Ir-N(5) 2.192(4), Ir-C(12) 2.033(5), Ir-C(22) 2.020(6).
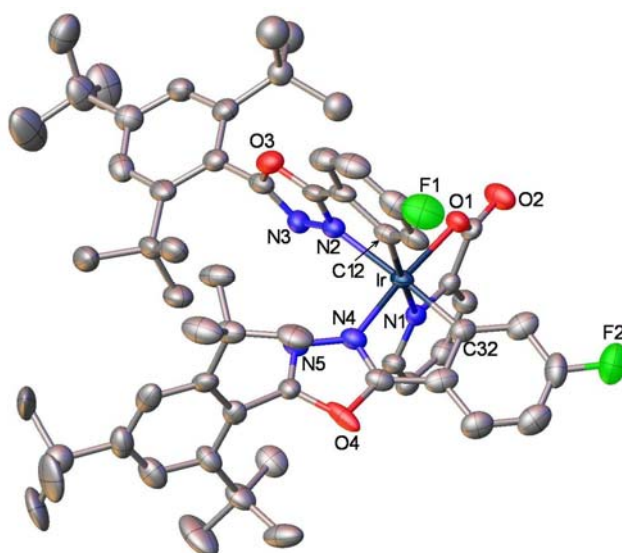
Figure 3.7. Crystal structure of **92** (thermal ellipsoids at 50% probability level, solvent and all H atoms are omitted). Selected bond distances (Å): Ir-O(1) 2.055(4), Ir-N(1) 2.108(5), Ir-N(2) 1.994(5), Ir-N(4) 2.097(6), Ir-C(12) 2.023(7), Ir-C(32) 2.033(7).

Table 3.1. Selected bond distances (Å) in complexes **86-88**.

	86	**87**	**88**, Ir(1)	**88**, Ir(2)
Ir-Cl	2.347(1)	2.3545(6)	2.356(1)	2.353(1)
Ir-N(1)	2.175(5)	2.159(2)	2.160(3)	2.166(3)
Ir-N(2´)	2.177(4)	2.172(2)	2.175(3)	2.184(3)
Ir-N(3)	2.033(4)	2.003(2)	2.020(3)	2.026(3)
Ir-C (*a*)	2.023(5)	2.025(2)	2.030(4)	2.028(4)
Ir-C (*b*)	2.035(6)	2.025(2)	2.028(4)	2.037(4)
Ir…Ir	4.299	4.298	4.313	

The question is why are complexes **90** and **92** formed? We can explain this by the formation of the unusual intermediate complexes **86-89**. We believe that steric hindrance caused by the alkyl substituents on the aryl substituent of the cyclometalling ligands results in organoiridium complexes with novel and unexpected structures.

3.2.3 Photophysical and Electrochemical Properties

Photophysical data are shown in Table 3.2. The absorption and emission spectra of complexes **90** and **91** and the absorption spectra of ligands **66** and **67** in oxygen-free dichloromethane solution are illustrated in Figure 3.8. Both complexes show strong absorption bands between 250-300 nm, which can assigned[110] to ligand-centred $\pi-\pi^*$ transitions and closely resemble the absorption spectra of the free ligands **66** and **67**. Furthermore, the complexes demonstrate absorption bands with lower extinction coefficients in the range of 300-425 nm, which can ascribed to singlet and triplet metal-to-ligand charge-transfer (^{1}MLCT and ^{3}MLCT) states, following literature precedents and the calculations of Hay.[111] It is not possible to distinguish the singlet and triplet absorptions, although the precedent is that the lower energy bands are predominantly triplet in character.

Luminescence in DCM at 293 K, with very low photoluminescence quantum yields (PLQYs), due to non-radiative decay, is observed for **90** (λ_{max}^{em} 482(sh), 518 nm), **91** (λ_{max}^{em} 471, 496 nm) and **92** (λ_{max}^{em} 462 nm) which is visible as green (**90**) and blue-green emission (**91** and **92**). It is well-established for heteroleptic Ir complexes that a pic ancillary ligand leads to blue shifted emission (usually by ca. 20 nm) compared to the analogous acac complex.[112,113] This trend is observed for **91** (pic) compared to **90** (acac). The emission of **92** is blue shifted in comparison to **91**, which can be explained by reduced conjugation in the OXD ligands of **92**, due to their increased torsion angles, compared to **91**. Lifetime data at 293 K are consistent with the following emission features: for **90** and **91** emission is a combination of fluorescence and phosphorescence; for **92** only fluorescence is observed, with an excited state lifetime in the nanosecond regime. The increased vibronic fine structure for **90** and **91** at 293 K is consistent with a combination of ^{3}MLCT states and LC $^3\pi-\pi^*$ transitions. At 77 K strong phosphorescence is observed for all three complexes; the spectra show the characteristic vibronic fine structure (see Figure 3.9). Excited state lifetimes at 77 K are all in the microsecond regime. Such long lived excited states suggest that the emitting state has triplet character. The luminescence decay profiles are shown in the Supporting Information. Further photophysical studies on these and analogous complexes will be undertaken to probe the interesting interplay of fluorescence and phosphorescence.
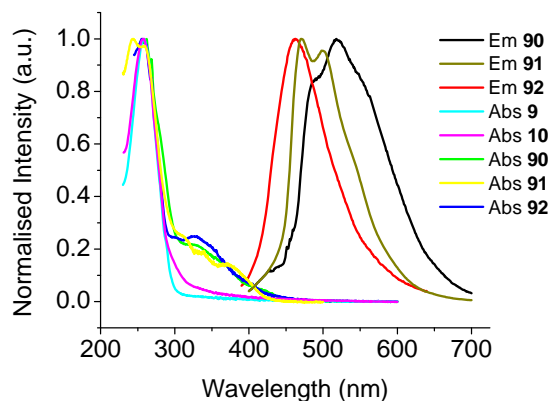
Figure 3.8. Normalized absorption and emission spectra of complexes **90**, **91** and **92** and absorption spectra of ligands **66** and **67** in oxygen-free dichloromethane solution at 293 K.

Table 3.2. Photophysical data of complexes **90-92**.

Complex	λ_{max}^{ab} /nm (293 K)[a]	λ_{max}^{em} /nm (293 K)[a]	λ_{max}^{em} /nm (77 K)[b]	Lifetime/ τ (293K)[b]	Lifetime/ τ (77 K)[b]	PLQY, Φ (293 K)[a,c]
90	263	482(sh), 518	496(sh), 529, 574(sh)	3.8 μs	4.6 μs	< 0.01
91	243	471, 496	470, 504, 543(sh)	0.3 μs	4.2 μs	< 0.01
92	256	462	483(sh), 519, 563(sh)	6.3 ns	5.7 μs	< 0.01

[a] Measured in CH_2Cl_2 solution, λ^{ex} 350 nm; [b] Measured in EPA; [c] Measured using an integrating sphere. [d] A fluorescent component with a lifetime in the nanosecond region was also observed.
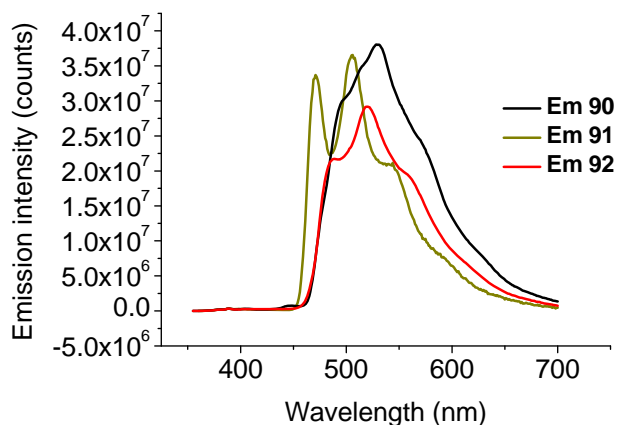
Figure 3.9. Emission spectra of complexes **90**, **91** and **92** in EPA (a mixture of diethyl ether : 2-methylbutane : ethanol, 5:5:2 v/v) at 77 K.

The electrochemical properties of **90** and **92** were studied by cyclic voltammetry in dichloromethane solution which established that each complex has a quasi-reversible single-wave oxidation ascribed to a metal-centred Ir^{3+}/Ir^{4+} process at E^{ox} 1.28 V (**90**) and 1.50 V (**92**) in dichloromethane vs. $FcMe_{10}/FcMe_{10}^+$.
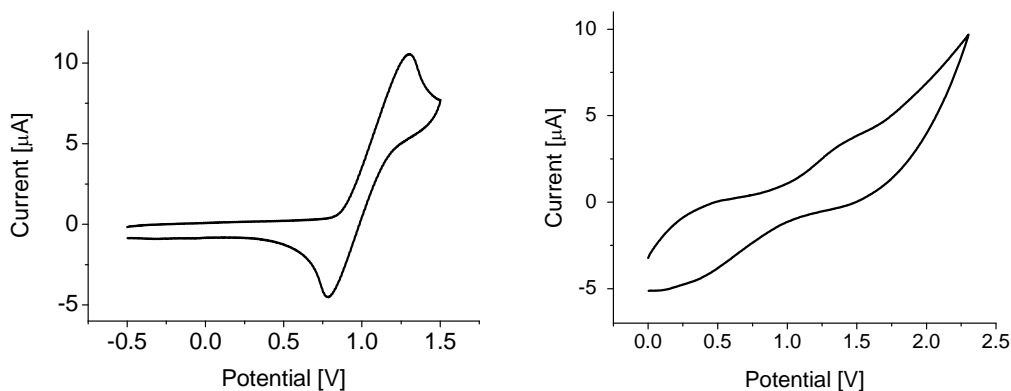
Figure 3.10. Cyclic voltammogram of complexes **90** (left) and **91** (right) in DCM, vs. $FcMe_{10}/FcMe_{10}^+$.

Figure 3.11. Cyclic voltammogram of complex **92** in DCM, vs. $FcMe_{10}/FcMe_{10}^+$.

3.2.4 Synthesis of Pyridine-Carbazole Complexes

Our group has previously investigated Ir(III) complexes of carbazolylpyridine ligands as emitting guests in blends with host materials for OLED applications.[114] Two isomeric series (labelled as S1 and S2) of complexes **95-100** are shown in Figure 3.12.

Figure 3.12. Structures of Ir(III) complexes **95-100**. S1 (H) **95**, S1 (CF$_3$) **96**, S1 (OMe) **97**, S2 (H) **98** and S2 (CF$_3$) **99** and S2 (OMe) **100**

The difference between these two series is the carbazole coupling position to the pyridine unit. The ligands for S2 are more conjugated (linear system) than the corresponding ligands for S1 (bent system), resulting in a red shift of the emission for S2. Moreover, S1 complexes display high device efficiency (>30 lm/W) by single-active-layer spin-coating method. On the contrary, the devices from S2 complexes are less efficient. S1 complexes have shown great potential in OLEDs. However, a

challenge for studying these complexes is the low yields for the cyclometalation step (only 2-8%).[63] Also, attempts for preparing the complex **97** with a methoxy group *para* to the pyridine were unsuccessful.

The aim for my work was to increase the yield for the formation of the complexes and to find a successful synthetic route for the complex where the methoxy group is *para* to the pyridine nitrogen. Two approaches are shown below in Scheme 3.2.
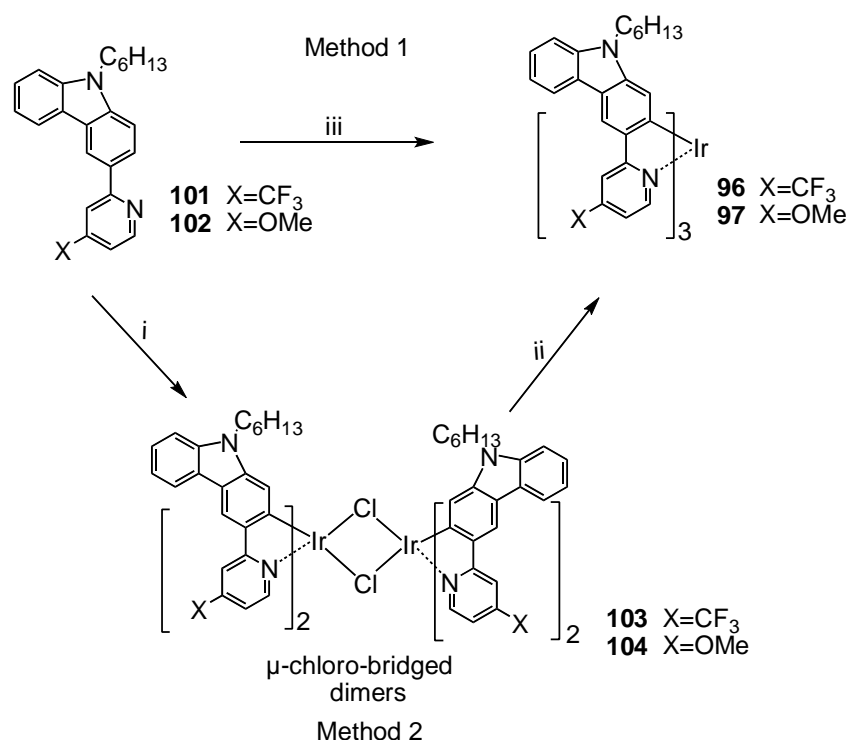
Scheme 3.2. Synthetic routes for complex **96** and **97**. i: IrCl$_3$, 2.3 eq **101** or **102**, 3:1 2-ethoxyethanol : water, 130 °C, ii: Ethylene glycol, **101** or **102**, acetylacetone, NEt$_3$, 190 °C, iii: Ir(acac)$_3$, glycerol, 220 °C.

Method 1 is a standard route to synthesise homoleptic iridium complexes. Some reports suggested that for some systems this reaction is known to proceed in reasonable yields of ca. 40%.[44,115] However, a few groups reported that formation of homoleptic complexes *via* Ir(acac)$_3$ was low yielding.[57,116] Also, experiences from within our group[114,117,118] showed that the yields of this method varied between 2% to 85% with different ligands. The reason for this could be the different reactivity of the ligands to the iridium under the conditions applied, e.g. temperatures >220 °C, depending on the chemical structure. We, therefore, explored an alternative approach

for the synthesis of homoleptic complexes. The preparation of ligand **101** and **102** followed a procedure from within the group.[63] The formation of an intermediate, assumed to be the μ-chloro-bridged dimer **103**, was achieved *via* standard iridium cyclometalation conditions. No purification of the dimer was required, which was used for the final step. An excess (15 eq.) of acetylacetone and triethylamine were added to **101** and **103** in ethylene glycol and the mixture refluxed at 190 °C to form complex **96**. The isolated yield of **96** by this method was 40%, which is much higher than the yield reported (8%).[63] This 40% yield was repeated. During the reaction a precipitate was detected after 2 hours refluxing, which was complex **96**. The reason for using triethylamine as the base is that NEt₃ can break the iridium-acac bonds, giving way for the free coordination between ligands and the iridium centre to form the homoleptic complex. Overall, this new reaction route has less side products than Method 1.

The synthesis of complex **97** was attempted previously in our group by Tom Moore who observed a new fluorescent product by TLC, but isolation of the compound failed.[63] Therefore, the formation of complex **97** was now attempted following the new Method 2. Upon reaction of **102** with **104**, a precipitate was detected after 30 min. TLC was performed which showed a new luminescent spot in addition to the ligand **102**. The mixture was left to react overnight which resulted in disappearance of the precipitate as well as the new luminescent spot on TLC. Interestingly, luminescent materials still remained in the solution. Hence, further reactions were carried out under the same reaction conditions to try and optimise the formation of the new luminescent material. TLC analysis of the reaction mixture was performed every hour after precipitate formation. The results showed that after 30 min reaction time, two new spots formed; only one of which was luminescent. After an additional 30 min only the luminescent spot remained and further precipitate was detected. After another 6 h, the amount of precipitate was reduced. The reaction was left overnight. Again, no precipitate was present and no luminescent spot could be seen on TLC. We, therefore, assumed that the luminescent material was complex **97**. The non-luminescent spot observed after 30 min could be the *mer*-isomer. To prove this assumption, another reaction was performed and monitored every 15 min. The reaction was stopped after 1 h when. The non-luminescent spot had disappeared. The luminescent material was isolated by chromatography in 68% yield and shown by ¹H

NMR spectra and mass spectrometry to be complex **97**. Moreover, complex 97 is not stable in CDCl$_3$.

Accordingly, we can conclude that complex **97** is thermally unstable and the correct reaction time is vital for its isolation. The photophysics and device properties complex **97** are now being studied by our collaborators.

3.2.5 Theoretical Studies on Azacarbazole Complexes

As discussed above, Ir complexes of ligands which combine carbazole and pyridine units have provided promising devices with EL λ_{max} from 504 to 637 nm. These complexes are thermally stable, soluble and possess high PLQYs. As discussed in Chapter 1, thermally stable, soluble and efficient blue complexes are precious. The aim of this section is, therefore, to build up blue complexes with similar carbazole and pyridine frameworks. The general idea was to move the nitrogen atom from the pyridine ring into the carbazole ring to form the isomeric phenylazacarbazole systems **106** and **108** (see Figure 3.13).
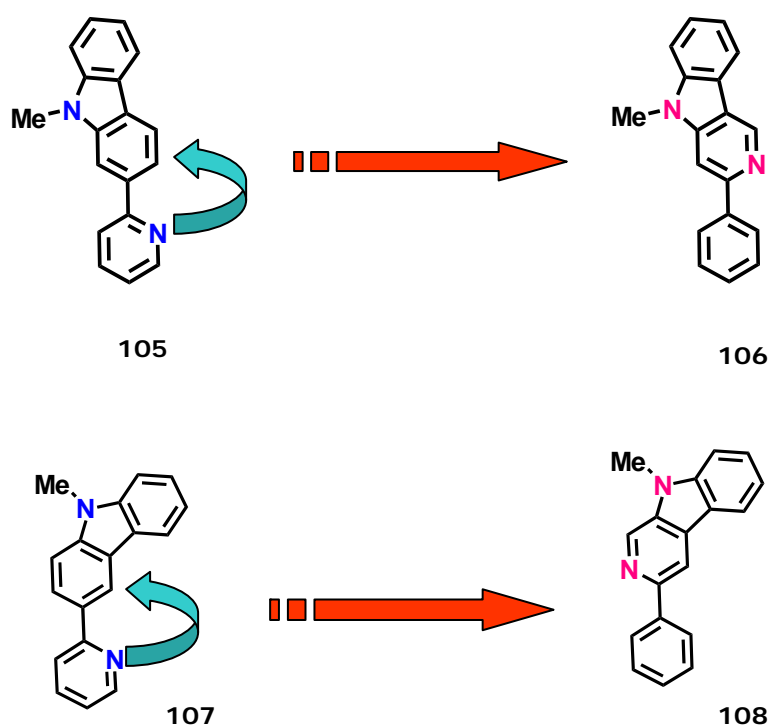
Figure 3.13. Schematic showing the relationship of structures **105** and **107** to the azacarbazole systems **106** and **108**.

Compounds **106** and **108** can be seen as derivatives of 2-phenylpyridine. It can, therefore, be expected that by attaching electron withdrawing groups on the phenyl ring a blue shift to the emission would be induced. DFT calculations on these ligands were performed using the basis set B3LYP/6-31G(d). The HOMO-LUMO levels of compounds **105** and **107** were calculated as 4.15 and 4.43 eV, respectively, which suggests that compound **107** is less conjugated than **105**. However, the singlet energies of compounds **106** and **108** are 4.43 and 4.26 eV, respectively, which does not follow the conjugation behaviour of **105** and **107**. The reason could be that moving the position of nitrogen from the pyridine ring to the carbazole affects the molecular conjugation length. DFT calculations for complexes **108-111** were performed using the basis set B3LYP/LAN2DZ. HOMO-LUMO energy diagrams are shown in Figure 3.14.
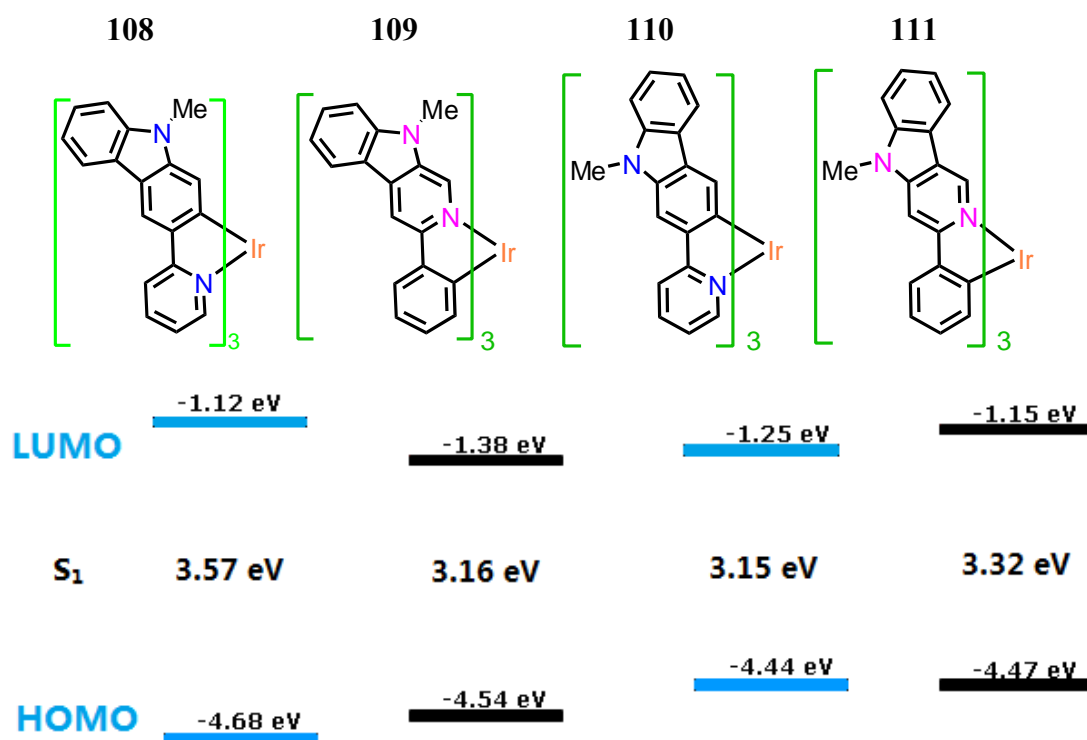
Figure 3.14. HOMO-LUMO energy diagrams of complexes **108-111**.

These diagrams show that the singlet energy of complex **109** is smaller than for the parent **108**, while complex **111** possesses a bigger singlet HOMO-LUMO gap than its parent **110**. This suggests that the size of the singlet gap of the ligand influences the singlet state of the complex. In theory, the emission of complex **111** should be deeper blue than complex **109**. Therefore, complex **111** was used as the

parent to achieve blue emission. The HOMO-LUMO orbitals of complex **111** are shown in Figure 3.15.

Figure 3.15. HOMO-LUMO orbitals of complex **111**.

Complex **111** shows a similar HOMO-LUMO distribution to Ir(ppy)₃. (Chapter 1, Figure 1.15). The majority of the HOMO orbital is located on the phenyl rings and iridium centre, which can be destabilised by attaching electron withdrawing groups to blue shift the emission. In comparison, the LUMO orbital spreads out over all ligands. Here, colour tuning modifications can be operated on the azacarbazole site. The focus in this section is directed towards colour tuning by substitution on the phenyl ring. More DFT calculations were performed on the complexes with various modifications on the phenyl ring, which were aiming to enlarge the HOMO-LUMO gap of the parent complex **110** (see Figure 3.16).

Figure 3.16. HOMO-LUMO energy diagrams of complexes **111-113**.

The HOMO-LUMO gap of complex **111** was calculated to be 3.32 eV. Introducing an electron withdrawing group on the phenyl ring increases the singlet energy gap to 3.66 eV (complex **112**). The gap of complex **113** is 3.97 eV, which is larger than of complex **108**. Therefore, complex **113** has the most potential to be a blue emitter of all the calculated species above.

3.2.6 Synthesis of Azacarbazole Complexes

The synthetic routes used for the azacarbazole derivatives have been developed by Zhang *et al*.[119,120] The formation of compound **119** is shown in Scheme 3.3. The 2-ethylhexyl side chain on the nitrogen was chosen to aid solubility of the final complex. The literature precedent had a methyl substituent on nitrogen.
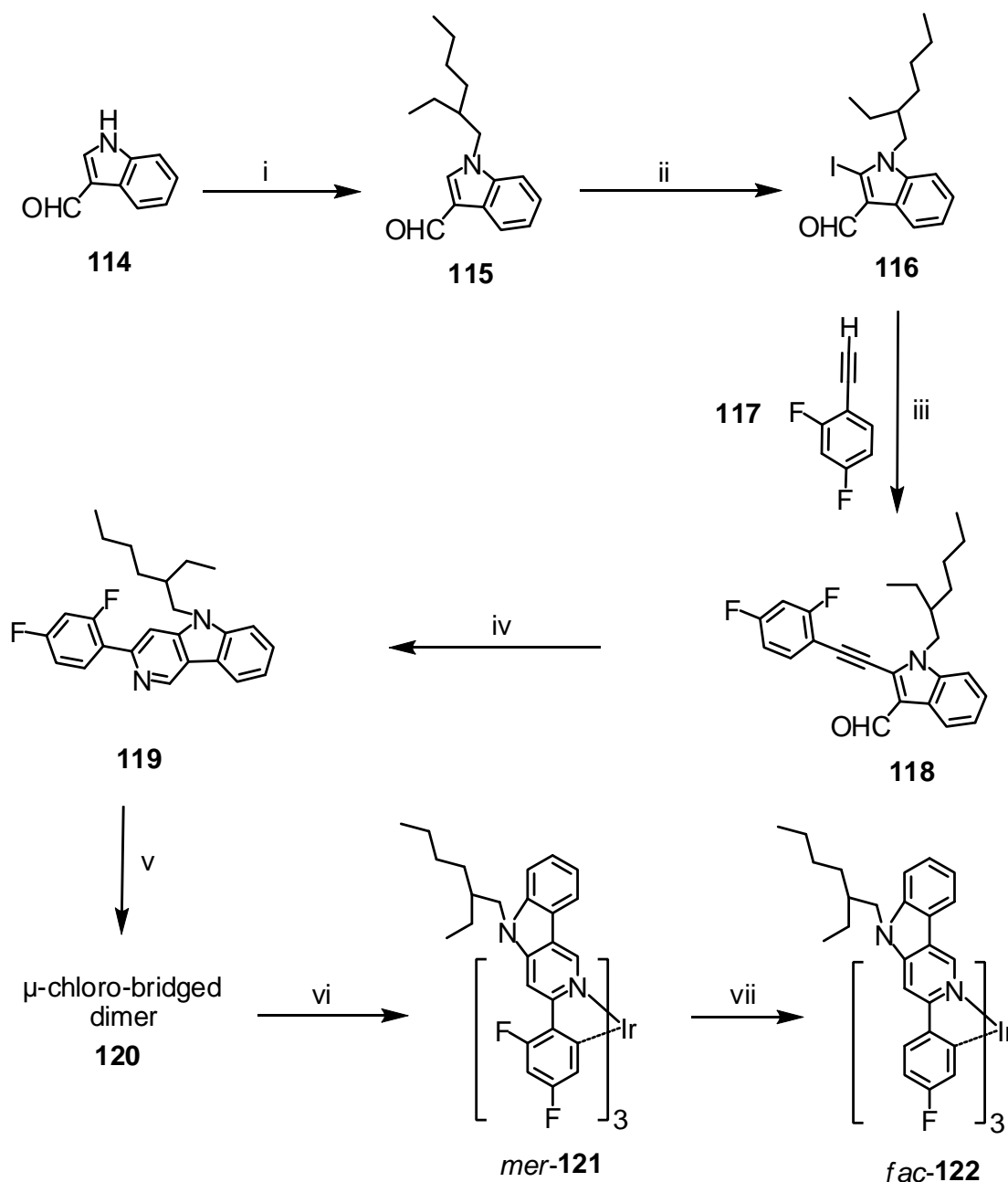
Scheme 3.3. Synthetic routes to ligand **119**, complex *mer*-**121** and *fac*-**122**: i: Acetone, K_2CO_3, 60 °C (90% yield), ii: ^nBuLi, I_2, THF, -23 °C (60% yield), iii: $Pd(PPh_3)_4$, CuI, NEt_3 and **117** (90% yield), iv: *tert*-butylamine, Toluene, 100 °C, 48 h (60% yield), v:$IrCl_3$, 2.3 eq **119**, 3:1 (2-ethoxyethanol : water), 130 °C (67% yield), vi: Ethylene glycol, **119**, acetylacetone, NEt_3, 190 °C (63% yield), vii: glycerol, 290 °C (58% yield).

The first three steps were performed in moderate to high yields of 60-90%. For the last reaction step it was claimed that for the N-Me analogue the yield was ca. 90% after reaction at 100 °C for 24 h. A reaction solvent was not stated in the paper.[120]

Heating **118** with *tert*-butylamine in toluene at 100 °C for 48 h produced the desired product **119** in 60% yield along with some unreacted starting material. Lower yields of **119** were obtained when using DMF as solvent under comparable conditions.

Compound **119** was subsequently used to form the cyclometalated iridium complex **121**. The intermediate complex, presumably the μ-bridged dimer **120** was not isolated.

The same reaction conditions were applied as for the preparation of complex **96** (Scheme 3.2) A yellow solid was collected and purified by column chromatography. Mass spectrometry confirmed the mass of the yellow compound to be consistent with complex **121** (63% yield). In contrast, the ^{1}H and ^{19}F NMR spectrum were not what we expected (Figures 3.17 and 3.18). In the aromatic region there were more than the expected 8 hydrogen peaks for the *fac*-isomer of **121** and the ^{19}F spectrum showed more than the expected two peaks. We concluded that the product was either the pure *mer*-isomer or a mixture of *fac*- and *mer*-isomers.
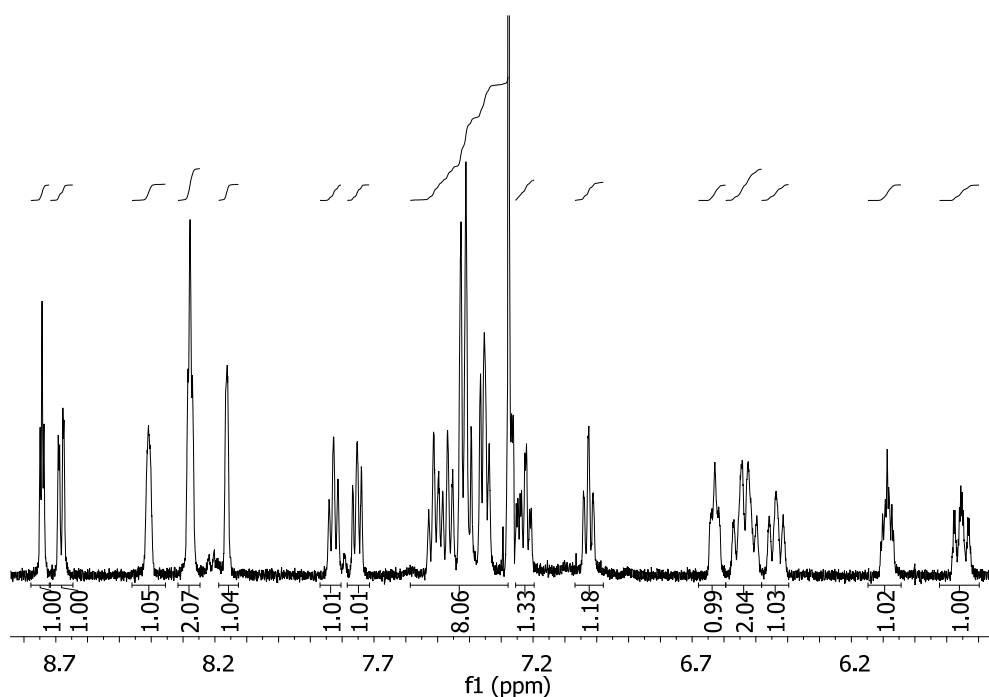
Figure 3.17. Expansion of the aromatic region of ^{1}H NMR spectrum of complex *mer*-**121** in CDCl₃
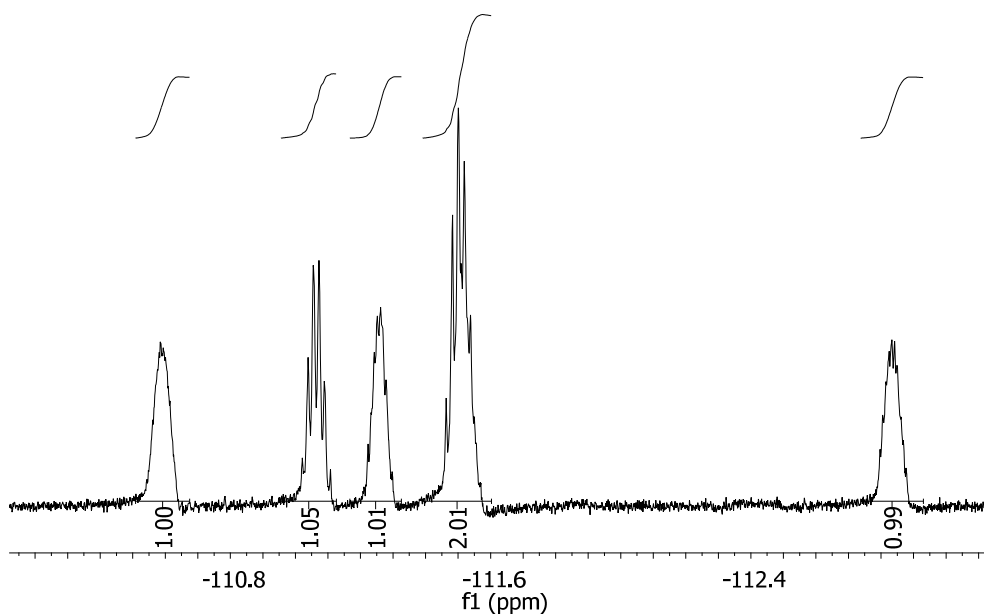
Figure 3.18. ^{19}F NMR spectrum of complex *mer*-**121** in CDCl$_3$.

HPLC analysis gave only a broad peak which did not help in the assignment. An X-ray single crystal structure was obtained which clearly showed that complex is the *mer*-isomer **121** (Figure 3.19). The iridium atom adopts a *mer*-octahedral coordination with three C,N-chelating **119** ligands. The Ir-N(1) and Ir-N(3) bonds, in trans-positions to each other, are shorter (2.063(4) and 2.048(5) Å, respectively) than the Ir-N(2) bond (2.151(6) Å) which is trans to Ir-C(3) bond of 1.975(7) Å, whereas the latter is shorter than Ir-C(1) and Ir-C(2) bonds (2.038(7) and 2.068(8) Å) which are trans to each other. These differences are in full agreement with the rules of trans-influence. In each ligand, the phenyl-azacarbazole system is planar within experimental error; one of them [N(2)∩C(2)] shows strong librational movement within its own plane. Nevertheless, the aromatic core of the molecule is reasonably ordered, and π-π stacking of these moieties define the packing motif. The channels in this motif are occupied by the intensely disordered alkyl side-chains
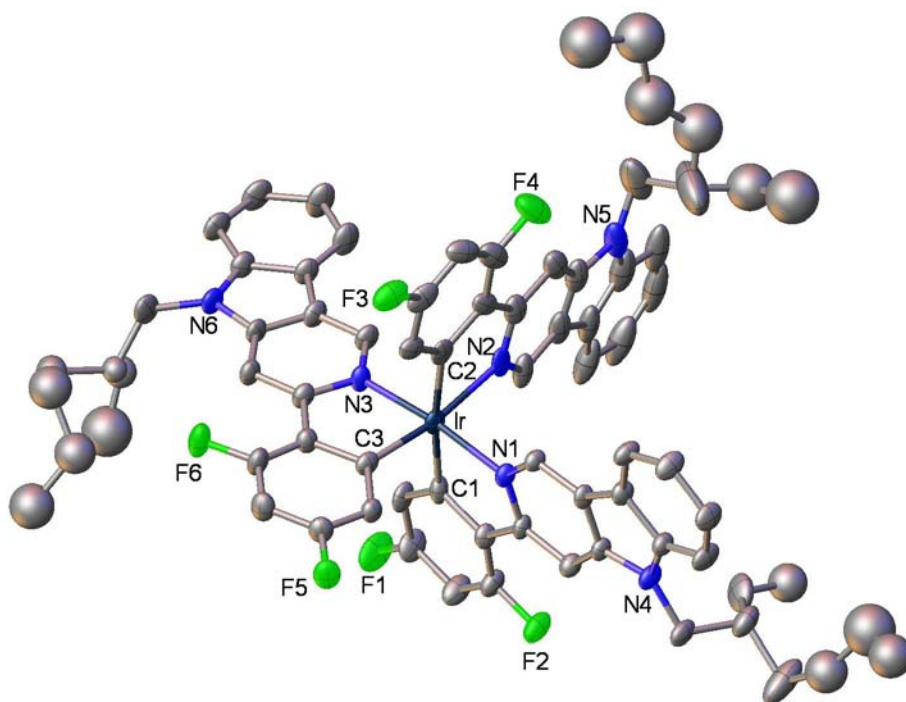
Figure 3.19. Crystal structure of complex *mer*-**121**, showing only one conformation of the disordered side-chains. Thermal ellipsoids are drawn at the 50% probability level 50% atomic displacement ellipsoids.

Indeed, the integration of the proton peaks in the aromatic region of the ^{1}H NMR spectrum matches the number of protons of the *mer*-isomer **121**. It is generally the case that *mer*-isomers are not suitable for OLED applications due to thermal instability and low emission quantum yield.[44] We then asked the question: Can the *fac*-isomer **121** be formed and isolated? Several reaction conditions were applied as shown in Table 3.2. When *mer*-isomers have been isolated in previous cases, the *fac*-isomer can sometimes be obtained by using a higher reaction temperature.[44]

Table 3.3. Different conditions used for the attempted synthesis of *fac*-**121**.

Reaction	Temperature / °C	Solvent	Base	Reagents	Reaction time/h	Products
1	190	Ethylene glycol	NEt₃	acac, **119**, **120**	18	*mer*-**121**
2	190	Ethylene glycol	NEt₃	acac, **119**, **120**	40	*mer*-**121**
3	250	glycerol	NEt₃	acac, **119**, **120**	18	*mer*-**121**
4	265	glycerol	NEt₃	acac, **119**, **120**	18	*mer*-**121**
5	270	glycerol	NEt₃	acac, **119**, **120**	18	*mer*-**121** + *fac*-**122**
6	290	glycerol	NEt₃	acac, **119**, **120**	18	*mer*-**121** + *fac*-**122**
7	290	glycerol	NEt₃	*mer*-**121**	72	*fac*-**122**
8	290	glycerol	none	*mer*-**121**	72	*fac*-**122**
9	290	glycerol	K₂CO₃	**119**, Ir(acac)₃	24	none

Under the conditions of reactions 1 and 2, the *mer*-**121** was the major product and no *fac*-isomer was detected. Increasing the reaction temperature from 190 to 265 °C, as well as changing the solvent from ethylene glycol to glycerol, also did not produce the *fac*-**121** isomer. Interestingly, when the temperature was further increased to ≥270 °C, as in reaction 5, a new complex was detected. If the reaction temperature was increased still further, e.g. 290 °C, the new complex became the major product. At that point it was unclear if that meant that complex *mer*-**121** was thermally unstable or base sensitive. Therefore, two more reactions (entries 7 and 8, Table 3.3)

were carried out to identify the possible reason for the formation of the new complex. Results showed that complex *mer*-**121** was indeed thermally unstable.

After isolation of the new complex, the ^{1}H and ^{19}F NMR spectra established that a fluorine atom had been lost and the complex was identified as *fac*-**122** (58% yield). The ^{1}H and ^{19}F NMR spectrum of *fac*-**122** (Figure 3.20 and 3.21) confirmed that all three of the less sterically hindered fluorine atoms in complex *mer*-**121** were lost during the synthesis (reactions 5-9). Loss of fluorine in the iridium complex FIrpic has been observed previously by Sivasubramaniam *et al.*[99] They analysed the complex after thermal evaporation by mass spectrometry. New peaks were found which indicated loss of fluorine atoms. However, they did not isolate any defluorinated complexes and their data were consistent with a mixture of defluorinated products.
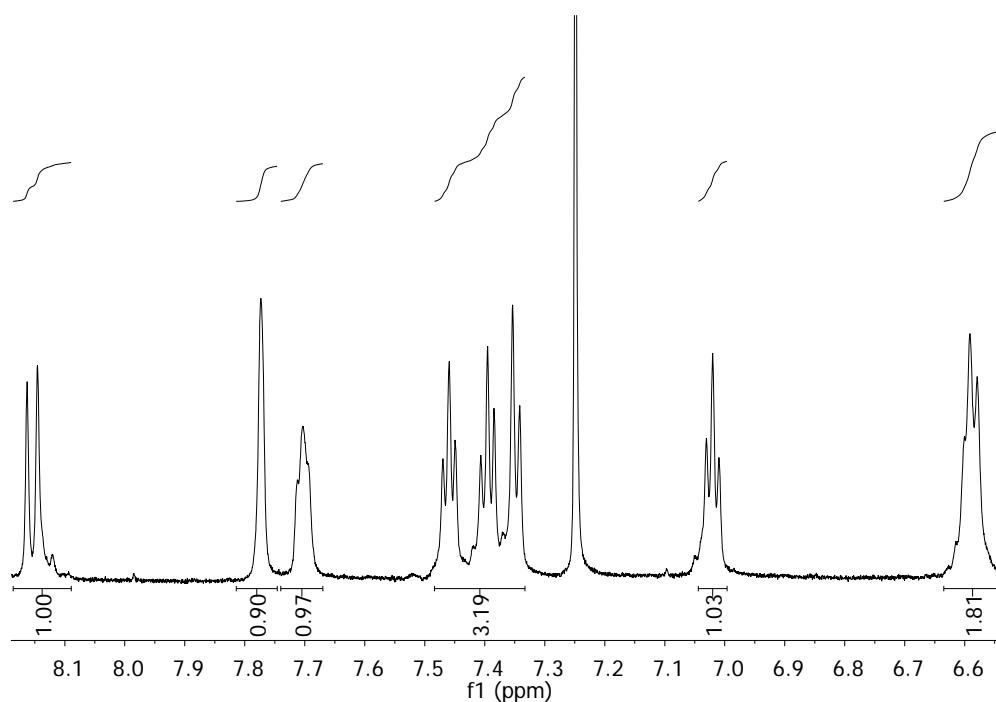
Figure 3.20. Expansion of the aromatic region of ^{1}H NMR spectrum of complex *fac*-**122** in CDCl$_3$.
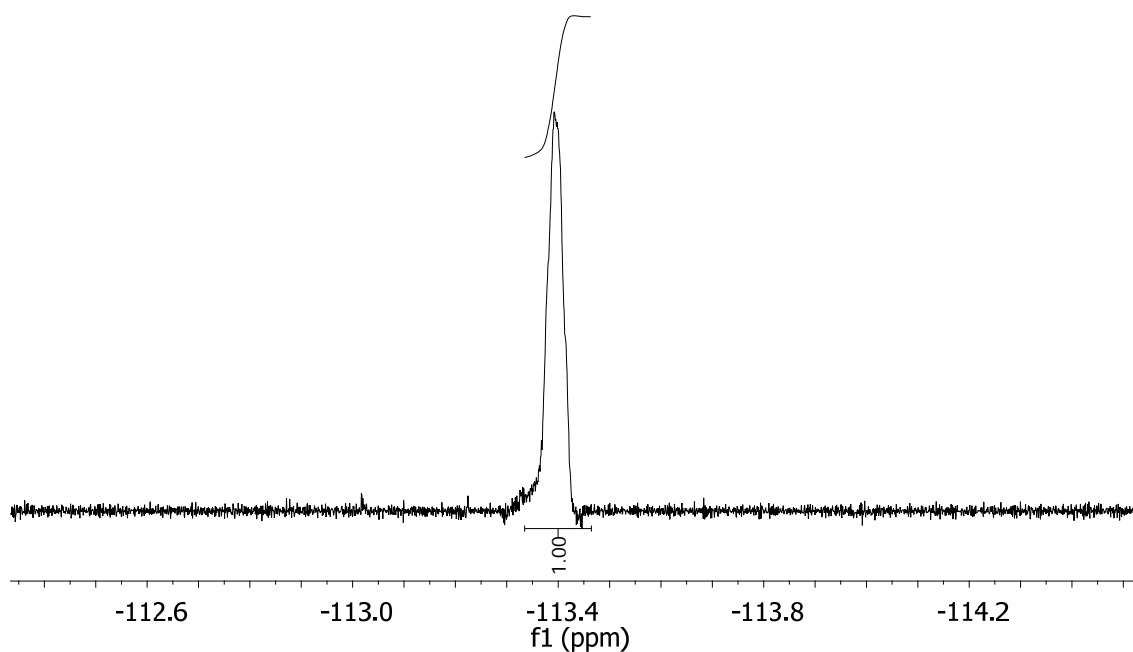
Figure 3.21. ^{19}F NMR spectrum of complex *fac*-**122**.

mer-**121** was not stable enough to survive at high temperature ($\geq$270 $^{\circ}$C). Therefore, photochemical conversion experiments were carried out by Robert M. Edkins in the Chemistry Department of Durham University. *mer*-**121** was dissolved in CD$_2$Cl$_2$ (0.5 ml) in a Young's tap NMR tube and degassed three times by freeze-pump-thaw techniques. The sample was irradiated by two LEDs at 365 nm for a total period of 5 h with intermittent agitation. The conversion was monitored by ^{19}F NMR until the isomerisation was judged to have reached completion. *fac*-**121** complex was comfirmed and characterised by ^{1}H, ^{19}F NMR and mass spectrometry. In the aromatic region of the ^{1}H NMR spectrum there were the expected 8 hydrogen peaks for the *fac*-**121** (see Figure 3.22) and the ^{19}F spectrum showed the expected two peaks (see Figure 3.23). Hence, *fac*-**121** can be obtained photochemically not thermally.
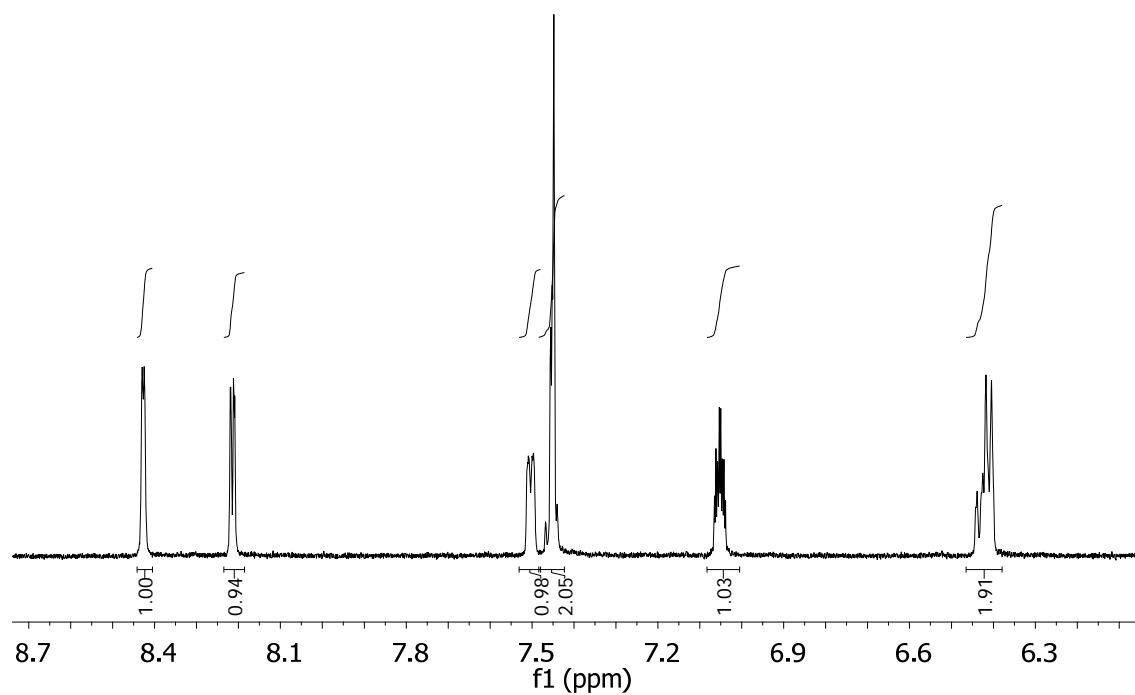
Figure 3.22. Expansion of the aromatic region of ^{1}H NMR spectrum of complex *fac*-**121** in CD$_2$Cl$_2$.
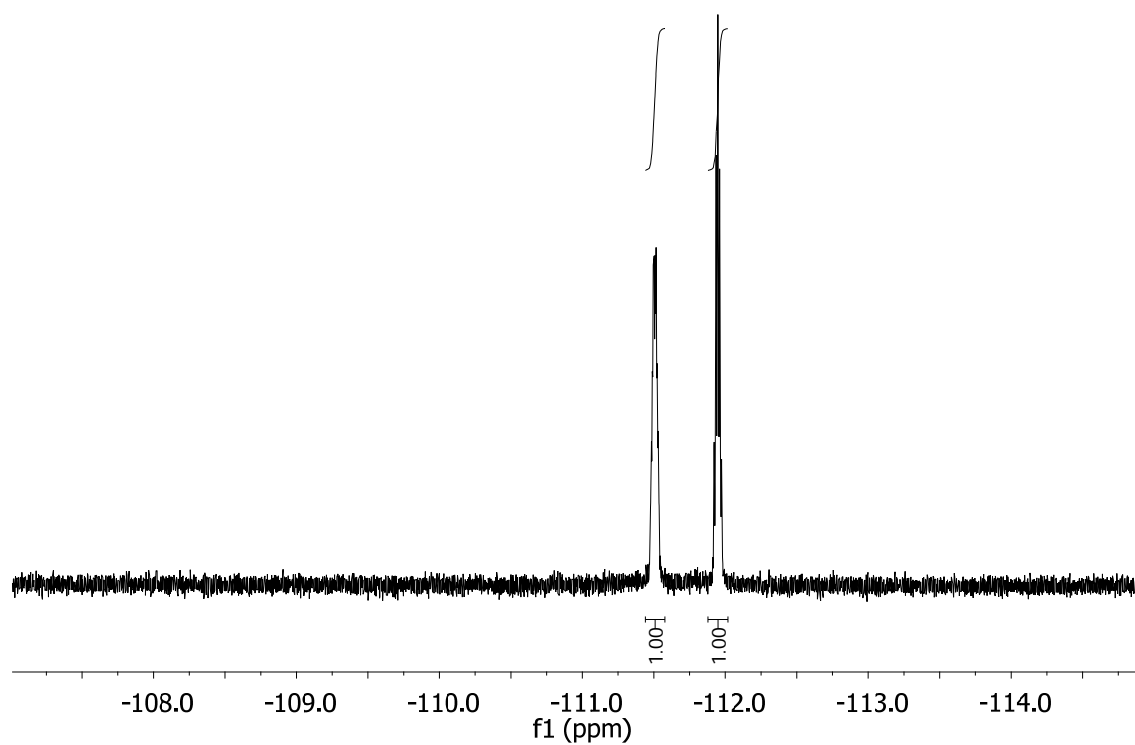
Figure 3.23. ^{19}F NMR spectrum of complex *fac*-**121**.

From the previous experiments, we knew that thermally-induced defluorination occurred, leading to conversion of *mer*-**121** to *fac*-**122**. We then asked the question: how is the *fac*-**122** being formed? So, a thermal conversion of *fac*-**121** to *fac*-**122** was carried out in glycerol at 290 °C. No defluorination was observed by either ^{19}F NMR or by mass spectrometry. Starting material *fac*-**121** was recovered (see Scheme 3.3).

mer-**121**   *fac*-**121**   *fac*-**122**
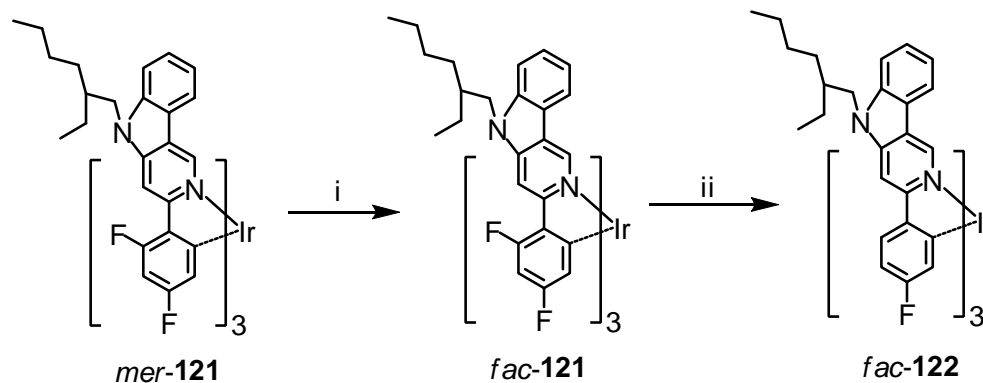
Scheme 3.3. Synthetic route to complex *fac*-**121**: i: UV light, CD$_2$Cl$_2$, 5 h (100% conversion), ii: glycerol, 290 °C, 48 h.

In conclusion, the *mer*-**121** isomer is an unusually stable *mer*-isomer. The *fac*-isomer could not be isolated due to the fluorine cleavage at higher temperatures which led to *fac*-**122** being formed. However, *fac*-**121** was succssfully synthesised by photochemical conversion. Meanwhile, the formation of *fac*-**122** was a subject of defluorination of *mer*-**121** instead of *fac*-**121**.

3.2.7 Photophysical Properties

The absorption and emission spectra of complexes *mer*-**121**, *fac*-**121** and *fac*-**122** in dichloromethane solution are shown in Figure 3.24.
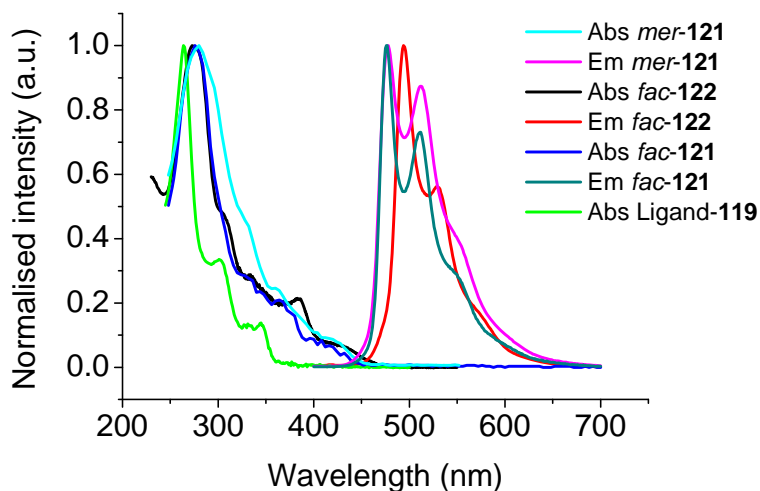
Figure 3.24. Normalised absorption and emission spectra of complexes *mer*-**121**, *fac*-**121** and *fac*-**122** and absorption spectra of ligand **119** in DCM solution.

all complexes show strong absorption bands in the 270-300 nm region which are assigned[110] to ligand-centered $\pi-\pi^*$ transitions. The complexes show absorption bands with lower extinction in the range 325-450 nm which are ascribed to singlet and triplet metal-to-ligand charge-transfer (^{1}MLCT and ^{3}MLCT) states, following literature precedents and the calculations of Hay.[111] It is not possible to distinguish the singlet and triplet absorptions, although the precedent is that the lower energy bands are predominantly triplet in character. Luminescence is observed for *mer*-**121** (λ_{max}^{em} 477(sh), 510 nm in DCM), *fac*-**121** (λ_{max}^{em} 476(sh), 511 nm in DCM) and *fac*-**122** (λ_{max}^{em} 494, 529 nm in DCM) which is visible as blue, blue and green emission, respectively. The results have shown that more electron withdrawing groups on the phenyl ring blue shift the emission. Measured photophysical and electrochemical data of *mer*-**121**, *fac*-**121** and *fac*-**122** are shown in Table 3.4. The PLQY and lifetime of *mer*-**121** cannot be obtained accurately, due to formation of *fac*-**121** triggered by UV light.

The thermally induced defluorination of *mer*-**121** is interesting and merits further discussion as fluorinated aryl groups are widely used to shift the emission of cyclometalated Ir complexes to the blue.[44,121] However, Holmes *et al.* recognised that there may be drawbacks to this strategy as the large electronegativity of fluorine could make the ligands electrochemically reactive potentially reducing device lifetimes.[122]

Table 3.4. Absorption (λ_{max}), emission (λ_{max}), PLQY, lifetime and oxidation potential of complexes *mer*-**121**, *fac*-**121** and *fac*-**122**.

Complex	λ_{max}^{abs}/nm	λ_{max}^{PL}/nm	PLQY, Φ_{PL}	Lifetime at RT/µs	$E^{ox}_{1/2}$ /V^a
mer-**121**	278	477	None	None	0.65
fac-**121**	280	476	0.31	4.5	0.70
fac-**122**	272	494	0.22	4.3	0.60

^{a} Values are reported vs. $FcMe_{10}/FcMe_{10}^+$

The electrochemical properties of *mer*-**121**, *fac*-**121** and *fac*-1**22** were studied by cyclic voltammetry in dichloromethane solution which established that each complex has a quasi-reversible single-wave oxidation ascribed to a metal-centred Ir^{3+}/Ir^4 in dichloromethane vs. $FcMe_{10}/FcMe_{10}^+$ (see Figure 3.25 and 3.26).
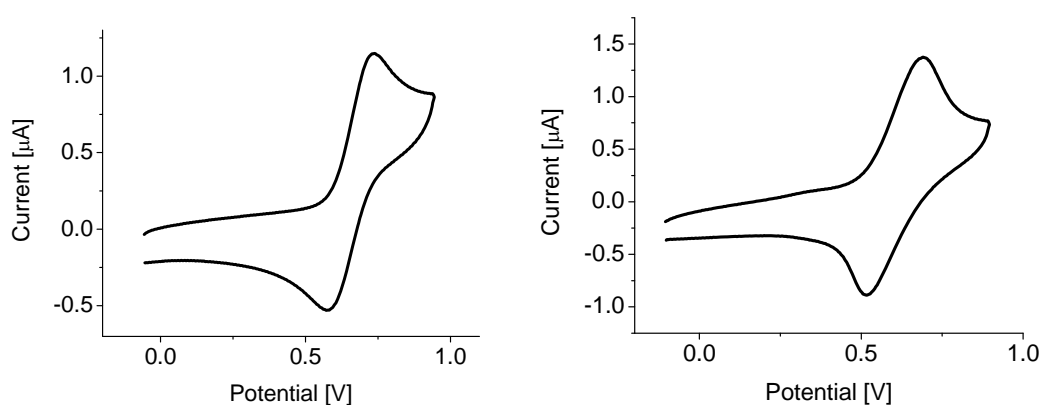
Figure 3.25. Cyclic voltammogram of complex *mer*-**121** (left) and *fac*-**122** (right) in DCM.
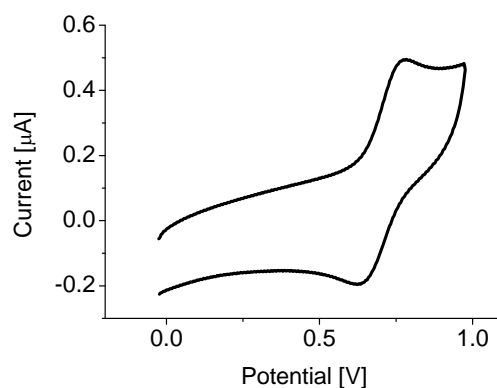
Figure 3.26. Cyclic voltammogram of complex *fac*-**121** in DCM.

3.3 Conclusions

The work described in this chapter showed that steric factors on the cyclometalling ligand can lead to organoiridium complexes with novel and unexpected structures. Reactions of OXDs derivatives, bearing *ortho*-alkyl substituents on one of the phenyl rings, with iridium(III) chloride under standard conditions did not lead to the expected μ-dichloro-bridged diiridium C^N ligand complexes. Instead, the dinuclear complexes **86-88** and the mononuclear complex **89** were isolated and characterised crystallographically. The concept of metal chelation to sterically-hindered OXDs derivatives can now be exploited in the synthesis of other luminescent transition metal-ligand systems which may possess unusual structural properties. Luminescence for **90** (λ_{max}^{em} 482(sh), 518 nm) and **91** (λ_{max}^{em} 471, 496 nm) and **92** (λ_{max}^{em} 462 nm) is observed in DCM at room temperature in the green (**90**) and blue-green regions (**91** and **92**). Complexes **90-92** are phosphorescent at low temperature, with triplet lifetimes of 4.2-5.7 μs at 77 K. The scope of metal chelation to sterically-hindered ligands can now be explored in other luminescent complexes with different metal-ligand combinations in the search for complexes with unusual structural properties.

Building on previous work in our group, reaction conditions for complexes **96** and **97** were optimised to give significantly increased yields of ca. 40%. The reaction time was found to be a crucial factor to successfully synthesise complex **97**.

Complex *mer*-**121** was obtained under various conditions. The interesting defluorinated complex *fac*-**122** was isolated and characterised. This suggests that the less sterically protected fluorine atoms are more labile at high temperatures. *fac*-**121** was succssfully synthesised by photochemical conversion method. Meanwhile, the formation of *fac*-**122** was a subject of defluorination of *mer*-**121** instead of *fac*-**121**. The formation of *fac*-**122** was proved that defluorination can be occoured under certain conditions.Luminescence is observed for *mer*-**121** (λ_{max}^{em} 477(sh), 510 nm in DCM), *fac*-**121** (λ_{max}^{em} 476(sh), 511 nm in DCM) and *fac*-**122** *(*λ_{max}^{em} 494, 529 nm in DCM) at room temperature which is visible as blue and green emission, respectively. The triplet lifetimes of complexes *fac*-**121** and *fac*-**122** are 4.5 and 4.3 µs at room temperature, respectively. Unfortunately, the lifetime of *mer*-**121** could not be obtained.

Chapter 4 – High Triplet Electron-Transporting Materials

4.1 Introduction

Electron-transporting (ET) materials, which conduct electrons from the cathode to the emissive zone of the device, play an important role in OLED applications. Small molecule devices require vacuum-deposition processes, which offer the advantages of the controllability of thickness, surface smoothness and the flexibility of changing the underlying layers. However, the biggest limitation for small molecule devices is that ca. 95% of the sample is lost during the device fabrication process. Therefore, polymeric phosphorescent light-emitting devices have been considered to be one of the most promising candidates for future applications due to their low-cost large-area production by solution processing techniques.

A popular subject for device engineers has been the question of how the known ET materials influence device performances. On the other hand, there is less work on discovering novel ET materials. Recent progress on ET materials for small molecule and polymeric devices will be discussed below. A selection of electron-transporting small molecules with their triplet energy levels is shown in Figure 4.1.

11 PBD (T_1= 2.5 eV)[85] **12** OXD-7 (T_1= 2.7 eV)[84] **15** TPBI (T_1= 2.6 eV)[123] (chemical structure see Chapter 1, Figure 1.5)
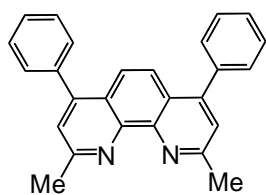
123 BCP (T_1= 2.5 eV)[124]
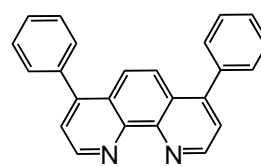
124 BPhen (T_1= 2.5 eV)[125]

2,9-Dimethyl-4,7-diphenyl-1,10-phenanthroline   4,7-Diphenyl-1,10-phenanthroline

Figure 4.1. Chemical structure of different ET materials

The advantage of small molecule devices is that the thickness of the layer can be controlled which provides a good platform to study different ET materials in directly comparable device structures. The properties of electron mobility and triplet energy of ET materials are the main attractions for device engineers to investigate.

Chopra *et al.* have demonstrated the effect on balancing the charge injection by varying the ET materials.[97] **123** (BCP), **124** (BPhen) and Tris[3-(3-pyridyl)mesityl]borane (3TPYMB) have been studied using the same device structures, which is shown in Figure 4.2.
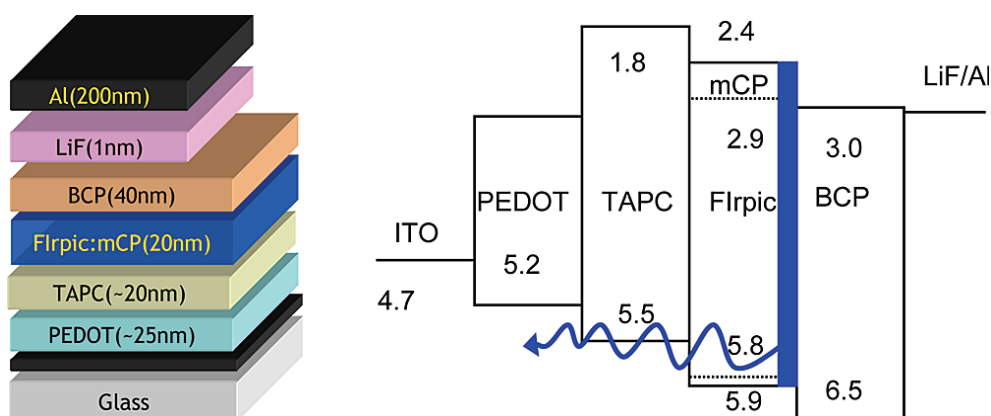
Figure 4.2. Device structure used to compare BCP, BPhen and 3TPYMB. Hole-transporting layer: PEDOT: PSS; TAPC: 1,1-Bis[(di-4-tolylamino)phenyl]cyclohexane; mCP: 3,5′-*N,N′*-Dicarbazolebenzene. Emissive zone; **48** (Flrpic). All the numbers are in eV.

The thickness of the ET layer (on the top of the Flrpic: mCP layer) for all three ET materials was the same, which allowed direct studies on how the electron mobility and triplet energy of different ET materials influence the device efficiency. The electron mobilities of BCP[126], BPhen[127] and 3TPYMB[128] were found to be 5.5×10^{-6}, 5.2×10^{-4} and 5.0×10^{-5} cm^2 V^{-1} s^{-1} and triplet energies are 2.5, 2.5 and 3.0 eV, respectively. The current efficiency of devices for these materials can be seen in Figure 4.3.
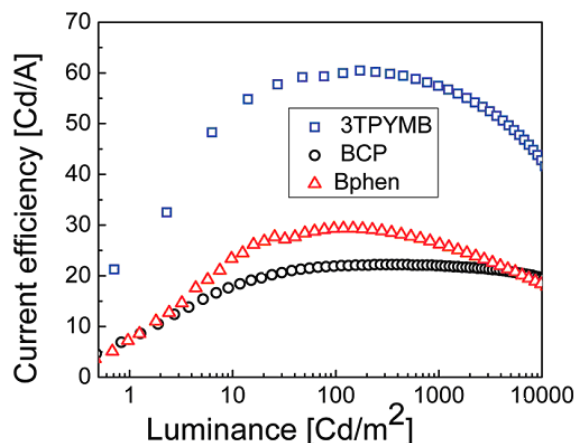
Figure 4.3. Current efficiencies of BCP, BPhen and 3TPYMB in devices

The recombination zone was located at the EML/ETL interface. Therefore, the low triplet energy of BCP and BPhen partially quenched the Flrpic (T_1= 2.62 eV) emission,[129] which led to lower current efficiencies than for 3TPYMB. The BCP device had the lowest efficiency, which agreed with its lowest mobility and low triplet energy. The electron mobility of BPhen was substantially higher than those of the other two ET materials, but the device efficiency was slightly higher than that of the BCP device due to its low triplet energy compared to 3TPYMB. Moreover, the 3TPYMB device showed the highest efficiency compared to the other two devices. In conclusion, the high triplet energy of ET materials was crucial for high current efficiency devices in these studies.

Lee *et al.* have reported that the electron mobility of the ETLs plays a dominant role in determining the device efficiency.[130] They compared BCP, BPhen and OXD-7. The current efficiencies of devices for these materials are shown in Figure 4.4.
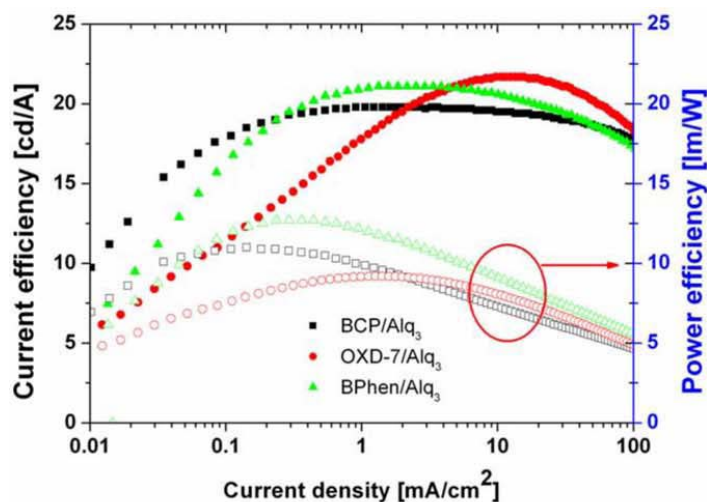
Figure 4.4. Current efficiencies of BCP, BPhen and OXD-7 in devices (Alq$_3$= Tris(8-hydroxyquinoline)aluminium). Luminous efficiency (solid symbols) and power efficiency (open symbols) of the devices. Device architecture: ITO/PEDOT:PSS/TAPC/mCP:3% Flrpic/BCP or BPhen or OXD-7/Alq$_3$/LiF/Al.

The triplet energy of OXD-7 was determined as 2.7 eV, significantly higher than that of BCP (2.5 eV) and BPhen (2.5 eV). The device efficiency of OXD-7 was found to be 21.7 cd/A, only slightly better than BPhen (21.1 cd/A) and BCP (19.8 cd/A). Meanwhile, the electron mobility of OXD-7 was 2.5×10^{-4} cm^2 V^{-1} s^{-1}, which was similar to BPhen.[131] They concluded that no noticeable correlation between the triplet energy of the ET materials and the device efficiency existed.

Interestingly, Lo *et al.* have demonstrated that excitons formed near the EML:ETL interface and were quenched by the low triplet energy ETL. The triplet energies of ET materials TPBI and PBD were 2.6 and 2.5 eV, respectively, which were lower than the emission energy of the deep blue Ir complex. Therefore, the device efficiencies were low for both of these two ET materials.[65]

Polymer phosphorescent light-emitting devices (PPLEDs) have recently started to attract broad attention, as a result of their potentially low cost and the ability to fabricate large area panels. For PPLEDs, the polymer host should have high triplet energy in order to confine the excitons on the phosphorescent emissive zone. PVK has been widely used as a host because of its high triplet energy. TPBI, PBD and OXD-7 are very popular ET materials. There are two different approaches to employ ET materials to provide stable and efficient polymeric devices. A total solution processable approach is to mix ET material, dopant and polymer host in one solution

and then spin-coat the mixture onto the ITO. The great advantage is that there is almost no waste of materials. The other approach is to deposit the ET materials on top of the emissive layer (spin-coated) under high vacuum conditions. With this approach, a considerable amount of ET materials would be lost during the device fabrication.

Yang *et al.* have studied the influence of PBD and OXD-7 as ET materials in polymeric devices. Devices were fabricated by spin-coating the mixture of ET materials, Flrpic and PVK onto ITO, followed by deposition of the CsF/Al cathode. The results suggested that the device incorporating OXD-7 was better than PBD due to triplet quenching in the PBD device. The triplet energy of Flrpic is higher than PBD, but OXD-7 leads to an energy transfer from the complex to PBD.[132]

In 2009, Lee *et al.* demonstrated the effect of triplet energy of ET materials within the PVK host.[98] They fabricated the same device as Yang *et al.*, and obtained consistent results. Moreover, they carried out another approach to separate the ET materials from the host to form an electron-transporting layer. Luminous efficiencies of OXD-7 and PBD are show in Figure 4.5 and 4.6, respectively.
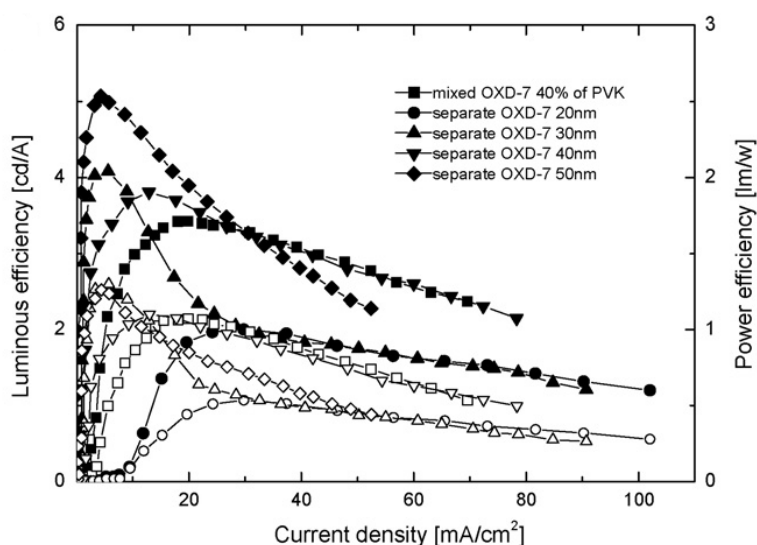
Figure 4.5. Performance of PVK:OXD-7 (40 wt.%) based single-layer devices and PVK based two-layer devices with four different thicknesses of a separate OXD-7 layer, both with 10% FIrpic in the emissive layer. Luminous efficiency (solid symbols) and power efficiency (open symbols) of the devices. (from ref. 98)

For a PVK device with 40% incorporation of OXD-7, the luminous efficiency of the optimised single layer device was 3.7 cd/A, which is slightly lower than the device with 50 nm of OXD-7 layer (the thicknesses of the emissive layers are the same).

Unlike the OXD-7 device, the single layer PBD device showed a low luminous efficiency, merely 0.4 cd/A (see Figure 4.6). Surprisingly, the luminous efficiency of the device with 50 nm of PBD layer was about five times higher than a single layer device. This confirmed that significant back-energy transfer from Flrpic to PBD occurs in single layer but not in double layer devices.[98]

In this Chapter, twisted 2,5-diaryl-1,3,4-oxadiazoles have been designed for use as high triplet electron-transporting materials. Theoretical, photophysical and device studies have been carried out.
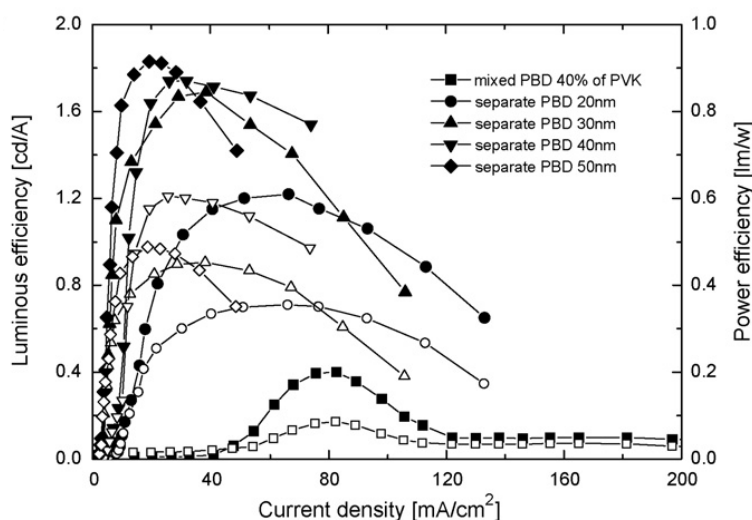
Figure 4.6. Performance of PVK:PBD (40 wt.%) based single-layer devices and PVK-based two-layer devices with four different thicknesses of separate PBD layer, both with 10% FIrpic in the emissive layer. Luminous efficiency (solid symbols) and power efficiency (open symbols) of the devices.

4.2 Results and Discussion

4.2.1 Synthesis of 2,5-Diaryl-1,3,4-oxadiazole Derivatives

The synthesis of the twisted diaryloxadiazole compounds was already discussed in Chapter 2. The twisted diaryloxadiazoles **126, 129** and **130** were synthesised in moderate to high yields (43-65%) (see Scheme 4.1 and 4.2).
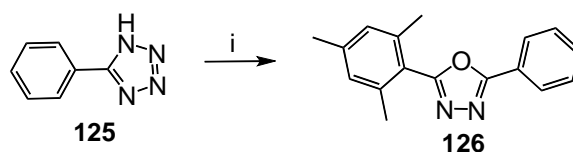
Scheme 4.1. Synthetic route to **126**: i: 2,4,6-trimethylbenzoyl chloride, pyridine, reflux (85% yield).
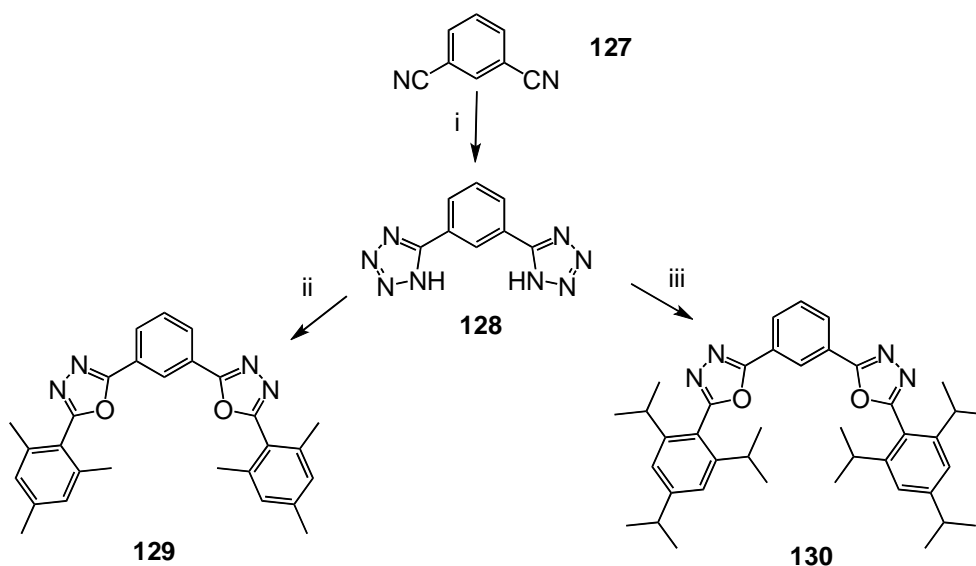
Scheme 4.2. Synthetic route to **129-130**: i: NaN$_3$, NH$_4$Cl, DMF, 105 ^{o}C (56% yield) ii: 2,4,6-trimethylbenzoyl chloride, pyridine, reflux (73% yield), iii: 2,4,6-triisopropylbenzoyl chloride, pyridine, reflux (62% yield).

4.2.2 Theoretical and Photophysical Studies

The HOMO-LUMO calculations were optimised using the B3LYP method with the 6-31G(d) atomic basis set 32. The HOMO-LUMO distributions and orbital

energies of compounds **126**, **129**, **130** and OXD-7 are shown in Figure 4.7, respectively.

LUMO -1.43 eV   **126**   HOMO -6.04 eV

LUMO -1.75 eV   **129**   HOMO -6.11 eV

LUMO -1.69 eV   **130**   HOMO -6.34 eV
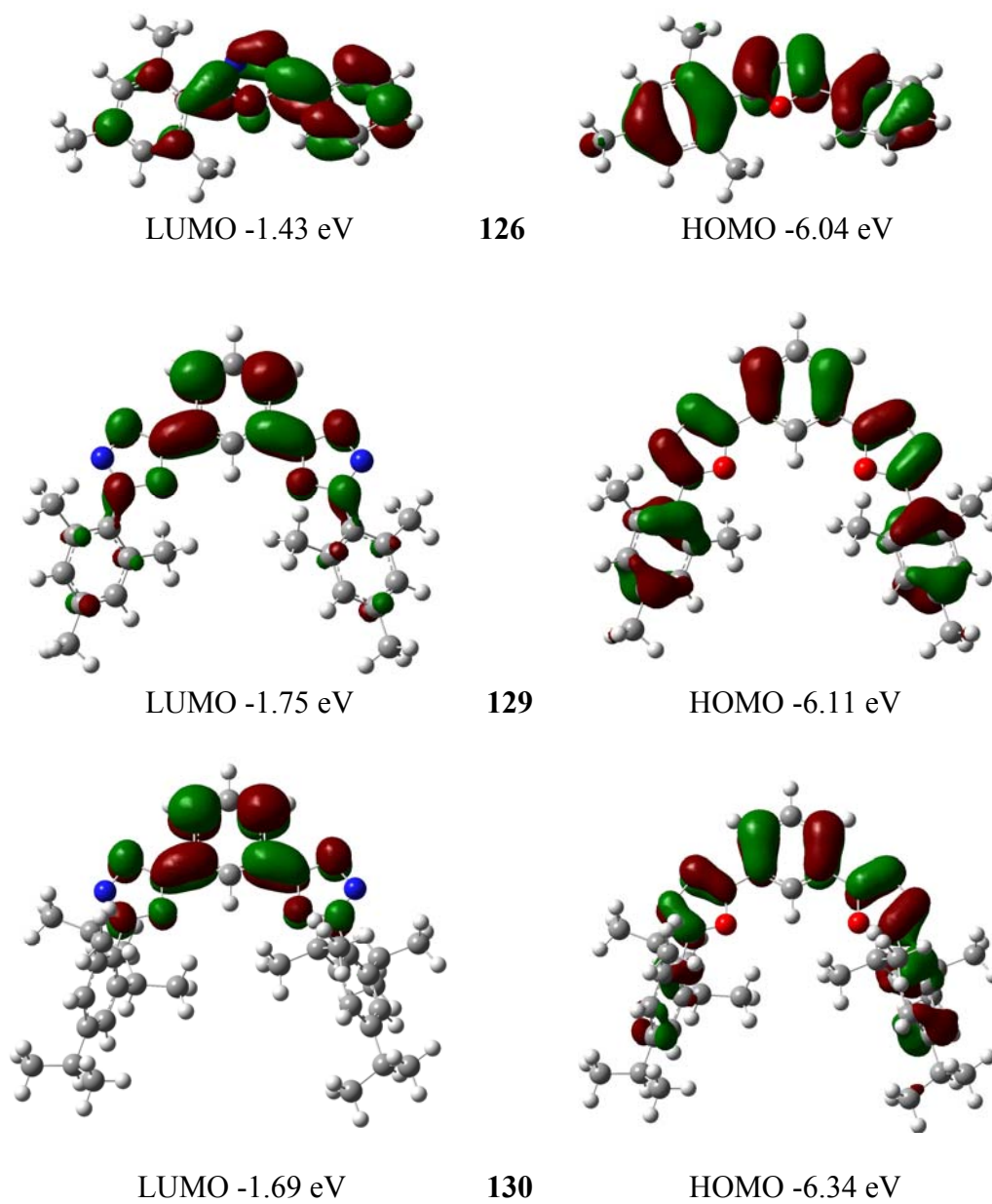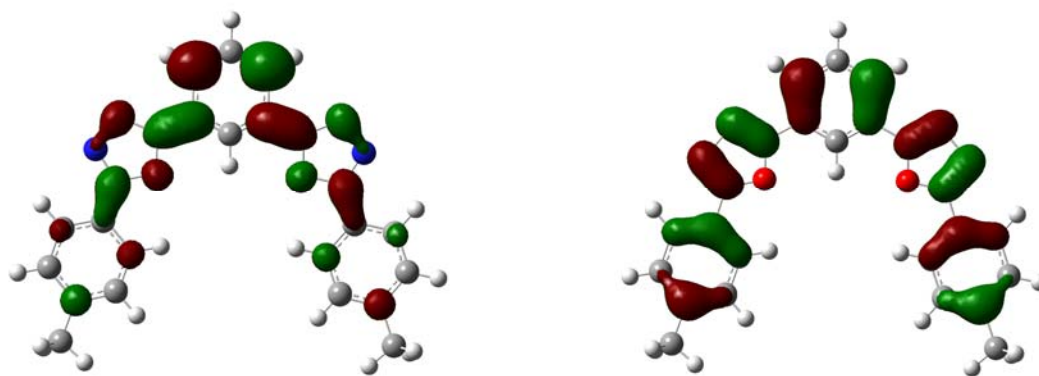
LUMO -1.83 eV   **OXD-7**   HOMO -6.10 eV

Figure 4.7. HOMO-LUMO orbital maps of compounds **126**, **129**, **130** and OXD-7.

The HOMO orbitals of compounds **126**, **129** and OXD-7 are quite similar, which subsequently also leads to similar HOMO energy levels (ca. -6.10 eV). Interestingly, the HOMO level of compound **130** is ca. -6.34 eV, which is a much lower value than for the other oxadiazole derivatives. On the other hand, the LUMO density on the terminal phenyl ring decreases from OXD-7 to **130**. Twisting the terminal phenyl moiety reduces the π-conjugation on the aryloxadiazole fragment. Hence, the LUMO levels of compounds **126**, **129**, **130** are higher than that of OXD-7.
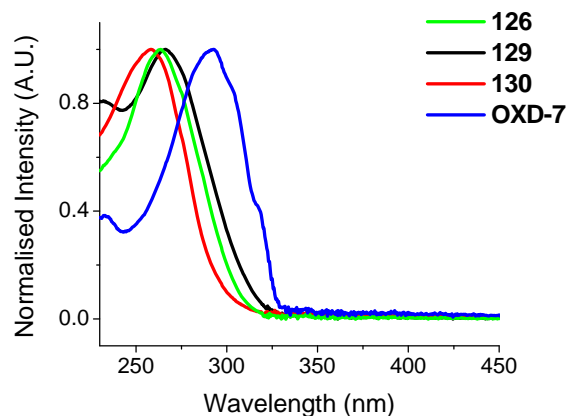
Figure 4.8. Normalised absorption spectra of compounds **126**, **129**, **130** and OXD-7 in DCM solution.

Table 4.1. Absorption band (λ_{max}) and calculated HOMO, LUMO and S_1 energy levels of compounds OXD-7, **126**, **129**, and **130**.

Compound	Absorption λ_{max} (nm)	LUMO (eV)	HOMO (eV)	$S_1(E_{HOMO}-E_{LUMO})$ (eV)
OXD-7	293	-1.83	-6.10	4.27
126	263	-1.43	-6.04	4.61
129	266	-1.75	-6.11	4.36
130	258	-1.69	-6.34	4.65

The absorption of **129** and **130** is shifted to lower wavelengths compared to OXD-7, Figure 4.8 and Table 4.1, due to the reduced π-conjugation between the terminal phenyl ring and the oxadiazole unit. It thus indicates that **129** and **130** both possess a larger HOMO-LUMO gap than OXD-7, which agrees with the calculated results. On the other hand, compound **126** possesses a relatively large HOMO-LUMO gap, which is due to its smaller aromatic system and the twisting effect at the terminal phenyl ring.

Triplet measurements of compounds **126**, **129** and **130** were carried out by Vygintas Jankus in the Physics Department at Durham University. Unfortunately, no reliable spectra could be obtained as a result of the limited capability of the equipment used for measuring high energy compounds. However, the concept of increasing the triplet energy of the molecule by interrupting the π-conjugation between the terminal phenyl ring and the oxadiazole moiety was proven in Chapter 2. Therefore, it is reasonable to assume that compounds **129** and **130** should possess a higher triplet energy than OXD-7.
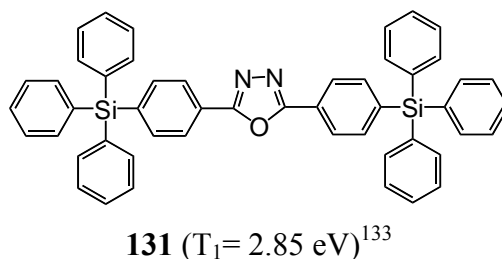
131 (T₁= 2.85 eV)[133]

Figure 4.9. Structure of compound **131.**

The triplet energy of compound **131** was determined as 2.85 eV.[133] The triphenylsilanyl group does not affect the electronic structure of the diaryloxadiazole. We, therefore, believe that the triplet energy of 2,5-diphenyl-1,3,4-oxadiazoles to be ca. 2.85 eV. Also, the triplet energy of compound **126** should be higher than that of compound **131**, due to the twisting effect between the terminal phenyl group and the oxadiazole unit.

4.2.3 Device Studies

The device fabrications of high triplet ET materials were performed by Gareth C. Griffiths in the Physics Department of Durham University. The device structure used was ITO/PVKH/2% Flrpic and 30 wt% ET compound (the concentration was with respect to PVKL) doped in PVKL/Ba:Al. (PVKH= high molecular weight PVK; M_W= 110K g/mol); PVKL= low molecular weight PVK; M_W= 40-70K g/mol). Devices were fabricated by spin-coating a 81 nm thick layer of a blend containing PVKL, the blue-emitting FIrpic and electron transporter onto indium tin oxide substrates covered with a 25 nm thick layer of PVKH. The samples were annealed at 80 °C for 30 min before deposition of the Ba/Al cathode. The diodes were characterised by the data shown in Figure 4.10.

The electroluminescence (EL) spectra shown in Figure 4.10a are dominated by the emission of Flrpic (472 nm). For all four devices a turn on voltage of 10 to 11 V (0.1 cd/m^2) was obtained, which led to similar brightness (Figure 4.10b and 4.10d). In comparison to devices with OXD-7, the device containing compound **126** exhibits a slightly higher turn on voltage. This can be partially attributed to the fact that OXD-7 is a better electron transporter because of its lower LUMO level compared to compound **126**. The device efficiency of the four devices was similar (Figure 4.10f), all around 1.0 cd/A, which suggested that compounds **126**, **129** and **130** are as good as OXD-7 as electron-transporting molecules. Device structures could probably be optimised further to achieve better results, e.g. changes in layer thickness and concentration of the ET material.
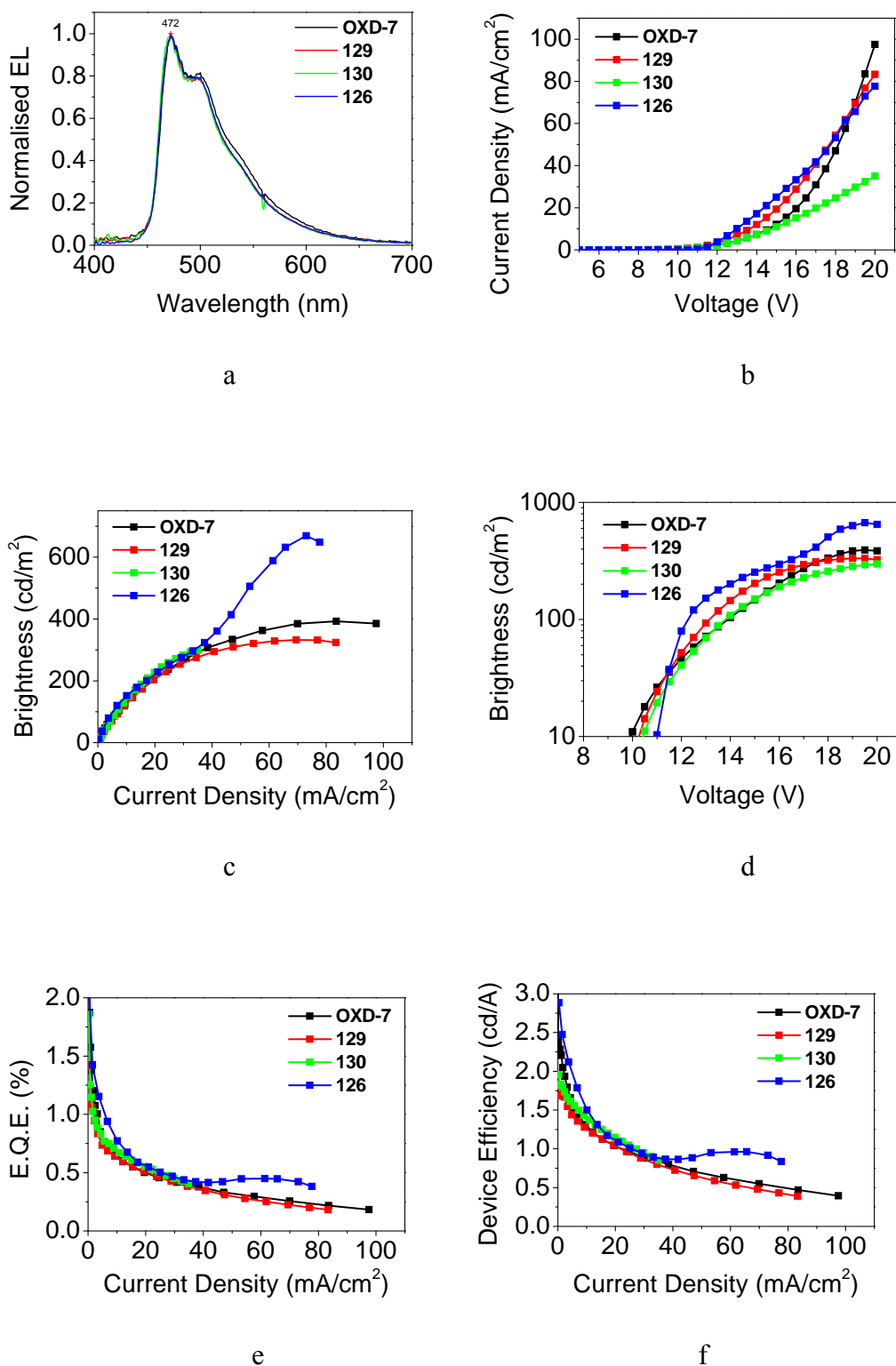
Figure 4.10. Device characteristics of compounds **126** (blue), **129** (red), **130** (green) and OXD-7 (black).

Furthermore, exciplex studies were carried out to understand how these four oxadiazole-based electron-transporting materials influence the device performances. An exciplex can be defined as a complex formed by the interaction of an excited molecular unit with a ground state counterpart of a different molecule. In our research, we were looking for the interaction between the excited state of PVK and the ground state of the various ET-materials.

Device structures were similar to the devices examined above; the only difference was that no heavy metal complexes were employed in the device. This is due to the fact that heavy metal complexes would strongly harvest excitons leading to difficulties in observing exciplex formation. The device characteristics are shown in Figure 4.11.

a

b

c

d

e

f

g
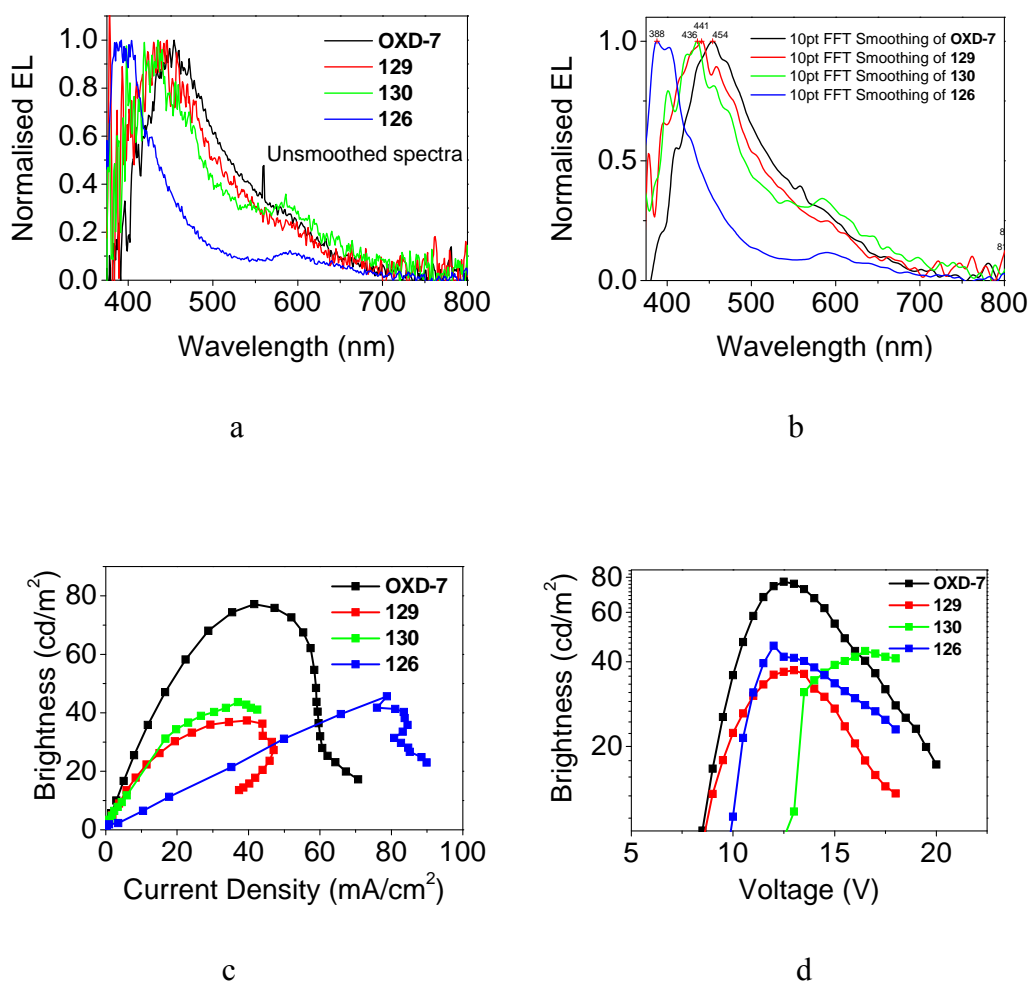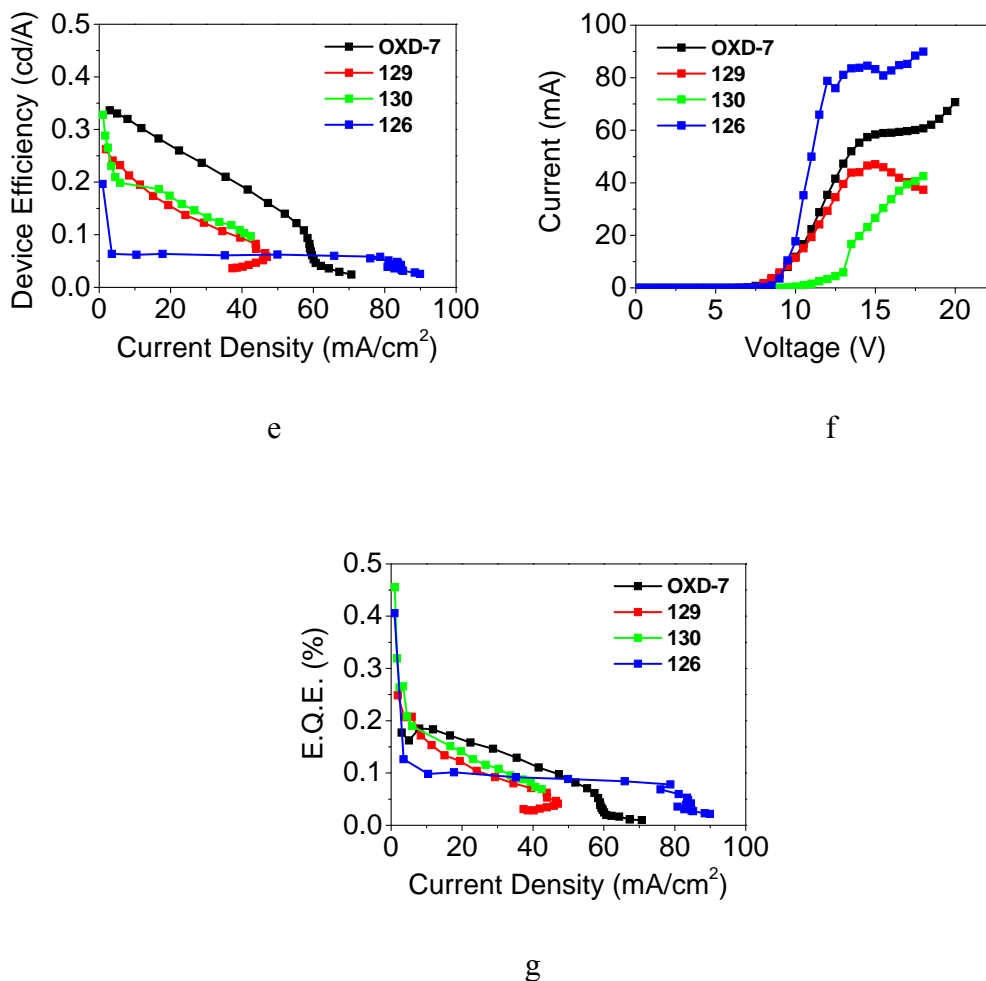
Figure 4.11. Exciplex studies on different oxadiazole-based ET-materials, compounds **126** (blue), **129** (red), **130** (green) and OXD-7 (black).

Figures 4.11a and 4.11b show the EL spectra of PVK with different ET materials. The emission of all four devices analysed was not very intense because of only weak interactions between PVK and the electron transporter. The maximum emission of the PVK:OXD-7 device was observed at 454 nm, which showed the reddest emission of all the devices. In comparison, the emission maximum of the PVK:**130** device was 18 nm bluer, while the emission maximum of PVK:**129** was at 441 nm, which was intermediate between the OXD-7 and compound **129** devices.

Surprisingly, the emission from the device containing compound **126** was found to be the emission of PVK. Therefore, a model of exciplex formation is introduced (Figure 4.12) to explain the emission wavelengths of the different devices. We propose that a HOMO electron in PVK is excited to the LUMO orbital to form an exciton. The exciton subsequently interacts with the ground state of the electron

transporter, which has a lower LUMO energy level. Finally, the exciton relaxes back to the HOMO orbital of PVK and emits light with lower energy. The model of exciplex formation shown in Figure 4.12 demonstrates that the shorter emissive wavelength from compounds **129** and **130** compared to the emission of OXD-7, is due to their higher LUMO energy levels. On the other hand, compound **126** does not form an exciplex with PVK, because **126** possesses a higher LUMO energy level than PVK. We believe that the exciplex emission studies are an alternative way to assess the LUMO energy levels of a series of compounds.
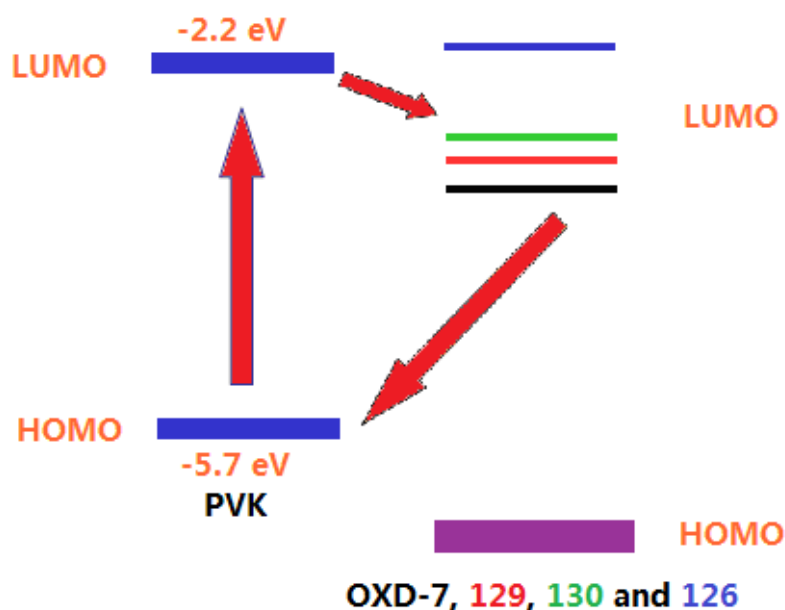
Figure 4.12. Model of exciplex formation with different electron transporter devices, assuming that the HOMO orbitals for these ET materials are similar and LUMO orbitals of **OXD-7** (black), compound **129** (red), **130** (green) and **126** (blue).

The turn-on voltage of the OXD-7 device is ca 8.3 V, which is very similar to that of compound **129** (Figure 4.11d), while the OXD-7 device has the highest efficiency (about 0.3 cd/A, shown in Figure 4.11e). In contrast, compound **130** possesses the highest turn-on voltage and lower device efficiency than OXD-7. In summary, the LUMO levels of compound **129** and **130** are higher than OXD-7, leading to higher turn-on voltages and poorer device efficiencies.

4.3 Conclusions

An efficient electron-transporting molecule must possess two important properties, which are high triplet energy and good electron mobility. High triplet energy is to prevent energy back transfer from emitter. Electron mobility is to identify how well a molecule can transport electrons.

In this chapter, ET materials with high singlet and triplet energy levels have been studied. Absorption spectra and computational results demonstrate that the singlet level can be raised by twisting the terminal phenyl group of the oxadiazole derived materials. Unfortunately, we were not able to measure the triplet energies of these materials due to the limited capability of the equipment. But, we believe that the triplet energies of twisted OXD compounds are higher than commercial OXD-7. In addition, exciplex studies demonstrated that OXD-7 has the lowest LUMO level among the four compounds studied, and overall OXD-7 is a better electron-transporting material. Meanwhile, compound **126** did not interact with the excited state of PVK, leading to undetectable sufficient energy transfer from PVK. This is potentially a great advantage for OLED device applications.

Chapter 5 – High Triplet Polymeric Host Materials

5.1 Introduction

Phosphorescent polymer light-emitting diodes (PPLEDs) have attracted great attention due to solution processability and potential 100% internal quantum efficiency.[134-137] Also, PPLEDs are more suitable for the preparation of large area displays. All three primary colours are necessary for applications. However, the performance of blue PPLEDs devices is far behind that of green and red PPLEDs, due to the limited availability of appropriate polymeric host materials.[138-140]

Non-conjugated PVK (Poly 9-vinylcarbazole) is a universal polymeric host for phosphorescent dopants.[139,141] The advantages of PVK as a host are its high triplet energy, [142] high molecular weight, wide band gap[143] and commercial availablity. However, PVK transports only holes and requires the use of additional ET materials, leading to possible phase separation during device operation. Also, PVK's high resistivity leads to rather high operating voltages of the resulting devices. The triplet energy levels of host materials are a crucial factor for efficient devices. When the triplet energy of the host is higher than the dopant, it can prevent back energy transfer from emitter to the host, thus leading to efficient devices. The reported triplet energy of PVK is 3.0[142] and/or 2.5[144] eV. The actual triplet value of PVK still remains an open question. A small emission peak at about 600 nm was observed in EL spectra from PVK, which has been attributed to the triplet excimers.[145] Therefore, energy back transfer from dopants to hosts may occur during device operation, resulting in lowering the device efficiency. However, blue PPLEDs typically use PVK as hosts. The best reported result for a PVK device with **48** (Flrpic) (blue emitter) was 22 cd/A[146] in the device structure: ITO/PEDOT:PSS/10% Flrpic and 40 wt% OXD-7 doped in host PVK/CsF:Al.

Conjugated polymers have been demonstrated to be excellent hosts for red and green PPLEDs with low driving voltage and high device efficiency.[137] However, they are not suitable for use in blue PPLEDs due to their low triplet energy levels (E_T).[38] Therefore, it is a challenge to develop conjugated polymer hosts with high triplet energy. Liu *et al.* reported a poly(*meta*-phenylene) derivative **132** with triplet energy of 2.64 eV as a conjugated polymer host for high efficiency blue PPLEDs.[147] They

claimed that polymer **132** possesses the highest triplet energy within all known conjugated polymers. The maximum device efficiency was found to be 4.7 cd/A with Flrpic as the emitter.[147] Furthermore, a wide band gap (E_S = 3.26 eV) polymer **38** has been developed by Fei *et al.*[41] and it was used as the host for iridium complexes; the maximum luminous efficiency for blue devices was 3.4 cd/A. The triplet energy of polymer **38** was not reported in the paper. Other examples are noted in Chapter 1, Section 1.5.2.

132   **38**
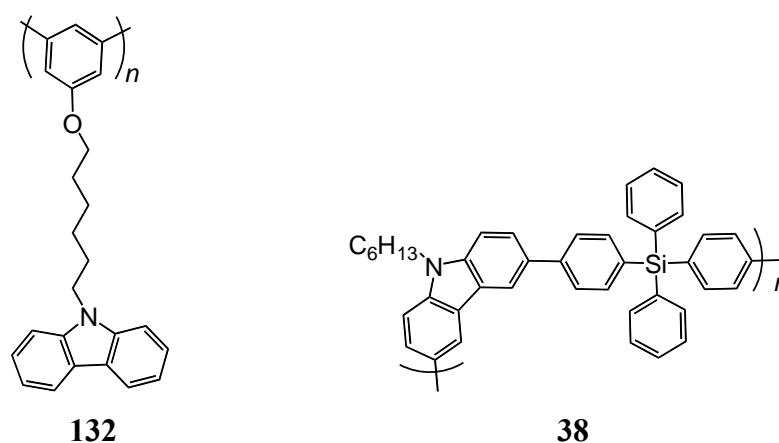
Figure 5.1. Structure of polymer **132** and **38**.

In this chapter, new high triplet energy carbazole-based host polymers have been designed for blue PPLEDs. The reasons for choosing carbazole have been discussed in Chapter 1. Our study sheds new light on designing high triplet polymers and we have demonstrated a strategy for achieving a high triplet energy by interrupting the conjugation in the polymer backbone.

5.2 Results and Discussion

5.2.1 Syntheses of Carbazole Based Polymers

The aim of this work is to understand how the triplet energy level of a polymer can be influenced by varying the polymer structure. The non-conjugated polymer **133** has been designed for possessing high triplet energy to host deep blue phosphorescent emitters. As discussed in Chapter 1, conjugated polymers possess low triplet energy and non-conjugated polymers are less conductive. To achieve a better balance, semi-

conjugated polymer **134** was designed for possessing relatively high triplet energy and reasonable conductivity. The synthesis of these two polymers is reported in this chapter (see Figure 5.2). The *n*-octyl and *t*-butyl substituents in **133** and **134**, respectively, were attached to provide solubility of the polymers in organic solvents.

133   **134**
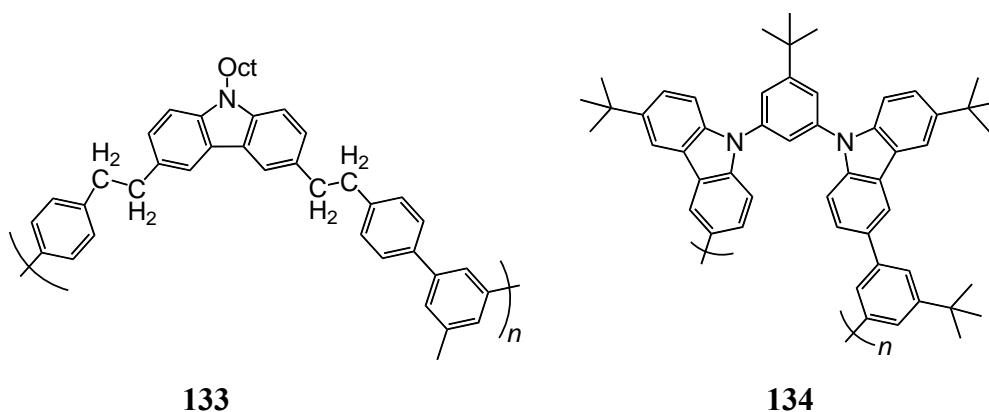
Figure 5.2. Structures of polymers **133** and **134**.

The synthesis of polymer **133** is shown in Scheme 5.1. All reactions proceeded in high yields. *N*-*n*-octylcarbazole **135** was di-iodinated to yield compound **136**[148] in 74% yield. Compound **137** was obtained from **136** under standard Sonogashira cross-coupling conditions[149] in high yield (ca. 90%). Deprotection of the trimethylsilyl groups to synthesise compound **138** was a high yielding step and under mild conditions. Compound **138** was converted into **139** by two-fold Sonogashira reaction with 4-iodophenylboronic acid pinacol ester. Finally, hydrogenation[150] of compound **139** was applied to form **140** (yield 85%).

Compounds **140** and 3,5-dibromotoluene were purified serveral times by recrystallistion before their use in the polymerisation reaction to obtain **133**. The purity of the monomer is a crucial factor for synthesising high molecular weight polymers. The purity of compounds **140** and 3,5-dibromotoluene were 99.4% and 100%, respectively, as judged by HPLC analysis. Polymer **133** was synthesised through Suzuki cross-coupling[151] and obtained in high yield (83%). The work up involved pouring the reaction mixture into vigorously stirring methanol solution, resulting in a grey precipitate of the crude polymer which was dissolved in toluene and was mixed with a solution of sodium diethyldithiocarbamate trihydrate to scavenge palladium residues, for 18 h at 60 °C. The product was precipitated from methanol to give a white solid which was isolated, redissolved in toluene and re-

precipitated from methanol again. Finally, pure white polymer **133** was obtained. Polymer **133** is soluble in common organic solvents, such as toluene, chloroform, and THF. The weight-average molecular weight (Mw) is 40,000 Da with a polydispersity index (PDI) of 3.4, as determined by gel permeation chromatography using a poly(styrene) standard.
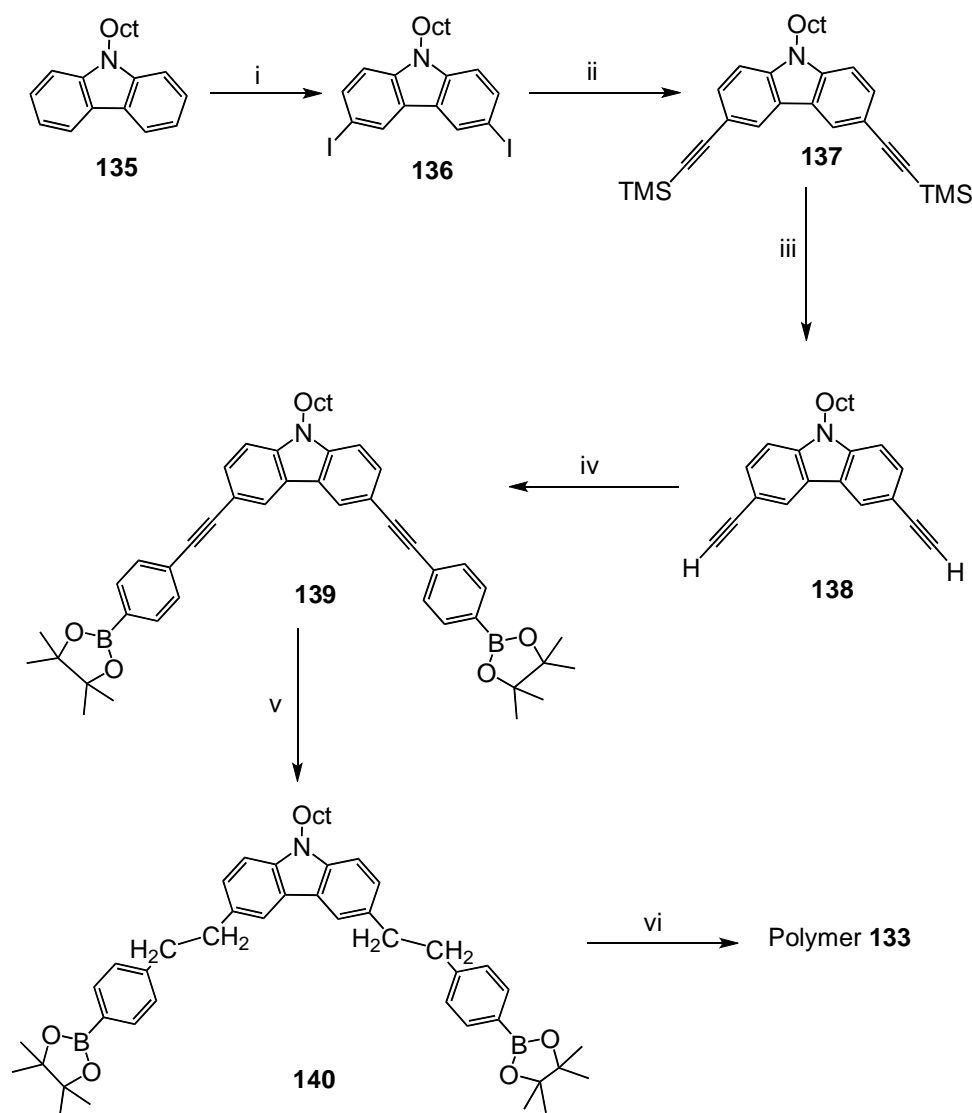
Scheme 5.1. Synthetic route to compound **140** and polymer **133**: i: N-Iodosuccinimide, DCM, AcOH (74% yield), ii: Trimethylsilylacetylene, Pd(PPh$_3$)$_4$, NEt$_3$, CuI (95% yield), iii: K$_2$CO$_3$, MeOH (91% yield), iv: 4-Iodophenylboronic acid pinacol ester, Pd(PPh$_3$)$_4$, NEt$_3$, CuI (92% yield), v: EtOAc, H$_2$, 5% Pd(0) in charcoal (85% yield), vi: Pd(P(*o*-Tol)$_3$)$_2$Cl$_2$, 20wt% tetraethylammonium hydroxide, 3,5-Dibromotoluene, Toluene, 115 °C (83% yield).
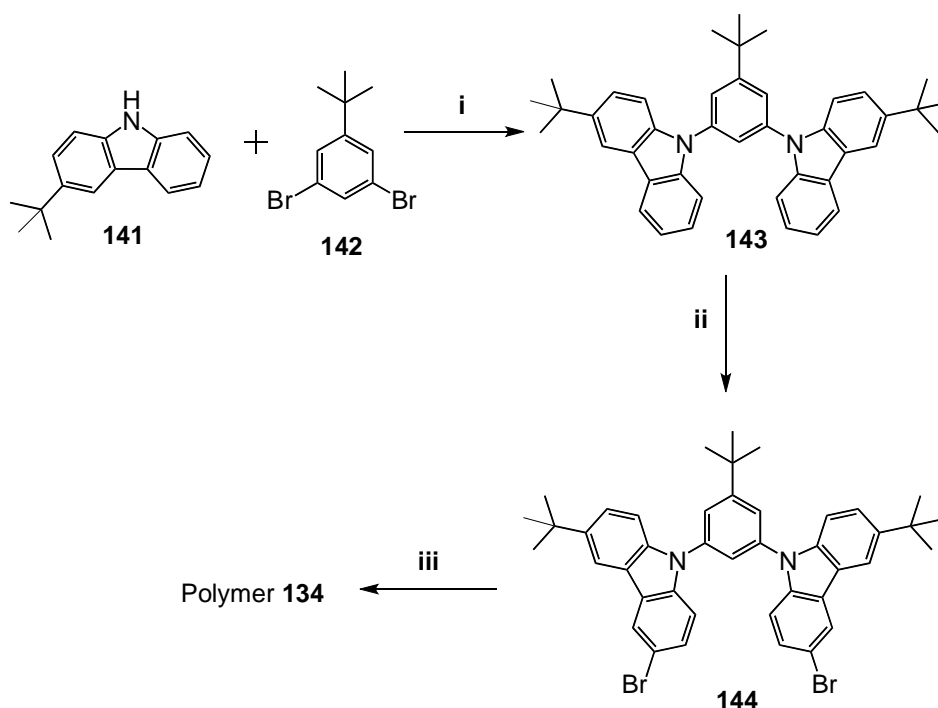
Scheme 5.2. Synthetic route to compound **144** and polymer **134**: i: Pd(OAc)$_2$, Johnphos, NaO^{t}Bu, Toluene, 115 ^{o}C (90% yield), ii: NBS, THF (94% yield), iii: Pd(P(o-Tol)$_3$)$_2$Cl$_2$, 20wt% tetraethylammonium hydroxide, 2,2'-[5-*tert*-Butyl-1,3-phenylene]bis[4,4,5,5-tetramethyl-1,3,2-dioxaborolane], Toluene, 115 ^{o}C (62% yield).

The synthesis of polymer **134** starting from **141** is shown in Scheme 5.2. All reactions proceeded in high yields. Compound **143** was synthesised by a two-fold C-N palladium catalysed cross-coupling reaction in high yield (90%). Bromination of **143** using NBS gave compound **144** as a white solid in 94% yield.

Polymer **134** was obtained from **144** in modest yield (62%) using 2,2'-[5-*tert*-Butyl-1,3-phenylene]bis[4,4,5,5-tetramethyl-1,3,2-dioxaborolane] as co-monomer. The work up and purification of polymer **134** reaction was the same as for polymer **133**. Polymer **134** is also soluble in common organic solvents, such as toluene, chloroform, and THF. The Mw is low, 7,286 Da with a PDI of 1.7, as determined by gel permeation chromatography using a poly(styrene) standard. The low molecular weight of polymer **134** could be due to low purity of the monomers.

5.2.2 Photophysical Studies of Carbazole Based Polymers

The absorption and fluorescence spectra of polymers **133**, **134** and PVK were obtained in DCM solution (Figure 5.3). The λ_{max} values of absorption for all three polymers are not clear. Therefore, the red edge values of the absorption spectra of polymer **133**, **134** and PVK were recorded, which are in the range of 363-370 nm. The PVK emission spectrum is broader than that of polymers **133** and **134**. Also, the peak of emission is less clear. Hence, the singlet energy levels of all three polymers were compared with each other based on the values taken from the onset and peaks of the fluorescence spectra. The fluorescence spectrum of PVK gives the onset at 327 nm (see Figure 5.3), which was used to calculate the E_S to be 3.79 eV. The onset fluorescence values of polymers **133** and **134** are 3.58 and 3.60 eV, respectively, which are remarkably lower than that of PVK. In contrast, the peak values of all three polymers' fluorescence spectra are similar (ca. 3.37 eV). The structure of the fluorescence spectra of polymer **133** and **134** are more defined. Hence, the values of the band gaps of polymers **133** and **134** were obtained from the peak values. Table 5.1 shows the values of offset absorption, onset emission and peak phosphorescence of polymers **133**, **134** and PVK.
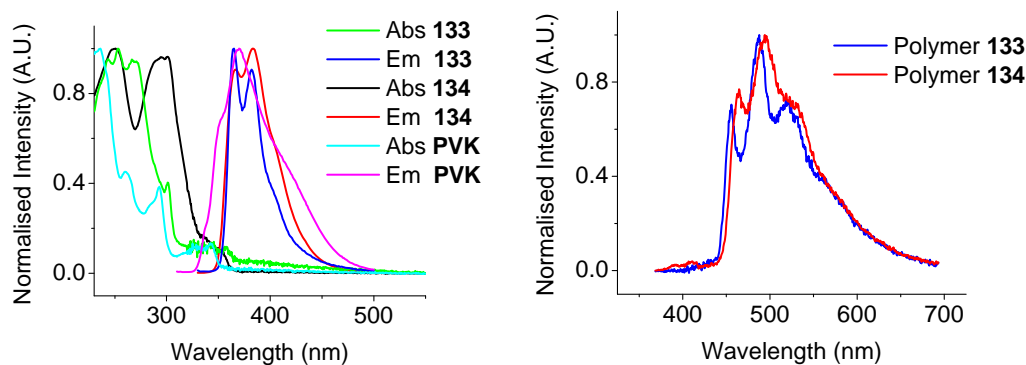
Figure 5.3. Absorption and emission spectra of polymers **133**, **134** and PVK in CH$_2$Cl$_2$ solution (left). Phosphorescent spectra recorded at 77 K of polymers **133** and **134** as thin film samples prepared by spin-coating (right).

Triplet measurements of polymers **133** and **134** were carried out by Vygintas Jankus in the Physics Department of Durham University. The phosphorescent spectrum of polymer **133** gives the higher energy peak at 454 nm (see Figure 5.3),

which was used to calculate E_T as 2.73 eV (Table 5.1). This value is higher than that of most conjugated and non-conjugated polymer hosts.[147,152] Most importantly, the triplet energy of polymer **133** is higher than that of sky-blue Ir complex FIrpic (E_T= 2.62 eV). This should prevent the triplet back energy transfer from FIrpic to host **133**, which is a prerequisite for high device efficiency. Also, as with other deep blue phosphorescent dopants with high triplet energy, such as iridium(III) bis(4,6-difluorophenylpyridinato)tetrakis(1-pyrazolyl)borate (FIr6, E_T= 2.70 eV), the triplet energy of polymer **133** is still high enough to prevent triplet energy back transfer. On the other hand, the phosphorescent spectrum of polymer **134** gives the higher energy peak at 464 nm with E_T of 2.67 eV, which is 0.06 eV lower than that of polymer **133,** but still higher than the triplet energy of Flrpic (Table 5.1).

Table 5.1. The values of offset absorption, emission at the onset, emission at the peak and phosphorescent emission at the peak of polymer **133**, **134** and PVK.

Polymer	$Abs^{red\ edge}$ (nm)	E_S^{onset} (eV)	E_T^{peak} (eV)
133	370	3.58	2.73
134	364	3.60	2.67
PVK	363	3.79	3.0^{142} and 2.5^{144}

5.2.3 Device Studies of Polymers 133 and PVK

The device fabrication and characterisation were performed by Dr. Hameed A. Al-Attar in the Physics Department of Durham University. Polymer **133** was compared with PVK. The device structure used was ITO/PEDOT:PSS/5% Ir(ppy)$_3$ and 40 wt% PBD doped in host **133** or PVK/Ba:Al. (The concentrations of Ir(ppy)$_3$ and PBD were w/w % with respect to the host). Devices were fabricated by spin-coating a layer of a blend containing the polymer host **133**, the green-emitting Ir(ppy)$_3$ and the electron transporter PBD onto indium tin oxide substrates covered with a 20 nm thick layer of PEDOT:PSS. The samples were annealed at 80 °C for 30 min before deposition of the Ba/Al cathode. The thickness of PVK and polymer **133** layers was 79 and 91 nm, respectively. The diodes were characterised by the data shown in Figure 5.4.

a

b

c

d
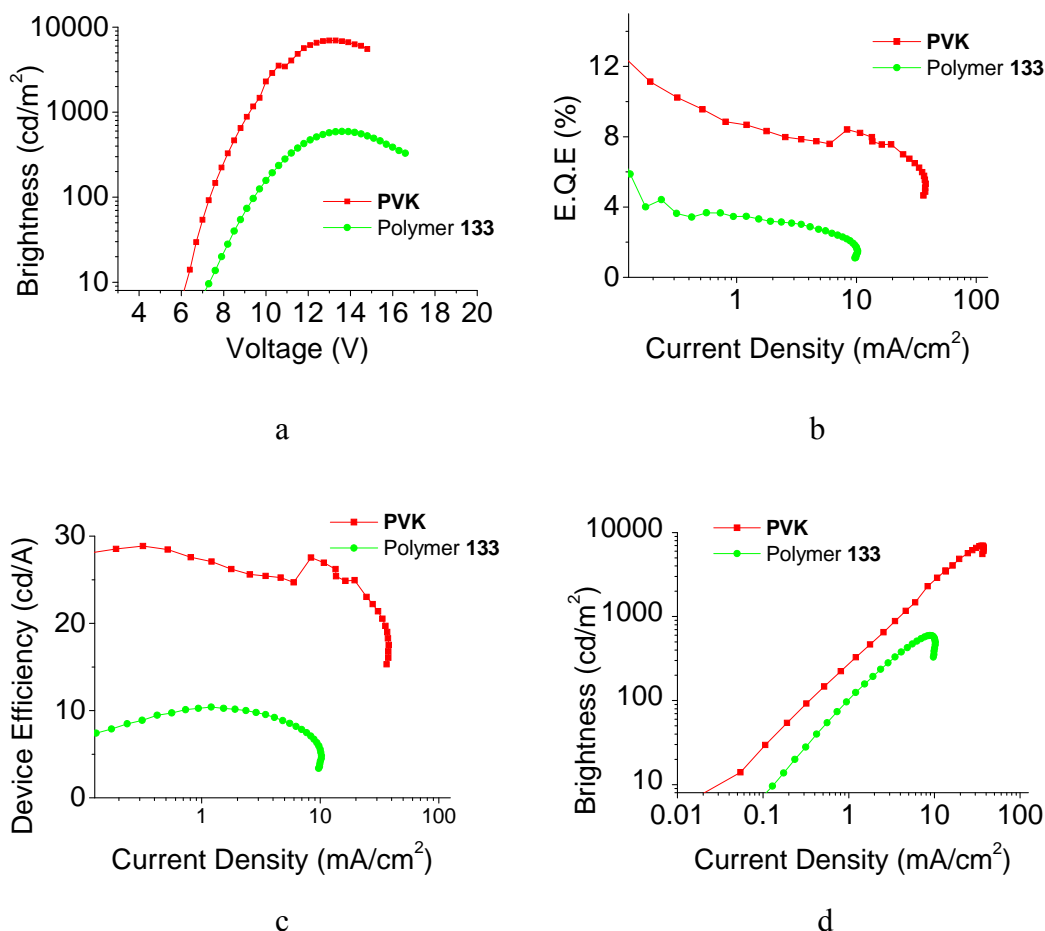
Figure 5.4. Device characteristics of PVK (red) and polymer **133** (green). Device architecture: ITO/PEDOT:PSS/5% Ir(ppy)$_3$ and 40 wt% PBD doped in host **133** or PVK/Ba:Al.

The efficiency of polymer **133** device is quite good (ca. 10 cd/A) but significantly lower than that of the PVK device (ca. 28 cd/A) (Figure 5.4c), and the turn-on voltage for polymer **133** is slightly higher (see Figure 5.4a). One reason why PVK is better than polymer **133** as a green host, is that the device conditions have been specifically optimised for PVK. Hence, it is probable that the device performance with polymer **133** could be improved by optimising the thickness of the emissive layer and other parameters. The purpose of these sets of device data is to examine how the new host material responds under the optimised PVK green device conditions.

Polymer **133** is designed for hosting blue emitters. Bearing that in mind, we employed a new blue complex **145** (G2IrG2) developed within our group.[153] It is a Flrpic-based complex, possessing the same triplet energy as Flrpic with the advantage

of increased solubility in organic solvents. Device fabrication incorporating polymer **133** and complex **145** were then performed.
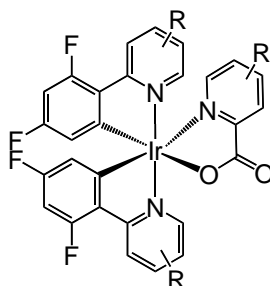
G2IrG2-**145** R = bulky aryl

Figure 5.5. Structure of compound **145**. (Details of group R are withheld for reasons of confidentiality).

The device structure used was ITO/PEDOT:PSS/X% **145** and 40 wt% OXD-7 doped in polymer **133**/Ba:Al (X=1, 2, 5, 8). The reason for incorporating OXD-7 in devices instead of PBD is preventing the energy back transfer from emitter to electron-transporting materials. Devices were fabricated by spin-coating a 100 nm thick layer of blend containing polymer **133**, the blue-emitter **145** and OXD-7 onto indium tin oxide substrates covered with a 20 nm thick layer of PEDOT:PSS. The samples were annealed at 80 °C for 30 min before deposition of the Ba/Al cathode. The diodes were characterised by the data shown in Figure 5.5.

Figure 5.6a shows that the EL spectra are dominated by **145**. But only at ≥5 wt% complex **145**, a full energy transfer occurs from polymer **133** to **145**. Below ca 5 wt% concentration the higher energy emission from polymer **133** was observed, which indicates no triplet energy back-transfer from **145** to polymer **133** and is consistent with the fact that the triplet energy of polymer **133** is higher than that of emitter **145**.

a

b

c

d

e

Figure 5.6. Device characteristics of polymer **133** with different percentage of dopant **145**.
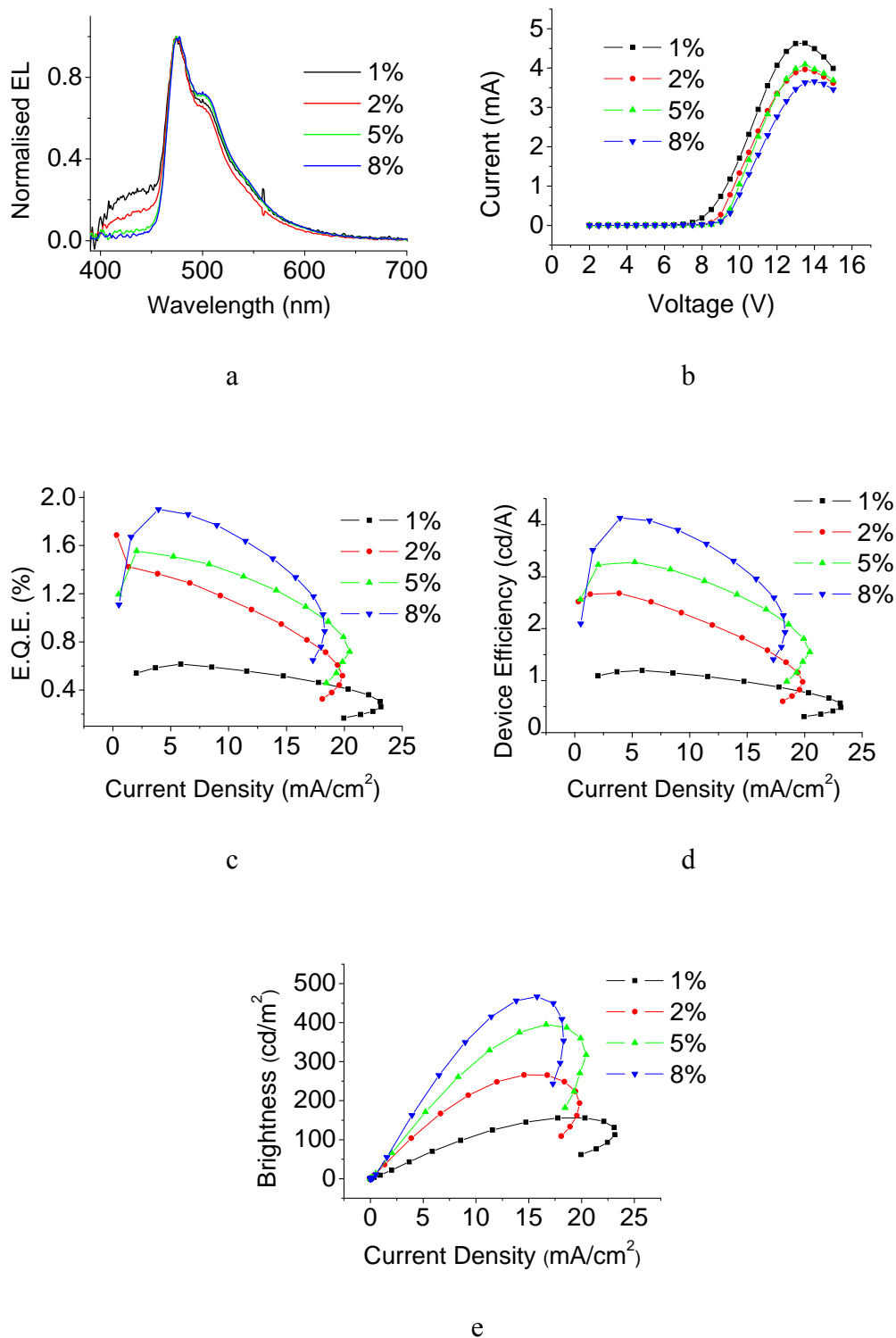
The best EL performance, as judged by Figures 5.6c,d,e, is achieved at a **145** content of 8 wt%. The turn-on voltage of the devices increases with increasing concentration of emitters (see Figure 5.6b). The increased turn-on voltage resulted

from the charge trapping of the emitter; thus the device with 8 wt% of emitter possesses the highest turn-on voltage (ca. 9.5 V). The brightness of the device with 8 wt% complex **145** reaches 450 cd/m^2 at 15 mA/cm^2. At a current density of 4.9 mA/cm^2, it exhibits a device efficiency of 4.3 cd/A and E.Q.E. of 1.9%. PPLEDs generally exhibit higher luminance efficiency with decreasing current density because of the long diffusion distance of triplet excitons and triplet-triplet annihilation.[8] However, the device based on 8 wt% dopant shows low device efficiency at low current densities. It is probably due to an inbalance of charge carriers. Device optimisation with balancing the charge and varying the thickness of the emissive layer is expected to lead to improved EL performance. These studies are ongoing.

One point worth noting is that the actual triplet energy of PVK is still not clear (as stated above). Moreover, electrophosphorescence has been observed from a triplet excimer in PVK at room temperature. Two extra emissions were observed at 560 and 600 nm.[145] Therefore, back energy transfer may occur when PVK hosts high triplet energy emitters such as Flrpic. In contrast, polymer **133** shows no electrophosphorescence during device operations. Further studies, e.g. a direct device comparison between PVK and polymer **133** with Flrpic as guest, will be carried out by Dr. Hameed A. Al-Attar.

5.3 Conclusions

New non-conjugated carbazole based polymers have been developed. The tripelt energy of polymers **133** and **134** is 2.73 and 2.67 eV, respectively, which is higher than that of FIrpic. Hence, polymers **133** and **134** are considered to be suitable host materials for blue PPLEDs. High E_T polymers can prevent triplet energy back transfer thus confining triplet excitons in FIrpic to emit light, potentially allowing the use of low content of FIrpic for high EL efficiency. Double-layer PPLEDs using the blend containing 8 wt% of complex **145** emits sky-blue light exclusively from **145** with a maximum luminance efficiency of 4.3 cd/A. Our results provide a novel avenue for the design of polymer host materials for phosphorescent dopants. Studies are ongoing to optimise the device performance by changing the thickness of the emissive layer and the concentration of ET materials and to use polymer **133** with deeper blue phosphorescent guest.

Chapter 6 – Future Work

Chapter 2: We have established that chemical modifications on carbazole-oxadiazole ambipolar molecules can independently tune the singlet and triplet energy levels of the molecules. Also, the origin of the interesting feature of phosphorescence at low temperature from dimethoxycarbazole substitutied molecules is still unknown. Hence, the future work from this chapter is to understand the reason for this unusual phosphorescence emission for organic molecules, and to further modify the structures to tailor the HOMO-LUMO levels and energy gaps.

Chapter 3: Ir(III) complexes with different ligands have been studied in detail. The iridium-oxadiazole complexes, **90-92** possess phosphorescent emission at low temperature, which is quite unusual for Ir(III) complexes. Therefore, temperature dependent experiments could be carried out in the future to probe the low temperature phosphorescence behaviour. New analogues could be studied to explore this further.a

Chapter 4: Exciplex studies on the twisted oxadiazole molecules have shown a great advantage of possessing a high lying LUMO level to avoid energy transfer from host to ET molecules. Therefore, more device studies will be required to confirm the benefit of having high lying LUMO level.

Chapter 5: More device studies will be needed to confirm the benefit of having a high triplet energy level. Also, temperature dependent experiments on phosphorescence emission will be carried out to examine the potential aggregation and/or dimer formation at higher temperature, more importantly at room temperature.

Chapter 7 – Experimental Procedures

7.1 General Methods

All air-sensitive reactions were conducted under a blanket of argon which was dried by passage through a column of phosphorus pentoxide. All commercial chemicals were used without further purification unless otherwise stated. Anhydrous toluene and tetrahydrofuran (THF) were dried through an HPLC column on an Innovative Technology Inc. solvent purification system. Column chromatography was carried out using 40-60 μm mesh silica. Analytical thin layer chromatography was performed on 20 mm pre-coated plates of silica gel (Merck, silica gel $60F_{254}$), visualisation was made using ultraviolet light (254 nm). NMR spectra were recorded on: Bruker Avance-400, Varian Mercury-200, Varian Mercury-400, Varian Inova-500 and Varian VNMRS-700 spectrometers. Chemical shifts are reported in ppm downfield of tetramethylsilane (TMS) using TMS or the residual solvent as an internal reference. Melting points were determined in open-ended capillaries using a Stuart Scientific SMP3 melting point apparatus at a ramping rate of 5 °C/min. Electron ionisation (EI) mass spectra were recorded on Thermoquest Trace or Thermo-Finnigan DSQ instruments. Atmospheric Solids Analysis Probe (ASAP) was recorded on Waters Xevo QTOF equipped with Atmospheric Pressure Gas Chromatography. MALDI TOF MS was recorded on Bruker Daltonics Autoflex II ToF/ToF.

Elemental analyses were obtained on an Exeter Analytical Inc. E-440 elemental analyser. Ion analyses were performed on a Dionex 120 Ion Chromatography detector.Molecular weight of the polymers was measured by the gel permeation chromatography (GPC) method using polystyrene as the standard and THF as the eluent.

UV-Vis spectra were recorded using a Varian Cary 5 spectrophotometer at ambient temperatures. Excitation and emission photoluminescence spectra were recorded on a Horiba Jobin Yvon SPEX Fluorolog FL3-22 spectrofluorometer. Samples were held in quartz fluorescence cuvettes, l = 1 cm x 1 cm, degassed by repeated freeze-pump-thaw cycles until the pressure gauge showed no further

movement upon a new pump phase and sealed by way of a Teflon Young's tap. Solutions had A = 0.10-0.15 at 400 nm to minimize inner filter effects. The fluorescence lifetimes were measured by time-correlated single photon counting (TCSPC) using a pulsed diode laser (396 nm) providing a 1 MHz train of pulses of < 100 ps. The fluorescence emission was collected at right angles to the excitation source, with the emission wavelength selected using a monochromator and detected by a cooled photomultiplier tube module photon (IBH TBX-04). The instrument response function was measured using a dilute LUDOX$^{®}$ suspension as the scattering sample, setting the monochromator at the emission wavelength of the laser, giving an instrument response function (IRF) of 250 ps at 396 nm. The resulting intensity decay was a convolution of the fluorescence decay with the IRF, and iterative reconvolution of the IRF with a decay function and non-linear least-squares analysis were used to analyze the convoluted data. Phosphorescence measurements were performed using a home-made set-up, a N_2 laser (337 nm, 10 μJ, 10 Hz) was used as an excitation source. Emission was detected in a 90° geometry by a photomultiplier tube (Hamamatsu R928) as a function of time, selecting a wavelength close to the peak emission by way of a monochromator (Horiba Jobin Yvon Triax 320) with a 0.1-2.0 nm bandpass. The signal was averaged and converted to a digital signal by a digital storage oscilloscope (Tetronix TDS 340). The data were fitted to single exponential functions of the form $I(t) = I_0 \exp(-t/\tau)$. Low temperature measurements were conducted using an Oxford Instruments DN1704 optical cryostat. Solution-state PLQYs were measured using intergrating sphere technique.

Cyclic voltammograms were recorded at scan rate 100 mVs^{-1} at room temperature using an air-tight single-compartment three-electrode cell equipped with a Pt disk working electrode, Pt wire counter electrode, and Pt wire pseudo-reference electrode. The cell was connected to a computer-controlled Autolab PG-STAT 30 potentiostat. The solutions contained the compound together with n-Bu$_4$NPF$_6$ (0.1 M) as the supporting electrolyte in dichloromethane. All potentials are reported with reference to an internal standard of the Fc/Fc$^+$ or FcMe$_{10}$/FcMe$_{10}^+$ $=0.00$ V.

Density function theory calculations were carried out using Becke's three-parameter hybrid exchange functional with Lee-Yang-Parr gradient-corrected correlation functional (B3LYP).Thus, the geometries of organic molecules were

optimised with a B3LYP/6-31G(d) level of theory. Meanwhile, the geometries of iridium complexes were optimised with a B3LYP/LAN2DZ level of theory.[154]

7.2 Experimental Procedures for Chapter 2

5-(4-Fluorophenyl)-tetrazole (58)
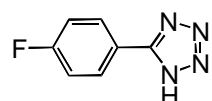
5-(4-Fluorophenyl)-tetrazole **58** was prepared following the procedure of Koyama *et al.*[91] An argon-purged flask was charged with 4–fluorobenzonitrile **56** (5.00 g, 41.3 mmol), sodium azide (3.22 g, 49.4 mmol), ammonium chloride (2.63 g, 49.4 mmol) and anhydrous dimethylformamide (DMF) (100 ml). The solution was refluxed overnight. The solution was cooled and water added before the solution was acidified with dilute hydrochloric acid to precipitate the product which was filtered and dried. A pale yellow solid **58** (5.30 g, 78%) was obtained and used for the next step without further purification.

5-(4-Fluoro-3-methylphenyl)-tetrazole (59)
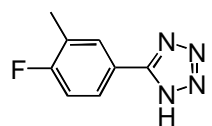
An argon-purged flask was charged with 4–fluoro-3-methylbenzonitrile **57** (1.50 g, 11.1 mmol), sodium azide (0.80 g, 12.2 mmol), ammonium chloride (0.65 g, 12.2 mmol) and anhydrous DMF (30 ml). The solution was refluxed overnight. The solution was cooled and water added before the solution was acidified with dilute hydrochloric acid to precipitate the product which was filtered and dried. A pale yellow solid **59** (1.32 g, 66%) was obtained and used for the next step without further purification; mp: 200.5-201.8 $^{\circ}$C; Anal. Calc. for $C_8H_7FN_4$: C, 53.93; H, 3.96; N, 31.45. Found: C, 53.81; H, 4.00; N, 31.49; δ_H (700 MHz, DMSO-d_6) 7.96 (1H, d, J 7.1), 7.86 (1H, d, J 5.3), 7.37 (1H, t, J 9.1), 2.31 (3H, s) (NH not observed); δ_C (176 MHz, DMSO-d_6) 162.64 (d, J 248.3), 130.90 (d, J 5.8), 127.19 (d, J 9.0), 126.21 (d, J 18.1), 116.61 (d, J 23.2), 109.99, 14.57 (d, J 3.2); MS (EI): m/z (EI) 177.9 (M$^+$, 20%), 149.7 (100%).

2-(4-Fluorophenyl)-5-(2,4,6-trimethylphenyl)-1,3,4-oxadiazole (65)
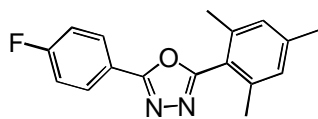
An argon-purged flask was charged with 5-(4-fluorophenyl)-tetrazole **58** (0.13 g, 0.8 mmol), 2,4,6-trimethylbenzoyl chloride **61** (0.15 g, 0.8 mmol) and pyridine (5 ml). The solution was refluxed overnight. The solution was cooled and water added. The precipitate was collected and dried. The crude product was purified by column chromatography (SiO$_2$, 19:1 DCM: EtOAc) followed by recrystallisation from ethanol yielding compound **65** (0.18 g, 85%) as colourless crystals; mp: 102.2-102.8 °C; Anal. Calc. for C$_{17}$H$_{15}$FN$_2$O: C, 72.32; H, 5.36; N, 9.92. Found: C, 72.27; H, 5.30; N, 10.10; δ_H (700 MHz, CDCl$_3$) 8.09 (2H, dt, J 6.9, 13.9), 7.21 (2H, t, J 8.6), 6.99 (2H, s), 2.35 (3H, s), 2.31 (6H, s); δ_C (176 MHz, CDCl$_3$) 164.74 (d, J 252.4), 163.91, 141.09, 138.71, 129.10 (d, J 8.9), 128.87, 128.47, 120.95, 120.40 (d, J 3.3), 116.40 (d, J 22.3), 21.27, 20.47; λ_{abs} (CH$_2$Cl$_2$) (ε,10^{4}dm^3.M^{-1}cm^{-1}) 264 nm (1.62); MS (EI): m/z 282.0 (M$^+$, 100%).

**2-(4-Fluorophenyl)-5-(2,4,6-triisopropylphenyl)-1,3,4-oxadiazole (66)**
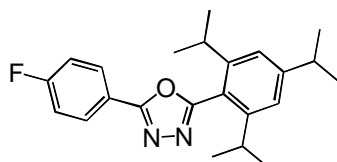
An argon-purged flask was charged with 5-(4-fluorophenyl)-tetrazole **58** (1.50 g, 9.1 mmol), 2,4,6-triisopropylbenzoyl chloride **62** (2.68 g, 10.0 mmol) and pyridine (10 ml). The solution was refluxed overnight. The solution was cooled and water added. The precipitate was collected and dried. The crude product was purified by column chromatography (SiO$_2$, 19:1 DCM: EtOAc) followed by recrystallisation from ethanol yielding compound **66** (1.85 g, 55%) as colourless crystals; mp: 119.3-120.6 °C; Anal. Calc. for C$_{23}$H$_{27}$FN$_2$O: C, 75.38; H, 7.43; N, 7.64. Found: C, 75.32; H, 7.50; N, 7.60; δ_H (700 MHz, CDCl$_3$) 8.11 – 8.06 (2H, m), 7.23 – 7.19 (2H, m), 7.12 (2H, s), 2.96 (1H, hept, J 6.9), 2.65 (2H, hept, J 6.9), 1.29 (6H, d, J 6.9), 1.21 (12H, t, J 8.2); δ_C (176 MHz, CDCl$_3$) 164.84 (d, J 218.0), 164.02, 163.86, 152.46, 149.45, 129.08 (d, J 8.8), 121.20, 120.47, 119.56, 116.42 (d, J 22.3), 34.57, 31.47, 24.07, 23.87; λ_{abs} (CH$_2$Cl$_2$) (ε,10^{4}dm^3.M^{-1}cm^{-1}) 258 nm (2.49); MS (MALDI+): m/z 367.3 (M$^+$, 100%).

2-(4-Fluorophenyl)-5-(2,4,6-*tert*-butylphenyl)-1,3,4-oxadiazole (67)
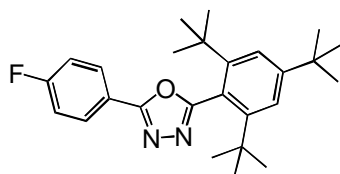
An argon-purged flask was charged with 5-(4-fluorophenyl)-tetrazole **58** (1.23 g, 7.5 mmol), 2,4,6-*tert*-butylbenzoyl chloride **63** (1.92g, 6.3 mmol) and pyridine (10 ml). The solution was refluxed overnight. The solution was cooled and water added. The precipitate was collected and dried. The crude product was purified by column chromatography (SiO$_2$, 100% DCM) followed by recrystallisation from ethanol yielding compound **67** (1.20 g, 47%) as colourless crystals; mp: 168.9-170.3 ^{o}C; Anal. Calc. for C$_{26}$H$_{33}$FN$_2$O: C, 76.44; H, 8.14; N, 6.86; Found: C, 76.52; H, 8.02; N, 7.02; δ_H (700 MHz, CDCl$_3$) 8.14 – 8.02 (2H, m), 7.25 (2H, s), 7.20 (2H, t, *J* 8.6), 1.36 (9H, s), 1.18 (18H, s); δ_C (176 MHz, CDCl$_3$) 165.49, 164.69, 164.06, 163.18, 152.90, 151.51, 129.06, 129.01, 122.19, 117.94, 116.51, 116.39, 37.17, 32.16, 31.23, 15.24; λ_{abs} (CH$_2$Cl$_2$) (ε,10^{4}dm^3.M^{-1}cm^{-1}) 257 nm (2.54); MS (EI): *m/z* 408.1 (M$^+$, 15%), 393.1 (100%).

2-(4-Fluoro-3-methylphenyl)-5-phenyl-1,3,4-oxadiazole (68)
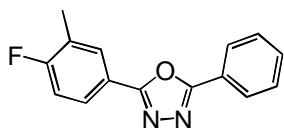
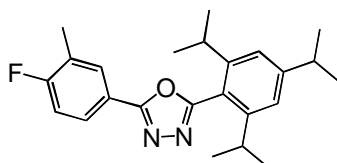An argon-purged flask was charged with 5-(4-fluoro-3-methylphenyl)-tetrazole **59** (0.33 g, 1.7 mmol), benzoyl chloride **61** (0.28 g, 2.0 mmol) and pyridine (5 ml). The solution was refluxed overnight. The solution was cooled and water added. The precipitate was collected and dried. The crude product was purified by column chromatography (SiO$_2$, 19:1 DCM: EtOAc) followed by recrystallisation from ethanol yielding compound **68** (0.36 g, 84%) as a white solid; mp: 139.5-140.8 ^{o}C; Anal. Calc. for C$_{15}$H$_{11}$FN$_2$O: C, 70.86; H, 4.36; N, 11.02. Found: C, 70.93; H, 4.24; N, 11.05; δ_H (700 MHz, CDCl$_3$) 8.14 (2H, dd, *J* 10.0, 16.6), 8.00 (1H, d, *J* 7.3), 7.98 – 7.90 (1H, m), 7.63 – 7.44 (3H, m), 7.15 (1H, t, *J* 8.9), 2.37 (3H, s); δ_C (176 MHz, CDCl$_3$) 164.51, 163.96, 163.40 (d, *J* 251.9), 131.70, 130.35 (d, *J* 6.0), 129.05, 126.88, 126.46 (d, *J* 8.9), 126.22 (d, *J* 18.2), 123.88, 119.86 (d, *J* 3.5), 115.95 (d, *J* 23.4), 14.52 (d, *J* 3.5); MS (EI): *m/z* 254.0 (M$^+$, 100%).

2-(4-Fluoro-3-methylphenyl)-5-(2,4,6-trimethylphenyl)-1,3,4-oxadiazole (69)
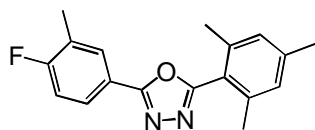
An argon-purged flask was charged with 5-(4-fluoro-3-methylphenyl)-tetrazole **59** (0.30 g, 1.7 mmol), 2,4,6-trimethylbenzoyl chloride **61** (0.360 g, 2.0 mmol) and pyridine (5 ml). The solution was refluxed overnight. The solution was cooled and water added. The precipitate was collected and dried. The crude product was purified by column chromatography (SiO$_2$, 19:1 DCM: EtOAc) followed by recrystallisation from ethanol yielding compound **69** (0.28 g, 56%) as a white solid; mp: 93.7-94.8 ^{o}C; Anal. Calc. for C$_{18}$H$_{17}$FN$_2$O: C, 72.95; H, 5.78; N, 9.45; Found: C, 72.64; H, 5.90; N, 9.50; δ_H (700 MHz, CDCl$_3$) 7.96 (1H, d, J 7.1), 7.89 (1H, dd, J 3.9, 7.0), 7.14 (1H, t, J 8.9), 6.98 (2H, s), 2.35 (3H, s), 2.34 (3H, s), 2.30 (6H, s); δ_C (176 MHz, CDCl$_3$) 164.23, 164.22, 164.06, 163.80, 162.63, 141.04, 138.70, 130.31, 130.28, 128.77, 126.41, 126.36, 126.25, 126.14, 121.04, 120.00, 116.01, 115.87, 30.89, 21.24, 20.45. MS (EI): m/z 296.0 (M$^+$, 70%), 146.7 (100%).

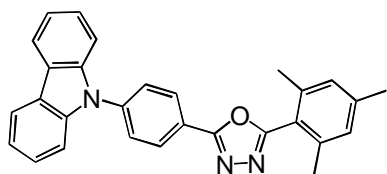**2-(4-Fluoro-3-methylphenyl)-5-(2,4,6-triisopropylphenyl)-1,3,4-oxadiazole (70)**

An argon-purged flask was charged with 5-(4-fluoro-3-methylphenyl)-tetrazole **59** (0.20 g, 1.1 mmol), 2,4,6-triisopropylbenzoyl chloride **62** (0.30 g, 1.1 mmol) and pyridine (5 ml). The solution was refluxed overnight. The solution was cooled and water added. The precipitate was collected and dried. The crude product was purified by column chromatography (SiO$_2$, 19:1 DCM: EtOAc) followed by recrystallisation from ethanol yielding compound **70** (0.29 g, 70%) as a white solid; mp: 99.3-101.0 ^{o}C; Anal. Calc. for C$_{24}$H$_{29}$FN$_2$O: C, 75.76; H, 7.68; N, 7.36; Found: C, 75.42; H, 7.60; N, 7.60; δ_H (700 MHz, CDCl$_3$) 7.94 (1H, d, J 7.0), 7.88 (1H, dd, J 4.1, 7.1), 7.16 − 7.09 (3H, m), 2.96 (1H, dt, J 6.9), 2.64 (2H, hept, J 6.8), 2.35 (3H, s), 1.29 (6H, d, J 6.9), 1.20 (12H, d, J 6.8); δ_C (176 MHz, CDCl$_3$) 164.41, 163.76, 163.35 (d, J 251.7), 152.41, 149.44, 130.29 (d, J 6.0), 126.36 (d, J 8.9), 126.21 (d, J 18.2), 121.17, 120.06 (d, J 3.9), 119.65, 119.65, 115.96 (d, J 23.4), 34.57, 31.45, 24.06, 23.87, 14.52 (d, J 3.4). MS (EI): m/z 380.1 (M$^+$, 15%), 230.5 (100%).

2-[4-(9*H*-Carbazol-9-yl)phenyl]-5-phenyl-1,3,4-oxadiazole (71)
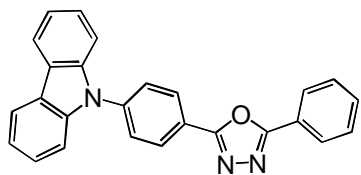
A flask was charged with 2-(4-fluorophenyl)-5-phenyl-1,3,4-oxadiazole **64** (0.22 g, 0.6 mmol), carbazole (0.10 g, 0.6 mmol), K_2CO_3 (200 mg) and DMSO (10 ml). The solution was heated at 150 °C overnight. The solution was cooled and water added. The mixture was extracted with DCM (3 × 30 ml). The organic layers were combined and dried over $MgSO_4$. A brown solid which was obtained after removing the solvent, was purified by column chromatography (SiO$_2$, 98:2 DCM: EtOAc) followed by recrystallisation from EtOH yielding compound **71** (0.13g, 55%) as a white solid; mp: 223.5-224.8 °C; Anal. Calc. for $C_{26}H_{17}N_3O$: C, 80.60; H, 4.42; N, 10.85. Found: C, 80.61; H, 4.40; N, 10.83; δ_H (500 MHz, CDCl$_3$) 8.46 − 8.39 (2H, m), 8.25 − 8.19 (2H, m), 8.18 (2H, d, *J* 7.7), 7.85 − 7.78 (2H, m), 7.64 − 7.51 (5H, m), 7.50 − 7.44 (2H, m), 7.38 − 7.32 (2H, m); δ_C (126 MHz, CDCl$_3$) 165.05, 159.75, 141.17, 140.50, 132.15, 129.46, 128.84, 127.51, 127.25, 126.47, 124.06, 122.71, 120.83, 120.74, 109.99, 109.95; MS (EI): *m/z* 387.1 (M$^+$, 100%).

2-[4-(9*H*-Carbazol-9-yl)phenyl]-5-(2,4,6-trimethylphenyl)-1,3,4-oxadiazole (72)

A flask was charged with 2-(4-fluorophenyl)-5-(2,4,6-trimethylphenyl)-1,3,4-oxadiazole **65** (0.18 g, 0.67 mmol), carbazole (0.11 g, 0.69 mmol), K_2CO_3 (200 mg) and DMSO (10 ml). The solution was heated at 150 °C overnight. The solution was cooled and water added. The mixture was extracted with DCM (3 × 30 ml). The organic layers were combined and dried over $MgSO_4$. A brown solid was obtained after removing solvent and purified by column chromatography (SiO$_2$, 98:2 DCM: EtOAc) followed by recrystallisation from ethanol yielding compound **72** (0.16 g, 55%) as a white solid; mp: 191.8-192.6 °C; Anal. Calc. for $C_{29}H_{23}N_3O$: C, 81.09; H, 5.40; N, 9.78. Found: C, 81.10; H, 5.36; N, 9.76; δ_H (700 MHz, CDCl$_3$) 8.35 (2H, d, *J* 8.2), 8.15 (2H, d, *J* 7.5), 7.77 (2H, d, *J* 8.3), 7.49 (2H, d, *J* 8.1), 7.43 (2H, t, *J* 7.6), 7.32 (2H, t, *J* 7.4), 7.02 (2H, s), 2.36 (9H, s); δ_C (176 MHz, CDCl$_3$) 164.26, 164.12, 141.16, 140.86, 140.27, 138.78, 128.93, 128.49, 127.28, 126.19, 123.77, 122.64, 120.98, 120.55, 120.45, 109.66, 21.29, 20.53; MS (EI): *m/z* 429.1 (M$^+$, 100%).

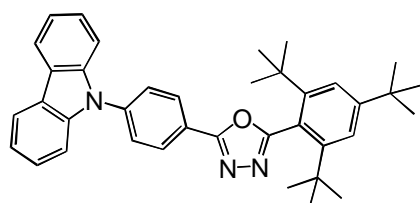**2-[4-(9*H*-Carbazol-9-yl)phenyl]-5-(2,4,6-triisopropylphenyl)-1,3,4-oxadiazole (73)**
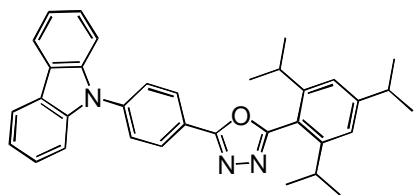
A flask was charged with 2-(4-fluorophenyl)-5-(2,4,6-triisopropylphenyl)-1,3,4-oxadiazole **66** (0.50 g, 1.4 mmol), carbazole (0.23 g, 1.4 mmol), K_2CO_3 (400 mg) and DMSO (20 ml). The solution was heated at 150 ^{o}C overnight. The solution was cooled and water added. The mixture was extracted with DCM (3 × 30 ml). The organic layers were combined and dried over $MgSO_4$. A brown solid was obtained after removing solvent and purified by column chromatography (SiO_2, 98:2 DCM: EtOAc) followed by recrystallisation from ethanol yielding compound **73** (0.36 g, 52%) as colourless crystals. Crystals for X-ray analysis were grown by slowly cooling a solution of **73** in MeCN; mp: 216.2-217.0 ^{o}C; Anal. Calc. for $C_{35}H_{35}N_3O$: C, 81.84; H, 6.87; N, 8.18. Found: C, 81.75; H, 6.88; N, 8.11; δ_H (700 MHz, $CDCl_3$) 8.33 (2H, d, *J* 8.5), 8.15 (2H, d, *J* 7.7), 7.77 (2H, d, *J* 8.5), 7.49 (2H, d, *J* 8.2), 7.43 (2H, t, *J* 7.6), 7.32 (2H, t, *J* 7.4), 7.16 (2H, s), 2.98 (1H, hept, *J* 7.0), 2.71 (2H, hept, *J* 6.8), 1.31 (6H, d, *J* 6.9), 1.25 (12H, d, *J* 6.8); δ_C (176 MHz, $CDCl_3$) 164.46, 164.08, 152.52, 149.50, 140.88, 140.27, 128.47, 127.31, 126.19, 123.77, 122.69, 121.25, 120.55, 120.45, 119.59, 109.66, 34.60, 31.54, 24.13, 23.89; MS (MALDI+): *m/z* 513.4 (M$^+$, 100%).

2-[4-(9*H*-carbazol-9-yl)phenyl]-5-(2,4,6-*tert*-butylphenyl)-1,3,4-oxadiazole (74)

A flask was charged with 2-(4-fluorophenyl)-5-(2,4,6-*tert*-butylphenyl)-1,3,4-oxadiazole **67** (0.10 g, 0.25 mmol), carbazole (0.05 g, 0.30 mmol), K_2CO_3 (200 mg) and DMSO (20 ml). The solution was heated at 150 ^{o}C overnight. The solution was cooled and water added. The mixture was extracted with DCM (3 × 30 ml). The organic layers were combined and dried over $MgSO_4$. A brown solid was obtained after removing solvent and purified by column chromatography (SiO_2, 97:3 DCM: EtOAc) followed by recrystallisation from acetonitrile yielding compound **74** (0.08 g, 59%) as colourless crystals. Crystals for X-ray analysis were grown by slowly cooling a solution of **74** in MeCN; mp: 222.0-223.0 ^{o}C; Anal. Calc. for $C_{38}H_{41}N_3O$: C, 82.12; H, 7.44; N, 7.56; Found: C, 81.96; H,

7.45; N, 7.54; δ_H (700 MHz, CDCl$_3$) 8.33 (2H, d, J 8.7), 8.15 (2H, d, J 7.1), 7.77 (2H, d, J 8.7), 7.58 (2H, s), 7.51 (2H, d, J 8.2), 7.43 (2H, t, J 7.7), 7.32 (2H, t, J 7.9), 1.39 (9H, s), 1.25 (18H, s). δ_C (176 MHz, CDCl$_3$) 164.91, 163.42, 152.96, 151.57, 140.94, 140.28, 128.40, 127.34, 126.18, 123.77, 122.59, 122.25, 120.55, 120.44, 117.98, 109.72, 37.24, 35.32, 32.25, 31.26. MS (MALDI+): m/z 555.3 (M$^+$, 100%).

2-[4-(9*H*-Carbazol-9-yl)-3-methylphenyl]-5-phenyl -1,3,4-oxadiazole (75)
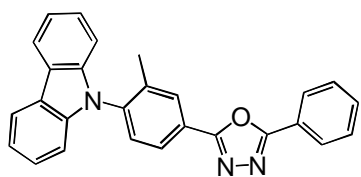
A flask was charged with 2-(4-fluoro-3-methylphenyl)-5-phenyl-1,3,4-oxadiazole **68** (0.23 g, 0.9 mmol), carbazole (0.15 g, 0.9 mmol), K$_2$CO$_3$ (200 mg) and DMSO (10 ml). The solution was heated at 150 ^{o}C overnight. The solution was cooled and water added. The mixture was extracted with DCM (3 × 30 ml). The organic layers were combined and dried over MgSO$_4$. A brown solid was obtained after removing the solvent and purified by column chromatography (SiO$_2$, 98:2 DCM: EtOAc) followed by recrystallisation from ethanol yielding compound **75** (0.19 g, 53%) as a white solid; mp: 197.1-197.8 ^{o}C; Anal. Calc. for C$_{27}$H$_{19}$N$_3$O: C, 80.78; H, 4.77; N, 10.47. Found: C, 80.36; H, 4.71; N, 10.31; δ_H (700 MHz, CDCl$_3$) 8.29 (1H, s), 8.19 (2H, d, J 7.9), 8.17 (3H, d, J 7.9), 7.62 − 7.48 (4H, m), 7.41 (2H, t, J 7.6), 7.31 (2H, t, J 7.5), 7.07 (2H, d, J 8.1), 2.11 (3H, s); δ_C (176 MHz, CDCl$_3$) 164.86, 164.06, 140.75, 139.36, 138.53, 131.89, 130.12, 130.09, 129.09, 127.07, 126.06, 125.85, 124.12, 123.78, 123.11, 120.46, 120.09, 109.72, 17.54; MS (MALDI+): m/z 401.1 (M$^+$, 100%).
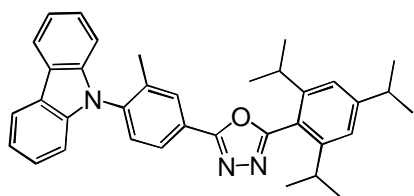
2-[4-(9*H*-Carbazol-9-yl)-3-methylphenyl]-5-(2,4,6-trimethylphenyl)-1,3,4-oxadiazole (76)
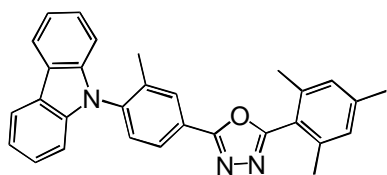
A flask was charged with 2-(4-fluoro-3-methylphenyl)-5-(2,4,6-triisopropylphenyl)-1,3,4-oxadiazole **69** (0.15 g, 0.5 mmol), carbazole (0.08 g, 0.9 mmol), K$_2$CO$_3$ (200 mg) and DMSO (10 ml). The solution was heated at 150 ^{o}C overnight. The solution was cooled and water added.

The mixture was extracted with DCM (3 × 30 ml). The organic layers were combined and dried over MgSO$_4$. A brown solid was obtained after removing solvent and purified by column chromatography (SiO$_2$, 98:2 DCM: EtOAc) followed by recrystallisation from acetonitrile yielding compound **76** (0.12 g, 45%) as colourless crystals; mp: 191.3-192.6 ^{o}C; Anal. Calc. for C$_{30}$H$_{25}$N$_3$O: C, 81.24; H, 5.68; N, 9.47; Found: C, 81.34; H, 5.73; N, 9.61; δ_H (700 MHz, CDCl$_3$) 8.25 (1H, s), 8.17 (2H, d, J 7.6), 8.13 (1H, d, J 10.1), 7.54 (1H, d, J 8.1), 7.41 (2H, t, J 7.6), 7.30 (2H, t, J 7.9), 7.06 (2H, d, J 8.1), 7.02 (2H, s), 2.37 (3H, s), 2.36 (6H, s), 2.09 (3H, s); δ_C (176 MHz, CDCl$_3$) 164.35, 164.25, 141.15, 140.72, 139.29, 138.76, 138.54, 130.14, 130.04, 128.90, 126.09, 125.83, 124.23, 123.28, 120.99, 120.46, 119.97, 109.63, 21.29, 20.49, 17.83. MS (MALDI+): *m/z* 443.2 (M$^+$, 100%).

2-[4-(9*H*-Carbazol-9-yl)-3-methylphenyl]- 5-(2,4,6-triisopropylphenyl)-1,3,4-oxadiazole (77)

A flask was charged with 2-(4-fluoro-3-methylphenyl)-5-(2,4,6-triisopropylphenyl)-1,3,4-oxadiazole **70** (0.12 g, 0.31 mmol), carbazole (0.05 g, 0.31 mmol), K$_2$CO$_3$ (200 mg) and DMSO (20 ml). The solution was heated at 150 ^{o}C overnight. The solution was cooled and water added. The mixture was extracted with DCM (3 × 30 ml). The organic layers were combined and dried over MgSO$_4$. A brown solid was obtained after removing solvent and purified by column chromatography (SiO$_2$, 98:2 DCM: EtOAc) followed by recrystallisation from acetonitrile yielding compound **77** (0.10 g, 57%) as colourless crystals. Crystals for X-ray analysis were grown by slowly cooling a solution of **77** in MeCN; mp: 202.6-203.8 ^{o}C; Anal. Calc. for C$_{36}$H$_{37}$N$_3$O: C, 81.94; H, 7.07; N, 7.96; Found: C, 81.80; H, 7.12; N, 8.07; δ_H (700 MHz, CDCl$_3$) 8.24 (1H, s), 8.16 (2H, d, J 7.8), 8.12 (1H, d, J 8.2), 7.54 (1H, d, J 8.1), 7.40 (2H, t, J 7.6), 7.30 (2H, t, J 7.8), 7.15 (2H, s), 7.06 (2H, d, J 8.1), 2.97 (1H, dt, J 6.9, 13.8), 2.70 (2H, dt, J 6.8, 13.5), 2.08 (3H, s), 1.30 (6H, t, J 9.1), 1.25 (12H, d, J 6.8); δ_C (176 MHz, CDCl$_3$) 164.55, 164.16, 152.53, 149.48, 140.74, 139.30, 138.56, 130.17, 130.02, 126.08, 125.78, 124.27, 123.28, 121.23, 120.45, 119.97, 119.59, 109.63, 34.60, 31.53, 24.11, 23.88, 17.80; MS (MALDI+): *m/z* 527.3 (M$^+$, 100%).

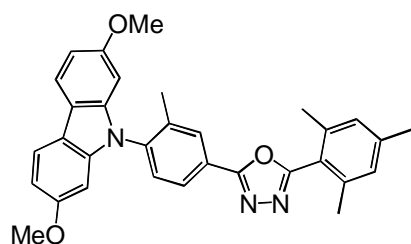## 2-[4-(2,7-Dimethoxy-9*H*-carbazol-9-yl)phenyl]-5-(2,4,6-trimethylphenyl)-1,3,4-oxadiazole (78)

A flask was charged with 2-(4-fluoro-3-methylphenyl)-5-(2,4,6-trimethylphenyl)-1,3,4-oxadiazole **69** (0.07 g, 0.2 mmol), 2,7-dimethoxycarbazole (0.07 g, 0.3 mm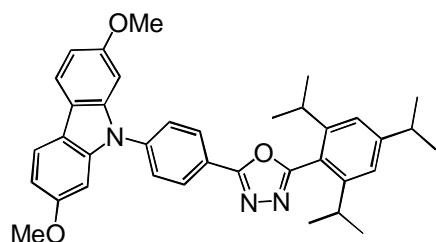ol), K_2CO_3 (200 mg) and DMSO (10 ml). The solution was heated at 150 ^{o}C overnight. The solution was cooled and water added. The mixture was extracted with DCM (3 × 30 ml). The organic layers were combined and dried over $MgSO_4$. A brown solid was obtained after removing solvent and purified by column chromatography (SiO_2, 98:2 DCM: EtOAc) followed by recrystallisation from acetonitrile yielding compound **78** (0.05 g, 50%) as colourless crystals; mp: 186.3-187.2 ^{o}C; Anal. Calc. for $C_{32}H_{29}N_3O_3$: C, 76.32; H, 5.80; N, 8.34; Found: C, 76.27; H, 5.85; N, 8.40; δ_H (500 MHz, $CDCl_3$) 8.28 (1H, s), 8.16 (1H, d, *J* 9.8), 7.94 (2H, d, *J* 8.5), 7.56 (1H, d, *J* 8.1), 7.05 (2H, s), 6.90 (2H, dd, *J* 3.3, 9.5), 6.49 (2H, d, *J* 2.2), 3.82 (6H, s), 2.40 (3H, s), 2.38 (6H, s), 2.14 (3H, s); δ_C (126 MHz, $CDCl_3$) 164.65, 164.49, 158.69, 142.38, 141.47, 139.42, 139.01, 138.86, 130.40, 129.18, 126.23, 124.58, 121.21, 120.57, 117.47, 108.55, 94.26, 55.93, 21.59, 20.79, 18.23; MS (ASAP+): *m/z* 504.2 (M+H$^+$, 100%).

2-[4-(2,7-Dimethoxy-9*H*-carbazol-9-yl)phenyl]-5-(2,4,6-triisopropylphenyl)-1,3,4-oxadiazole (79)

A flask was charged with 2-(4-fluoro-3-methylphenyl)-5-(2,4,6-triisopropylphenyl)-1,3,4-oxadiazole **66** (0.2 g, 0.5 mmol), 2,7-dimethoxycarbazole (0.2 g, 1.2 mmol), K_2CO_3 (400 mg) and DMSO (20 ml). The solution was heated at 150 ^{o}C overnight. The solution was cooled and water added. The mixture was extracted with DCM (3 × 30 ml). The organic layers were combined and dried over $MgSO_4$. A brown solid was obtained after removing solvent and purified by column chromatography (SiO_2, 98:2 DCM: EtOAc) followed by recrystallisation from

acetonitrile yielding compound **79** (0.17 g, 60%) as colourless crystals; mp: 192.5-194.0 °C; Anal. Calc. for $C_{37}H_{39}N_3O_3$: C, 77.46; H, 6.85; N, 7.32; Found: C, 77.35; H, 6.93; N, 7.35; δ_H (500 MHz, CDCl$_3$) 8.36 (2H, d, *J* 8.5), 7.93 (2H, d, *J* 9.2), 7.77 (2H, d, *J* 8.5), 7.18 (2H, s), 6.97 − 6.88 (4H, m), 3.86 (6H, s), 3.01 (1H, dt, *J* 7.0, 13.9), 2.79 − 2.67 (2H, m), 1.34 (6H, d, *J* 6.9), 1.28 (12H, d, *J* 6.8); δ_C (126 MHz, CDCl$_3$) 164.72, 164.37, 158.67, 152.82, 149.75, 141.96, 141.07, 128.85, 127.61, 123.10, 121.53, 120.55, 119.81, 117.96, 108.91, 94.61, 55.99, 34.88, 31.82, 24.41, 24.18; MS (ASAP+): *m/z* 574.3 (M+H$^+$, 100%).

2-[4-(9*H*-carbazol-9-yl)phenyl]-5-methyl-1,3,4-oxadiazole (80)
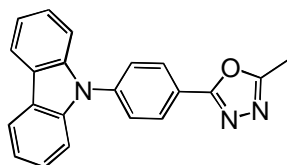
A flask was charged with 2-(4-fluorophenyl)-5-methyl-1,3,4-oxadiazole **82** (0.50 g, 2.8 mmol), carbazole (0.47 g, 2.8 mmol), K$_2$CO$_3$ (1.9 g) and DMSO (40 ml). The solution was heated at 150 °C overnight. The solution was cooled and water added. The mixture was extracted with DCM (3 × 100 ml). The organic layers were combined and dried over MgSO$_4$. A brown solid was obtained after removing solvent and purified by column chromatography (SiO$_2$, 100%DCM) followed by recrystallisation from acetonitrile yielding compound **80** (0.55 g, 61%) as colourless crystals. Crystals for X-ray analysis were grown by slowly cooling a solution of **80** in MeCN; mp: 202.8-203.8 °C; Anal. Calc. for $C_{21}H_{15}N_3O$: C, 77.52; H, 4.65; N, 12.91; Found: C, 77.52; H, 4.67; N, 13.13; δ_H (500 MHz, CDCl$_3$) 8.30 (2H, d, *J* 8.6), 8.17 (2H, d, *J* 7.7), 7.77 (2H, d, *J* 8.6), 7.54 − 7.43 (4H, m), 7.34 (2H, t, *J* 7.4), 2.70 (3H, s); δ_C (126 MHz, CDCl$_3$) 164.58, 164.12, 140.99, 140.50, 128.62, 127.46, 126.45, 124.00, 122.78, 120.80, 120.72, 109.94, 11.47; MS (EI): *m/z* 325.0 (M$^+$, 100%).

2-[4-(2,7-Dimethoxy-9*H*-carbazol-9-yl)phenyl]-5-methyl-1,3,4-oxadiazole (81)
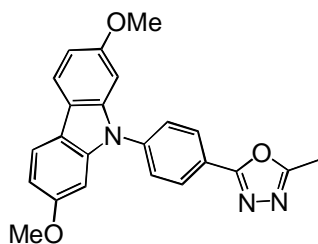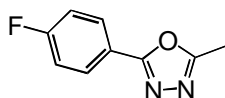
A flask was charged with 2-(4-fluorophenyl)-5-methyl-1,3,4-oxadiazole **82** (0.24 g, 1.4 mmol), 2,7-dimethoxycarbazole (0.30 g, 1.4 mmol), K_2CO_3 (800 mg) and DMSO (40 ml). The solution was heated at 150 °C overnight. The solution was cooled and water added. The mixture was extracted with DCM (3 × 100 ml). The organic layers were combined and dried over $MgSO_4$. A brown solid was obtained after removing solvent and purified by column chromatography (SiO_2, 100% DCM) followed by recrystallisation from acetonitrile yielding compound **81** (0.36 g, 73%) as colourless crystals; mp: 226.9-228.3 °C; Anal. Calc. for $C_{23}H_{19}N_3O_3$: C, 71.67; H, 4.97; N, 10.90; Found: C, 71.27; H, 4.96; N, 10.81; δ_H (700 MHz, $CDCl_3$) 8.27 (2H, d, *J* 8.5), 7.89 (2H, d, *J* 8.4), 7.72 (2H, d, *J* 8.5), 6.91 – 6.86 (4H, m), 3.83 (6H, s), 2.67 (3H, s); δ_C (176 MHz, $CDCl_3$) 164.29, 163.84, 158.41, 141.72, 140.69, 128.46, 127.22, 122.71, 120.26, 117.71, 108.59, 94.41, 55.71, 11.16. MS (EI): *m/z* 385.0 (M^+, 100%).

2-(4-Fluorophenyl)-5-methyl-1,3,4-oxadiazole (82)

2-(4-Fluorophenyl)-5-methyl-1,3,4-oxadiazole **82** was prepared following procedure of Barrett *et al.*[155] An argon-purged flask was charged with 4-fluorobenzoic hydrazide (1.0 g, 6.5 mmol) and triethyl orthoformate (20 ml). The solution was refluxed overnight. The solution was cooled and water added. The precipitate was collected and dried. The crude product was recrystallised from ethanol yielding compound **82** (0.82 g, 71%) as a white solid; MS (EI): *m/z* 178.0 (M^+, 15%), 123.0 (100%).

7.3 Experimental Procedures for Chapter 3

2-(4-Methoxyphenyl)-5-(2,4,6-triisopropylphenyl)-1,2,4-oxadiazole (85)
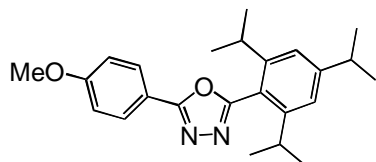
Following the procedure for **65**, 5-(4-Methoxyphenyl)-tetrazole (1.50 g, 9.1 mmol), 2,4,6-triisopropylbenzoyl chloride **62** (2.68 g, 10.0 mmol) and pyridine (10 ml) gave **85** (1.85 g, 55%) as colourless crystals; mp: 160.5-161.3 °C; Anal. Calc. for $C_{24}H_{30}N_2O_2$: C, 76.16; H, 7.99; N, 7.40; O, 8.45. Found: C, 76.01; H, 7.74; N, 8.60; δ_H (700 MHz, CDCl$_3$) 8.02 (2H, d, J 8.9), 7.12 (2H, s), 7.02 (2H, d, J 8.9), 3.87 (3H, s), 2.95 (1H, dt, J 7.0, 14.0), 2.67 (2H, hept, J 6.8), 1.29 (6H, d, J 6.9), 1.20 (12H, d, J 6.8); δ_C (176 MHz, CDCl$_3$) 164.93, 163.28, 162.27, 152.26, 149.46, 128.57, 121.14, 119.88, 116.65, 114.52, 55.45, 34.57, 31.41, 24.08, 23.88; λ_{abs} (CH$_2$Cl$_2$) (ε,10^{4}dm^3.M^{-1}cm^{-1}) 270 nm (2.29); MS (ASAP+): m/z 379 (M$^+$, 100%).

Complex (86)
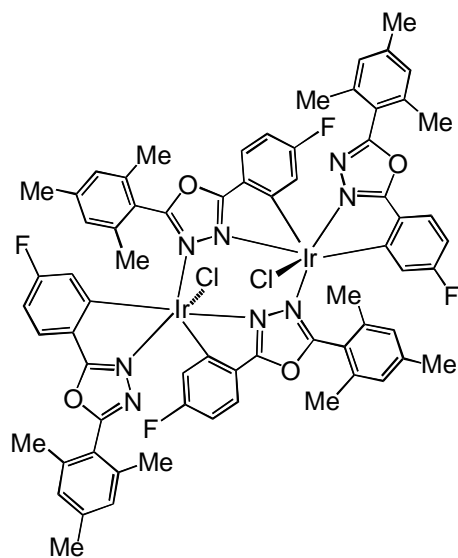
A mixture of the ligand **65** (780 mg, 2.8 mmol), iridium chloride (400 mg, 1.1 mmol) and 2-ethoxyethanol: water (10 ml, 3:1 v/v) was stirred at 120 °C overnight. The solid was collected and recrystallised from DCM: hexane to afford complex **86** (88 mg, 10%) as yellow crystals. Crystals for X-ray analysis were grown by slow cooling of a solution of **86** in DMSO. δ_H (700 MHz, CDCl$_3$) 7.69 (2H, dd, J 2.4, 10.3), 7.35 (2H, dd, J 5.6, 8.4), 7.24 – 7.22 (2H, m), 6.88 (4H, s), 6.86 (2H, s), 6.66 (2H, td, J 2.4, 8.5), 6.47 (2H, td, J 2.4, 8.5), 6.40 (2H, s), 5.65 (2H, dd, J 2.4, 10.9), 2.44 (6 H, s), 2.28 (12H, s), 2.18 (12H, s), 1.54 (6 H, s); Anal. Calc. for $C_{68}H_{56}Cl_2F_4Ir_2N_8O_4$: C, 51.67; H, 3.57; N, 7.09; Found: C, 51.48; H, 3.50; N, 7.14; HRMS (FTMS+ESI): calcd for [$C_{68}H_{56}Cl_2F_4Ir_2N_8O_4$+H$^+$]: 1581.3074. Found: 1581.3049.

Complex (87)
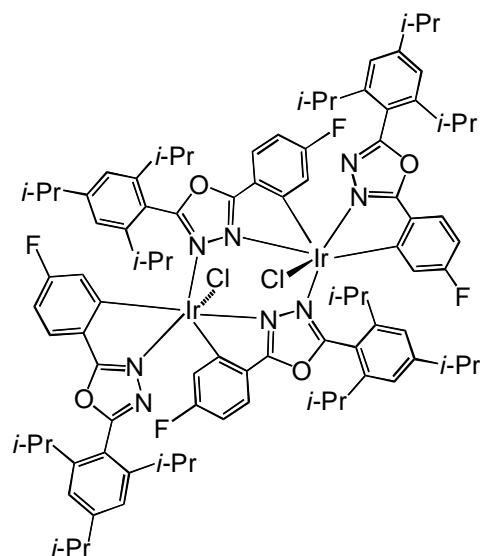
Following the procedure for **86**, **66** (533 mg, 1.5 mmol), iridium chloride (200 mg, 0.6 mmol) and 2-ethoxyethanol: water (10 ml; 3:1 v/v) gave complex **87** (230 mg, 40%) as yellow crystals. Crystals for X-ray analysis were grown by slow cooling of a solution of **86** in DCM/hexane. δ_H (700 MHz, CDCl$_3$) 7.63 (2H, dd, J 2.4, 10.1), 7.27 (4H, ddd, J 5.7, 8.5, 19.7), 7.13 (2H, s), 7.01 (4H, s), 6.59 (2H, s), 6.51 (2H, td, J 2.5, 8.3), 6.47 (2H, td, J 2.4, 8.4), 5.52 (2H, dd, J 2.4, 10.8), 3.55 (2H, dt, J 6.6, 13.4), 2.89 (4H, t, J 6.9, 14.0), 2.16 (4H, dt, J 6.8, 13.6), 2.05 (2H, dt, J 6.8, 13.6), 1.44 (6H, d, J 6.4), 1.30 (12H, d, J 6.9), 1.24 (12H, d, J 6.9), 1.01 (18H, d, J 6.8), 0.96 (12H, d, J 6.8), 0.81 (6H, d, J 6.8), 0.77 (6H, d, J 6.9); Anal. Calc. for C$_{92}$H$_{104}$Cl$_2$F$_4$Ir$_2$N$_8$O$_4$: C, 57.64; H, 5.47; N, 5.84; Found: C, 57.48; H, 5.40; N, 5.72 HRMS (FTMS+ESI): calcd for [C$_{92}$H$_{104}$Cl$_2$F$_4$Ir$_2$N$_8$O$_4$+H$^+$]: 1917.6830. Found: 1917.6828.

Complex (88)
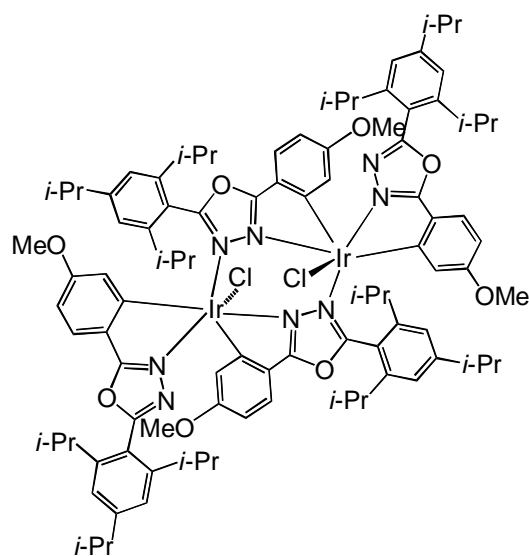
Following the procedure for **86**, **85** (280 mg, 0.7 mmol), iridium chloride (115 mg, 0.3 mmol) and 2-ethoxyethanol: water (10 ml, 3:1 v/v) gave complex **88** (100 mg, 40%) as yellow crystals. Crystals for X-ray analysis were grown by slow cooling of a solution of **88** in DCM/hexane. δ_H (700 MHz, CDCl$_3$) 7.46 (2H, d, J 2.4), 7.18 (4H, dd, J 8.4, 11.3), 7.04 (2H, s), 7.00 (4H, s), 6.55 (2H, s), 6.36 (2H, dd, J 2.4, 8.3), 6.27 (2H, dd, J 2.4, 8.5), 5.35 (2H, d, J 2.4), 3.75 (6H, s), 3.41 (2H, dt, J 6.7, 13.4), 3.29 (6H, s), 2.90 (2H, dt, J 6.9, 13.8), 2.85 (2H, dt, J 7.0, 13.9), 2.25 – 2.14 (6H, m), 1.42

(6H, d, *J* 6.4), 1.28 (12H, t, *J* 7.3), 1.25 (12H, d, *J* 6.9), 1.02 (6H, d, *J* 6.7), 0.99 (24H, t, *J* 7.3), 0.79 (12H, t, *J* 6.5); Anal. Calc. for $C_{96}H_{116}Cl_2Ir_2N_8O_8$: C, 58.67; H, 5.95; N, 5.70; Found: C, 58.50; H, 5.73; N, 5.76; HRMS (FTMS+ESI): calcd for $[C_{96}H_{116}Cl_2Ir_2N_8O_8+H^+]$: 1965.7630. Found: 1965.7627.
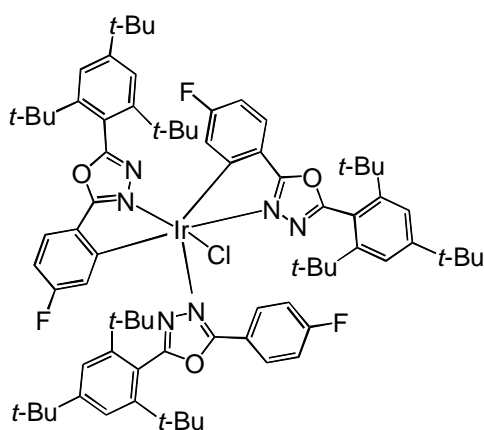
Complex (89)

Following the procedure for **86**, **67** (640 mg, 1.6 mmol), iridium chloride (230 mg, 0.7 mmol) and 2-ethoxyethanol: water (10 ml, 3:1 v/v) gave complex **89** (140 mg, 14%) as yellow crystals. Crystals for X-ray analysis were grown by slow cooling of a solution of **89** in DCM/hexane. Anal. Calc. for $C_{78}H_{97}ClF_3IrN_6O_3$: C, 65.45; H, 7.52; F, 3.70; Ir, 12.47; N, 5.45; Found: C, 66.12; H, 7.80; N, 5.31; Ir, 12.63; δ_H (400 MHz, CDCl₃) 8.18 – 8.05 (3H, m), 7.63 (1H, d, *J* 1.6), 7.54 (1H, d, *J* 1.6), 7.47 – 7.33 (6 H, m), 7.05 (2H, d, *J* 8.7), 6.88 – 6.78 (1H, m), 6.60 – 6.49 (1H, m), 6.02 (1H, dd, *J* 10.2, 2.4), 1.39 (9H, s), 1.38 (9H, s), 1.33 (9H, s), 1.31 (9H, s), 1.18 (9H, s), 1.00 (9H, s), 0.85 (9H, s), 0.81 (9H, s), 0.60 (9 H, s); MS (MALDI+) *m/z* = 1042.3 (M - 408).

Complex (90)
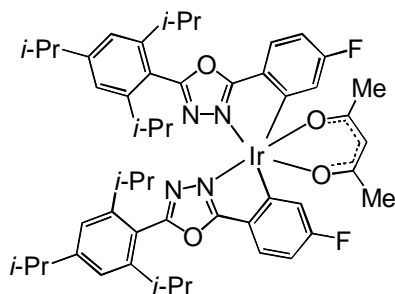
A mixture of complex **87** (80 mg, 0.04 mmol), acetylacetone (0.1 ml), Na₂CO₃ (100 mg, 0.8 mmol) and 2-ethoxyethanol (10 ml) was stirred at 120 °C overnight. The solvent was removed under reduce pressure and the product was purified by column chromatography [SiO₂, eluent DCM/hexane (2:3 v/v)] followed by recrystallisation from DCM/hexane to give **90** as yellow crystals (50 mg, 61%). Crystals for X-ray analysis were grown by slow cooling of a solution of **90** in DCM/hexane. δ_H (700 MHz, CDCl₃) 7.58 (1H, dd, *J* 5.5, 8.3), 7.44 (1H, dd, *J* 5.6,

8.3), 7.21 (1H, dd, J 2.4, 9.6), 7.11 (2H, s), 7.03 (2H, s), 6.91 (1H, td, J 2.4, 8.7), 6.58 (1H, td, J 2.5, 8.6), 6.18 (1H, dd, J 2.4, 10.1), 5.37 (1H, s), 2.95 (1H, dt, J 7.0, 13.9), 2.90 (1H, dt, J 6.9, 13.8), 2.74 (2H, hept, J 6.9), 2.32 (2H, hept, J 6.8, 13.7), 1.88 (6H, d, J 3.6), 1.28 (6H, d, J 6.9), 1.24 (6H, d, J 6.9), 1.17 (12H, d, J 6.8), 1.05 (6H, d, J 6.8), 1.00 (6H, d, J 6.8); λ_{abs} (CH$_2$Cl$_2$) (ε,10^{4}dm^3.M^{-1}cm^{-1}) 263 nm (3.80); Anal. Calc. for C$_{51}$H$_{59}$F$_2$IrN$_4$O$_4$: C, 59.92; H, 5.82; N, 5.48. Found: C, 59.74; H, 5.93; N, 5.20; HRMS (FTMS+ESI): calcd for [C$_{51}$H$_{59}$F$_2$IrN$_4$O$_4$+H$^+$]: 1023.4213. Found: 1023.4189.

Complex (91)
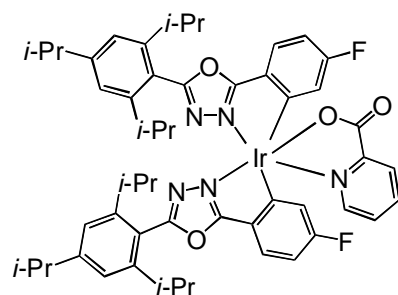
Following the procedure for **90**, **87** (100 mg, 0.05 mmol), picolinic acid (40 mg, 0.5 mmol), Na$_2$CO$_3$ (55 mg, 0.6 mmol) and 2-ethoxyethanol (10 ml) gave yellow crystals of complex **91** (30 mg, 28%). δ_H (700 MHz, CDCl$_3$) 8.25 (1H, d, J 7.7), 7.87 (2H, dd, J 6.2, 12.2), 7.58 (1H, dd, J 5.5, 8.4), 7.54 (1H, dd, J 5.4, 8.3), 7.39 – 7.30 (1H, m), 7.12 (2H, s), 7.10 (2H, s), 6.83 – 6.75 (1H, m), 6.75 – 6.70 (1H, m), 6.47 (1H, dd, J 2.3, 9.7), 6.43 (1H, dd, J 2.3, 9.5), 2.94 (2H, dt, J 7.0, 14.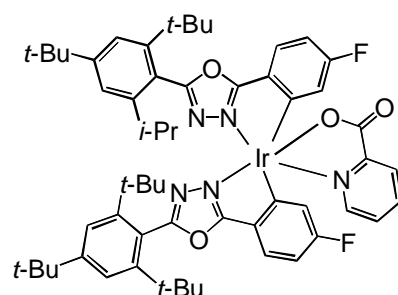0), 2.68 (2H, dt, J 6.8, 13.7), 2.54 (2H, dt, J 6.8, 13.5), 1.29 – 1.24 (18H, m), 1.20 (6H, d, J 6.8), 1.18 (6H, d, J 6.8), 1.12 (6H, d, J 6.8); λ_{abs} (CH$_2$Cl$_2$) (ε,10^{4}dm^3.M^{-1}cm^{-1}) 243 nm (4.35); %). Anal. Calc. for C$_{52}$H$_{56}$F$_2$IrN$_5$O$_4$: C, 59.75; H, 5.40; N, 6.70. Found: C, 59.65; H, 5.48; N, 6.55; HRMS (FTMS+ESI): calcd for [C$_{52}$H$_{56}$F$_2$IrN$_5$O$_4$+H$^+$]: 1046.4008. Found: 1046.3987.

Complex (92)

Following the procedure for **90**, **89** (70 mg, 0.05 mmol), picolinic acid (50 mg, 0.5 mmol), Na$_2$CO$_3$ (55 mg, 0.6 mmol) and 2-ethoxyethanol (10 ml) gave yellow crystals of complex **92** (40 mg, 69%). Crystals for X-ray analysis were grown by slow

cooling of a solution of **92** in DCM/hexane. δ_H (700 MHz, CDCl$_3$) 8.18 (1H, d, J 7.8), 8.07 (1H, d, J 5.3), 7.88 (1H, td, J 1.4, 7.7), 7.56 (1H, dd, J 5.3, 8.4), 7.53 – 7.43 (6H, m), 7.38 – 7.33 (1H, m), 6.87 (1H, td, J 2.4, 8.6), 6.64 (1H, td, J 2.4, 8.6), 6.12 (1H, dd, J 2.4, 9.9), 1.35 (9H, s), 1.30 (9H, s), 1.25 (9H, s), 1.11 (18H, s), 0.71 (9H, s); λ_{abs} (CH$_2$Cl$_2$) (ε,10^{4}dm^3.M^{-1}cm^{-1}) 256 nm (4.30); Anal. Calc. for C$_{58}$H$_{68}$F$_2$IrN$_5$O$_4$: C, 61.68; H, 6.07; N, 6.20. Found: C, 61.75; H, 6.16; N, 6.02; HRMS (FTMS+ESI): calcd for [C$_{58}$H$_{68}$F$_2$IrN$_5$O$_4$+H$^+$]: 1130.4977. Found: 1130.4927.

Complex (96)
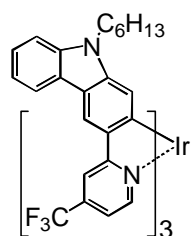
A mixture of **101** (0.23 g, 0.58 mmol), iridium chloride (0.09 g, 0.25 mmol) and 2-ethoxyethanol: water (10 ml, 3:1) was stirred at 120 ^{o}C overnight. The precipitate was collected by suction filtration and the orange solid was dried. A mixture of the **101** (0.24 g, 6.0 mmol), the orange solid **103** (0.28 g, 0.13 mmol) and ethylene glycol (10 ml), acetylacetone (0.1 ml) and NEt$_3$ (0.1 ml) was stirred at 190 ^{o}C overnight. The precipitate was collected by suction filtration. The crude product was purified by column chromatography (SiO$_2$, 40:60 DCM: hexane) yielding **96** (0.15 g, 40%) as an orange solid. The NMR data is in agreement with previous characterisation.[63]

Complex (97)
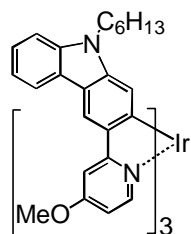
A mixture of the ligand **102** (0.67 g, 1.9 mmol), iridium chloride (0.32g, 0.89 mmol) and 2-ethoxylethanol: water (10 ml, 3:1) was stirred at 120 ^{o}C overnight. The precipitate was collected by suction filtration and the yellow solid **104** was dried. A mixture of the ligand **102** (0.08 g, 0.23 mmol), **104** (0.11 g, 0.06 mmol) and ethylene glycol (10 ml), acetylacetone (0.1 ml) and NEt$_3$ (0.1 ml) was stirred at 190 ^{o}C for 1 h. The precipitate was collected by suction filtration. The crude product was purified by column chromatography (SiO$_2$, 40:60 DCM: hexane) yielding complex **97** (0.10 g, 70%) as a yellow solid; Anal. Calc. for C$_{72}$H$_{75}$N$_6$O$_3$Ir: C, 68.38; H, 5.98; N, 6.65;.

Found: C, 68.18; H, 5.92; N, 6.37; δ_H (500 MHz, acetone-d$_6$) 8.63 (3H, s), 8.05 (3H, d, J 7.6), 7.78 (3H, d, J 2.6), 7.66 (3H, t, J 6.6), 7.31 − 7.23 (6H, m), 7.07 (3H, ddd, J 13.0, 7.5, 4.5), 6.94 (3H, s), 6.64 (3H, dd, J 6.4, 2.6), 3.98 (9H, s), 3.86 − 3.71 (6H, m), 1.55 − 1.26 (12H, m), 1.02 − 0.81 (12H, m), 0.66 (9H, m).MS (MALDI+): m/z 1264.4 (M$^+$, 100%).

1-(2-Ethylhexyl)-2-iodo-1*H*-indole-3-carbaldehyde (116)
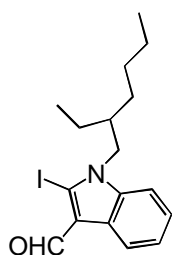
To a solution of *N*-methylpiperazine (6.0 mL, 50.6 mmol) in THF (100 mL) was added ^{n}BuLi in hexane (2.5 M, 18.7 mL, 46.7 mmol) at −78 °C. After 20 min, compound **115**[156] (10.0 g, 38.9 mmol) was added and the mixture was stirred for 20 min at the same temperature. Then ^{n}BuLi in hexane (2.5 M, 47 mL, 116.7 mmol) was added dropwise, and the mixture was warmed to −23 °C. After 3.5 h, a solution of I$_2$ (49.0 g, 194.5 mmol) in THF (40 mL) was added to the mixture. After 1 h, the reaction was quenched by addition of saturated aqueous Na$_2$S$_2$O$_3$, and the mixture was extracted with DCM. The organic layers were combined, dried (MgSO$_4$) and filtered. A brown solid was obtained after removing solvent and purified by column chromatography (SiO$_2$, 50:50 DCM: hexane) yielding **116** (8.91 g, 60%) as a brown oil; Anal. Calc. for C$_{17}$H$_{22}$NOI: C, 53.27; H, 5.79; N, 3.65;. Found: C, 53.20; H, 5.62; N, 3.75; δ_H (700 MHz, CDCl$_3$) 9.85 (1H, s), 8.36 − 8.30 (1H, m), 7.38 − 7.30 (1H, m), 7.29 − 7.22 (2H, m), 4.13 (2H, dd, J 7.6, 3.0), 2.14 − 1.95 (1H, m), 1.53 − 1.18 (8H, m), 0.91 (3H, t, J 7.5), 0.86 (3H, t, J 7.1); δ_C (176 MHz, CDCl$_3$) 187.95, 139.28, 126.58, 123.85, 122.78, 120.79, 119.10, 110.38, 100.48, 51.87, 39.81, 30.67, 28.64, 24.07, 22.92, 13.95, 10.94; MS (ASAP+): m/z 328.2 (M$^+$, 100%).

2-[(2,4-Difluorophenyl)ethynyl]-1-(2-ethylhexyl)-1*H*-indole-3-carbaldehyde (118)
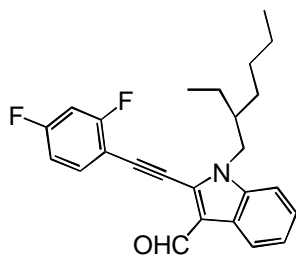
An argon-purged flask was charged with **115** (2.00 g, 5.2 mmol) and dry triethylamine (30 ml). The solution was degassed for 20 min before Pd(PPh$_3$)$_2$Cl$_2$ (60 mg),

commercial **117** (0.86 g, 6.3 mmol) and copper(I) iodide (0.01 mg) were added. The reaction was stirred for 18 h at room temperature. The NEt$_3$ was removed under reduced pressure. The residue was extracted with DCM (3 × 100 ml). The organic layers were combined, dried (MgSO$_4$) and filtered. A pale yellow oil was obtained after removing solvent and purified by column chromatography (SiO$_2$, 80:20 DCM: EtOAc) yielding **118** (1.81 g, 90%) as a brown solid; mp: 70.6-71.5 ^{o}C; δ_H (700 MHz, CDCl$_3$) 10.28 (1H, s), 8.35 (1H, d, J 7.8), 7.63 – 7.50 (1H, m), 7.40 – 7.29 (3H, m), 7.02 – 6.90 (2H, m), 4.22 (2H, dd, J 7.6, 2.2), 2.11 – 2.00 (1H, m), 1.48 – 1.14 (8H, m), 0.92 (3H, t, J 7.5), 0.84 (3H, t, J 7.1); δ_C (176 MHz, CDCl$_3$) 185.13, 164.20 (dd, J 48.9, 12.3), 162.74 (dd, J 50.1, 12.3), 137.30, 134.18 (dd, J 8.3, 3.9), 131.16, 125.06, 124.61, 123.45, 122.31, 120.11, 112.14 (dd, J 21.3, 4.6), 110.28, 106.67 (dd, J 13.5, 6.2), 104.87 – 104.56 (m), 93.26, 82.90, 49.40, 39.74, 30.62, 28.55, 23.99, 22.95, 13.90, 10.68; HRMS (MS ASAP+): calcd for [C$_{25}$H$_{25}$F$_2$NO+H$^+$]: 394.1982. Found: 394.1968.

3-(2,4-Difluorophenyl)-5-(2-ethylhexyl)-5H-pyrido[4,3-b]indole (119)
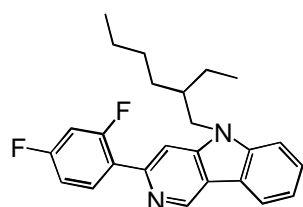
An argon-purged flask was charged with **118** (1.81 g, 4.6 mmol), *tert*-butylamine (2 ml) and toluene (20 ml). The solution was heated at 100 ^{o}C for 48 h. The solvent was removed under reduced pressure. The crude product was purified by column chromatography (SiO$_2$, 60:40 DCM: EtOAc) yielding **119** (1.09 g, 60%) as a brown oil; δ_H (700 MHz, CDCl$_3$) 9.36 (1H s), 8.16 (2H, t, J 10.0), 7.76 (1H, s), 7.57 – 7.49 (1H, m), 7.44 (1H, d, J 8.2), 7.33 (1H, t, J 7.4), 7.08 – 7.01 (1H, m), 6.95 (1H, ddd, J 11.2, 8.9, 2.3), 4.18 (2H, dd, J 7.5, 3.0), 2.06 (1H, dt, J 12.7, 6.2), 1.47 – 1.21 (8H, m), 0.93 (3H, t, J 7.4), 0.85 (3H, t, J 7.2); δ_C (176 MHz, CDCl$_3$) 163.51 (d, J 12.2), 162.09 (d, J 12.0), 161.12 (d, J 11.7), 159.69 (d, J 11.6), 147.46, 145.57, 142.21, 141.45, 132.58 (dd, J 9.5, 4.3), 126.80, 121.23, 120.75, 120.57, 111.80 (dd, J 20.9, 3.5), 109.57, 104.91, 104.29 (dd, J 27.2, 25.4), 47.40, 39.35, 30.97, 28.72, 24.34, 22.94, 13.91, 10.79; HRMS (MS ASAP+): calcd for [C$_{25}$H$_{26}$F$_2$N$_2$+H$^+$]: 393.2142. Found: 393.2147.

Complex (*mer*-121)
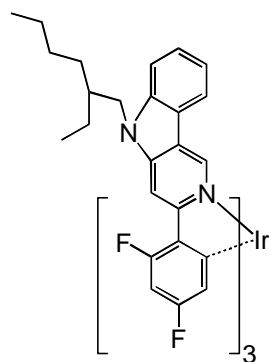
A mixture of the **119** (0.60 g, 1.5 mmol), iridium chloride (0.24 g, 0.67 mmol) and 2-ethoxyethanol: water (10 ml, 3:1) was stirred at 120 °C overnight. The precipitate was collected by suction filtration and the yellow solid was dried. A mixture of the **119** (0.12 g, 3.1 mmol), the yellow solid **120** (0.15 g, 0.07 mmol) and ethylene glycol (10 ml), acetylacetone (0.1 ml) and NEt$_3$ (0.1 ml) was stirred at 190 °C overnight. The precipitate was collected by suction filtration. The crude product was purified by column chromatography (SiO$_2$, 40:60 DCM: hexane) yielding *mer*-**121** (0.12 g, 63%) as a yellow solid. Crystals for X-ray analysis were grown by slow cooling of a solution of **121** in DCM/hexane; δ_H (500 MHz, CDCl$_3$) 8.74 (1H, t, *J* 3.0), 8.68 (1H, d, *J* 7.4), 8.41 (1H, s), 8.28 (2H, s), 8.16 (1H, s), 7.83 (1H, t, *J* 7.1), 7.79 – 7.71 (1H, m), 7.54 – 7.33 (8H, m), 7.23 (1H, dd, *J* 14.2, 6.7), 7.03 (1H, t, *J* 7.6), 6.63 (1H, s), 6.53 (2H, dd, *J* 22.8, 13.0), 6.48 – 6.40 (1H, m), 6.09 (1H, t, *J* 7.3), 5.94 – 5.80 (1H, m), 4.29 – 4.08 (6H, m), 2.07 (3H, d, *J* 8.9), 1.50 – 1.13 (24H, m), 1.07 – 0.78 (18H, m). δ_F (470 MHz, CDCl$_3$) -110.59, -111.06 (dd, *J* 15.8, 7.5), -111.26, -111.42 – -111.57 (2F, m), -112.84; HRMS (FTMS+ESI): calcd for [C$_{75}$H$_{75}$F$_6$IrN$_6$]: 1366.5587; Found: 1366.5579.

Complex (*fac*-121)
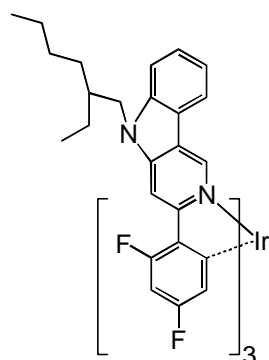
mer-**121** (4.3 mg, 3.1 µmol) was dissolved in CD$_2$Cl$_2$ (0.5 ml) in a Young's tap NMR tube and degassed three times by freeze-pump-thaw. The sample was irradiated by two LEDs at 365 nm (*ca.* 100 mW each) for a total period of 5 h with intermittent agitation. The conversion was monitored by ^{19}F NMR until the isomerisation was judged to have reached completion (yield, 100% by NMR). δ_H (700 MHz, CD$_2$Cl$_2$) 8.43 (3H, d, *J* 3.5), 8.21 (3H, m), 7.50 (3H, m), 7.45 (6H, m), 7.05 (3H, m), 6.40 (6H, m), 4.27 (6H, m), 2.13 (3H, m), 1.52-1.24 (24H, m) 0.99 (9H, dt, *J* 28.4, 7.4 Hz) 0.88 (9H, dt, *J* 24.9, 7.3 Hz); δ_F (658 MHz, CD$_2$Cl$_2$) -111.51 (1F, m), -11.95 (1F, quintet, *J* 6.6); HRMS (MS AP+): calcd for [C$_{75}$H$_{75}$F$_6$IrN$_6$]: 1366.5587. Found: 1366.5583.

Complex (*fac*-122)
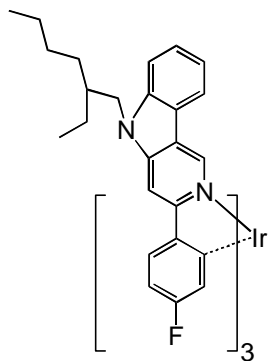
A mixture of the *mer*-**121** (0.06 g, 0.04 mmol) and glycol (10 ml) was stirred at 290 °C overnight. The residue was extracted with DCM (3 × 10 ml). The organic layers were combined, dried (MgSO₄) and filtered. The yellow solid which was obtained after removing the solvent was purified by column chromatography (SiO₂, 30:70 DCM : EtOAc) yielding *fac*-**122** (0.03 g, 58%) as a yellow solid; δ_H (700 MHz, CDCl₃) 8.15 (3H, d, *J* 12.2), 7.77 (3H, s), 7.70 (3H, s), 7.46 (3H, t, *J* 7.0), 7.40 (3H, t, *J* 7.7), 7.35 (3H, d, *J* 8.4), 7.02 (3H, t, *J* 7.3), 6.59 (6H, d, *J* 8.6), 4.36 – 4.10 (6H, m), 2.10 (3H, s), 1.51 – 1.19 (24H, m), 1.06 – 0.78 (18H, m); δ_F (658 MHz, CDCl₃) -113.40 (3F, dd, *J* 14.8, 8.2); HRMS (FTMS+ESI): calcd for [C₇₅H₇₈F₃IrN₆+H⁺]: 1313.5948. Found: 1313.5927.

7.4 Experimental Procedures for Chapter 4

2-(4-Phenyl)-5-(2,4,6-trimethylphenyl)-1,3,4-oxadiazole (126)
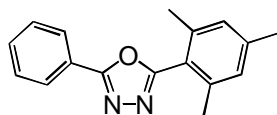
An argon-purged flask was charged with 5-(4-phenyl)-tetrazole **125** (0.25 g, 1.7 mmol), 2,4,6-trimethylbenzoyl chloride **61** (0.31 g, 1.7 mmol) and pyridine (5 ml). The solution was refluxed overnight. The solution was cooled and water added. The precipitate was collected and dried. The crude product was purified by column chromatography (SiO$_2$, 19:1 DCM: EtOAc) followed by recrystallisation from ethanol yielding compound **126** (0.38 g, 85%) as colourless crystals; mp: 98.6-99.7 $^{\mathrm{o}}$C; Anal. Calc. for C$_{17}$H$_{16}$N$_2$O: C, 77.25; H, 6.10; N, 10.60; Found: C, 77.20; H, 6.05; N, 10.71; δ_H (700 MHz, CDCl$_3$) 8.15 – 8.09 (2H, m), 7.59 – 7.50 (3H, m), 7.00 (2H, s), 2.36 (3H, s), 2.33 (6H, s); δ_C (176 MHz, CDCl$_3$) 164.81, 163.89, 141.01, 138.74, 131.63, 129.06, 128.85, 126.84, 124.06, 121.10, 21.26, 20.46; λ_{abs} (CH$_2$Cl$_2$) (ε,10^{4}dm^3.M^{-1}cm^{-1}) 263 nm (3.22); MS (EI): *m/z* 263.9 (M$^+$, 70%), 146.5 (100%).

1,3-Di(1*H*-tetrazol-5-yl)benzene (128)
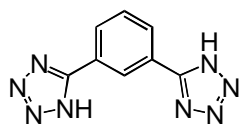
An argon-purged flask was charged with 1,3-dicyanobenzene **127** (1.50 g, 11.7 mmol), sodium azide (2.28 g, 35.0 mmol), ammonium chloride (1.86 g, 35.0 mmol) and anhydrous DMF (30 ml). The solution was refluxed overnight. The solution was cooled and water added before the solution was acidified with dilute hydrochloric acid to precipitate compound **128** which was filtered and dried to yield a pale yellow solid (1.43 g, 56%)[157] which was used for next step without further purification.

1,3-Bis(5-mesityl-1,3,4-oxadiazol-2-yl)benzene (129)
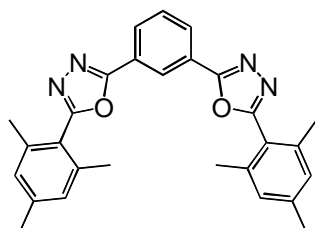
An argon-purged flask was charged with **128** (0.30 g, 1.4 mmol), 2,4,6-trimethylbenzoyl chloride **61** (0.56 g, 3.1 mmol) and pyridine (5 ml). The solution was refluxed overnight. The solution was cooled and water added. The precipitate was collected and dried. The crude product was purified by column chromatography (SiO$_2$, 19:1 DCM: EtOAc) followed by recrystallisation from ethanol yielding compound **129** (0.46 g, 73%) as colourless crystals; mp: 238.0-239.0 $^{\circ}$C; Anal. Calc. for C$_{28}$H$_{26}$N$_4$O$_2$: C, 74.65; H, 5.82; N, 12.44; Found: C,74.46; H, 5.71; N, 11.96; δ_H (500 MHz, CDCl$_3$) 8.77 (1H, t, *J* 1.4), 8.32 (2H, dd, *J* 7.9, 1.7), 7.72 (1H, t, *J* 7.9), 7.00 (4H, s), 2.36 (6H, s), 2.33 (12H, s); δ_C (126 MHz, CDCl$_3$) 164.67, 164.16, 141.51, 139.00, 130.36, 129.94, 129.19, 125.44, 125.21, 120.99, 21.58, 20.80; λ_{abs} (CH$_2$Cl$_2$) (ε,10^{4}dm^3.M^{-1}cm^{-1}) 266 nm (4.31); MS (ASAP+): *m/z* 451.2 (M$^+$, 100%).

1,3-Bis(5-(2,4,6-triisopropylphenyl)-1,3,4-oxadiazol-2-yl)benzene (130)
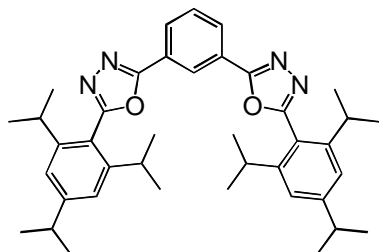
An argon-purged flask was charged with **128** (0.30 g, 1.4 mmol), 2,4,6-triisopropylbenzoyl chloride **62** (0.82 g, 3.1 mmol) and pyridine (5 ml). The solution was refluxed overnight. The solution was cooled and water added. The precipitate was collected and dried. The crude product was purified by column chromatography (SiO$_2$, 19:1 DCM: EtOAc) followed by recrystallisation from ethanol yielding compound **130** (0.38 g, 62%) as colourless crystals; mp: 228.6-229.5 $^{\circ}$C; Anal. Calc. for C$_{40}$H$_{50}$N$_4$O$_2$: C, 77.63; H, 8.14; N, 9.05; Found: C, 77.09; H, 8.14; N, 8.75; δ_H (700 MHz, CDCl$_3$) 8.71 (1H, t, *J* 1.4), 8.31 (2H, dd, *J* 7.9, 1.7), 7.71 (1H, t, *J* 7.9), 7.12 (4H, s), 2.95 (2H, hept, *J* 7.1), 2.63 (4H, hept, *J* 6.9), 1.28 (12H, d, *J* 6.9), 1.20 (24H, d, *J* 6.8); δ_C (176 MHz, CDCl$_3$) 164.36, 164.06, 152.56, 149.42, 130.12, 129.62, 125.27, 124.92, 121.20, 119.34, 24.06, 23.86; λ_{abs} (CH$_2$Cl$_2$) (ε,10^{4}dm^3.M^{-1}cm^{-1}) 258 nm (3.88); MS (MALDI+): *m/z* = 619.4 (M$^+$, 100%).

7.5 Experimental Procedures for Chapter 5

3,6-Bis((trimethylsilyl)ethynyl)-9-octyl-9*H*-carbazole (137)
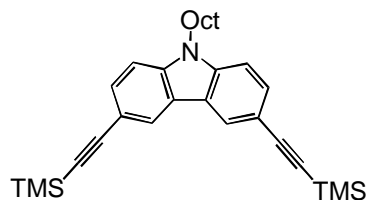
An argon-purged flask was charged with 9-octyl-3,6-diiodo-9*H*-carbazole **136**[148](4.00 g, 7.5 mmol) and dry triethylamine (30 ml). The solution was degassed for 20 min before Pd(PPh$_3$)$_2$Cl$_2$ (60 mg), TMSA (1.88 g, 18.6 mmol) and copper(I) iodide (0.01 mg) were added. The reaction was stirred for 18 h at room temperature. The NEt$_3$ was removed under reduced pressure. The residue was extracted with DCM (3 × 100 ml). The organic layers were combined, dried (MgSO$_4$) and filtered. A pale yellow oil which was obtained after removing the solvent was purified by column chromatography (SiO$_2$, 50:50 DCM: hexane) yielding **137** (3.70 g, 82%) as a pale yellow oil; Anal. Calc. for C$_{30}$H$_{41}$NSi$_2$: C, 76.37; H, 8.76; N, 2.97; Found: C, 76.30; H, 8.65; N, 2.82; δ_H (500 MHz, CDCl$_3$) 8.19 (2H, d, *J* 1.4), 7.57 (2H, dd, *J* 8.5, 1.5), 7.30 (2H, d, *J* 8.5), 4.25 (2H, t, *J* 7.3), 1.82 (2H, dt, *J* 14.4, 7.3), 1.35 – 1.23 (10H, m), 0.86 (3H, t, *J* 6.8), 0.29 (18H, s); δ_C (126 MHz, CDCl$_3$) 140.75, 130.21, 124.92, 122.53, 113.92, 109.02, 106.60, 92.27, 43.55, 31.98, 29.54, 29.39, 29.15, 27.47, 22.83, 14.31, 0.41; MS (ASAP+): *m/z* 472.1 (M+H$^+$, 100%).

3,6-Diethynyl-9-octyl-9*H*-carbazole (138)
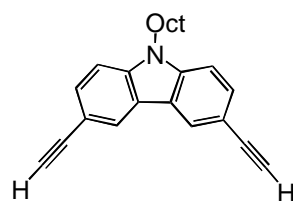
A flask was charged with **137** (3.70 g, 7.8 mmol), K$_2$CO$_3$ (5.30 g, 39.0 mmol) and methanol (50 ml). The solution was stirred overnight. The solvent was removed under reduced pressure and to the residue water was added and the mixture was extracted with DCM (3 × 100 ml). The organic layers were combined, dried (MgSO$_4$) and filtered. A brown solid which was obtained after removing the solvent was purified by column chromatography (SiO$_2$, 50:50 DCM: hexane) yielding compound **138** (2.30 g, 90%) as a yellow solid; mp: 66.2-67.5 °C; Anal. Calc. for C$_{24}$H$_{25}$N: C, 88.03; H, 7.70; N, 4.28. Found: C, 87.51; H, 7.77; N, 4.25; δ_H (500 MHz, CDCl$_3$) 8.24 (2H, d, *J* 1.1), 7.62 (2H, dd, *J* 8.5, 1.6), 7.36 (2H, d, *J* 8.5), 4.29 (2H, t, *J*

7.3), 3.10 (2H, s), 1.84 (2H, dt, J 14.3, 7.3), 1.43 – 1.14 (10H, m), 0.87 (3H, t, J 7.1); δ_C (126 MHz, CDCl$_3$) 140.89, 130.36, 125.01, 122.48, 112.89, 109.20, 84.97, 75.69, 43.58, 31.99, 29.55, 29.38, 29.16, 27.48, 22.83, 14.31; MS (ASAP+): m/z 328.2 (M$^+$, 100%).

3,6-Bis[(4-(4,4,5,5-tetramethyl-1,3,2-dioxaborolan-2-yl)phenyl)ethynyl]-9-octyl-9*H*-carbazole (139)
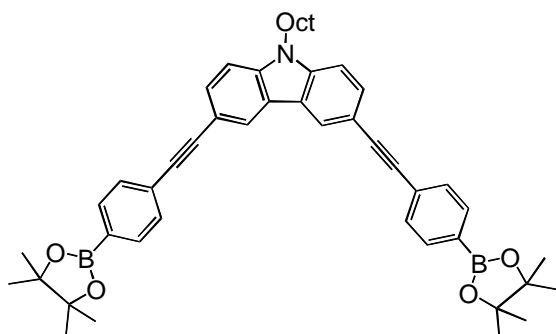
An argon-purged flask was charged with **139** (1.87 g, 5.7 mmol) and dried triethylamine (50 ml). The solution was degassed for 20 min before catalyst Pd(PPh$_3$)$_4$ (60 mg), 4-Iodophenylboronic acid pinacol ester (3.94 g, 11.7 mmol) and copper(I) iodide (0.01 mg) were added. The reaction was stirred for 18 h at room temperature. The NEt$_3$ was removed under reduced pressure. The residue was extracted with DCM (3 × 100 ml). The organic layers were combined, dried (MgSO$_4$) and filtered. A pale yellow oil obtained after removing the solvent was purified by column chromatography (SiO$_2$, 20:10:70 hexane: EtOAc: DCM) yielding **139** (3.86 g, 92%) as a yellow solid; mp: 228.5-229.8 ^{o}C; *Anal.* Calc. for C$_{48}$H$_{55}$NB$_2$O$_4$: C, 78.80; H, 7.58; N, 1.91; Found: C, 78.79; H, 7.40; N, 1.70; δ_H (700 MHz, CDCl$_3$) 8.29 (2H, d, J 1.1), 7.80 (4H, d, J 8.2), 7.66 (2H, dd, J 8.4, 1.6), 7.57 (4H, d, J 8.2), 7.37 (2H, d, J 8.4), 4.29 (2H, t, J 7.3), 1.87 (2H, dt, J 14.4, 7.4), 1.41 – 1.22 (34H, m), 0.87 (3H, t, J 7.1); δ_C (176 MHz, CDCl$_3$) 140.49, 134.57, 130.59, 129.75, 126.51, 124.24, 122.49, 113.76, 108.98, 92.00, 88.09, 83.88, 43.36, 31.72, 29.29, 29.12, 28.93, 27.24, 24.87, 22.56, 14.02; MS (MALDI+): m/z = 731.6 (M$^+$, 100%).
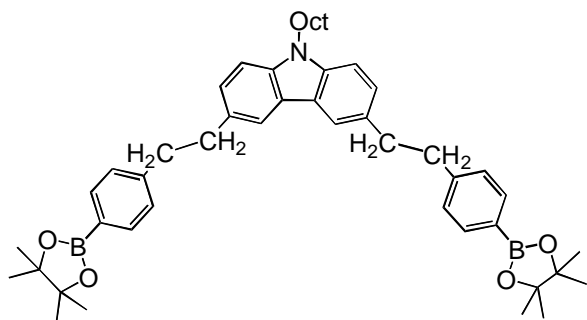
3,6-Bis(4-(4,4,5,5-tetramethyl-1,3,2-dioxaborolan-2-yl)phenethyl)-9-octyl-9*H*-carbazole (140)

A hydrogen-purged flask was charged with **139** (0.30 g, 0.4 mmol) and EtOAc (20 ml). 5% Pd/C (0.03 g) was added slowly. The reaction was judged to be finished within 2 h by TLC analysis. Ethyl acetate was removed under reduced pressure. The residue was purified by column chromatography (SiO$_2$, 30:70 DCM: hexane) yielding **140** (0.30 g, 98%) as a white solid; mp: 165.3-165.8 ^{o}C; Anal. Calc. for C$_{48}$H$_{63}$B$_2$NO$_4$: C, 77.95; H, 8.59; N, 1.89;. Found: C, 78.00; H, 8.63; N, 1.91; δ$_H$ (700 MHz, CDCl$_3$) 7.89 (2H s,), 7.74 (4H, d, *J* 8.0), 7.29 – 7.23 (8H, m), 4.23 (2H, t, *J* 7.3), 3.08 (4H, t, *J* 10.0), 3.02 (4H, t, *J* 9.9), 1.83 (2H, dt, *J* 14.9, 7.5), 1.39 – 1.20 (34H, m), 0.85 (3H, t, *J* 7.1); δ$_C$ (176 MHz, CDCl$_3$) 145.59, 139.32, 134.86, 131.86, 127.96, 126.15, 122.75, 119.68, 108.35, 83.60, 43.17, 39.15, 37.92, 31.77, 29.35, 29.15, 29.00, 27.31, 24.84, 22.57, 14.04; MS (MALDI+): *m/z* 739.6 (M$^+$, 100%).

9,9'-(5-*tert*-Butyl-1,3-phenylene)bis(3-*tert*-butyl-9*H*-carbazole) (143)
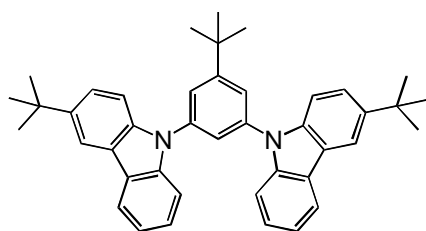
An argon-purged flask was charged with 3-bromo-9-H-carbazole **141** (1.51 g, 6.8 mmol), 3,5-dibromo-1-*tert*-butybenzene **142** (0.98 g, 3.4 mmol), sodium *tert*-butoxide (0.79 g, 8.0 mmol), Pd$_2$(dba)$_3$. (0.07 g, 0.08 mmol), (2-Biphenylyl)di-*tert*-butylphosphine (JohnPhos) (0.055g, 0.15 mmol) and toluene (50 ml). The solution was refluxed overnight. Toluene was removed under reduced pressure. The mixture was extracted three times by DCM (200 ml). The organic layers were combined and dried over MgSO$_4$. The crude product was obtained after removing solvent and purified by column chromatography (SiO$_2$, 30:70 DCM : hexane) yielding **143** (1.86 g, 90%) as a white solid; mp: 148.0-149.1 ^{o}C; δ$_H$ (700 MHz, CDCl$_3$) 8.21 – 8.15 (4H, m), 7.69 (2H, d, *J* 1.9), 7.62 (1H, t, *J* 1.9), 7.55 – 7.51 (4H, m), 7.49 (2H, d,

J 8.6), 7.44 – 7.40 (2H, m), 7.31 – 7.27 (2H, m), 1.47 (s, 18H), 1.46 (s, 9H); δ_C (176 MHz, CDCl₃) 154.91, 143.28, 140.84, 138.97, 138.73, 125.83, 124.00, 123.76, 123.22, 122.59, 121.63, 120.22, 119.91, 116.48, 109.69, 109.24, 35.32, 34.72, 31.94, 31.31; HRMS (MS ASAP+): calcd for $[C_{42}H_{44}N_2+H^+]$: 577.3583. Found: 577.3574.

9,9'-(5-*tert*-Butyl-1,3-phenylene)bis(3-bromo-6-*tert*-butyl-9*H*-carbazole) (144)
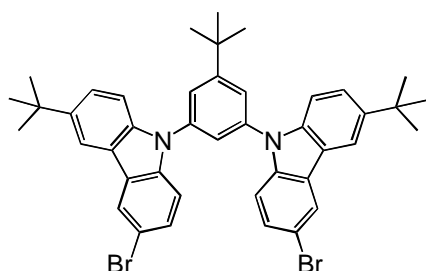
A flask covered with aluminium foil was charged with **143** (0.66 g, 1.14 mmol) and dried THF (50 ml), and cooled to 0 °C. NBS (0.42 g, 2.34 mmol) was added in small portions. The mixture was allowed to warm to room temperature and stirred overnight. To the solution, water was added to quench excess NBS. The THF was evaporated and the cloudy solution was extracted with DCM (3 × 50 ml). The organic layers were combined and dried over MgSO₄. The crude product was obtained after removing solvent and purified by column chromatography (SiO₂, 50:50 DCM: hexane) followed by recrystallisation from DCM/hexane yielding **144** (0.79 g, 94%) as a white solid; mp: 328.0-330.0 °C; δ_H (700 MHz, CDCl₃) 8.30 (2H, d, *J* 1.8), 8.12 (2H, d, *J* 1.7), 7.67 (2H, d, *J* 1.7), 7.58 – 7.55 (3H, m), 7.50 (2H, dt, *J* 6.9, 3.5), 7.47 (2H, d, *J* 8.7), 7.39 (2H d, *J* 8.7), 1.47 (27H, s,); δ_C (176 MHz, CDCl₃) 155.35, 143.89, 139.47, 139.06, 138.69, 128.53, 125.58, 124.88, 123.07, 122.81, 122.22, 121.45, 116.69, 112.80, 111.11, 109.43, 35.38, 34.77, 31.95, 31.89, 31.31, 31.29; HRMS (ASAP+): calcd for $[C_{42}H_{42}N_2Br_2+H^+]$: 735.1773. Found: 735.1728.

Polymer (133)
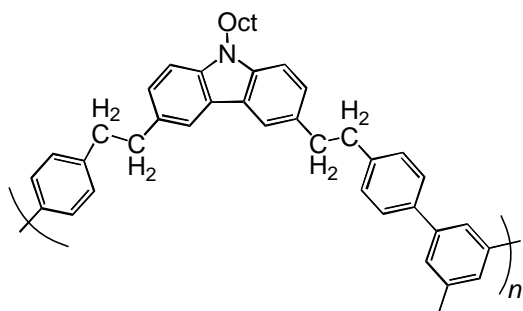
An argon-purged flask was charged with 3,5-dibromotoluene (0.415 g, 1.71 mmol), **140** (1.23 g, 1.71 mmol) and toluene (20 ml). The solution was degassed for 30 min before Pd(P(*o*-Tol)₃)₂Cl₂ (20 mg) and degassed 20% wt Et₄NOH aqueous (water)

solution (7 ml) were added. The reaction was stirred for 18 h at 115 ^{o}C. Bromobenzene (0.10 ml) was added and stirring continued for 1 h. Benzeneboronic acid (100 mg) was added and stirring continued for 1 h. After cooling, a grey precipitate was obtained by slowly pouring the reaction mixture into vigorously stirred MeOH (350 ml). The precipitate was dissolved in toluene (20 ml) and the scavenger solution (sodium diethyldithiocarbamate trihydrate) [1.0 g in water (10 ml)] was added and the mixture was stirred at 65 - 75 ^{o}C for 18 h. The polymer solution was separated by separatory funnel and filtered through a celite plug. The filtrate (i.e. the polymer solution) was concentrated under vacuum (to ca. 3 ml) and added dropwise into methanol (400 ml) to precipitate polymer **133** as a white solid (0.89 g, 86%); δ_H (400 MHz, CDCl$_3$) 7.93 (1H, br), 7.62 – 7.50 (3H, br), 7.40 – 7.27 (6H, br), 4.30 – 4.21 (2H, br), 3.19 – 2.98 (4H, br), 2.45 (3H, br), 1.84 (2H, br), 1.41-1.15 (8H, br), 0.88 – 0.82 (3H, br).

Polymer (134)
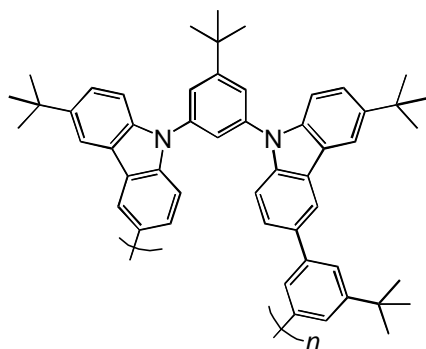
Following the procedure for polymer **133,** An argon-purged flask was charged with 2,2'-[5-*tert*-butyl-1,3-phenylene]bis[4,4,5,5-tetramethyl-1,3,2-dioxaborolane] (0.11 g, 0.27 mmol), **144** (0.20 g, 0.27 mmol), Pd(P(*o*-Tol)$_3$)$_2$Cl$_2$ (10 mg), 20% wt Et$_4$NOH solution (1 ml) and toluene (5 ml) gave polymer **134** (0.12 g, 64%) as a white solid; δ_H (400 MHz, CDCl$_3$) 8.46 (2H, br), 8.24 (2H, br), 7.92 (1H, br), 7.80 (2H, br), 7.73 (5H, br), 7.65 (2H, br), 7.54 (5H, br), 1.51 (9H, br), 1.49 (9H, br), 1.46 (18H, br).

Chapter 8 - References

(1) Borchardt, J. K. *Materials Today* **2004**, *7*, 42.

(2) http://www.treehugger.com/files/2007/03/ge_accelerates.php; Last accessed, Nov 2010.

(3) Burn, P. L.; Bradley, D. D. C.; Friend, R. H.; Halliday, D. A.; Holmes, A. B.; Jackson, R. W.; Kraft, A. *J. Chem. Soc., Perkin Trans. 1.* **1992**, 3225.

(4) Burroughes, J. H.; Bradley, D. D. C.; Brown, A. R.; Marks, R. N.; Mackay, K.; Friend, R. H.; Burn, P. L.; Holmes, A. B. *Nature* **1990**, *347*, 539.

(5) Scherf, U. T. *Curr. Chem.* **1999**, *201*, 163.

(6) Grimsdale, A. C.; Leok Chan, K.; Martin, R. E.; Jokisz, P. G.; Holmes, A. B. *Chem. Rev.* **2009**, *109*, 897.

(7) Perepichka, I.; Perepichka, D.; Meng, H.; Wudl, F. *Adv. Mater.* **2005**, *17*, 2281.

(8) Tang, C. W.; VanSlyke, S. A. *Appl. Phys. Lett.* **1987**, *51*, 913.

(9) http://electronics.howstuffworks.com/oled.htm/printable; Last accessed, Oct 2010.

(10) Kafafi, Z. *Organic Electroluminescence*; Taylor & Francis Group: Boca Raton, 2005.

(11) Kuwabara, Y.; Ogawa, H.; Inada, H.; Noma, N.; Shirota, Y. *Adv. Mater.* **1994**, *6*, 677.

(12) Zhang, Q.; Chen, J.; Cheng, Y.; Wang, L.; Ma, D.; Jing, X.; Wang, F. *J. Mater. Chem.* **2004**, *14*, 895.

(13) Ishikawa, W.; Noguchi, K.; Kuwabaru, Y.; Shirota, Y. *Adv. Mater.* **1993**, *5*, 559.

(14) Inada, H.; Shirota, Y. *J. Mater. Chem.* **1993**, *3*, 319.

(15) Okumoto, K.; Doi, H.; Shirota, Y. *J. Photopolym. Sci. Technol.* **2002**, *15*, 239.

(16) O'Brien, D. F.; Burrows, P. E.; Forrest, S. R.; Koene, B. E.; Loy, D. E.; Thompson, M. E. *Adv. Mater.* **1998**, *10*, 1108.

(17) Koene, B. E.; Loy, D. E.; Thompson, M. E. *Chem. Mater.* **1998**, *10*, 2235.

(18)   Salbeck, J.; Yu, N.; Bauer, J.; Weissörtel, F.; Bestgen, H. *Synth. Met.* **1997**, *91*, 209.

(19)   Tokito, S.; Iijima, T.; Suzuri, Y.; Kita, H.; Tsuzuki, T.; Sato, F. *Appl. Phys. Lett.* **2003**, *83*, 569.

(20)   Adachi, C.; Tsutsui, T.; Saito, S. *Appl. Phys. Lett.* **1989**, *55*, 1489.

(21)   O'Brien, D.; Bleyer, A.; Lidzey, D. G.; Bradley, D. D. C.; Tsutsui, T. *J. Appl. Phys.* **1997**, *82*, 2662.

(22)   Bettenhausen, J.; Strohriegl, P. *Adv. Mater.* **1996**, *8*, 507.

(23)   Ogawa, H.; Okuda, R.; Shirota, Y. *Mol. Cryst. liq. Cryst.,* **1998**, *315*, 187.

(24)   Kido, J.; Ohtaki, C.; Hongawa, K.; Okuyama, K.; Nagai, K. *Jpn. J. Appl. Phys.* **1993**, *32*, L917.

(25)   Jandke, M.; Strohriegl, P.; Berleb, S.; Werner, E.; Brutting, W. *Macromolecules* **1998**, *31*, 6434.

(26)   Lee, J.; Chopra, N.; Eom, S.-H.; Zheng, Y.; Xue, J.; So, F.; Shi, J. *Appl. Phys. Lett.* **2008**, *93*, 123306.

(27)   Yersin, H. *Highly Efficient OLEDs with Phosphorescent Materials*; WILEY-VCH: Weinheim, 2008.

(28)   Birks, B. J. *Photophysics of Aromatic Compounds*; Wiley: New York, 1970.

(29)   Mohamad, D.; Johnson, R. G.; Janeliunas, D.; Kirkus, M.; Yi, H.; Lidzey, D. G.; Iraqi, A. *J. Mater. Chem.* **2010**, *20*, 6990.

(30)   Brunner, K.; van Dijken, A.; Börner, H.; Bastiaansen, J. J. A. M.; Kiggen, N. M. M.; Langeveld, B. M. W. *J. Am. Chem. Soc.* **2004**, *126*, 6035.

(31)   Tsai, M.-H.; Ke, T.-H.; Lin, H.-W.; Wu, C.-C.; Chiu, S.-F.; Fang, F.-C.; Liao, Y.-L.; Wong, K.-T.; Chen, Y.-H.; Wu, C.-I. *ACS Appl. Mater. Interfaces* **2009**, *1*, 567.

(32)   Su, S.-J.; Sasabe, H.; Takeda, T.; Kido, J. *Chem. Mater.* **2008**, *20*, 1691.

(33)   Tao, Y.; Wang, Q.; Yang, C.; Wang, Q.; Zhang, Z.; Zou, T.; Qin, J.; Ma, D. *Angew. Chem., Int. Ed.* **2008**, *120*, 8224.

(34)   Lamansky, S.; Djurovich, P.; Murphy, D.; Abdel-Razzaq, F.; Kwong, R.; Tsyba, I.; Bortz, M.; Mui, B.; Bau, R.; Thompson, M. E. *Inorg. Chem.* **2001**, *40*, 1704.

(35)   Van Slyke, S. A.; Chen, C. H.; Tang, C. W. *Appl. Phys. Lett.* **1996**, *69*, 2160.

(36)   Kim, J. H.; Yoon, D. Y.; Kim, J. W.; Kim, J.-J. *Synth. Met.* **2007**, *157*, 743.

(37)   Kawamura, Y.; Yanagida, S.; Forrest, S. R. *J. Appl. Phys.* **2002**, *92*, 87.

(38)   Van Dijken, A.; Bastiaansen, J. J. A. M.; Kiggen, N. M. M.; Langeveld, B. M. W.; Rothe, C.; Monkman, A.; Bach, I.; Stössel, P.; Brunner, K. *J. Am. Chem. Soc.* **2004**, *126*, 7718.

(39)   Zhang, K.; Tao, Y.; Yang, C.; You, H.; Zou, Y.; Qin, J.; Ma, D. *Chem. Mater.* **2008**, *20*, 7324.

(40)   Van Dijken, A.; Brunner, K.; Langeveld, B. M. W.; Schoo, H. F. M.; Bastiaansen, J. J. A. M.; Kiggen, N. M. M. USA, 2007; Vol. WO 2007/072240 A1.

(41)   Fei, T.; Cheng, G.; Hu, D.; Lu, P.; Ma, Y. *J. Polym. Sci. Part A: Polymer Chem.* **2009**, *47*, 4784.

(42)   Gao, F. G.; Bard, A. J. *Chem. Mater.* **2002**, *14*, 3465.

(43)   Balzani, V.; Juris, A.; Venturi, M.; Campagna, S.; Serroni, S. *Chem. Rev.* **1996**, *96*, 759.

(44)   Tamayo, A. B.; Alleyne, B. D.; Djurovich, P. I.; Lamansky, S.; Tsyba, I.; Ho, N. N.; Bau, R.; Thompson, M. E. *J. Am. Chem. Soc.* **2003**, *125*, 7377.

(45)   Brooks, J.; Babayan, Y.; Lamansky, S.; Djurovich, P. I.; Tsyba, I.; Bau, R.; Thompson, M. E. *Inorg. Chem.* **2002**, *41*, 3055.

(46)   Baldo, M. A.; Thompson, M. E.; Forrest, S. R. *Nature* **2000**, *403*, 750.

(47)   Baldo, M. A.; O'Brien, D. F.; You, Y.; Shoustikov, A.; Sibley, S.; Thompson, M. E.; Forrest, S. R. *Nature* **1998**, *395*, 151.

(48)   Wilson, J. S.; Dhoot, A. S.; Seeley, A. J. A. B.; Khan, M. S.; Kohler, A.; Friend, R. H. *Nature* **2001**, *413*, 828.

(49)   Chou, P. T.; Chi, Y. *Chem. Eur. J.* **2007**, *13*, 380.

(50)   Lakowicz., R. J. *Principles of Fluorescence Spectroscopy*; 2nd ed.; Kluwer Academic/Plenum: New York, 1999.

(51)   Nonoyama, M. *Bull. Chem. Soc. Jpn.* **1974**, *47*, 767.

(52)   Karatsu, T.; Nakamura, T.; Yagai, S.; Kitamura, A.; Yamaguchi, K.; Matsushima, Y.; Iwata, T.; Hori, Y.; Hagiwara, T. *Chem. Lett.* **2003**, *32*, 886.

(53)   Adachi, C.; Kwong, R. C.; Djurovich, P.; Adamovich, V.; Baldo, M. A.; Thompson, M. E.; Forrest, S. R. *Appl. Phys. Lett.* **2001**, *79*, 2082.

(54)   Yeh, S. J.; Wu, M. F.; Chen, C. T.; Song, Y. H.; Chi, Y.; Ho, M. H.; Hsu, S. F.; Chen, C. *Adv. Mater.* **2005**, *17*, 285.

(55)   Deaton, J. C.; Young, R. H.; Lenhard, J. R.; Rajeswaran, M.; Huo, S. *Inorg. Chem.* **2010**, *49*, 9151.

(56)   Sajoto, T.; Djurovich, P. I.; Tamayo, A. B.; Oxgaard, J.; Goddard, W. A.; Thompson, M. E. *J. Am. Chem. Soc.* **2009**, *131*, 9813.

(57)   Lee, S. J.; Park, K.-M.; Yang, K.; Kang, Y. *Inorg. Chem.* **2008**, *48*, 1030.

(58)   Laskar, I. R.; Hsu, S.-F.; Chen, T.-M. *Polyhedron* **2005**, *24*, 189.

(59)   Sajoto, T.; Djurovich, P. I.; Tamayo, A.; Yousufuddin, M.; Bau, R.; Thompson, M. E.; Holmes, R. J.; Forrest, S. R. *Inorg. Chem.* **2005**, *44*, 7992.

(60)   Dedeian, K.; Djurovich, P. I.; Garces, F. O.; Carlson, G.; Watts, R. J. *Inorg. Chem.* **1991**, *30*, 1685.

(61)   Tsuboyama, A.; Iwawaki, H.; Furugori, M.; Mukaide, T.; Kamatani, J.; Igawa, S.; Moriyama, T.; Miura, S.; Takiguchi, T.; Okada, S.; Hoshino, M.; Ueno, K. *J. Am. Chem. Soc.* **2003**, *125*, 12971.

(62)   Ostrowski, J. C.; Robinson, M. R.; Heeger, A. J.; Bazan, G. C. *Chem. Commun.* **2002**, 784.

(63)   Moore, T. *MSc. Thesis, Durham University.* 2008.

(64)   Chen, L.; You, H.; Yang, C.; Ma, D.; Qin, J. *Chem. Commun.* **2007**, 1352.

(65)   Lo, S.-C.; Harding, R. E.; Shipley, C. P.; Stevenson, S. G.; Burn, P. L.; Samuel, I. D. W. *J. Am. Chem. Soc.* **2009**, *131*, 16681.

(66)   Yeh, Y. S.; Cheng, Y. M.; Chou, P. T.; Lee, G. H.; Yang, C. H.; Chi, Y.; Shu, C. F.; Wang, C. H. *ChemPhysChem* **2006**, *7*, 2294.

(67)   Adams, D. M.; Brus, L.; Chidsey, C. E. D.; Creager, S.; Creutz, C.; Kagan, C. R.; Kamat, P. V.; Lieberman, M.; Lindsay, S.; Marcus, R. A.; Metzger, R. M.; Michel-Beyerle, M. E.; Miller, J. R.; Newton, M. D.; Rolison, D. R.; Sankey, O.; Schanze, K. S.; Yardley, J.; Zhu, X. *J. Phys. Chem. B* **2003**, *107*, 6668.

(68)   Maruccio, G.; Cingolani, R.; Rinaldi, R. *J. Mater. Chem.* **2004**, *14*, 542.

(69)   Forrest, S. R.; Thompson, M. E. *Chem. Rev.* **2007**, *107*, 923.

(70)   Gust, D.; Moore, T. A.; Moore, A. L. *Accts. Chem. Res.* **2000**, *34*, 40.

(71)   Laquai, F.; Park, Y.-S.; Kim, J.-J.; Basché, T. *Macromol. Rapid Commun.* **2009**, *30*, 1203.

(72)   Shirota, Y.; Kageyama, H. *Chem. Rev.* **2007**, *107*, 953.

(73)   Giacalone, F.; Segura, J. L.; Martín, N.; Ramey, J.; Guldi, D. M. *Chem. Eur. J.* **2005**, *11*, 4819.

(74)   Thompson, A. L.; Ahn, T.-S.; Thomas, K. R. J.; Thayumanavan, S.; Martínez, T. J.; Bardeen, C. J. *J. Am. Chem. Soc.* **2005**, *127*, 16348.

(75)   Adhikari, R. M.; Mondal, R.; Shah, B. K.; Neckers, D. C. *J. Org. Chem.* **2007**, *72*, 4727.

(76)   Kamtekar, K. T.; Wang, C.; Bettington, S.; Batsanov, A. S.; Perepichka, I. F.; Bryce, M. R.; Ahn, J. H.; Rabinal, M.; Petty, M. C. *J. Mater. Chem.* **2006**, *16*, 3823.

(77)   Zhu, Y.; Kulkarni, A. P.; Wu, P.-T.; Jenekhe, S. A. *Chem. Mater.* **2008**, *20*, 4200.

(78)   Kulkarni, A. P.; Zhu, Y.; Babel, A.; Wu, P.-T.; Jenekhe, S. A. *Chem. Mater.* **2008**, *20*, 4212.

(79)   Lo, S.-C.; Burn, P. L. *Chem. Rev.* **2007**, *107*, 1097.

(80)   Iraqi, A.; Wataru, I. *J. Polym. Sci. Part A: Polym. Chem.* **2004**, *42*, 6041.

(81)   Iraqi, A.; Simmance, T. G.; Yi, H.; Stevenson, M.; Lidzey, D. G. *Chem. Mater.* **2006**, *18*, 5789.

(82)   O'Brien, D. F.; Baldo, M. A.; Thompson, M. E.; Forrest, S. R. *Appl. Phys. Lett.* **1999**, *74*, 442.

(83)   Tanaka, I.; Tabata, Y.; Tokito, S. *Chem. Phys. Lett.* **2004**, *400*, 86.

(84)   Tokito, S.; Suzuki, M.; Sato, F.; Kamachi, M.; Shirane, K. *Org. Electron.* **2003**, *4*, 105.

(85)   Suzuki, M.; Tokito, S.; Sato, F.; Igarashi, T.; Kondo, K.; Koyama, T.; Yamaguchi, T. *Appl. Phys. Lett.* **2005**, *86*, 103507.

(86)   Hayes, F. N.; Rogers, B. S.; Ott, D. G. *J. Am. Chem. Soc.* **1955**, *77*, 1850.

(87)   Abshire, C. J.; Marvel, C. J. *Makromol. Chem.* **1961**, *44*, 388.

(88)   Huisgen, R.; Sauer, J.; Sturm, H. J. *Chem. Ber.* **1960**, *93*, 2106.

(89)   Thomas, J. K. R.; Lin, J. T.; Tao, Y.-T.; Chuen, C.-H. *Chem. Mater.* **2004**, *16*, 5437.

(90)   Guan, M.; Qiang Bian, Z.; Feng Zhou, Y.; You Li, F.; Jun Li, Z.; Hui Huang, C. *Chem. Commun.* **2003**, 2708.

(91)   Koyama, M.; Ohtani, N.; Kai, F.; Moriguchi, I.; Inouye, S. *J. Med. Chem.* **1987**, *30*, 552.

(92)   Allen, F. H.; Taylor, R. *Chem. Soc. Rev.* **2004**, *33*, 463.

(93)   Tao, Y.; Gong, S.; Wang, Q.; Zhong, C.; Yang, C.; Qin, J.; Ma, D. *Phys. Chem. Chem. Phys.* **2010**, *12*, 2438.

(94)   Ulbricht, C.; Beyer, B.; Friebe, C.; Winter, A.; Schubert, U. S. *Adv. Mater.* **2009**, *21*, 4418.

(95)   Wong, W.-Y.; Ho, C.-L. *J. Mater. Chem.* **2009**, *19*, 4457.

(96)   Jeon, S. O.; Yook, K. S.; Joo, C. W.; Son, H. S.; Lee, J. Y. *Thin Solid Films* **2010**, *518*, 3716.

(97)   Chopra, N.; Lee, J.; Zheng, Y.; Eom, S.-H.; Xue, J.; So, F. *ACS Appl. Mater. Interfaces* **2009**, *1*, 1169.

(98)   Lee, D. H.; Xun, Z.; Chae, H.; Cho, S. M. *Synth. Met.* **2009**, *159*, 1640.

(99)   Sivasubramaniam, V.; Brodkorb, F.; Hanning, S.; Loebl, H. P.; van Elsbergen, V.; Boerner, H.; Scherf, U.; Kreyenschmidt, M. *J. Fluorine Chem.* **2009**, *130*, 640.

(100)   You, Y.; Seo, J.; Kim, S. H.; Kim, K. S.; Ahn, T. K.; Kim, D.; Park, S. Y. *Inorg. Chem.* **2008**, *47*, 1476.

(101)   Chen, L.; Yang, C.; Qin, J.; Gao, J.; Ma, D. *Inorg. Chim. Acta.* **2006**, *359*, 4207.

(102)   Chen, L.; Yang, C.; Qin, J.; Gao, J.; You, H.; Ma, D. *J. Organomet. Chem.* **2006**, *691*, 3519.

(103)   Xu, Z.; Li, Y.; Ma, X.; Gao, X.; Tian, H. *Tetrahedron* **2008**, *64*, 1860.

(104)   Kulkarni, A. P.; Tonzola, C. J.; Babel, A.; Jenekhe, S. A. *Chem. Mater.* **2004**, *16*, 4556.

(105)   Huo, S.; Deaton, J. C.; Rajeswaran, M.; Lenhart, W. C. *Inorg. Chem.* **2006**, *45*, 3155.

(106)   Chen, L.; Yang, C.; Li, M.; Qin, J.; Gao, J.; You, H.; Ma, D. *Crystal Growth & Design* **2006**, *7*, 39.

(107)   Michon, C.; Djukic, J.-P.; Pfeffer, M.; Gruber-Kyritsakas, N.; de Cian, A. *J. Organomet. Chem.* **2007**, *692*, 1092.

(108)   Kothari, P. J.; Singh, S. P.; Parmar, S. S.; Stenberg, V. I. *J. Heterocycl. Chem.* **1980**, *17*, 1393.

(109)   Tejel, C.; Ciriano, M. A.; Millaruelo, M.; López, J. A.; Lahoz, F. J.; Oro, L. A. *Inorg. Chem.* **2003**, *42*, 4750.

(110)   Lamansky, S.; Djurovich, P.; Murphy, D.; Abdel-Razzaq, F.; Lee, H.-E.; Adachi, C.; Burrows, P. E.; Forrest, S. R.; Thompson, M. E. *J. Am. Chem. Soc.* **2001**, *123*, 4304.

(111)   Hay, P. J. *J. Phys. Chem. A* **2002**, *106*, 1634.

(112)   Coppo, P.; Plummer, E. A.; De Cola, L. *Chem. Commun.* **2004**, 1774.

(113)   Schneidenbach, D.; Ammermann, S.; Debeaux, M.; Freund, A.; Zöllner, M.; Daniliuc, C.; Jones, P. G.; Kowalsky, W.; Johannes, H.-H. *Inorg. Chem.* **2009**, *49*, 397.

(114)   Bettington, S.; Tavasli, M.; Bryce, M. R.; Beeby, A.; Al-Attar, H.; Monkman, A. P. *Chem. Eur. J.* **2007**, *13*, 1423.

(115)   Mi, B. X.; Wang, P. F.; Gao, Z. Q.; Lee, C. S.; Lee, S. T.; Hong, H. L.; Chen, X. M.; Wong, M. S.; Xia, P. F.; Cheah, K. W.; Chen, C. H.; Huang, W. *Adv. Mater.* **2009**, *21*, 339.

(116)   Beyer, B.; Ulbricht, C.; Escudero, D.; Friebe, C.; Winter, A.; González, L.; Schubert, U. S. *Organometallics* **2009**, *28*, 5478.

(117)   Tavasli, M.; Bettington, S.; Perepichka, I. F.; Batsanov, A. S.; Bryce, M. R.; Rothe, C.; Monkman, A. P. *Eur. J. Inorg. Chem.* **2007**, *2007*, 4808.

(118)   Tavasli, M.; Bettington, S.; Bryce, M. R.; Attar, H. A. A.; Dias, F. B.; King, S.; Monkman, A. P. *J. Mater. Chem.* **2005**, *15*, 4963.

(119)   Zhang, H.; Larock, R. C. *Org. Lett.* **2001**, *3*, 3083.

(120)   Zhang, H.; Larock, R. C. *J. Org. Chem.* **2002**, *67*, 9318.

(121)   Ragni, R.; Plummer, E. A.; Brunner, K.; Hofstraat, J. W.; Babudri, F.; Farinola, G. M.; Naso, F.; De Cola, L. *J. Mater. Chem.* **2006**, *16*, 1161.

(122)   Holmes, R. J.; Forrest, S. R.; Sajoto, T.; Tamayo, A.; Djurovich, P. I.; Thompson, M. E.; Brooks, J.; Tung, Y.-J.; D'Andrade, B. W.; Weaver, M. S.; Kwong, R. C.; Brown, J. J. *Appl. Phys. Lett.* **2005**, *87*, 243507.

(123)   Fukagawa, H.; Watanabe, K.; Tokito, S. *Org. Electron.* **2009**, *10*, 798.

(124)   Baldo, M. A.; Forrest, S. R. *Phys. Rev. B.* **2000**, *62*, 10958.

(125)   Xin, Q.; Li, W. L.; Su, W. M.; Li, T. L.; Su, Z. S.; Chu, B.; Li, B. *J. Appl. Phys.* **2007**, *101*, 044512.

(126)   Li, Y. Q.; Fung, M. K.; Xie, Z.; Lee, S. T.; Hung, L. S.; Shi, J. *Adv. Mater.* **2002**, *14*, 1317.

(127)   Naka, S.; Okada, H.; Onnagawa, H.; Tsutsui, T. *Appl. Phys. Lett.* **2000**, *76*, 197.

(128)   Tanaka, D.; Takeda, T.; Chiba, T.; Watanabe, S.; Kido, J. *Chem. Lett.* **2007**, *36*, 262.

(129)   Holmes, R. J.; Forrest, S. R.; Tung, Y.-J.; Kwong, R. C.; Brown, J. J.; Garon, S.; Thompson, M. E. *Appl. Phys. Lett.* **2003**, *82*, 2422.

(130)   Lee, J.; Chopra, N.; Eom, S.-H.; Zheng, Y.; Xue, J.; So, F.; Shi, J. *Appl. Phys. Lett.* **2008**, *93*, 123306.

(131)   Yokoyama, D.; Sakaguchi, A.; Suzuki, M.; Adachi, C. *Appl. Phys. Lett.* **2009**, *95*, 243303.

(132)   Yang, X. H.; Jaiser, F.; Klinger, S.; Neher, D. *Appl. Phys. Lett.* **2006**, *88*, 021107.

(133)   Jung, S. O.; Kim, Y.-H.; Kwon, S.-K.; Oh, H.-Y.; Yang, J.-H. *Org. Electron.* **2007**, *8*, 349.

(134)   Kawamura, Y.; Yanagida, S.; Forrest, S. R. *J. Appl. Phys.* **2002**, *92*, 87.

(135)   Deng, L.; Furuta, P. T.; Garon, S.; Li, J.; Kavulak, D.; Thompson, M. E.; Fréchet, J. M. J. *Chem. Mater.* **2006**, *18*, 386.

(136)   Chen, X. W.; Liao, J. L.; Liang, Y.; Ahmed, M. O.; Tseng, H. E.; Chen, S. A. *J. Am. Chem. Soc.* **2003**, *125*, 636.

(137)   Evans, N. R.; Devi, L. S.; Mak, S. S. K.; Watkins, S. E.; Pascu, S. I.; Köhler, A.; Friend, R. H.; Williams, C. K.; Holmes, A. B. *J. Am. Chem. Soc.* **2006**, *128*, 6647.

(138)   Huang, F.; Shih, P. I.; Liu, M. S.; Shu, C. F.; Jen, A. K. Y. *Appl. Phys. Lett.* **2008**, *93*, 243512.

(139)   Yang, X.; Müller, D. C.; Neher, D.; Meerholz, K. *Adv. Mater.* **2006**, *18*, 948.

(140)   Fei, T.; Cheng, G.; Hu, D.; Lu, P.; Ma, Y. *J. Polym. Sci. Part A: Polym. Chem.* **2009**, *47*, 4784.

(141)   Zacharias, P.; Gather, M. C.; Rojahn, M.; Nuyken, O.; Meerholz, K. *Angew. Chem., Int. Ed.* **2007**, *46*, 4388.

(142)   Pina, J.; Seixas de Melo, J.; Burrows, H. D.; Monkman, A. P.; Navaratnam, S. *Chem. Phys. Lett.* **2004**, *400*, 441.

(143)   Daubler, T. K.; Glowacki, I.; Scherf, U.; Ulanski, J.; Horhold, H.-H.; Neher, D. *J. Appl. Phys.* **1999**, *86*, 6915.

(144)   Lei, G. T.; Wang, L. D.; Duan, L.; Wang, J. H.; Qiu, Y. *Synth. Met.* **2004**, *144*, 249.

(145)   Qian, L.; Bera, D.; Holloway, P. H. *Appl. Phys. Lett.* **2007**, *90,* 103511.

(146)   Mathai, M. K.; Choong, V.-E.; Choulis, S. A.; Krummacher, B.; So, F. *Appl. Phys. Lett.* **2006**, *88*, 243512.

(147)   Liu, J.; Pei, Q. *Macromolecules* **2010**, *43*, 9608.

(148)   Grigalevicius, S.; Grazulevicius, J. V.; Gaidelis, V.; Jankauskas, V. *Polymer* **2002**, *43*, 2603.

(149)   Sonogashira, K.; Tohda, Y.; Hagihara, N. *Tetrahedron Lett.* **1975**, *16*, 4467.

(150)   Lo, S.-C.; Harding, R. E.; Brightman, E.; Burn, P. L.; Samuel, I. D. W. *J. Mater. Chem.* **2009**, *19*, 3213.

(151)   Miyaura, N.; Suzuki, A. *Chem. Commun.* **1979**, 866.

(152)   Fei, T.; Cheng, G.; Hu, D.; Dong, W.; Lu, P.; Ma, Y. *J. Polym. Sci. Part A: Polym. Chem.* **2010**, *48*, 1859.

(153)   Dahms, K.; Kamtekar, K. T.; Sidde, J.; Bryce, M. R. Unpublished results.

(154)   Frisch, M. J.; Trucks, G. W.; Schlegel, H. B.; Scuseria, G. E.; Robb, M. A.; Cheeseman, J. R.; Montgomery, J. A. J.; Vreven, T.; Kudin, K. N.; Burant, J. C.; Millam, J. M.; Iyengar, S. S.; Tomasi, J.; Barone, V.; Mennucci, B.; Cossi, M.; Scalmani, G.; Rega, N.; Petersson, G. A.; Nakatsuji, H.; Hada, M.; Ehara, M.; Toyota, K.; Fukuda, R.; Hasegawa, J.; Ishida, M.; Nakajima, T.; Honda, Y.; Kitao, O.; Nakai, H.; Klene, M.; Li, X.; Knox, J. E.; Hratchian, H. P.; Cross, J. B.; Adamo, C.; Jaramillo, J.; Gomperts, R.; Stratmann, R. E.; Yazyev, O.; Austin, A. J.; Cammi, R.; Pomelli, C.; Ochterski, J. W.; Ayala, P. Y.; Morokuma, K.; Voth, G. A.; Salvador, P.; Dannenberg, J. J.; Zakrzewski, V. G.; Dapprich, S.; Daniels, A. D.; Strain, M. C.; Farkas, O.; Malick, D. K.; Rabuck, A. D.; Raghavachari, K.; Foresman, J. B.; Ortiz, J. V.; Cui, Q.; Baboul, A. G.; Clifford, S.; Cioslowski, J.; Stefanov, B. B.; Liu, G.; Liashenko, A.; Piskorz, P.; Komaromi, I.; Martin, R. L.; Fox, D. J.; Keith, T.; Al-Laham, M. A.; Peng, C. Y.; Nanayakkara, A.; Challacombe, M.; Gill, P. M. W.; Johnson, B.; Chen, W.; Wong, M. W.; Gonzalez, C.; Pople, J. A. *Gaussian 03*, revision C.02; Gaussian, Inc., Wallingford CT. **2004**.

(155)   Barrett, D. G.; Boncek, V. M.; Catalano, J. G.; Deaton, D. N.; Hassell, A. M.; Jurgensen, C. H.; Long, S. T.; McFadyen, R. B.; Miller, A. B.; Miller, L. R.;

Payne, J. A.; Ray, J. A.; Samano, V.; Shewchuk, L. M.; Tavares, F. X.; Wells-Knecht, K. J.; Willard Jr, D. H.; Wright, L. L.; Zhou, H.-Q. Q. *Bioorg. Med. Chem. Lett.* **2005**, *15*, 3540.

(156)   Chun, H.; Moon, I. K.; Shin, D.-H.; Song, S.; Kim, N. *J. Mater. Chem.* **2002**, *12*, 858.

(157)   Huisgen, R.; Axen, C.; Seidl, H. *Chem. Ber.* **1965**, *98*, 2966.